

Understanding the architecture and biology of the type II protein secretion system in plant-pathogenic *Xanthomonas* bacteria

Doctoral thesis

submitted in fulfilment of the requirements for the degree of *Doctor rerum naturalium*
(Dr. rer. nat.)

at the Faculty of Natural Sciences I – Biosciences
Of the Martin-Luther-University
Halle-Wittenberg

by Samuel Goll

Examiners:

Apl. Prof. Dr. Daniela Büttner

Prof. Dr. Gary Sawers

Prof. Dr. Marc Erhardt

Dissertation handed in: 23. March 2025

Dissertation defended: 02. July 2025

1 Summary

The genus *Xanthomonas* entails Gram-negative plant-pathogenic bacteria that infect a large variety of agriculturally relevant crops. Virulence depends on protein secretion systems, such as the type II and type III secretion (T2S/T3S) systems. T2S systems are widespread among Gram-negative pathogens and transport substrates from the periplasm into the extracellular milieu, however, mechanisms of substrate recognition remain enigmatic. Focus of this study is the architecture of the Xps-T2S system and its role in infection.

When infecting pepper and tomato plants, *X. euvesicatoria* employs the Xps-T2S system composed of eleven different components: an outer membrane secretin (XpsD), inner membrane assembly platform components (XpsE, F, C, L, M) and periplasmic pseudopilins (XpsG, H, I, J and K). A modularized, plasmid-borne *xps* gene cluster enabled rapid generation of individual gene deletions and -variants to study the assembly of the complete secretion apparatus from these different components. Structural modelling, fluorescence microscopy, *in vitro* and *in vivo* protein interaction studies revealed three independently assembling subcomplexes of the T2S system: the XpsD secretin channel, an inner membrane XpsCLM assembly platform complex and an XpsF-XpsIJK complex which connects the pseudopilus with an assembly platform component. The trimeric XpsCLM complex appears to be structurally conserved in other T2S systems, and a conserved, positively charged, potential docking site for substrates in the second periplasmic (2P) region of XpsC was identified. Additionally, the membrane protein XpsF interacts with the pseudopilus tip complex composed of XpsI, J and K, forming an additional independent subcomplex. A mechanism of T2S system assembly and of T2S secretion is proposed, with the preformed XpsCLM and XpsF-IJK subcomplexes binding to the XpsD secretin channel, thereby forming a scaffold for the oligomerization of the hexameric ATPase XpsE in the cytoplasm. Substrates are presumably then secreted through the secretin channel via extension of the pseudopilus.

As substrates of the T2S system are delivered into the plant apoplast in nature, mass spectrometry of apoplastic proteins in infected plants identified novel T2S substrates including various proteases and cell wall degrading enzymes such as cellulases, xylanases and polygalacturonases. Analysis of plant cell wall composition revealed specific degradation of hemicelluloses and pectins as a result of T2S. Growth assays demonstrated that T2S enables utilization of amino acids from degraded extracellular proteins and of cell wall carbohydrates from cellulose and hemicelluloses like xylan. Taken together, these findings shed light on the role of T2S in nutrient acquisition of *Xanthomonas* during infection.

1.1 Table of contents

| | | |
|--------|--|----|
| 1 | Summary..... | I |
| 1.1 | Table of contents..... | II |
| 1.2 | List of abbreviations | IV |
| 1.3 | Table of figures..... | V |
| 2 | Introduction | 1 |
| 2.1 | Bacteria and secretion systems | 1 |
| 2.1.1 | One-step secretion systems..... | 2 |
| 2.1.2 | Two-step secretion systems | 3 |
| 2.2 | Architecture and function of the T2S system | 5 |
| 2.3 | T2S in phytopathogenic <i>Xanthomonas</i> species..... | 9 |
| 2.3.1 | The Biology of <i>Xanthomonas</i> plant infections..... | 10 |
| 2.3.2 | The role of T2S in <i>Xanthomonas</i> infection of plants | 11 |
| 2.3.3 | Nutrient acquisition of bacterial pathogens in the host plant | 13 |
| 2.4 | Goals of this study | 16 |
| 3 | Materials and methods | 17 |
| 3.1 | Material..... | 17 |
| 3.1.1 | Buffers and media | 17 |
| 3.1.2 | Bacterial strains, plasmids and primers | 18 |
| 3.2 | Methods..... | 20 |
| 3.2.1 | Cloning and strain construction | 20 |
| 3.2.2 | Plant infection studies | 24 |
| 3.2.3 | Isolation of cell wall extracts..... | 25 |
| 3.2.4 | Growth curves in modified XVM2 minimal medium..... | 25 |
| 3.2.5 | Extracellular protease activity assays..... | 26 |
| 3.2.6 | Identification of apoplastic T2S substrates | 26 |
| 3.2.7 | Secretion assays..... | 26 |
| 3.2.8 | Immunoblot analysis of bacterial protein extracts | 27 |
| 3.2.9 | Protein-Protein interaction studies..... | 27 |
| 3.2.10 | Fluorescence microscopy..... | 29 |
| 3.2.11 | Statistical analyses..... | 29 |
| 3.2.12 | <i>In-silico</i> structural protein modelling | 30 |
| 4 | Results..... | 31 |
| 4.1 | Characterization of the Xps-T2S in <i>X. euvesicatoria</i> | 31 |
| 4.1.1 | Generation of a modular <i>xps</i> gene cluster by Golden Gate cloning | 31 |
| 4.1.2 | The modularized <i>xps</i> gene cluster expedites functional studies | 33 |
| 4.1.3 | Independent assembly of the oligomeric secretin structure | 34 |
| 4.1.4 | The assembly platform components XpsC, XpsL and XpsM are essential for T2S | 37 |
| 4.1.5 | <i>In-silico</i> modeling suggests a structurally conserved trimeric XpsCLM complex in diverse bacterial species | 38 |
| 4.1.6 | <i>In vitro</i> characterization of XpsC, XpsL, XpsM and XpsE interactions | 40 |
| 4.1.7 | Stability of XpsC and XpsL depend on each other and XpsM | 42 |
| 4.1.8 | Identification of the XpsCLM complex by <i>in vivo</i> crosslinking experiments | 43 |

| | | |
|--------|--|-----|
| 4.1.9 | Conserved positive charges in the 2P region of XpsC regulate T2S efficiency .. | 45 |
| 4.1.10 | XpsF and all pseudopilins aside from XpsH are essential to T2S in <i>X. euvesicatoria</i> | 49 |
| 4.1.11 | XpsF oligomerization requires XpsI, XpsJ and XpsK | 50 |
| 4.1.12 | Structural modelling suggests docking of the pseudopilus tip in a trimeric XpsF channel | 51 |
| 4.1.13 | The pseudopilus tip assembles independently of XpsF and XpsE | 53 |
| 4.1.14 | XpsK interacts with XpsF as predicted | 55 |
| 4.1.15 | Alphafold3 predictions suggest that XpsHIJK may form the tip of the extending pseudopilus and interact with T2S substrates | 57 |
| 4.2 | Function of T2S substrates | 59 |
| 4.2.1 | <i>In planta</i> identification of novel T2S substrates | 59 |
| 4.2.2 | Multiple T2S secreted proteins have proteolytic activity | 62 |
| 4.2.3 | The T2S-dependent serine protease XCV3671 requires autocatalytic cleavage for secretion and oligomerization | 63 |
| 4.2.4 | Virulence and protease secretion of the Xps-T2S system are conserved in different <i>Xanthomonas</i> species | 66 |
| 4.2.5 | T2S enables utilization of amino acids from extracellular proteins | 67 |
| 4.2.6 | <i>Xanthomonas</i> infection alters plant cell wall composition in a T2S-dependent manner | 67 |
| 4.2.7 | Cell wall carbohydrates are utilized by <i>Xanthomonas</i> in a T2S dependent manner | 70 |
| 5 | Discussion | 74 |
| 5.1 | Insights into the architecture and the assembly of the Xps-T2S system | 74 |
| 5.1.1 | The XpsD secretin channel assembles independently of the remaining T2S system components | 76 |
| 5.1.2 | The trimeric assembly platform XpsCLM complex links the secretin to the cytoplasmic ATPase | 76 |
| 5.1.3 | Pseudopilus initiation at an XpsF channel? | 79 |
| 5.1.4 | A proposed functional mechanism of the Xps-T2S system | 81 |
| 5.1.5 | How does the pseudopilus retract? | 85 |
| 5.2 | The role of T2S in plant infection | 86 |
| 5.2.1 | T2S and nutrient acquisition | 86 |
| 5.2.2 | Degradation of apoplastic defense components by the T2S system | 89 |
| 5.2.3 | Functional interplay between T2S and T3S in virulence? | 91 |
| 5.3 | Employing the Xps-T2S to expand the metabolic capabilities of <i>E. coli</i> | 92 |
| 6 | References | 94 |
| 7 | Appendix | 105 |
| 7.1 | Supplemental tables | 105 |
| 7.2 | Supplemental figures | 122 |
| 7.3 | Acknowledgements | 128 |
| 7.4 | Curriculum vitae | 129 |
| 7.5 | Declaration of authorship | 130 |

1.2 List of abbreviations

2P region: second periplasmic

AIR: alcohol insoluble residue

ATP: adenosine triphosphate

BACTH assay/system: bacterial adenylate cyclase two-hybrid assay/system

cAMP: cyclic adenosine monophosphate

CTE: C-terminal extension domain

CWDE: cell wall degrading enzyme

Cya: adenylate cyclase

DAMP: damage-associated molecular pattern

DNA: deoxyribonucleic acid

ETI: effector-triggered immunity

ETS: effector-triggered susceptibility

FA: formaldehyde

Gsp: general secretory pathway

GST: glutathione S-transferase

HPAEC-PAD: high-pressure anion-exchange chromatography with pulsed-amperometric detection

HR: homology region

IM: inner membrane

IPTG: isopropyl β -D-thiogalactopyranoside

N1E/N2E: N-terminal extension domain

OM: outer membrane

PAMP: pathogen-associated molecular pattern

PEP: plant elicitor peptides

PGIP: polygalacturonase-inhibiting protein

PRR: pattern recognition receptor

PTI: PAMP-triggered immunity

RNA: ribonucleic acid

ROS: reactive oxygen species

Sec system: general secretory system

T1S: type I secretion

T2S: type II secretion

T3S: type III secretion

T4S: type IV secretion

T5S: type V secretion

T6S: type VI secretion

Tat system: twin-arginine translocation system

Xag: *Xanthomonas axonopodis* pv. *Glycines*

Xcc: *Xanthomonas campestris* pv. *Campestris*

Xe: *Xanthomonas euvesicatoria*

X-gal: 5-bromo-4-chloro-3-indolyl- β -D-galactopyranoside

XIP: xylanase-inhibiting protein

1.3 Table of figures

| | |
|---|-----|
| Figure 1: Overview of several secretion systems employed by Gram-negative bacteria | 2 |
| Figure 2: Schematic representation of the T2S system | 6 |
| Figure 3: schematic representation of a non-vascular <i>Xanthomonas</i> infection of a plant | 10 |
| Figure 4: potential roles of T2S in <i>Xanthomonas</i> virulence..... | 13 |
| Figure 5: schematic structures of abundant plant cell wall polysaccharides | 15 |
| Figure 6: Modular Cloning of the <i>xps</i> -T2S gene cluster from <i>X. euvesicatoria</i> | 32 |
| Figure 7: The modular <i>xps</i> -T2S system expedites functional characterization of <i>xpsD</i> and <i>xpsE</i> mutants | 34 |
| Figure 8: Assembly of the outer membrane secretin XpsD is independent of T2S system components. | 36 |
| Figure 9: Assembly platform components XpsC, XpsL and XpsM are essential for T2S in <i>X. euvesicatoria</i> | 38 |
| Figure 10: XpsCLM form a predicted trimeric complex which is structurally conserved | 40 |
| Figure 11: <i>In vitro</i> protein-protein interaction studies with assembly platform components from <i>X. euvesicatoria</i> | 41 |
| Figure 12: <i>In vivo</i> crosslinking experiments verify a trimeric XpsCLM complex | 43 |
| Figure 13: Positively charged residues of 2P-region of XpsC are highly conserved | 46 |
| Figure 14: the 2P region of XpsC may interact with substrates electrostatically and regulates T2S efficiency | 48 |
| Figure 15: XpsF and the pseudopilins XpsG, XpsI, XpsJ and XpsK are essential to T2S..... | 50 |
| Figure 16: Oligomerization of XpsF requires XpsI, XpsJ and XpsK..... | 51 |
| Figure 17: Predicted structure of a XpsI-J-K pseudopilus tip complex nested in a trimeric XpsF channel | 52 |
| Figure 18: A trimeric XpsIJK complex assembles independently of XpsF and XpsE <i>in vivo</i> | 54 |
| Figure 19: XpsK interacts with XpsF via the hydrophobic tail region | 56 |
| Figure 20: AlphaFold3 predictions of the XpsHIJK tip complex with XpsG and with T2S substrates ... | 58 |
| Figure 21: Apoplastic <i>X. euvesicatoria</i> proteins reduced in an <i>xps</i> mutant | 60 |
| Figure 22: <i>In vitro</i> verification of novel <i>X. euvesicatoria</i> Xps-T2S substrates | 61 |
| Figure 23: five extracellular proteases from <i>X. euvesicatoria</i> show proteolytic activity | 63 |
| Figure 24: Autocatalytic cleavage of the N-terminal domain of XCV3671 is required for T2S | 65 |
| Figure 25: The T2S system contributes to extracellular protease activity and virulence in <i>Xanthomonas</i> | 66 |
| Figure 26: Xps-T2S allows for utilization of amino acids from extracellular proteins | 67 |
| Figure 27: Plant cell wall monosaccharide composition is altered in an Xps-dependent manner during infection | 69 |
| Figure 28: <i>Xanthomonas</i> utilization of cell wall carbohydrates depends on the Xps-T2S | 71 |
| Figure 29: <i>Xanthomonas</i> utilization of xylan and cellulose depends on the Xps-T2S system..... | 72 |
| figure 30: A proposed integrated model of the assembly and function of the T2S system: | 75 |
| Figure 31: proposed model of substrate secretion via the T2S system | 82 |
| Figure 32: Potential inhibition of PTI responses by T2S substrates..... | 90 |
| Figure 33: The modular T2S system restores bacterial spot formation in an <i>xps</i> -T2S gene cluster mutant..... | 122 |
| Figure 34: Predicted secondary structures in XpsC and corresponding GspC proteins..... | 122 |
| Figure 35: Synthesis and immunological detection of T18 and T25 fusions of assembly platform components | 123 |
| Figure 36: AlphaFold3 structural model of XpsE ₆ -XpsF ₃ complex: | 123 |
| Figure 37: AlphaFold2 Structure predictions of assembly platform components from <i>X. euvesicatoria</i> , <i>P. aeruginosa</i> , <i>D. dadantii</i> and <i>V. cholerae</i> | 124 |
| Figure 38: AlphaFold2 structure predictions of additional T2S proteins..... | 125 |
| Figure 39: AlphaFold3 structure predictions of proteins used in this study | 126 |
| Figure 40: Principal component analysis of the cell wall monosaccharide composition of infected plants | 127 |

2 Introduction

2.1 Bacteria and secretion systems

Bacteria are an incredibly diverse and multifaceted group of single cell prokaryotic organisms that thrive in practically all environmental niches, from anaerobic organic sludge and deep-sea vents to alpine ridges. Colonization of such diverse habitats is made possible by an astounding metabolic diversity found in bacteria, ranging from photo- or chemosynthetic autotrophs to heterotrophs involved in recycling of complex biomass. In their natural habitat, heterotrophs need to access organic molecules from the extracellular environment for meta- and anabolism (Gralka *et al*, 2023). Frequently, bacteria cohabitate with other eukaryotic organisms mutualistically or as pathogens, ranging from beneficial nitrogen-fixing *Rhizobium* spp. in legume plants and intracellular *Shigella* spp. pathogens residing in human host cells.

Bacterial pathogens have specialized infection mechanisms to infect their respective hosts, including plants, animals and protists such as amoeba (Shi *et al*, 2021; Savary *et al*, 2019; Soni *et al*, 2024). To facilitate infection and growth, multiple protein secretion systems are employed to either transport proteins from the bacterial cell into the extracellular milieu or directly into host cells. Protein secretion systems are complex biomolecular nanomachines formed by multiple components that work together to recognize and translocate specific target proteins across membranes. These systems are frequently highly conserved and required for the virulence of pathogens infecting diverse hosts, including both animals and plants. To date at least 11 different bacterial secretion systems have been discovered, classified in the order of their discovery as type I secretion (T1S) through type XI secretion (T11S) systems (Filloux, 2022; Grossman *et al*, 2021). An overview of several important bacterial secretion systems in Gram-negative bacteria is given in Figure 1.

Generally, secretion systems can be classified as one-step or two-step processes. In a one-step process, the transport machinery translocates a substrate protein from the bacterial cytoplasm to the extracellular milieu or into a target host cell. On the other hand, a two-step process relies on the general secretory (Sec) or twin-arginine translocation (Tat) system to first transport proteins into the periplasm (Rêgo *et al*, 2010). From the periplasm, substrates are then recognized and transported across the outer membrane.

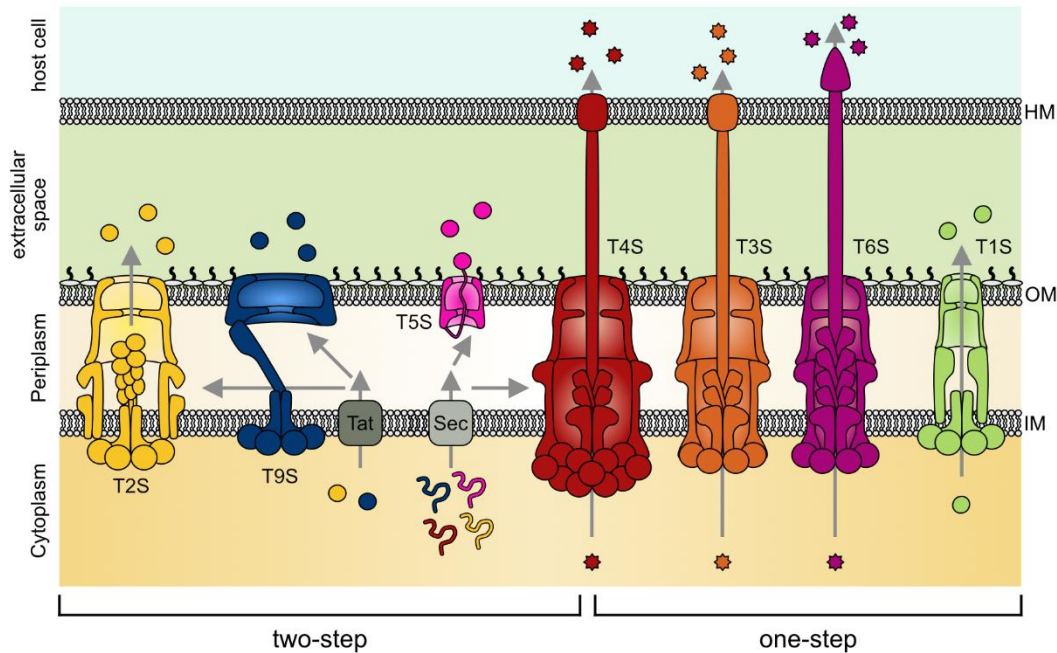


Figure 1: Overview of several secretion systems employed by Gram-negative bacteria

Secretion systems are employed by bacteria to transport substrate proteins into the extracellular milieu or into host cells. Secretion systems can be grouped as Sec/Tat-independent one-step processes (T1S: green, T3S: orange, T4S: red, and T6S: purple) or Sec/Tat dependent two-step processes (T2S: yellow, T5S: purple and T9S: blue). The Sec system transports unfolded substrates across the inner membrane, while the Tat system can secrete fully folded proteins. IM: inner membrane, OM: outer membrane, HM: host membrane

2.1.1 One-step secretion systems

One-step secretion systems include the T1S, T3S, T4S and T6S systems (Figure 1). The T1S system transports toxins and adhesins directly from the cytoplasm into the extracellular milieu and can secrete extremely large substrates, with a molecular mass of up to 1.5 MDa (Guo *et al*, 2017). Prior to secretion, a conserved amino acid sequence in the C-terminal region of substrate proteins is recognized (Wagner *et al*, 2011). T1S substrates that play a role in bacterial pathogenicity include hemolysin A from pathogenic *Escherichia coli* which forms a pore in host membranes (Pourhassan N. *et al*, 2022), and CyaA from *Bordetella pertussis* which translocates itself into the cytosol of a host cell where it manipulates cyclic adenosine monophosphate (cAMP) levels (Voegelé *et al*, 2018).

The T3S system, related to the bacterial flagellum, is an important virulence factor of many human- and plant-pathogens. It forms a syringe-like injectosome that secretes substrate proteins called effectors from the bacterial cytoplasm into the cytosol of eukaryotic host cells (Halte & Erhardt, 2021). T3S substrates are recognized by an export signal in their N-terminal region (Büttner, 2016). Upon secretion, effector proteins manipulate the metabolism of host cells to inhibit pathogen detection and immune responses and provide favorable conditions for pathogen proliferation (Deng *et al*, 2017). Sequential secretion of different effectors to reprogram host cells in various ways in the course of infection was demonstrated

for animal-pathogens (Braet *et al*, 2022). T3S systems are employed by prominent human pathogens such as *Salmonella enterica*, *Shigella flexneri*, pathogenic *E. coli* species and *Yersinia* spp. (Notti & Stebbins, 2016), by plant pathogens including *Pseudomonas syringae*, *Ralstonia solanacearum* and *Xanthomonas* spp, (Büttner, 2016) and even by symbiotic Rhizobia to establish symbiosis with legume plants (Teulet *et al*, 2022). Typically, T3S systems are expressed and assembled in a tightly regulated fashion in response to exogenous signals indicative of host organisms (Büttner, 2012).

T4S systems are highly complex and versatile, involved in DNA transfer and protein secretion (Costa *et al*, 2021). While most substrates are transported from the cytoplasm into a host cell, recent findings have shown that cargo proteins may also be recruited from the periplasm, rendering this system both a one-step or a two-step system, depending on the substrate involved (Llosa & Alkorta, 2017). A classical representative is the *Rhizobium radiobacter* (formerly *Agrobacterium tumefaciens*) VirB/D4 secretion system that transports T-DNA into host plants where it can be integrated into the chromosome and manipulates plant hormone levels and metabolism to favor bacterial proliferation (Cascales & Christie, 2004). Since its discovery, this system has been exploited as one of the prime tools for genetic modification of plants (Brown *et al*, 2023). Additional examples of T4S systems employed by human pathogens include the *Legionella pneumophila* Dot/Icm system and the *Helicobacter pylori* Cag system (Costa *et al*, 2021). Furthermore, T4S systems are employed in conjugative transfer of DNA between bacteria, exemplified by the F-pilus encoded Tra system, as well as in active killing of competing bacteria by toxin delivery, as demonstrated in *Xanthomonas citri* (Souza *et al*, 2015).

The T6S system is a contractile injection system. A needle-like structure is loaded with cargo proteins and subsequently thrust through the target membrane followed by cargo release (Cherrak *et al*, 2019). It is employed by a wide variety of bacteria for translocation of proteins into both eukaryotic and prokaryotic cells, very frequently involved in inter-bacterial competition and for delivering toxic effectors to bacterial rivals to reduce competition in a biofilm (Coulthurst, 2019). T6S effectors from human pathogens such as *Vibrio cholerae* or *Aeromonas hydrophila* were shown to target actin or tubulin rearrangement to prevent phagocytosis (Cherrak *et al*, 2019).

2.1.2 Two-step secretion systems

Two-step secretion systems including the T5S, T9S and T2S systems depend on the Sec or Tat system for translocation of substrate proteins into the periplasm. The Sec system is the most fundamental protein secretion system, conserved in nearly all forms of life, which translocates unfolded proteins across the inner membrane (IM) (Beckwith, 2013; Albers *et al*, 2006). Substrates are recognized by the system at a conserved signal peptide found at the

N-terminus of substrates, which is cleaved from the mature protein after translocation (Beckwith, 2013). Similarly, the Tat system recognizes an N-terminal twin-arginine signal peptide on the substrate protein which is cleaved after translocation. In contrast to the Sec system, the Tat system transports fully folded proteins (Palmer & Berks, 2012). In a second step, translocation of proteins across the outer membrane (OM) relies on one of several OM spanning secretion systems in Gram-negative bacteria. In contrast, Gram-positive bacteria possess one membrane, so Sec- and Tat-dependent secretion release proteins into the extracellular space.

The T5S system is often termed autotransporter secretion as it entails OM passage of an extracellular “passenger” domain of a substrate protein through a β -barrel domain of the same protein (Bernstein, 2019). The insertion of the β -barrel domain into the OM is assisted by the β -barrel assembly machinery (Leo *et al*, 2012). The passenger domain may then be cleaved and released into the extracellular space or remain bound to the OM. T5S substrates often play an important role in cell adhesion, but also in biofilm formation and immune evasion (Meuskens *et al*, 2019). T5S systems are found in diverse animal pathogens such as *Bordetella pertussis*, *Neisseria gonorrhoeae* and *Haemophilus influenzae* (Benz & Schmidt, 2011) as well as plant pathogens including *Xanthomonas citri* and *Rhizobium radiobacter* (Henderson & Nataro, 2005; Alvarez-Martinez *et al*, 2020).

The T9S system is found solely in bacteria of the phylum Bacteroidetes, transports various proteins including adhesins, proteases and cellulases into the extracellular milieu (Gorasia *et al*, 2020), and is involved in nutrient acquisition, surface adhesion, pathogenicity and gliding motility (Gao *et al*, 2020b).

Bacterial T2S systems deliver folded proteins across the outer membrane (OM) into the extracellular milieu and have been identified as virulence factors in many important human (e.g. *Klebsiella pneumoniae*, *Legionella pneumophila*, *Pseudomonas aeruginosa* and *Vibrio cholerae*) and plant pathogens (e.g. *Dickeya dadantii*, *Erwinia amylovora*, *Xanthomonas campestris* and *Xylella fastidiosa*) (Korotkov & Sandkvist, 2019; Abby *et al*, 2016). T2S substrates include degradative enzymes, toxins and proteins involved in bacterial adhesion, biofilm formation and nutrient acquisition (Naskar *et al*, 2021). One prominent example for a virulence-associated T2S substrate is cholera toxin from *V. cholerae* (Cianciotto & White, 2017). So far, no conserved recognition signal in substrate proteins has been described, and it is assumed that substrates are recognized by structural properties in their fully folded state (Gu *et al*, 2017)

2.2 Architecture and function of the T2S system

Focus of this study is the T2S system and its role in the virulence of plant pathogenic bacterium *Xanthomonas euvesicatoria*. T2S systems have historically been referred to as the main terminal branch of the General Secretory Pathway (GSP) which has given rise to the standardized Gsp nomenclature of T2S components (Desvaux *et al*, 2004). Nevertheless, multiple different nomenclatures exist for different species (Table 1) (Filloux, 2004; Patrick *et al*, 2010; Francetic *et al*, 2000; Buddelmeijer *et al*, 2009). Structural components of T2S systems are often encoded by a single operon containing 11 – 16 genes and are grouped into three subcomplexes: (i) an IM-associated assembly platform consisting of GspC, GspF, GspL, GspM and the cytoplasmic ATPase GspE, (ii) a periplasmic pseudopilus containing the major pseudopilin GspG capped by the minor pseudopilins GspH, GspI, GspJ and GspK, and (iii) an OM secretin assembled by GspD (Korotkov & Sandkvist, 2019; Naskar *et al*, 2021). A schematic representation of the T2S system is shown in Figure 2.

Table 1: Nomenclature of homologous components of prominent T2S systems of pathogenic bacteria (*Vibrio cholerae*, *Pseudomonas aeruginosa*, *Klebsiella* spp., *Erwinia* / *Dickeya* spp. and *Xanthomonas* spp.)

| Standardized Gsp | <i>Klebsiella</i> Pul | <i>Erwinia/Dickeya</i> Out | <i>Xanthomonas</i> Xps | <i>Vibrio</i> Eps | <i>Pseudomonas</i> Xcp | Function |
|------------------|-----------------------|----------------------------|------------------------|-------------------|------------------------|--------------------------|
| GspA | - | - | - | EpsA | - | Peptidoglycan remodeling |
| GspB | PulB | OutB | - | EpsB | - | Peptidoglycan remodeling |
| GspC | PulC | OutC | XpsC (N) | EpsC | XcpP | IM assembly platform |
| GspD | PulD | OutD | XpsD | EpsD | XcpQ | OM secretin |
| GspE | PulE | OutE | XpsE | EpsE | XcpR | ATPase |
| GspF | PulF | OutF | XpsF | EpsF | XcpS | IM assembly platform |
| GspG | PulG | OutG | XpsG | EpsG | XcpT | pseudopilus |
| GspH | PulH | OutH | XpsH | EpsH | XcpU | pseudopilus |
| GspI | PulI | OutI | XpsI | EpsI | XcpV | pseudopilus |
| GspJ | PulJ | OutJ | XpsJ | EpsJ | XcpW | pseudopilus |
| GspK | PulK | OutK | XpsK | EpsK | XcpX | pseudopilus |
| GspL | PulL | OutL | XpsL | EpsL | XcpY | IM assembly platform |
| GspM | PulM | OutM | XpsM | EpsM | XcpZ | IM assembly platform |
| GspN | PulN | - | - | EpsN | - | IM assembly platform |
| GspO | PulO | OutO | XpsO/PilD | EpsO | XcpA/PilD | pseudopilus processing |
| GspS | PulS | OutX | - | - | - | OM secretin insertion |

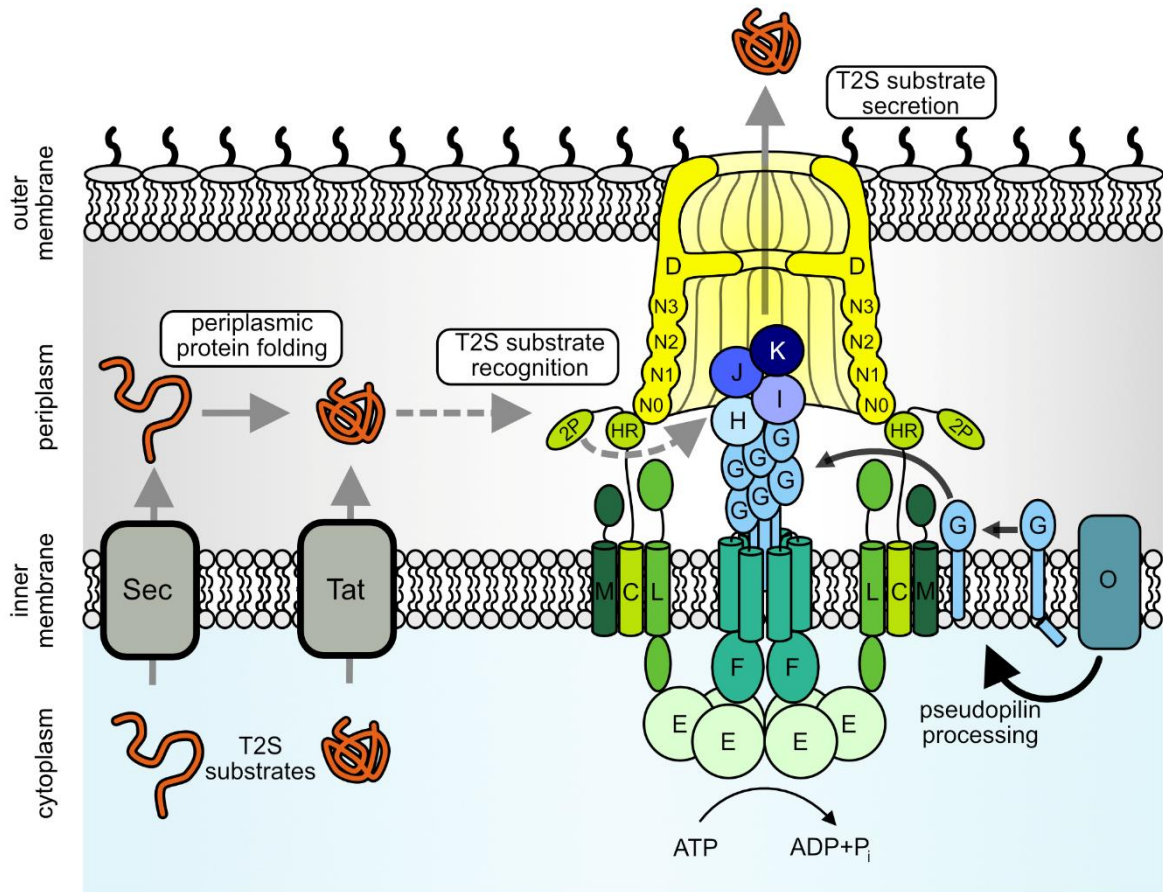


Figure 2: Schematic representation of the T2S system

A general model of the T2S system, composed of the assembly platform (shown in green; GspC, M, L and F and the hexameric ATPase GspE), the pseudopilus (blue; GspG, H, I, J and K) and the OM secretin complex (yellow; GspD). Pseudopilins are processed by the pseudopilin peptidase GspO (teal). T2S system substrates are exported into the periplasm via the general secretory (Sec) system or the Tat system (dark grey) and subsequently recruited by the T2S system. The HR domain of GspC interacts with the N0 domain of the secretin GspD, whereas the second periplasmic (2P) domain of GspC has been suggested to recognize and recruit T2S substrates. Letters refer to the nomenclature of Gsp proteins.

The outer membrane secretin GspD forms the pore through which T2S substrates are secreted. This secretin channel consists of a OM-spanning β -barrel structure formed by the C-terminal domains of 15 GspD proteins. Transport to the OM and oligomerization of the secretin depends on a small pilotin protein called GspS in some T2S systems, while in others lacking GspS homologues, GspD assembles independently (Korotkov & Sandkvist, 2019; Gu *et al*, 2017). Some bacteria require peptidoglycan remodeling by GspA and GspB for secretin assembly, while other T2S systems lack homologues of these proteins (Korotkov & Sandkvist, 2019). The N-terminal regions of GspD proteins form a periplasmic ring structure and consist of four subdomains designated N0, N1, N2 and N3. The N0 domains associate with the periplasmic “homologous regions” (HR) of the IM assembly platform protein GspC which is part of the assembly platform and presumably forms a cage-like structure upon interaction with the N0 domains (Korotkov & Sandkvist, 2019; Naskar *et al*, 2021; Yan *et al*, 2017; Korotkov *et al*, 2011; Chernyatina & Low, 2019).

The assembly platform is formed by four membrane proteins, GspC, L, M and F and the cytoplasmic ATPase GspE. In addition to connecting the assembly platform with the secretin channel via the HR domain, XpsC contains a second periplasmic region, hereafter designated “second periplasmic” (2P) region, likely acts as a docking site for T2S substrates in the periplasm (Pineau *et al*, 2014). The 2P region is variable in different GspC proteins; it is composed of a PDZ fold consisting of six β sheets flanked by two α helices in many T2S systems, but in others such as the *Pseudomonas aeruginosa* Xcp system, the 2P region simply entails a single α helix, (Gu *et al*, 2017; Korotkov *et al*, 2006; Pineau *et al*, 2014). GspC probably surrounds the central component of the assembly platform, GspF, and forms a complex with the IM proteins GspL and GspM which homo- and heterooligomerize via their periplasmic domains, possibly with variable assembly states in response to substrate binding (Gu *et al*, 2017; Chernyatina & Low, 2019; Dazzoni *et al*, 2023; Li *et al*, 2023; Thomassin *et al*, 2017; Michel-Souzy *et al*, 2018). A periplasmic protein complex likely corresponding to six copies of each GspL and GspM was visualized by cryo-electron tomography of the T2S system from *Legionella pneumophila* (Ghosal *et al*, 2019). Furthermore, cryo-electron microscopy and negative stain electron microscopy of an assembled T2S system from *Klebsiella pneumoniae* revealed a hexameric structure formed by GspL, GspM, and the ATPase GspE with each component predicted to interact with two copies of GspC (Korotkov & Sandkvist, 2019; Chernyatina & Low, 2019). Given the symmetry mismatch between 12 copies of GspC and the pentadecameric GspD secretin, it was speculated that the docking of the assembly platform to the secretin GspD leads to structural reorganizations in GspD. Alternatively, openings in the GspC-GspD complex and local rearrangements might control the access of T2S substrates (Chernyatina & Low, 2019; Gu *et al*, 2017; Barbat *et al*, 2023). In some T2S systems, such as those from *K. pneumoniae* and *Acinetobacter baumannii*, an additional non-essential membrane protein GspN protein is associated with the assembly platform (Naskar *et al*, 2021). However, no clear role of this accessory protein has been established to date (Chernyatina & Low, 2019; Waack *et al*, 2017).

GspF is a polytopic membrane protein that has been purified in a dimeric form (Abendroth *et al*, 2009) but recently demonstrated to form a trimeric inner membrane channel in the *Klebsiella* Pul system (Guilvout *et al*, 2024). This protein is thought to be located at the center of the assembly platform (Gu *et al*, 2017) and interacts with GspE and GspL (Py *et al*, 2001) potentially forming a base for the formation of the periplasmic pseudopilus. However, no direct interaction of XpsF with pseudopilins has yet been shown. The cytoplasmic ATPase provides the energy for T2S systems by hydrolysis of ATP (Patrick *et al*, 2011) and likely forms a hexamer (Lu *et al*, 2013). GspE contains three distinct domains: two N-terminal extension domains (N1E and N2E) and one C-terminal extension domain (CTE). Crystal structures suggest that the N2E and CTE domains of different GspE proteins interact with

each other to form the hexameric core ATPase, while the N1E domain is associated with the cytoplasmic domain of the assembly platform protein GspL (Lu *et al*, 2014b).

The transport of T2S substrates through the secretin is presumably mediated by the continuous assembly and disassembly of the periplasmic pseudopilus (Naskar *et al*, 2021). The periplasmic pseudopilus is composed of the major pseudopilin GspG and the minor pseudopilins GspH, I, J and K which form the tip complex at the end of the pseudopilus (Korotkov & Hol, 2008; Naskar *et al*, 2021). Pseudopilins contain a hydrophobic N-terminal region and a hydrophilic globular C-terminal domain. Both T2S pseudopilins and pilins of the closely related type IVa piliation system are processed by the prepilin peptidases of the GspO/PilD superfamily often encoded by a single gene for both systems (Filloux, 2004; Izadi-Pruneyre *et al*, 2024). These pseudopilin peptidases localize in the inner membrane and cleave an N-terminal leader peptide from the pre-pseudopilins at a conserved glycine residue, yielding mature pseudopilins that can subsequently assemble into the pilus structure of the respective secretion system by interactions of the hydrophobic N-terminal region (Marsh & Taylor, 1998; Singh & Donnenberg, 2023; Nunn & Lory, 1991; Hu *et al*, 1995). Presumably, oligomerization of multiple GspG proteins extends the pseudopilus, pushing the tip complex towards the secretin channel, so that bound T2S substrates can be released into the extracellular milieu (Naskar *et al*, 2021). Subsequently, the pseudopilus disassembles or is retracted by some mechanism not yet understood, potentially by a conformational change of GspG due to the release of a bound calcium ion, or by proteolytic cleavage (Nivaskumar & Francetic, 2014; López-Castilla *et al*, 2017).

While progress has been made regarding the interactions of individual Gsp proteins in a functional T2S system, much less is known regarding the assembly of the system. It has been suggested that the T2S is more dynamic and less static than other secretion systems (Dazzoni *et al*, 2023; Gu *et al*, 2017). It remains to be determined whether all T2S components assemble simultaneously to form the system or whether there is a hierarchy with individual subcomplexes independently assembling and subsequently coming together. Furthermore, while it is assumed that the pseudopilus assembles at the center of the assembly platform, direct interactions between pseudopilins and assembly platform components remain to be verified *in vivo*.

How T2S substrates are recognized is also poorly understood. The only apparent common feature between different T2S substrates is a cleavable Sec or Tat signal peptides; no conserved signal for T2S-dependent transport across the OM has yet been identified (Thomassin *et al*, 2017; Gu *et al*, 2017). Given that T2S substrates are folded in the periplasm prior to T2S-dependent transport, the secretion signal is likely part of a structural element which interacts with components of the assembly platform such as the secretin or

the 2P region of GspC (Korotkov & Sandkvist, 2019; Thomassin *et al*, 2017; Douzi *et al*, 2011). Additional potential substrate docking sites are provided by the periplasmic pseudopilus which presumably pushes T2S substrates through the secretin by continuous assembly and disassembly (Michel-Souzy *et al*, 2018; Naskar *et al*, 2021). Interactions of T2S components with substrates have been demonstrated for the secretin GspD, the assembly platform components GspC, GspL and GspM, as well as the pseudopilus tip complex formed by GspHIJK (Pineau *et al*, 2014; Douzi *et al*, 2011; Michel-Souzy *et al*, 2018).

2.3 T2S in phytopathogenic *Xanthomonas* species

A model for the study of T2S in phytopathogenic bacteria is the genus *Xanthomonas* (Jha *et al*, 2005; Luneau *et al*, 2022), which entails many agriculturally relevant pathogens that infect over 400 different host plants and lead to significant annual crop losses (Timilsina *et al*, 2020). *Xanthomonas* spp. have two T2S systems, an Xcs- and an Xps-T2S system, of which the Xps-T2S system is highly conserved across the genus and required for full virulence (Pfeilmeier *et al*, 2024; Alvarez-Martinez *et al*, 2020; Szczesny *et al*, 2010; Baptista *et al*, 2010). Additionally, the Xps-T2S system is the main virulence determinant in the closely related plant-pathogen *Xylella fastidiosa* that causes Pierce's disease in grapevine and Olive Quick Decline Syndrome, which presents a current and highly relevant agricultural challenge (Ingel *et al*, 2023).

Xanthomonas euvesicatoria (Xe) is the causal agent of bacterial spot disease in pepper and tomato plants and the main model organism used in this study. Components of the Xps-T2S system from Xe are encoded by a chromosomal cluster of eleven genes and include XpsE, F, G, H, I, J, K, L, M, C and D (Szczesny *et al*, 2010), and it was previously demonstrated that deletion of genes encoding the putative ATPase XpsE or the secretin XpsD led to reduced virulence and extracellular protease and xylanase activity (Szczesny *et al*, 2010). A homolog of the prepilin peptidase GspO, which processes the pseudopilins prior to pseudopilus assembly, is encoded outside of the xps-T2S gene cluster (Thieme *et al*, 2005; Korotkov & Sandkvist, 2019). Homologs of a GspS pilotin, GspA and GspB are missing in *X. euvesicatoria*. Furthermore, the GspC homolog of the Xps-T2S system was formerly misannotated as XpsN (Thieme *et al*, 2005). However, due to the presence of a predicted HR region and structural similarities with other known XpsC proteins, it is hereafter referred to as XpsC (Alvarez-Martinez *et al*, 2020; Lee *et al*, 2004). Prior to this study, known substrates of the Xps-T2S system of Xe were two xylanases (XCV0965 and XCV4358), an esterase (XCV0536) and a protease (XCV3671) (Solé *et al*, 2015; Szczesny *et al*, 2010; Apama *et al*, 2009). In addition to these, virulence-related T2S substrates identified in other *Xanthomonas* species include polygalacturonases in *X. campestris* pv. *campestris* and *X. oryzae* pv. *oryzae*

(Tayi *et al*, 2016; Wang *et al*, 2008) and endoglucanases such as cellulases in *X. oryzae* pv. *oryzae* and others (Jha *et al*, 2007; Paaauw *et al*, 2024; Pfeilmeier *et al*, 2024).

2.3.1 The Biology of *Xanthomonas* plant infections

Pathogenic *Xanthomonas* strains are generally host specific, with different pathovars of the same species sometimes infecting different hosts (Timilsina *et al*, 2020). Based on the plant tissue they invade, *Xanthomonads* are classified as either vascular, invading plant xylem elements, or non-vascular, invading the intercellular apoplastic space of leaf mesophyll tissues (Ryan *et al*, 2011). Entry points into a plant are typically stomata or wound sites, or hydathodes in the case of vascular pathogens (Ryan *et al*, 2011). An exemplary scheme of a non-vascular *Xanthomonas* infection is depicted in Figure 3. As a non-vascular pathogen *X. euvesicatoria* multiplies locally in the apoplast and utilizes the Xps-T2S system and a T3S system to secrete virulence factors into the extracellular milieu or directly into the plant cell, respectively (Timilsina *et al*, 2020; Alvarez-Martinez *et al*, 2020; Potnis *et al*, 2015; An *et al*, 2020; Büttner & Bonas, 2010; Thieme *et al*, 2005).

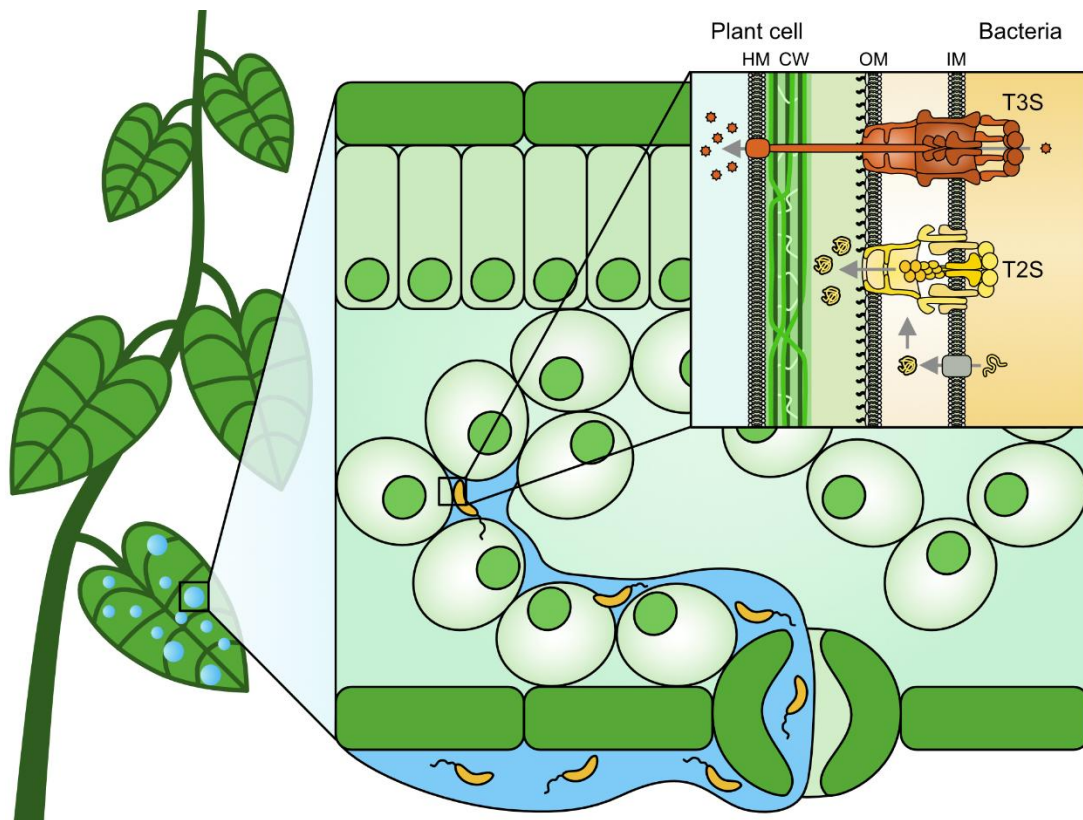


Figure 3: schematic representation of a non-vascular *Xanthomonas* infection of a plant

Xanthomonas pathogens, depicted in yellow, are transported to the plant in water droplets and can enter the plant mesophyll through stomata. In the apoplast, bacterial proliferation is assisted by both the T3S and T2S systems. T3S effector proteins (orange stars) are translocated by the T3S system (orange) through the plant cell wall and plasma membrane into host cells and T2S substrate proteins (depicted in yellow) are secreted into the apoplast by the T2S system (yellow) after translocation into the periplasm via the Sec or Tat system (grey box). (IM: inner membrane, OM: outer membrane, HM: host membrane, CW: cell wall)

Plants detect invading pathogens using pattern recognition receptors (PRRs) that detect molecular patterns, either conserved pathogen-associated molecular patterns (PAMPs) such as the bacterial flagellum and fungal chitin or plant-derived damage-associated molecular patterns (DAMPs) such as oligosaccharides derived from plant cell wall breakdown (Jones *et al*, 2024). Upon recognition of these, PRRs activate signal cascades that activate the plant cells immunity responses, called PAMP-triggered immunity (PTI) (Wang *et al*, 2022). These multi-faceted PTI-responses include the production of extracellular reactive oxygen species (ROS), strengthening of the cell wall, production of antimicrobial compounds called phytoalexins and secretion of CWDE-inhibiting proteins into the apoplast (Wang *et al*, 2022; Xiao *et al*, 2024; Tundo *et al*, 2022). Additionally plant-encoded elicitor peptides are released into the apoplast that are recognized by PRRs of surrounding cells, thereby accentuating PTI responses (Hou *et al*, 2019).

Many bacterial pathogens directly inhibit PTI by injecting effector proteins into host cells via a type III secretion system (Jones & Dangl, 2006). The T3S system is a main determinant of virulence in many *Xanthomonas* species, including *Xe* (Timilsina *et al*, 2020; Büttner & Bonas, 2010). This system has been studied in detail in the last decades and delivers effector protein directly into the plant cell cytoplasm (Deng *et al*, 2017). In *Xanthomonas*, Expression of T3S system genes is dependent on an exogenous signal detected *in planta* (Büttner & Bonas, 2010). Plant cell wall monosaccharides including xylose and galactose activate expression of T3S genes in *X. oryzae* pv. *oryzae* and *X. citri* pv. *citri* (Ikawa *et al*, 2018; Tsuge & Ikawa, 2023; Vieira *et al*, 2021). Additionally, once expressed, coordinated assembly of the complex T3S system is required before effector proteins are translocated into host cells (Otten & Büttner, 2021). There, those effector proteins may degrade PRRs and interfere with downstream signaling cascades to inhibit the plants PTI, leading to effector-triggered susceptibility (ETS) (Block & Alfano, 2011). However, many resistant plants can recognize these effector proteins in turn and respond with a much stronger immunity reaction, a programmed localized cell death called hypersensitive response to prevent further spread of the pathogen (Greenberg & Yao, 2004). This is called effector-triggered immunity (ETI).

2.3.2 The role of T2S in *Xanthomonas* infection of plants

In the complex biology of plant infection, at least four differing but not mutually exclusive roles of the proteases and CWDEs secreted by the T2S system of *Xanthomonas* spp. and related pathogens are conceivable, depicted in Figure 4. Firstly, breakdown of the plant cell wall and apoplastic proteins into more accessible sugars and amino acids may contribute to bacterial nutrient acquisition. Secondly, secreted proteins may degrade apoplastic and membrane-bound plant defense receptors to prevent recognition of PAMPs or DAMPs

released by pathogens in the course of infection and thereby inhibit PTI (Lee Erickson & Schuster, 2024). Thirdly, cell-wall degradation may release plant-derived signals such as xylose that can be sensed by bacteria and activate the expression of plant-specific virulence genes such as the T3S system (Tsuge & Ikawa, 2023). Fourthly, partial digestion of the plant cell wall may aid in the penetration of the T3S pilus through the plant cell wall to enable translocation of T3S effector proteins into the plant cell (Szczesny *et al*, 2010). Additionally, specific cellulases secreted by the T2S system have recently been linked to the ability of certain *Xanthomonas* species to penetrate and infect vascular tissue (Paauw *et al*, 2024; Gluck-Thaler *et al*, 2020).

Differentiating between these four plausible functions of the T2S system in virulence is difficult in the context of a non-vascular plant infection. The importance of the Xps-T2S system in *Xanthomonas* and *Xylella* pathogens lacking a T3S demonstrates T3S-independent roles of the T2S (1 and 2). But distinguishing between reduction of bacterial proliferation *in planta* due to decreased nutrient acquisition or due to increased immunity response is difficult in most experimental setups. Expression studies showed that the corresponding genes of T2S and T3S systems are coregulated and specifically activated during plant infection (Szczesny *et al*, 2010; Solé *et al*, 2015). However, establishing causality from coregulation is not possible as it can be explained both by interdependence of the secretion systems or by them having two independent roles that are required at the same time during infection. Beyond this, the finding that T3S effector translocation efficiency and subsequent hypersensitive response in resistant plant lines is reduced in T2S mutants (Szczesny *et al*, 2010) can be explained both by reduced bacterial fitness (expected for roles 1 and 2) or reduced expression or penetration of the T3S (roles 3 and 4). Therefore, clearly identifying the role of the T2S system in *Xanthomonas* virulence remains challenging.

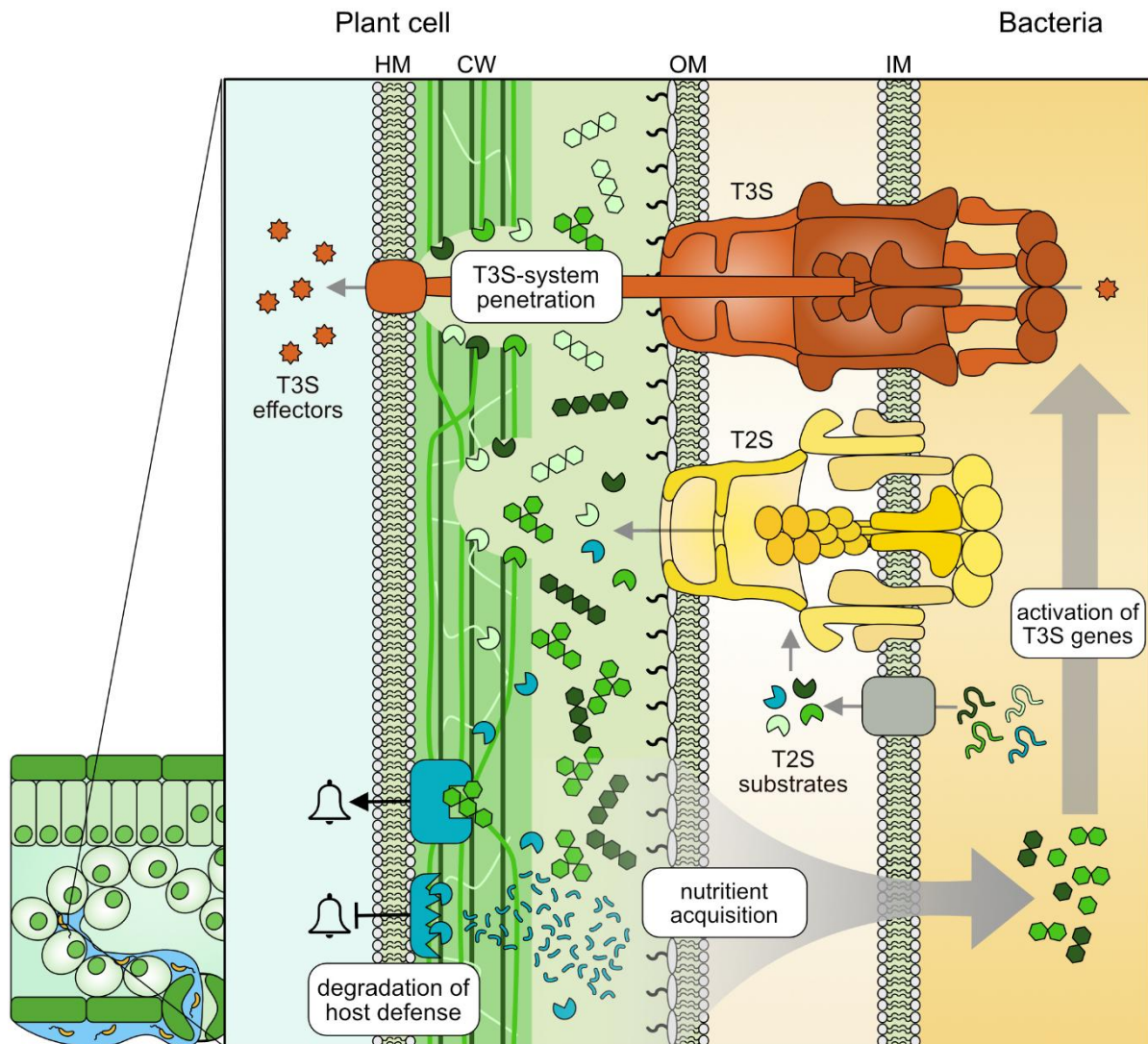


Figure 4: potential roles of T2S in *Xanthomonas* virulence

The interface of a bacterial cell and a plant cell in the context of a non-vascular infection is shown (IM: inner membrane, OM: outer membrane, HM: host membrane), including the T2S (yellow) and T3S system as well as T3S effectors (both orange). The plant cell wall (CW) is shown in green, with cellulose (dark green) hemicellulose (medium green) and pectin (light green). Membrane-bound plant pattern recognition receptors (shown in blue) can bind DAMPs or PAMPs and activate plant immunity responses. T2S substrates are first brought into the periplasm by the Sec or Tat system (grey box) and subsequently translocated into the apoplast by the T2S, where they can degrade their respective substrates (proteases: blue, cellulases: dark green, xylanases: medium green, polygalacturonases: light green). At least four roles of the T2S in the virulence of *Xanthomonas* are conceivable: Degradative enzymes secreted into the apoplast by the T2S system could contribute to virulence by degrading the plant cell wall (saccharides shown in green) of plant proteins (blue) for nutrient acquisition. Host defense could be inhibited by degradation of host defense receptors, or T3S pilus penetration through the plant cell wall could be enabled by cell wall breakdown. Furthermore, cell wall saccharides released by T2S substrate activity may be sensed by the bacterium and lead to the activation of T3S genes.

2.3.3 Nutrient acquisition of bacterial pathogens in the host plant

Both vascular and non-vascular pathogens need to acquire nutrients in their respective environments. The xylem inhabited by vascular *Xanthomonas* strains is mainly composed of non-living cells and is generally considered to be nutrient poor (Yadeta & Thomma, 2013). While the nutritional composition of the plant apoplast remains poorly characterized (O'Leary *et al*, 2016), sugar and amino acid availability in this niche is slightly higher than in the xylem

due to passive and active metabolite efflux from living mesophyll cells (Fatima & Senthil-Kumar, 2015). For some bacterial species, like *Pseudomonas* spp., apoplastic fluid containing limited metabolites were sufficient to support bacterial growth (Mithani *et al*, 2011; Rico & Preston, 2008). Nevertheless, for most bacteria, nutrient acquisition in the apoplast remains a challenge as most nutrients are either bound in the cell wall or inside the vacuole and not directly accessible (Fatima & Senthil-Kumar, 2015). Some *Xanthomonas* species employ certain T3S effector proteins to specifically upregulate sugar export into the apoplast via SWEET transporters (Chen *et al*, 2010; Boch *et al*, 2009). However, many *Xanthomonas* species lack such effectors and some even lack a T3S system and must therefore rely on other strategies to survive in the apoplast (Jacobs *et al*, 2015). One potential nutritional source is the plant cell wall. The primary cell wall is roughly composed of 25% cellulose, 25% hemicellulose and 35% pectin, as well as up to 8% structural proteins, although this can be highly variable between plant species (Fry, 2004; Zhang *et al*, 2021; Chylińska *et al*, 2014). The relatively high content of plant proteins in the cell wall is due to the involvement of these proteins in rearrangement of the complex carbohydrate network cell wall and cell-to-cell communication (Jacq *et al*, 2017).

Plant cell wall polysaccharides can be classified as celluloses, hemicelluloses and pectins, and a schematic representation is shown in Figure 5. Cellulose forms the backbone of the plant cell wall and is composed of long β -1,4-linked D-glucose oligomers arranged in crystalline cellulose microfibrils that confer mechanical stiffness (Cosgrove, 2023). Hemicelluloses are more diverse, containing a linear backbone that can bind to cellulose and decorated with short oligosaccharide side chains that increase their solubility, probably interconnecting different cellulose microfibrils (Cosgrove, 2023). Major hemicelluloses are xyloglucan composed of a β -1,4-glucan backbone with side chains containing xylose, galactose and fucose or arabinoxylan which is composed of a xylose backbone decorated with side chains containing arabinose, galactose, mannose or glucuronic acid (Cosgrove, 2023; Bhardwaj *et al*, 2019; Oliveira *et al*, 2010). Pectin is the most soluble and dynamic polysaccharide of the cell wall and forms a hydrated gel-matrix between cellulose microfibrils, important in determining wall thickness and porosity (Cosgrove, 2023). The most abundant pectin is homogalacturonan composed of linear α -1,4-linked galacturonic acid. Another abundant pectin is rhamnogalacturonan-I containing a backbone formed by alternating rhamnose and galacturonic acid residues and decorated with variable oligosaccharide side chains (Cosgrove, 2023). While the plant cell wall is a highly abundant source of sugars as well as amino acids from cell wall proteins, these nutrients are not as easily accessible as soluble metabolites. For the monosaccharides to be accessed by a bacterial pathogen, they must be enzymatically cleaved from cell wall polysaccharides by specialized enzymes such as cellulases, xylanases, or polygalacturonases (Lorrai & Ferrari, 2021), like the Xps-T2S

substrates identified in *Xanthomonas* pathogens. A link between the T2S system and utilization of plant cell wall oligosaccharides has already been demonstrated for certain saprophytic bacteria such as *Cellvibrio japonicus* that rely on the T2S system for growth on plant cell wall material (Gardner & Keating, 2010).

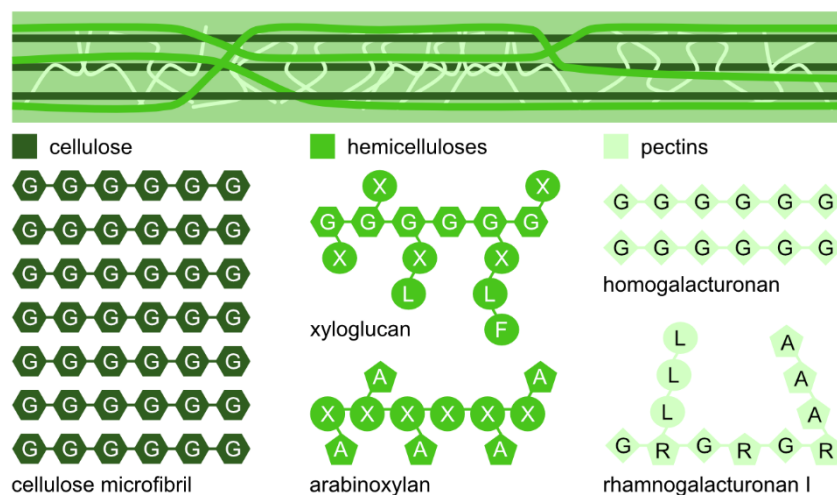


Figure 5: schematic structures of abundant plant cell wall polysaccharides

A schematic representation of a plant cell wall is shown above, composed of cellulose microfibrils (dark green), hemicelluloses (medium green) and pectins (light green). Representative structures of cellulose, the abundant hemicelluloses xyloglucan and arabinoxylan as well as the pectins homogalacturonan and rhamnogalacturonan I are shown below. Legend: G (rectangle): glucose, X (circle): xylose, L (circle): galactose, F (circle): fucose, A (pentagon): arabinose, G (diamond): galacturonic acid, R (pentagon): rhamnose

2.4 Goals of this study

Focus of this study is the architecture of the Xps-T2S system and understanding the role of secreted proteins in plant infection, specifically focusing on nutrient acquisition.

The architecture of the T2S system is still unclear in plant pathogenic bacteria, and this study was to analyze in what manner the components of the Xps-T2S assemble *in vivo* and what protein-interactions are involved in this process. Of specific interest was the formation of the assembly platform, secretin, and pseudopilus, and specifically interactions between pseudopilins and the assembly platform. In preliminary work, the entire *xps* gene cluster was modularized and hierarchically assembled by Golden Gate Cloning, yielding a plasmid-borne *xps* gene cluster construct that functionally complemented an Xe 85-10 Δxps strain. This modularized *xps*-T2S gene cluster was employed to rapidly generate and analyze gene deletions and gene fusions, accompanied by AlphaFold structural modelling, bacterial adenylate cyclase two hybrid assays, GST-pull-downs, fluorescence microscopy as well as *in vivo* formaldehyde- and cysteine-crosslinking.

Multiple roles of T2S substrates in plant infection are plausible, and this study focused on characterizing the influence of the T2S system on bacterial nutrient acquisition. To this end, proteins secreted *in planta* were identified by mass spectrometry, contribution of the T2S system to alterations of the plant cell wall composition was inspected and growth assays were performed in minimal media with various carbohydrate and amino acid sources.

3 Materials and methods

3.1 Material

3.1.1 Buffers and media

Buffers and media used in this study are listed in Table 2 and Table 3, respectively.

Table 2: buffers used in this study

| DNA buffers: | |
|---------------------------------------|---|
| 1 × TAE buffer | 40 mM Tris-Acetate, pH 8.0; 1 mM EDTA |
| 10 × Taq polymerase buffer | 100 mM Tris-HCl, pH 8.5; 500 mM KCl; 15 mM MgCl ₂ ; 1 % (v/v) Triton X-100; 0.1 % (w/v) gelatine |
| 10 × Hybrid buffer | 200 mM Tris-HCl pH 8.8; 20 mM MgSO ₄ ; 100 mM KCl; 100 mM (NH ₄) ₂ SO ₄ ; 1% Triton X-100; 1 mg/ml nuclease-free BSA, pH 8.5 – 9.1 |
| 5 × DNA loading buffer | 50 mM Tris-HCl, pH 8.0; 25 % (w/v) Saccharose; 0.1 % (w/v) SDS (sodium-dodecyl-sulfate); 0.05 % (w/v) Bromphenolblue |
| 10 × T4 ligase buffer | 400 mM Tris-HCl, 100 mM MgCl ₂ , 100 mM DTT, 5 mM ATP (pH 7.8 at 25°C) |
| Protein buffers | |
| 10 mM potassium phosphate | K ₂ HPO ₄ : 796mg/l, KH ₂ PO ₄ : 739mg/l (pH 6.8) |
| 1 × PBS | 140 mM NaCl; 2.7 mM KCl; 10.1 mM Na ₂ HPO ₄ ; 1.8 mM KH ₂ PO ₄ |
| 2 × Laemmli | 125 mM Tris-HCl, pH 6.8; 20 % (v/v) Glycerol; 10 % (v/v) β-Mercaptoethanol; 4 % (w/v) SDS; 0.05 % (w/v); Bromphenolblue |
| 2 × Laemmli (no β-Mercaptoethanol) | 125 mM Tris-HCl, pH 6.8; 20 % (v/v) Glycerol; 4 % (w/v) SDS; 0.05 % (w/v); Bromphenolblue |
| 1 × TBST | 150 mM NaCl; 10 mM Tris-HCl, pH 8.0; 0.05 % (v/v) Tween20 |
| 1 × Tank buffer pH 8.3 | 200 mM Glycine; 25 mM Tris; 0.1 % (w/v) SDS |
| Transfer buffer | 192 mM Glycine; 25 mM Tris-Base; 20 % (v/v) Methanol |
| Blocking solution | 5 % (w/v) skim milk powder; 3 % (w/v) BSA-Albumin Fraction V, in 1 x TBST |
| Chemiluminescence developing solution | 100 mM Tris-HCl pH 8.5; 1.25 mM 3-aminophthalhydrazid; 225 nM p-coumaric acid |

Table 3: media used in this study

| Medium | composition | Reference |
|-------------------------------|--|---------------------------------|
| Lysogeny broth (LB) | 1% Bacto Tryptone; 0.5% Bacto Yeast Extract; 0.5% NaCl; pH 7.5 | (Bertani, 1951) |
| Terrific broth (TB) | 24 g L ⁻¹ Yeast extract; 20 g L ⁻¹ Tryptone; 4 ml L ⁻¹ Glycerol; 0.017 M KH ₂ PO ₄ ; 0.072 M K ₂ HPO ₄ | (Tartoff & Hobbs, 1987) |
| Nutrient-yeast-glycerol (NYG) | 0.1% (w/v) Bacto Yeast Extract; 0.5% (w/v) Bacto Peptone; 0.2% (w/v) glycerol; pH 7.2 | (Daniels <i>et al</i> , 1984b) |
| XVM2 | 20 mM NaCl; 10 mM (NH ₄) ₂ SO ₄ ; 5 mM MgSO ₄ ; 1 mM CaCl ₂ ; 0.16 mM KH ₂ PO ₄ ; 0.32 mM K ₂ HPO ₄ ; 0.01 mM FeSO ₄ ; 10 mM fructose; 10 mM sucrose; 0.03% Casaminoacids; pH 6.7 | (Wengelnik <i>et al</i> , 1996) |

3.1.2 Bacterial strains, plasmids and primers

Bacterial strains used in this study are shown in Table 4, general plasmids are shown in Table 5, Modular Cloning plasmids are listed in Table 11 and Table 12 and primers are listed in Table 13.

Table 4: Bacterial strains used in this study

| Strain | Relevant characteristics | References |
|---|--|---|
| <i>X. euvesicatoria</i> | | |
| 85-10 | Pepper race 2, wild-type; Rif ^R | (Kousik & Ritchie, 1998; Minsavage, 1990) |
| 85-10Δ <i>xps</i> | Derivative of strain 85-10 deleted in the entire <i>xps</i> gene cluster (nucleotide positions 4212581-4224331) | This study |
| <i>X. axonopodis</i> pv. <i>glycines</i> | | |
| 8ra | wild-type; Rif ^R | (Hwang, 1992) |
| 8raΔ <i>xps</i> | Derivative of strain 8ra deleted in the entire <i>xps</i> gene cluster (nucleotide positions 4384268-4395300) | This study |
| <i>X. campestris</i> pv. <i>campestris</i> | | |
| 8004 | wild-type; Rif ^R | (Daniels <i>et al</i> , 1984a) |
| 8004Δ <i>xps</i> | Derivative of strain 8004 deleted in the entire <i>xps</i> gene cluster (nucleotide positions 4230359-4241531) | This study |
| <i>E. coli</i> | | |
| OneShot®TOP10 | F ⁻ <i>mcrA</i> Δ(<i>mrr-hsdRMS-mcrBC</i>) φ80 <i>lacZ</i> Δ <i>M15</i> Δ <i>lacX74</i> <i>recA1</i> <i>ara</i> Δ139 Δ(<i>ara-leu</i>)7697 <i>galU</i> <i>galK</i> <i>rpsL</i> <i>endA1</i> <i>nupG</i> ; Str ^R | Invitrogen |
| DH5α <i>λ</i> pir | F ⁻ <i>recA</i> <i>hsdR17</i> (r _K ⁻ , m _K ⁺) φ80 Δ <i>lacZ</i> Δ <i>M15</i> [<i>λ</i> pir] | (Platt <i>et al</i> , 2000) |
| JM109 | F ⁻ , <i>traD36</i> <i>proA</i> ⁺ <i>B</i> ⁺ <i>lacI</i> ^q Δ(<i>lacZ</i>) <i>M15</i> / Δ(<i>lac-proAB</i>) <i>glnV44</i> <i>e14</i> ⁻ <i>gyrA96</i> <i>recA1</i> <i>relA1</i> <i>endA1</i> <i>thi</i> <i>hsdR17</i> | (Yanisch-Perron <i>et al</i> , 1985) |
| DHM1 | F ⁻ , <i>cya</i> -854, <i>recA1</i> , <i>endA1</i> , <i>gyrA96</i> (<i>Nal</i> ^R), <i>thi1</i> , <i>hsdR17</i> , <i>spoT1</i> , <i>rfaD1</i> , <i>glnV44</i> | (Karimova <i>et al</i> , 2005) |
| BL21 Star™ (DE3) | F ⁻ <i>ompT</i> <i>hsdSB</i> (r _B ⁻ , m _B ⁻) <i>galdcmrne131</i> (DE3) | Invitrogen |

Table 5: General plasmids used in this study

| Plasmid | Relevant characteristics | References |
|----------------------------|--|---|
| General Plasmids | | |
| pAGM9121 | Derivative of pUC19, contains <i>lacZα</i> fragment flanked by <i>Bpil</i> sites, CTCA/CGAG overhangs; Sm ^R | Addgene #51833; (Weber <i>et al</i> , 2011) |
| pUC57Δ <i>BsaI</i> | Derivative of pUC57 with <i>BsaI</i> site mutated in the resistance cassette; Ap ^R | (Morbiter <i>et al</i> , 2011) |
| pICH41021 | Derivative of pUC19; Ap ^R | Gift from S. Marillonnet |
| pOGG2 | Golden Gate-compatible derivative of suicide vector pOK1, <i>sacB</i> <i>sacQ</i> <i>mobRK2</i> <i>oriR6K</i> ; Sm ^R | (Schulze <i>et al</i> , 2012) |
| pRK2013 | ColE1 replicon, TraRK ⁺ Mob ⁺ ; Km ^R | (Figurski & Helinski, 1979) |
| pBRM | Golden Gate-compatible derivative of pBBR1MCS-5 containing the <i>lac</i> promoter, a <i>lacZα</i> fragment flanked by <i>BsaI</i> recognition sites and a 3 × c-Myc epitope-encoding sequence, TATG/CACC overhangs; Gm ^R | (Szczesny <i>et al</i> , 2010) |
| pBRNM | Derivative of pBRM containing the <i>lac</i> promoter, an N-terminal 3 × c-Myc epitope-encoding sequence and a <i>lacZα</i> fragment flanked by <i>BsaI</i> recognition sites, TATG/CACC overhangs, Gm ^R | (Szczesny <i>et al</i> , 2010) |
| pBRM-P-stop | Derivative of pBRM lacking the <i>lac</i> promoter, contains a stop codon upstream of the 3× c-Myc epitope-encoding sequence, flanked by <i>BsaI</i> recognition sites, ATTC/CACC overhangs; Gm ^R | (Szczesny <i>et al</i> , 2010) |
| Deletion constructs | | |
| pOGG2Δ <i>xps</i> | Derivative of pOGG2 carrying flanking regions of the <i>X. euvesicatoria</i> <i>xps</i> gene cluster (upstream: nucleotide position 4224332-4225081; downstream: nucleotide position 4212580- | P. Martin, unpub. |

| Plasmid | Relevant characteristics | References |
|-----------------------------------|---|--------------------------------|
| | 4213329) for deletion of <i>xps</i> gene cluster (nucleotide position 4212581-4224331) | |
| pOGG2Δ <i>xps Xag</i> | Derivative of pOGG2 carrying flanking regions of the <i>Xag xps</i> gene cluster (upstream: nucleotide position 4395301-4396300; downstream: nucleotide position 4383268-4384267) for deletion of <i>xps</i> gene cluster (nucleotide position 4384268-4395300) | This study |
| pOGG2Δ <i>xps Xcc</i> | Derivative of pOGG2 carrying flanking regions of the <i>Xcc xps</i> gene cluster (upstream: nucleotide position 4241532-4242284; downstream: nucleotide position 4229609-4230358) for deletion of <i>xps</i> gene cluster (nucleotide position 4230359-4241531) | This study |
| Secretion assay constructs | | |
| pB-P3671 | pBRM-P derivative encoding XCV3671-3×c-Myc under the native XCV3672 promoter, Gm ^R | This study |
| pB-P3671 _{Δ31-150} | pBRM-P derivative encoding XCV3671 _{Δ31-150} -3×c-Myc under the native XCV3672 promoter, Gm ^R | This study |
| pB-P3671 _{Δ527-627} | pBRM-P derivative encoding XCV3671 _{Δ527-627} -3×c-Myc under the native XCV3672 promoter, Gm ^R | This study |
| pB-P3671 _{S448A} | pBRM-P derivative encoding XCV3671 _{S448A} -3×c-Myc under the native XCV3672 promoter, Gm ^R | This study |
| pB-P4358 | pBRM-P derivative encoding XCV4258-3×c-Myc under the native XCV4361 promoter, Gm ^R | This study |
| pB-P0722 | pBRM-P derivative encoding XCV0722-3×c-Myc under the native XCV0722 promoter, Gm ^R | This study |
| pB-P2571 | pBRM-P derivative encoding XCV2571-3×c-Myc under the native XCV2571 promoter, Gm ^R | This study |
| pB-P0670 | pBRM-P derivative encoding XCV0670-3×c-Myc under the native XCV0670 promoter, Gm ^R | This study |
| pB-P3634 | pBRM-P derivative encoding XCV3634-3×c-Myc under the native XCV3634 promoter, Gm ^R | This study |
| pB-P3406 | pBRM-P derivative encoding XCV3406-3×c-Myc under the native XCV3406 promoter, Gm ^R | This study |
| pB-P3407 | pBRM-P derivative encoding XCV3407-3×c-Myc under the native XCV3407 promoter, Gm ^R | This study |
| Protease test constructs | | |
| pB-XCV3671 | pBRM derivative encoding XCV3671-3×c-Myc under control of the <i>lac</i> promoter, Gm ^R | (Szczesny <i>et al</i> , 2010) |
| pB-XCV3671 _{S448A} | pBRM derivative encoding XCV3671 _{S448A} -3×c-Myc under control of the <i>lac</i> promoter, Gm ^R | This study |
| pB-XCV3013 | pBRM derivative encoding XCV3013-3×c-Myc under control of the <i>lac</i> promoter, Gm ^R | (Szczesny <i>et al</i> , 2010) |
| pB-XCV3406 | pBRM derivative encoding XCV3406-3×c-Myc under control of the <i>lac</i> promoter, Gm ^R | This study |
| pB-XCV3407 | pBRM derivative encoding XCV3407-3×c-Myc under control of the <i>lac</i> promoter, Gm ^R | This study |
| pB-XCV0845 | pBRM derivative encoding XCV0845-3×c-Myc under control of the <i>lac</i> promoter, Gm ^R | (Solé <i>et al</i> , 2015) |
| pB-XCV0722 | pBRM derivative encoding XCV0722-3×c-Myc under control of the <i>lac</i> promoter, Gm ^R | This study |
| BACTH-assay constructs | | |
| pKT25 _{GG} | Golden Gate-compatible derivative of pKT25 encoding the T25 fragment of CyaA downstream of a <i>lac</i> promoter and in frame with a C-terminal FLAG epitope-encoding sequence; contains <i>lacP-eforRed</i> flanked by <i>BsaI</i> sites downstream of the T25-FLAG fragment, TATG/CACC overhangs; Km ^R | (Otten & Büttner, 2021) |
| pKNT25 _{GG} | Golden Gate-compatible derivative of pKNT25, encodes the T25 fragment of CyaA in frame with an N-terminal FLAG epitope-encoding sequence downstream of the <i>lac</i> promoter, contains <i>lacP-eforRed</i> flanked by <i>BsaI</i> sites upstream of the T25-FLAG fragment, TATG/CACC overhangs; Km ^R | (Otten & Büttner, 2021) |
| pUT18 _{GG} | Golden Gate-compatible derivative of pUT18 containing <i>lacP-eforRed</i> flanked by <i>BsaI</i> sites upstream of the FLAG-T18 fragment, TATG/CACC overhangs; Gm ^R | (Otten & Büttner, 2021) |
| pUT18C _{GG} | Golden Gate-compatible derivative of pUT18C containing <i>lacP-eforRed</i> flanked by <i>BsaI</i> sites downstream of the T18-FLAG | (Otten & Büttner, 2021) |

| Plasmid | Relevant characteristics | References |
|----------------------------|--|--------------------------------|
| | fragment, TATG/CACC overhangs; Gm ^R | |
| pUT18C _{GG} -xpsC | Derivative of pUT18C _{GG} encoding T18-FLAG-XpsC | This study |
| pKT25 _{GG} -xpsC | Derivative of pKT25 _{GG} encoding T18-FLAG-XpsC | This study |
| pUT18C _{GG} -xpsM | Derivative of pUT18C _{GG} encoding T18-FLAG-XpsM | This study |
| pKT25 _{GG} -xpsM | Derivative of pKT25 _{GG} encoding T18-FLAG-xpsM | This study |
| pUT18C _{GG} -xpsL | Derivative of pUT18C _{GG} encoding T18-FLAG-XpsL | This study |
| pKT25 _{GG} -xpsL | Derivative of pKT25 _{GG} encoding T18-FLAG-XpsL | This study |
| pUT18C-xpsF | Derivative of pUT18C _{GG} encoding T18-FLAG-XpsF | This study |
| pKT25 _{GG} -xpsF | Derivative of pKT25 _{GG} encoding T18-FLAG-XpsF | This study |
| pUT18 _{GG} -xpsE | Derivative of pUT18 _{GG} encoding T18-FLAG-XpsE | This study |
| pUT18C _{GG} -xpsE | Derivative of pUT18C _{GG} encoding T18-FLAG-XpsE | This study |
| pKT25 _{GG} -xpsE | Derivative of pKT25 _{GG} encoding T18-FLAG-XpsE | This study |
| pKNT25 _{GG} -xpsE | Derivative of pKNT25 _{GG} encoding T18-FLAG-XpsE | This study |
| pUC57-ptac-GST | Derivative of pUC57 encoding GST downstream of the <i>tac</i> promoter flanked by <i>Bsa</i> I sites with ATTC/CATA overhangs; Ap ^R | (Drehkopf <i>et al</i> , 2020) |
| pB-P-stop-ptacGST-xpsE | Derivative of pBRM-P-stop encoding GST-XpsE under control of a <i>ptac</i> promoter; Gm ^R | This study |
| pBRNM-xpsL | Derivative of pBRNM encoding 3×c-Myc-XpsL under control of the <i>lac</i> promoter; Gm ^R | This study |

3.2 Methods

3.2.1 Cloning and strain construction

3.2.1.1 Bacterial strains and growth conditions

Escherichia coli strains were cultivated at 37°C in lysogeny broth (LB) or terrific broth (TB) medium and *Xanthomonas* strains at 30°C in nutrient-yeast extract-glycerol (NYG) or XVM2 medium. Plasmids were introduced into chemically competent *E. coli* strains (CaCl) by heat shock and into *Xanthomonas* strains by electroporation. Antibiotics and additives were added to the media at the following final concentrations: ampicillin, 100 µg ml⁻¹; gentamycin 15 µg ml⁻¹; kanamycin, 25 µg ml⁻¹; rifampicin, 100 µg ml⁻¹ and spectinomycin, 100 µg ml⁻¹; X-gal (5-Brom-4-chlor-3-indolyl-β-D-galactoside): 0.004 % (w/v).

3.2.1.2 Polymerase chain reactions (PCRs)

DNA fragments were amplified by Polymerase chain reaction (PCR) with either a Hybrid polymerase (EUR_x®, for cloning) or a *Taq*-polymerase (self-made, for colony PCRs to verify chromosomal deletions) in a thermocycler (Biometra TAdvanced Twin 48 G, Analytik Jena GmbH), with buffers and conditions as shown in table 6 and table 7.

table 6: PCR reaction compositions

| Taq PCR | | Hybrid PCR | |
|----------------------------|---------------------|-----------------------|----------|
| 10 × Taq polymerase buffer | 2 µl | 10 × Hybrid buffer | 5 µl |
| 10 mM dNTPs | 0.25 µl | 10 mM dNTPs | 1 µl |
| 10 mM primer 1 (10mM) | 1 µl | 10 µM primer 1 (10mM) | 2.5 µl |
| 10 mM primer 2 (10mM) | 1 µl | 10 µM primer 2 (10mM) | 2.5 µl |
| DMSO | 1.4 µl | DMSO | 2 µl |
| Taq polymerase | 0.3 µl (ca. 1.25 U) | Hybrid polymerase | 0.5 µl |
| Template DNA | variable | Template DNA | Variable |
| dH2O | Ad 20 µl | dH2O | Ad 50 µl |

table 7: PCR thermocycler programs

| Taq PCR | | | | Hybrid PCR | | | |
|----------------|------------|--------------|-----------|-------------------|------------|--------------|-----------|
| Step | Temp. (°C) | Time | Repeated? | Step | Temp. (°C) | Time | Repeated? |
| denaturation | 95 | 2 min | - | denaturation | 98 | 30 s | - |
| Denaturation | 95 | 30 s | 35 cycles | Denaturation | 98 | 10 s | 35 cycles |
| Annealing | 52-72 | 30 s | | Annealing | 52-65 | 10 s | |
| elongation | 72 | 1 min/kb | | elongation | 72 | 30 s/kb | |
| elongation | 72 | 5 min | - | elongation | 72 | 5 min | - |
| storage | 16 | indefinitely | - | storage | 16 | indefinitely | - |

3.2.1.3 One pot cut-ligation

For plasmid construction, one-pot cut-ligation reactions were performed in a thermocycler (Biometra TADVANCED Twin 48 G, Analytik Jena GmbH) with buffers and conditions as shown in Table 8 and Table 9.

Table 8: One-pot cut-ligation reaction mix

| | |
|--|--------------------------|
| Restriction enzyme | 5 U |
| T4 DNA ligase | 5 U |
| 10 × T4 DNA Ligase buffer | 2 µl |
| PCR amplicons or plasmids encoding inserts | Variable (ca. 75ng each) |
| Vector | Variable (ca. 50ng) |
| dH2O | Ad 10 µl |

Table 9: One-pot cut-ligation thermocycler program

| Step | Temperature | time | Repeated? |
|-------------------|------------------------------|------------|-----------|
| Restriction | 37°C (30°C for <i>Sma</i> I) | 2 min | 99 cycles |
| Ligation | 16°C | 5 min | |
| Final restriction | 37°C (30°C for <i>Sma</i> I) | 5 min | - |
| Inactivation | 65°C | 20 min | - |
| cooling | 16°C | Indefinite | |

3.2.1.4 Plasmid isolation

Plasmids were isolated from 2-4 ml overnight *E. coli* cultures in TB medium with appropriate antibiotics using a NucleoSpin® Plasmid kit (MACHEREY-NAGEL GmbH) following manufacturer's instructions.

3.2.1.5 Generation of *Xanthomonas* deletion strains

To generate strains *Xag* 8ra Δxps and *Xcc* 8004 Δxps in which the complete T2S gene cluster is deleted, DNA fragments flanking the *xps* gene cluster were amplified from *Xag* and *Xcc* by PCR using the primer pairs *Xag* Δxps -5'-fw+rv and *Xag* Δxps -3'-fw+rv or *Xcc* Δxps -5'-fw+rv and *Xcc* Δxps -3'-fw+rv, respectively (Table 13). PCR amplicons were cloned into the Golden-Gate-compatible suicide vector pOGG2 using *Bsa*I and ligase. The resulting deletion construct pOGG2- Δxps *Xag* containing a 11,032-bp deletion in the *xps*-T2S gene cluster and pOGG2- Δxps *Xcc* containing a 11,172-bp deletion in the *xps*-T2S gene cluster were introduced into *Xag* 8ra and *Xcc* 8004, respectively by triparental conjugation using the helper plasmid pRK2013. Transconjugants were selected as described previously (Huguet *et al*, 1998) and double crossovers resulted in strains 8ra Δxps and 8004 Δxps .

3.2.1.6 Generation of constructs for BACTH assays and pull-downs

To generate expression constructs for BACTH assays, *xps* genes were amplified by PCR from *X. euvesicatoria* using gene-specific primers listed in Table 13. PCR amplicons were cloned into vector pAGM9121 using *Bp*I and T4 ligase or into entry vectors pICH41021 or pUC57 by blunt-end cloning using *Sma*I and *Eco*RV, respectively. Genes were subsequently transferred to the Golden Gate-compatible BACTH vectors pKT25_{GG}, pKNT25_{GG}, pUT18_{GG} or pUT18C_{GG} using *Bsa*I and ligase as described previously (Otten & Büttner, 2021). For GST pull-down assays, *xpsE* and *xpsL* were amplified by PCR and subsequently either cloned into vector pBRNM (*xpsL*) downstream of an N-terminal c-Myc epitope-encoding sequence using *Bsa*I and ligase or assembled by Golden Gate cloning with an expression cassette encoding GST under control of the *ptac* promoter in the final destination vector pBRM-Pstop (*xpsE*). All constructs are listed in Table 5.

3.2.1.7 Generation of constructs for protease- and secretion assays

To generate constructs for protease- and secretion assays, genes (e.g. XCV4358 or XCV2571) and promoters (e.g. *p4361* or *p2571*) were amplified by PCR from *X. euvesicatoria* using gene-specific primers (e.g. 4358 fw+rv or 2571 1 fw+rv and 2571 2 fw+rv or p4358 fw+rv) listed in Table 13. Internal *Bsa*I recognition sites were removed using primers containing silent mutations in these. PCR amplicons were cloned into either vector pAGM9121 using *Bp*I and T4 ligase or into entry vectors pICH41021 or pUC57 by blunt-end cloning using *Sma*I and *Eco*RV, respectively and sequenced. Genes were subsequently

transferred to the Golden Gate-compatible expression vectors pBRM (for protease assays) or pBRM-P (for secretion assays) using *BsaI* and ligase.

Secretion constructs with variants of *XCV3671* were constructed using primer pairs p3672 fw+rv (for the promoter *p3672*), 3671 fw+rv (for *XCV3671_{WT}*) or 3671fw+3671 Δ 527-627 rv (for *XCV3671 Δ 527-627*) and cloned into either pAGM9121 with *BpiI* and ligase or pUC57 using *EcoRV*, or by mutagenesis PCR with the primer pair 3671 Δ 31-150 fw+rv on pUC-*XCV3671* for *XCV3671 Δ 31-150*. A construct of the catalytic mutant 3671_{S448A} (pUC-3671_{S448A}) was generated by Jessica Erickson (IPB, Halle). Promoter and ORF modules were subsequently cloned into the vector pBRM-P using *BsaI* and ligase (Table 5).

3.2.1.8 **Generation of a modular *xps* gene cluster by Golden Gate-based modular cloning**

For modular cloning of the *xps* gene cluster, the native promoters and coding sequences of *xpsE* and *xpsF* were amplified by PCR using primer pairs listed in Table 13. The resulting PCR amplicons were cloned into the level -1 vector pAGM1311 using *BsaI* and T4 ligase, thus resulting in constructs pT2S001 (contains *xpsE* and promoter) and pT2S005 (contains *xpsF* and promoter). Similarly, the native promoter of the *xpsG-xpsD* operon as well as *xpsG*, *xpsH*, *xpsI*, *xpsJ*, *xpsK*, *xpsL*, *xpsM*, *xpsC* and *xpsD* were amplified by PCR and cloned into the level -2 vector pAGM9121 using *BpiI* and T4 ligase, resulting in constructs pT2S011 to pT2S026. Primers and fragment sizes are listed in Table 13, nucleotide positions of 5' ends of the primers are indicated. Constructs pT2S011 – pT2S014, pT2S016 - pT2S020 and pT2S022 – pT2S026 were assembled by Golden Gate cloning in vector pAGM1311 (level -1) using *BsaI* and T4 ligase, thus generating constructs pT2S015 (contains *xpsG*, *xpsH* and *xpsI* including the native promoter), pT2S021 (contains *xpsJ*, *xpsK* and *xpsL*) and pT2S028 (contains *xpsM*, *xpsC* and *xpsD*). For the generation of level 0 constructs, gene modules from constructs pT2S001 (*xpsE* and promoter), pT2S005 (*xpsF* and promoter) as well as pT2S015, pT2S021 and pT2S028 were inserted into vector pICH41331 using *BpiI* and ligase, thus leading to level 0 constructs pT2S002 (*xpsE* and promoter), pT2S006 (*xpsF* and promoter) and pT2S030 (*xpsG* - *xpsD* operon and promoter). To generate level 1 constructs, inserts of level 0 constructs were ligated into different level 1 vectors which determine the positions of the individual modules in the final level M construct as shown in Fig. 1. This resulted in constructs pT2S32 (contains *xpsE* and promoter cloned in vector pICH47742 for insertion at position 2), pT2S34 (contains *xpsF* and promoter cloned in vector pICH47751 for insertion at position 3) and pT2S36 (contains *xpsG-xpsD* operon and promoter cloned in vector pICH47761 for insertion at position 4). Additional level 1 constructs pICH54011, pICH54055 and pICH50914 contained dummy modules for insertion at positions 1 and 5 and an end-linker, respectively, as shown in Fig. 1. The final level M construct pT2S038 was

constructed by assembly of level 1 modules in vector pAGM8031 using *BpiI* and T4 ligase. The end-linker connects the 3' end of the last module to the destination vector.

Constructs used for modular cloning are listed in Table 11 and Table 12. All constructs were verified by test restriction with appropriate enzymes and all plasmids containing PCR amplicons were sequenced by Sanger sequencing. As a template for PCRs, genomic DNA of *X. euvesicatoria* 85-10 was used.

3.2.1.9 Generation of modified *xps* gene clusters for functional analysis, microscopy and crosslinking

To construct modified *xps* gene cluster carrying individual gene deletions or epitope tagged *xps* genes, corresponding modules were generated and assembled hierarchically similar to pT2S038 with substituted modules as described in Table 12. Unless otherwise specified, pT2S038 was used as a template for PCRs to generate variant *xps* modules.

3.2.2 Plant infection studies

Capsicum annuum cultivar Early Cal Wonder (ECW) plants were grown at 25°C for 16 h of light and for 8 h in the darkness at 60 - 70% relative humidity. For syringe infections, *X. euvesicatoria* strains were infiltrated with a needleless syringe into the lower side of pepper leaves at concentrations of 2×10^7 CFU ml⁻¹ in 1mM MgCl₂. Symptoms were photographed 8 days post inoculation (dpi). For dip infections, leaves were incubated in 1 mM MgCl₂ solutions containing *X. euvesicatoria* at concentrations of 2×10^7 CFU ml⁻¹ and 0.02% Silwet for at least 30 seconds. The formation of bacterial spot symptoms was monitored 4 - 7 weeks after dipping. To quantify bacterial density in planta together with cell wall composition in syringe pepper plants infected with bacteria at 2×10^7 CFU ml⁻¹ in 1mM MgCl₂, infected plant material was harvested with cork borer size 3 at 5 dpi and ground in an Eppendorf cup with 1mM MgCl₂ and a large steel ball by shaking in a Retsch mill (30 bps, 40s). Subsequently samples were diluted and plated on NYG plates containing rifampicin and cyclohexamide. Bacterial growth was quantified after 2-3 days on plates containing 1:10⁶ dilutions.

Glycine max cultivar 'ROYKA' plants were grown at 25°C for 16 h of light and for 8 h in the darkness at 60 - 70% relative humidity. For syringe infections, *X. axopodopodis* pv. *glycines* strains were infiltrated with a needleless syringe into the lower side of trifoliate leaves at concentrations of 2×10^7 CFU ml⁻¹ in 1mM MgCl₂ in three-week-old plants. Symptoms were photographed 6 days post inoculation (dpi).

All experiments were performed at least three times with similar results. Representative results from one experiment are shown.

3.2.3 Isolation of cell wall extracts

Plant leaves were harvested at the end of the dark phase and shock frozen in liquid nitrogen in a safe-lock 2 ml Eppendorf tube with two small metal balls. Infected pepper plants were harvested at 5 dpi with a cork borer size 5 (at least 12 cut-outs); for growth experiments whole leaves were used, either of 4-week-old soya plants or *Arabidopsis* and tomato leaf material kindly provided by Jessica Erickson (IPB, Halle). Frozen material was pulverized in a Retsch mill (21 bps, 1 min), incubated in 1 ml 80% ethanol at 80°C for 10 min (shaking at 900rpm) and subsequently centrifuged at 17000g for 10 min at room temperature to allow for aspiration of the supernatant. Removal of alcohol soluble saccharides was repeated for a total of 3 times. Finally, the pellet was washed in 1 ml Acetone. Infected plant samples were vacuum dried for 3 minutes (Speed Vac® Plus SC110A), while non-infected samples for growth experiments were dried under a clean bench for sterility. Dried alcohol insoluble residue (AIR) containing cell wall polysaccharides was subjected to acid hydrolysis with sulfuric acid subsequently quantified in monosaccharide composition by high-pressure anion exchange chromatography with pulsed amperometric detection (HPAEC-PAD) in collaboration with Kristina Munzert and Timo Engelsdorf in the facility of Lars Voll (Philipps-University Marburg), as described (Zhang *et al*, 2024b).

3.2.4 Growth curves in modified XVM2 minimal medium

Growth experiments were performed in modified XVM2 minimal medium in which either Casamino acids were substituted with 3 g/l skim milk powder (XVM milk) or fructose and sucrose were substituted with AIR containing cell wall polysaccharides from *A. thaliana*, *G. max* or *S. lycopersicum* plants at 0.5 mg/ml, with pectin from citrus peel (Sigma-Aldrich, Steinheim) or carboxymethylcellulose (Sigma-Aldrich, Steinheim) at 4mg/ml or with xylan from corn cob (Carl-Roth, Karlsruhe) or glucose (Carl Roth, Karlsruhe) at 0.4 mg/ml. For this, the bacterial density of overnight cultures in NYG medium were measured, and appropriate volumes for an optical density of 0.4 were pelleted and washed once in XVM2 medium lacking casamino acids (for XVM milk assays) or lacking fructose and saccharose (for XVM carbohydrate assays) and resuspended in the appropriate medium. The bacterial density was again measured and appropriate volumes for a bacterial density of 2×10^7 CFU ml⁻¹ were added to 1 ml final medium in a 24-well plate (Greiner Cell Culture Plate, CELLSTAR®). Cultures were grown shaking at 200rpm at 30°C for 24 hours, either while bacterial density was quantified every 30 minutes in a plate reader (CLARIOstar, BMG Labtech) for XVM milk, in a growth chamber for various carbohydrates. At 24h, cultures growing on various carbohydrate sources were transferred to cuvettes and bacterial densities were quantified with a spectrophotometer after 5 minutes to allow for non-soluble AIR particles to settle. No difference on the optical density of cultures without AIR particles was observed when

vortexing cultures or waiting 5 minutes, indicating that *Xanthomonas* cells stay suspended in medium within this time frame.

3.2.5 Extracellular protease activity assays

For the analysis of extracellular protease activity, bacteria were grown over night in either NYG medium (*Xanthomonas*) or LB medium (*E. coli* BL21) with respective antibiotics. Forty microlitres of the over-night cultures adjusted to a density of 10^9 CFU ml⁻¹ were pipetted into holes, which were punched out from NYG or LB agar plates containing 2% skimmed milk as described previously (Szczesny *et al*, 2010). Plates were incubated at 30°C for 2 days and bacteria were removed prior to documentation of halo formation. Experiments were performed three times with similar results. One representative result is shown.

3.2.6 Identification of apoplastic T2S substrates

To identify *Xanthomonas* T2S substrates in infected *S. lycopersicum* moneymaker leaves, roughly 6-week-old plants were dip-infected with *Xe* wild-type and *xps* deletion mutants. Apoplastic wash fluid was extracted from leaves 3 days after infection by the infiltration-centrifugation method (O'Leary *et al*, 2014). Leaves were separated from plants with a sterile razor blade, washed in distilled water twice and infiltrated in a 60 ml syringe submerged in 40 ml water by manually applying a vacuum repeatedly until the entire leaf was infiltrated. Subsequently, leaves were removed, dried on the surface with a paper towel, rolled in parafilm, placed in a 50 ml Falcon with the leaf tip facing to the bottom and centrifuged at 1000 x g for 10 min at 4°C. Apoplastic wash fluid was subsequently transferred from the bottom of the falcon tube to a new Eppendorf cup and centrifuged at 15000 x g for 5 minutes to remove cell debris. Supernatants containing soluble proteins from tomato apoplast were transferred to a new Eppendorf cup and given to Jessica Erickson (IPB, Halle) for precipitation in acetone and subsequent mass spectrometry.

3.2.7 Secretion assays

For *in vitro* secretion assays with potential T2S substrates, 15 ml XVM2 medium was inoculated from an NYG overnight liquid culture with a bacterial density of 1.5×10^8 CFU ml⁻¹ and incubated at 30°C for 3-4 hours shaking at ca. 200 rpm. After measuring the cultures optical density, 1 ml culture was kept on ice as a total extract sample while supernatant samples were taken by filtering the remaining culture through a 0.45µm pore size Supor® Acrodisc® filter (Pall Corporation) and precipitation in 10% trichloroacetic acid (TCA) on ice for 30 minutes. Samples were subsequently centrifuged at 21000 x g for 10 minutes at 4°C. TCA precipitated proteins were washed in 500µl ice cold Ethanol, again centrifuged at 21000 x g for 10 minutes at 4°C and vacuum dried (Speed Vac® Plus SC110A). Protein samples

were resuspended in $2 \times$ Laemmli buffer (20 μ l for supernatant and 50 μ l for total extract), boiled for 10 min and separated by SDS-PAGE and immunoblotting. Loaded sample volumes were adjusted using the optical density of cultures to ensure equal protein loading.

3.2.8 Immunoblot analysis of bacterial protein extracts

For immunoblot analysis of protein extracts, bacterial cell pellets were resuspended in Laemmli buffer, denatured by boiling and analyzed by SDS-PAGE and immunoblotting, using antibodies specific to the c-Myc epitope (polyclonal antibody from rabbit, Sigma-Aldrich), the FLAG epitope (monoclonal antibody from mouse, Sigma-Aldrich), mCherry (polyclonal antibody from rabbit, Abcam Limited), GroEL (polyclonal antibody from rabbit, Enzo Life Sciences), RNA polymerase β (monoclonal antibody from mouse, Invitrogen), and GST (glutathione S-transferase; polyclonal antibody from goat, Cytiva). Horseradish peroxidase-labelled anti-mouse, anti-rabbit and anti-goat antibodies were used as secondary antibodies. Binding of antibodies was visualized by enhanced chemiluminescence using a Vilber FUSION-FX6 chemiluminescence imager. Results were reproduced at least twice. One representative blot is shown. Typically, SDS-polyacrylamid gels with a 10% running gel and a 4% stacking gel were used (Table 10) with 1x TANK buffer with a constant voltage of 135 V. For Western Blotting onto nitrocellulose Amersham™ Protran® membranes (Cytiva) was performed in transfer buffer at 95V, 400mA and 4°C for 1.5 h. Membranes were subsequently treated with blocking solution for at least 30 minutes, washed in TBST buffer and treated with primary antibodies overnight at 4°C and secondary antibodies for at least 1h.

Table 10: composition of polyacrylamide gels

| Component | Running gel (30 ml) | Stacking gel (15 ml) |
|----------------------|--------------------------------|---------------------------------|
| H ₂ O | 11.9 ml | 9 ml |
| Tris-HCl | 7.5 ml (1.5 M Tris-HCl pH 8,8) | 3.75 ml (0.5 M Tris-HCl pH 6,8) |
| 30 % (v/v) Acrylamid | 10 ml | 2 ml |
| 10 % (w/v) SDS | 0.3 ml | 0.15 ml |
| 10 % (w/v) APS | 0.3 ml | 0.15 ml |
| Temed | 0.012 ml | 0.009 ml |

3.2.9 Protein-Protein interaction studies

3.2.9.1 *Bacterial adenylate cyclase two-hybrid (BACTH) assays*

For protein-protein interaction studies, a modified version of the Euromedex BACTH system was used which allowed Golden Gate cloning of genes of interest in fusion with T18- and T25-encoding fragments (Otten & Büttner, 2021). For the analysis of protein synthesis, BACTH constructs were introduced into *E. coli* strain JM109 and gene expression was induced by IPTG (isopropyl- β -D-thiogalactopyranoside) for 2h at 37°C after the optical densities of the bacterial cultures at 600 nm (OD₆₀₀) had reached values between 0.6 and

0.8. Cells were resuspended in Laemmli buffer and analyzed by immunoblotting using a FLAG epitope-specific antibody. For interaction studies, the expression constructs encoding T18 and T25 fusion proteins were introduced into the *E. coli* reporter strain DHM1 and transformants were cultivated on LB agar plates containing kanamycin and gentamycin (Karimova *et al*, 2005). At least three transformants for each interaction were grown over night in liquid LB medium with appropriate antibiotics and 2 µl of each over-night culture was spotted on LB agar plates containing kanamycin, gentamycin, X-Gal (5-bromo-4-chloro-3-indolyl-β-d-galactopyranosid; 40 µg/mL) and 2 mM IPTG. Plates were incubated for up to seven days at room temperature and the colour of bacterial colonies was documented by photographs. Experiments were performed at least three times with bacteria from independent transformations. One representative colony is shown.

3.2.9.2 GST pull-down assays

For GST pull-down assays, *E. coli* TOP10 cells with expression constructs encoding GST, GST-XpsE and c-Myc-XpsL were grown in LB medium at 37°C. When the cultures reached an OD₆₀₀ of 0.6 - 0.8, gene expression was induced by addition of IPTG (isopropyl-β-D-thiogalactopyranoside) at a final concentration of 2 mM for two hours. Cells were harvested by centrifugation, resuspended in 1 × PBS buffer and lysed with a French press. Insoluble cell debris were removed by centrifugation and soluble GST and GST-XpsE fusion proteins were immobilized on a glutathione sepharose matrix according to the manufacturer's instructions (GE Healthcare). The glutathione sepharose with immobilized GST and GST fusion proteins was washed with 1 × PBS buffer and incubated with bacterial lysates containing c-Myc-XpsL for 1 h at 4°C on an overhead shaker. Unbound proteins were removed by washing in 1 × PBS. Bound proteins were eluted with Laemmli buffer and analyzed by SDS-PAGE and immunoblotting, using GST- and c-Myc epitope-specific antibodies. Experiments were repeated at least two times with similar results.

3.2.9.3 In vivo formaldehyde crosslinking

In vivo protein complex formation was analyzed after crosslinking with para-formaldehyde as described previously (Skare *et al*, 1993). Briefly, *X. euvesicatoria* strains were grown over night in NYG medium, resuspended at an OD₆₀₀ of 0.3 in fresh NYG medium and incubated on a tube rotator at 30°C. After 3 - 4 hours, cells from 1 ml cultures were collected by centrifugation, resuspended in 2 × Laemmli buffer and boiled for 10 minutes. These samples represented the "total cell extract". In parallel, cells of 1 ml of cultures were resuspended in 1 ml of 10 mM potassium phosphate buffer (pH 6.8) containing 1% formaldehyde. After incubation for 20 minutes at room temperature, cells were collected by centrifugation, washed in 1 ml of 10 mM potassium phosphate buffer (pH 6.8) without formaldehyde and resuspended in Laemmli buffer. Protein samples were incubated at 37°C for 10-20 minutes

to maintain formaldehyde cross-links. Total cell extracts and crosslinked samples were subsequently analyzed by SDS-PAGE and immunoblotting, using antibodies specific to the c-Myc epitope and the RNA polymerase β or GroEL, which was analyzed as loading control. Experiments were performed three times with similar results. One representative blot for each experiment is shown.

3.2.9.4 In vivo Cysteine crosslinking

In vivo protein complex formation using cysteine crosslinking was performed based on a described protocol (Guilvout *et al*, 2024). Briefly, *X. euvesicatoria* strains encoding proteins with appropriate cysteine substitutions were grown over night in NYG medium, resuspended at an OD₆₀₀ of 0.3 in fresh NYG medium and incubated on a tube rotator at 30°C. After 3 - 4 hours, cells from 1 ml cultures were collected by centrifugation, resuspended in 50 μ l normal 2 \times Laemmli buffer and boiled for 10 minutes. These samples represented the “total cell extract”. In parallel, cells of 1 ml of cultures were resuspended in 1 ml of 10 mM potassium phosphate buffer (pH 6.8) containing 0.3mM CuCl₂ for oxidation of neighbouring cysteine pairs. After incubation for 30 minutes at room temperature, 45 μ l 0.5M EDTA was added to terminate oxidation, and cells were collected by centrifugation resuspended 50 μ l normal 2 \times Laemmli buffer without β -Mercaptoethanol and boiled for 10-15 minutes. Total cell extracts and crosslinked samples were subsequently analyzed by SDS-PAGE and immunoblotting, using antibodies specific to the c-Myc epitope and GroEL, which was analyzed as loading control. Experiments were performed three times with similar results. One representative blot for each experiment is shown.

3.2.10 Fluorescence microscopy

To analyze the localization of an XpsD-mCherry fusion protein, bacteria were grown over night in NYG medium, resuspended in fresh NYG medium at an OD₆₀₀ of 0.15 and incubated on a tube rotator at 30°C for 2 hours. Bacterial cultures were placed on microscopy slides on top of a pad of 1% agarose dissolved in NYG medium as described previously (Hausner *et al*, 2019). mCherry fluorescence was visualized with a confocal laser scanning microscope (Zeiss LSM 780 AxioObserver. Z1) using filter sets for mCherry (excitation at 587 nm; emission at 610 nm). Experiments were performed with three different transconjugants per construct and repeated two times with comparable results. Fluorescent foci of at least 100 cells per transconjugant were counted. Results from one representative experiment are shown.

3.2.11 Statistical analyses

Plotting of data and statistical tests (Student's t-tests and one-way ANOVAs with post-hoc Tukey HSD tests) was performed in Microsoft Excel. Principal component analyses were

performed with an online tool from Statistics Kingdom (<https://www.statskingdom.com/pca-calculator.html>)

3.2.12 *In-silico* structural protein modelling

The AlphaFold2 algorithm was used for protein structure prediction using the Colabfold server (Mirdita *et al*, 2022; Goddard *et al*, 2018; Jumper *et al*, 2021). Single structure predictions were performed for XpsE and XpsD, and full-length predictions for complexes of XpsL-XpsE, XpsC-XpsL-XpsM and XpsC₃₆₋₁₆₉-XpsD₂₂₋₂₅₂, XpsF(3x)-XpsI-XpsJ-XpsK, as well as the interactions of the T2S substrates XCV0965, XCV4358, XCV3634, XCV0536 and XCV3671 with the 2P region of XpsC (XpsC₁₉₅₋₂₆₅). The AlphaFold2 structure prediction of XCV3671 was downloaded from the Uniprot database. Additionally, the AlphaFold3 algorithm was employed to generate structural models of an XpsG₈HIJK complex, an XpsE₆-XpsF₃ complex as well as HIJK-complexes with the substrates: XCV3634, XCV3406, XCV2571 and XCV0965. All structural predictions were visualized using the UCSF ChimeraX program (Goddard *et al*, 2018).

For the generation of an *in-silico* model of T2S system core components, the XpsD structure was superimposed on a pentadecameric crystal structure of the homologous *Pseudomonas aeruginosa* PAO1 XcpQ secretin channel (PDB: 5WLN) to generate a secretin channel. Furthermore, the XpsE structure was superimposed on the hexameric crystal structure of the homologous ATPase GspE from *Vibrio cholerae* (PDB: 4KSR). The XpsE-XpsL structure prediction was used to align six predicted XpsCLM complexes to the hexameric XpsE structure and the XpsC₃₆₋₁₆₉-XpsD₂₂₋₂₅₂ prediction was used to align the HR domains of the resulting hexameric XpsCLME complex to the N0 domains of the pentadecameric XpsD complex.

Conservation of individual residues of proteins were determined using the ConSurf-Webserver (Yariv *et al*, 2023; Ashkenazy *et al*, 2016) and visualized with UCSF ChimeraX.

4 Results

Sections of this chapter dealing with XpsD and XpsCLM (4.1.1-4.1.8) were originally written as part of an accepted PLOS pathogens manuscript entitled “Modularization of the type II secretion gene cluster from *Xanthomonas euvesicatoria* facilitates the identification of a structurally conserved XpsCLM assembly platform complex” by Samuel Goll, Patrick Martin, Sylvestre Marillonnet and Daniela Büttner.

4.1 Characterization of the Xps-T2S in *X. euvesicatoria*

4.1.1 Generation of a modular *xps* gene cluster by Golden Gate cloning

To expedite the functional characterization and gain insights into the mechanism of the Xps-T2S system from *X. euvesicatoria*, a plasmid-borne, modularized *xps*-T2S gene cluster was generated by hierarchical Golden Gate-based assembly of gene and promoter fragments (Weber *et al*, 2011) (Figure 6). For this, individual promoters and genes were subcloned and subsequently assembled by Golden Gate-based modular cloning, using the type IIs restriction enzymes *BsaI* and *BpiI*. Both enzymes cut DNA outside of their recognition sites. The resulting 4-bp overhangs enable the ordered assembly of DNA fragments by one-pot restriction/ligation reactions (Engler *et al*, 2008; Weber *et al*, 2011). This design allows the stepwise cloning of operons and multi-gene constructs in which the internal *BsaI* and *BpiI* sites have been removed by PCR-based mutagenesis prior to assembly (Engler *et al*, 2008). Two dummy modules, included upstream and downstream of the *xps*-T2S gene cluster, can be replaced by genes or reporter fusions in the final construct. A series of level 1 vectors with different *BpiI* fusion sites allows the ordered assembly of modules in the final, low copy, level M vector. This technique was previously used to modularize the T3S system of *Xanthomonas euvesicatoria* in a similar fashion, simplifying genetic manipulation by exchange of single gene modules in a multi-gene construct (Hausner *et al*, 2019).

Prior functional studies of the T2S system of *X. euvesicatoria* dealing with *xpsE* and *xpsD* encoding the ATPase and the secretin, respectively, relied on genomic deletions by homologous recombination (Szczeny *et al*, 2010). This is a time-consuming approach which involves several selection steps and the PCR-based analysis of recombination events (Schulze *et al*, 2012). Furthermore, complementation of the respective mutant phenotypes requires the reintroduction of the deleted gene, usually on a plasmid which leads to higher gene copy numbers and thus possibly interferes with protein function. The modularized *xps*-T2S gene cluster assembled by hierarchical Golden Gate-based cloning thus simplifies mutagenesis of *xps* genes and complementation studies.

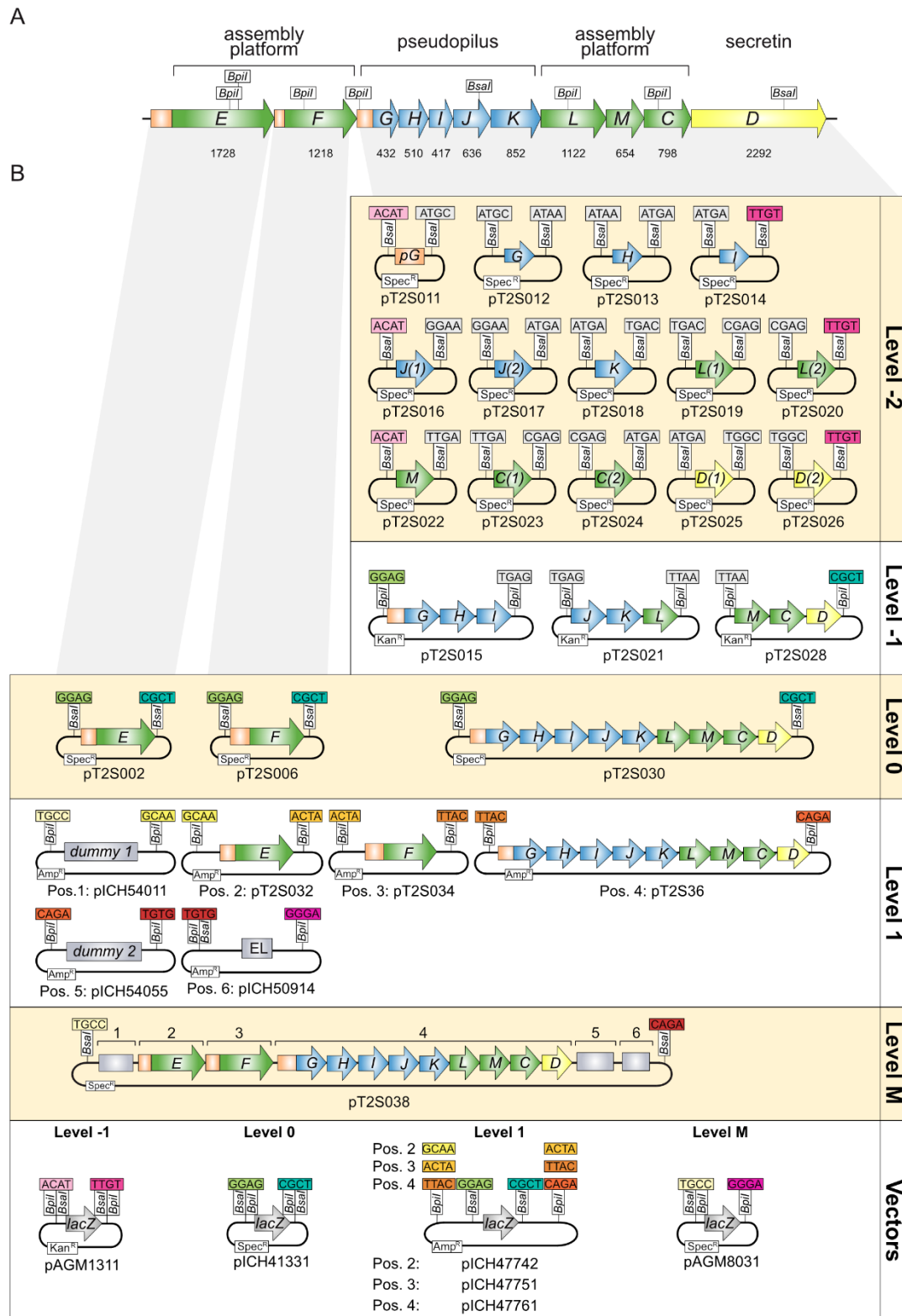


Figure 6: Modular Cloning of the *xps*-T2S gene cluster from *X. euvesicatoria*

A: Schematic representation of the *xps*-T2S gene cluster, genes are represented by arrows, promoters by orange boxes. Letters refer to the nomenclature of *xps* genes. The length of single genes is denoted in base pairs below the arrows and the position of internal *Bsal* and *Bpil* restriction sites is indicated. B: For the modular assembly, gene and promoter fragments were amplified by PCR and cloned into level -2 vectors (*xpsG* to *xpsD*) or level 0 vectors (*xpsE* and *xpsF*) as indicated. Restriction/ligation using the type II restriction enzymes *Bsal* and *Bpil* in alternating order led to the assembly of transcription units in level 0 and level 1 vectors and of the entire *xps*-T2S gene cluster in the level M vector. The final level M construct contains an end-linker (EL) and two dummy modules (grey boxes) which can be replaced by additional genes or reporter fusions.

4.1.2 The modularized *xps* gene cluster expedites functional studies

To test the functionality of the modularized T2S gene cluster, it was introduced into strain 85-10 Δ *xps*, in which the entire chromosomal *xps* gene cluster was deleted. Two T2S system-dependent phenotypes were examined: the ability of bacteria to secrete milk protein-degrading enzymes, and the ability of bacteria to induce disease in susceptible pepper plants. When extracellular protease activity was monitored on milk-containing agar plates, strain 85-10 leads to the formation of a cleared halo around the inoculation site due to the degradation of milk proteins, whereas halo formation was severely reduced for strain 85-10 Δ *xps* (Szczesny *et al*, 2010) (Figure 7). In the presence of the modular T2S gene cluster, extracellular protease activity was restored and even more prominent than in strain 85-10, suggesting that the plasmid-encoded modular *xps*-T2S gene cluster is functional. When bacteria were syringe-infiltrated into leaves of susceptible pepper plants, the wild-type strain 85-10 induced disease symptoms in form of water-soaked lesions while reduced symptoms were observed after infiltration of strain 85-10 Δ *xps* as reported previously for T2S mutants (Figure 7) (Szczesny *et al*, 2010). The wild-type phenotype was restored upon introduction of the modular T2S gene cluster.

Additionally, dip infection assays were performed which represent more natural conditions than the syringe infiltration experiments. Pepper leaves infected with the wild-type strain 85-10 led to the formation of bacterial spot symptoms, while spot formation was significantly reduced after infection in the T2S mutant (appendix, Figure 33). Spot formation in the strain 85-10 Δ *xps* was restored to wild-type levels by the modular T2S gene cluster (appendix, Figure 33).

Next, the gene modules encoding XpsE and XpsD were individually replaced by short linker sequences and reassembled modified T2S gene clusters were introduced into *X. euvesicatoria* 85-10 Δ *xps* (Figure 7). The absence of *xpsE* or *xpsD* led to reduced virulence and extracellular protease activity as reported previously (Figure 7) (Szczesny *et al*, 2010). For complementation studies, *xpsE* and *xpsD* were inserted under control of their native promoters at position 1 upstream of the modular *xps* gene clusters (Figure 7). The corresponding expression constructs fully restored virulence and extracellular protease activity in strain 85-10 Δ *xps*, suggesting that *xpsE* and *xpsD* were functional when inserted next to the modular *xps* gene cluster (Figure 7). Taken together, these experiments demonstrate the suitability of the modular T2S gene cluster for functional analysis of the Xps-T2S system in *X. euvesicatoria*.

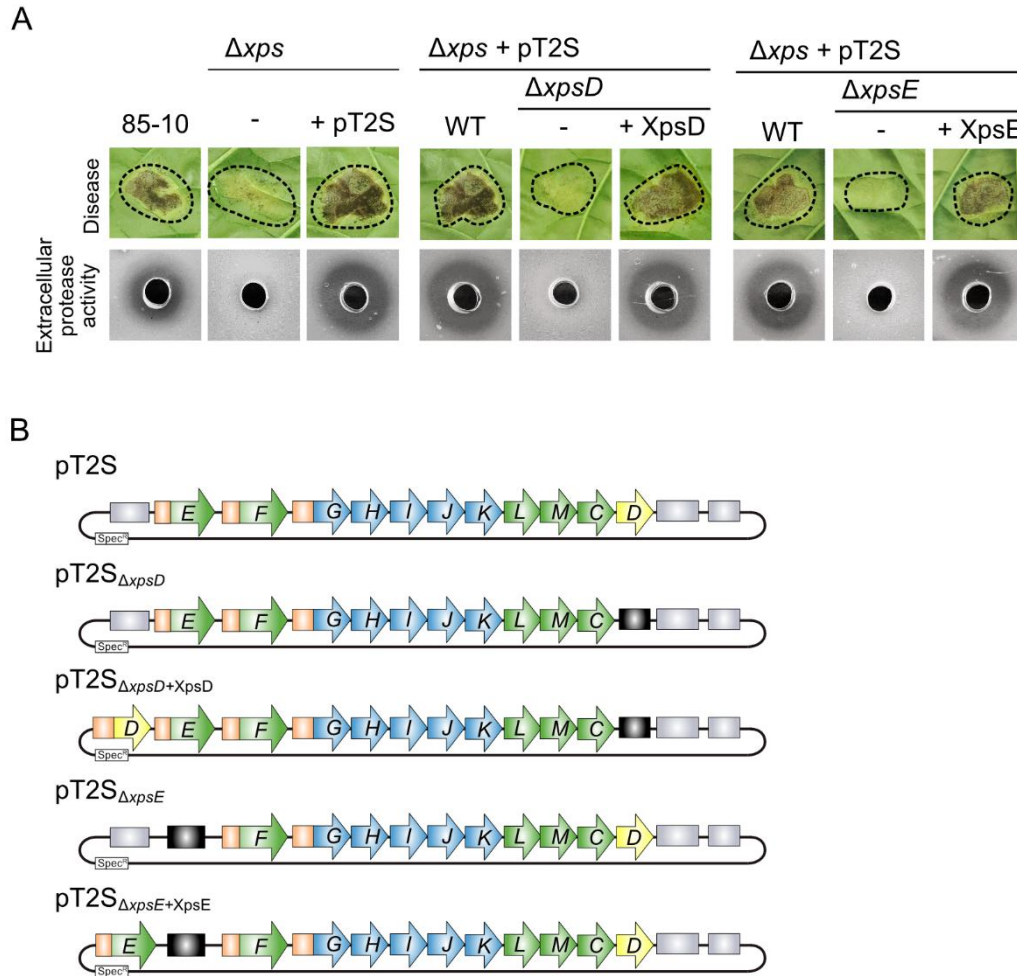


Figure 7: The modular *xps*-T2S system expedites functional characterization of *xpsD* and *xpsE* mutants

A: The wild-type strain 85-10 and the T2S deletion mutant 85-10 Δxps (Δxps) with (+) or without (-) the modular *xps*-T2S expression construct (+ pT2S) were analyzed for bacterial virulence and extracellular protease activity. For the analysis of *xpsD* and *xpsE* mutants, modular T2S gene cluster constructs lacking *xpsD* ($\Delta xpsD$) or *xpsE* ($\Delta xpsE$) were introduced into strain 85-10 Δxps . For complementation studies, *xpsD* (+XpsD) or *xpsE* (+XpsE) expression cassettes were inserted at position 1 of the respective constructs as depicted in (B). Bacteria were infiltrated at a density of 2×10^7 CFU ml⁻¹ into leaves of susceptible pepper plants and disease symptoms were photographed at 8 dpi. Dashed lines indicate the infiltrated areas. For the analysis of extracellular protease activity, bacterial cultures with a starting density of 10^9 CFU ml⁻¹ were grown on 1% milk plates for 2 days and halo formation was documented. Bacteria were removed from the holes prior to documentation. B: Overview on modular level M T2S constructs generated for the analysis of *xpsE* and *xpsD* mutants. Genes are represented by arrows, promoters by orange boxes. Deletions are indicated by black boxes. For complementation studies, *xpsE* and *xpsD* were reinserted at position 1 of the corresponding modular T2S gene cluster constructs as indicated.

4.1.3 Independent assembly of the oligomeric secretin structure

Fluorescent protein fusions have previously served as reporters to visualize membrane-bound protein complexes for the T3S system in *X. euvesicatoria*; unbound fluorescent fusion proteins produce a homogenous signal in the cytoplasm or periplasm, but form distinct fluorescent foci when part of a protein complex such as a protein secretion system (Hausner *et al*, 2019; Otten & Büttner, 2021). To investigate the assembly dynamics of the XpsD secretin channel, fluorescence microscopy-based *in vivo* localization studies were performed with XpsD fused to the red fluorescent reporter mCherry which is active in the periplasm

(Meiresonne *et al*, 2017). Typically, both the N- and C-termini of secretins are located in the periplasm (Barbat *et al*, 2023). As the N-terminal region of XpsD contains a predicted Sec signal cleaved upon translocation into the periplasm, mCherry was fused to the C-terminus of XpsD. Complex formation of XpsD-mCherry upon assembly of the secretin should result in the formation of fluorescent foci at the cell periphery as shown previously for PulD of *Klebsiella oxytoca* (Buddelmeijer *et al*, 2009). Prerequisite for the formation of fluorescent foci is the stability and functionality of the XpsD-mCherry fusion protein.

For functional studies, the native *xpsD* gene was deleted from the modular T2S gene cluster and an expression cassette encoding XpsD-mCherry under control of the native promoter was inserted at position 1 of the corresponding level M construct. XpsD-mCherry restored the wild-type phenotype when encoded in the flanking region of the modular T2S gene cluster lacking *xpsD*, suggesting that the mCherry fusion partner did not interfere with XpsD function (Figure 8). Immunoblot analyses of bacterial cell extracts showed that XpsD-mCherry was stably synthesized and forms high molecular weight complexes which were detected in the stacking gel and presumably correspond to XpsD-mCherry multimers (Figure 8). Complex formation was also detected in the absence of *xpsE* – *xpsD* genes, suggesting that the secretin assembles independently of other components of the T2S system including the assembly platform. To confirm this hypothesis, fluorescence microscopy studies with bacteria containing XpsD-mCherry in the presence or absence of other Xps proteins were performed. Fluorescent foci per cell were detected in both strains, indicative of the formation of XpsD-mCherry oligomers and thus the assembly of the secretin (Figure 8). Foci formation was specific to the presence of XpsD and was not detected in bacteria containing mCherry alone (data not shown). No significant differences in foci formation were detectable in the presence or absence of the remaining *xps* genes (Figure 8). This suggests that the secretin assembles independently of other components of the T2S system.

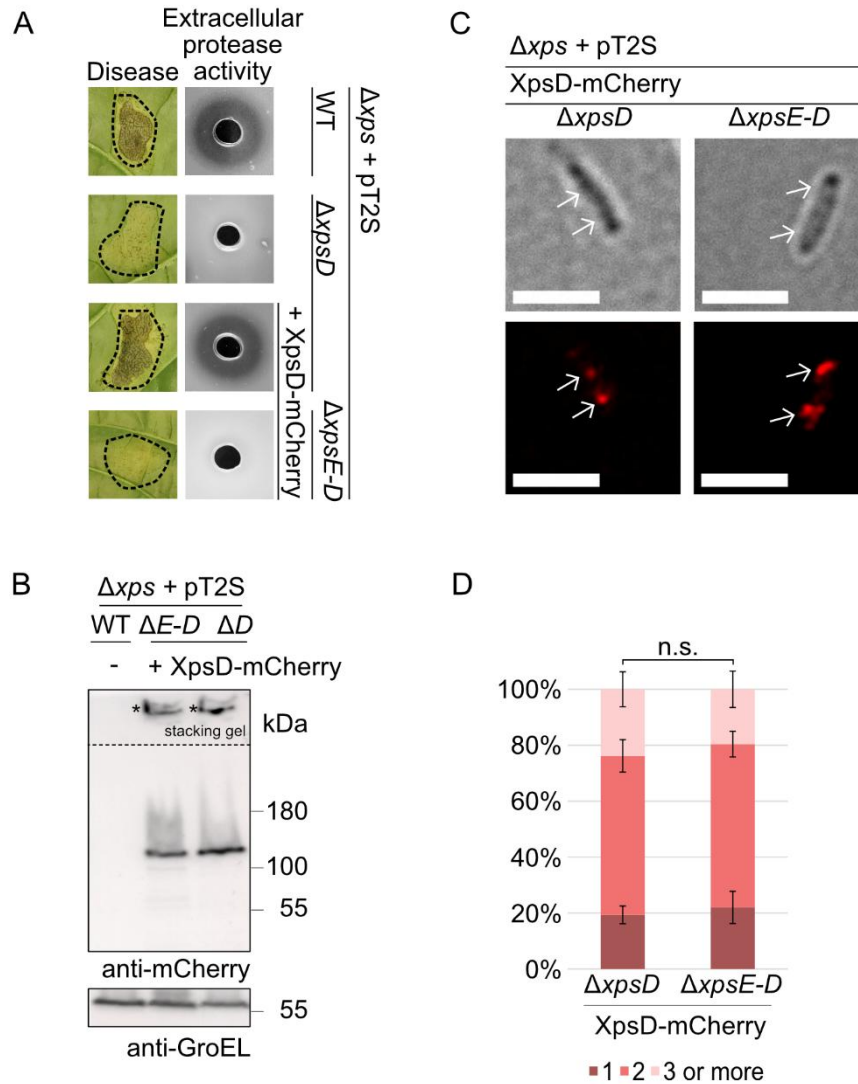


Figure 8: Assembly of the outer membrane secretin XpsD is independent of T2S system components.

A: Complementation studies with XpsD-mCherry in *X. euvesicatoria*. Strain 85-10 Δxps carrying the wild-type (WT) modular T2S gene cluster (pT2S) or derivatives thereof deleted in *xpsD* ($\Delta xpsD$) or *xpsE* – *xpsD* ($\Delta xpsE-D$) and encoding XpsD-mCherry as indicated were infiltrated at a density of 2×10^7 CFU ml⁻¹ into leaves of susceptible pepper plants and disease symptom formation was documented 8 dpi. Dashed lines indicate the infiltrated areas. For the analysis of extracellular protease activity, bacteria were grown on 1% milk plates. Halo formation resulting from the degradation of milk proteins was photographed after two days. B: XpsD-mCherry is stably synthesized and forms complexes. Bacterial strains as described in (A) were cultivated in NYG medium and equal amounts of protein extracts were analyzed by SDS-PAGE and immunoblotting using mCherry-specific antibodies. Blots were reprobed with antibodies directed against GroEL which was analyzed as a loading control. C: For fluorescence microscopy studies, strain 85-10 Δxps (Δxps) containing modular T2S gene cluster constructs (pT2S) deleted in *xpsD* ($\Delta xpsD$) or in the entire cluster ($\Delta xpsE-D$) and encoding XpsD-mCherry were incubated in NYG medium for 2 hours. Fluorescent foci formation was analyzed by fluorescence microscopy using a Zeiss LSM 780 AxioObserver Z1 microscope at 60x magnification. Fluorescent foci are indicated by white arrows. The scale bar corresponds to 3 μ m. D: Fluorescent foci were counted in at least 100 cells per strain in three different transconjugants and the mean values and standard deviations are shown as percentage of bacterial cells. Asterisks indicate a significant difference between the number of foci with a *p*-value < 0.05 based on the results of a chi-squared test. All experiments were performed three times with similar results. One representative image for each strain from one experiment is shown.

4.1.4 The assembly platform components XpsC, XpsL and XpsM are essential for T2S

Complexes of homologs of the assembly platform components XpsC, XpsL and XpsM have been detected in *E. amylovora* and *X. campestris* pv. *campestris*, however, their structure and contribution to the formation of the assembly platform is largely unknown (Tsai *et al*, 2002; Li *et al*, 2023). Therefore, the functions and interactions of XpsC, XpsL and XpsM were studied using the modular T2S gene cluster from *X. euvesicatoria*. To this end, level M expression constructs were generated in which the individual genes contained large in-frame deletions. For complementation studies, individual assembly platform genes were reinserted under control of the native *xpsG* promoter at position 1 of the corresponding modular gene clusters (compare complementation of *xpsD* mutant in Figure 7). When analyzed in strain 85-10 Δ *xps*, modular T2S gene cluster constructs deleted in *xpsC*, *xpsL* or *xpsM* led to reduced virulence and extracellular protease activity, indicative of a loss of T2S (Figure 9). Upstream expression of *xpsC* or *xpsM* in the corresponding mutant T2S gene clusters restored the wild-type phenotype, suggesting that reduced virulence and loss of detectable extracellular protease activity were specifically caused by the absence of XpsC or XpsM and not by a polar effect of the deletions on neighbouring genes (Figure 9).

In case of the *xpsL* mutant, however, reinsertion of *xpsL* under control of the native promoter did not restore the wild-type phenotype in the *xpsL* mutant. To prevent a possible polar effect of the deletion in *xpsL* on other genes, a nonsense mutation at codon position 147 of *xpsL* was inserted and the infection and complementation studies were repeated. Similarly to the *xpsL* deletion, the stop codon in *xpsL* led to reduced virulence and extracellular protease activity when the corresponding modular *xps*-T2S gene cluster construct was analyzed in strain 85-10 Δ *xps* (Figure 9). However, upstream expression of *xpsL* under control of the *xpsG* operon promoter in the corresponding modular expression construct did not complement the mutant phenotype. To investigate whether the lack of complementation was caused by alterations in the expression level of *xpsL*, the predicted Shine Dalgarno sequence in the *xpsG* promoter was replaced by the corresponding sequence upstream of *xpsL* (Figure 9). The resulting *xpsL* expression cassette restored the wild-type phenotype, suggesting that the function of XpsL is tightly linked to its level of translation which is controlled by the Shine Dalgarno sequence.

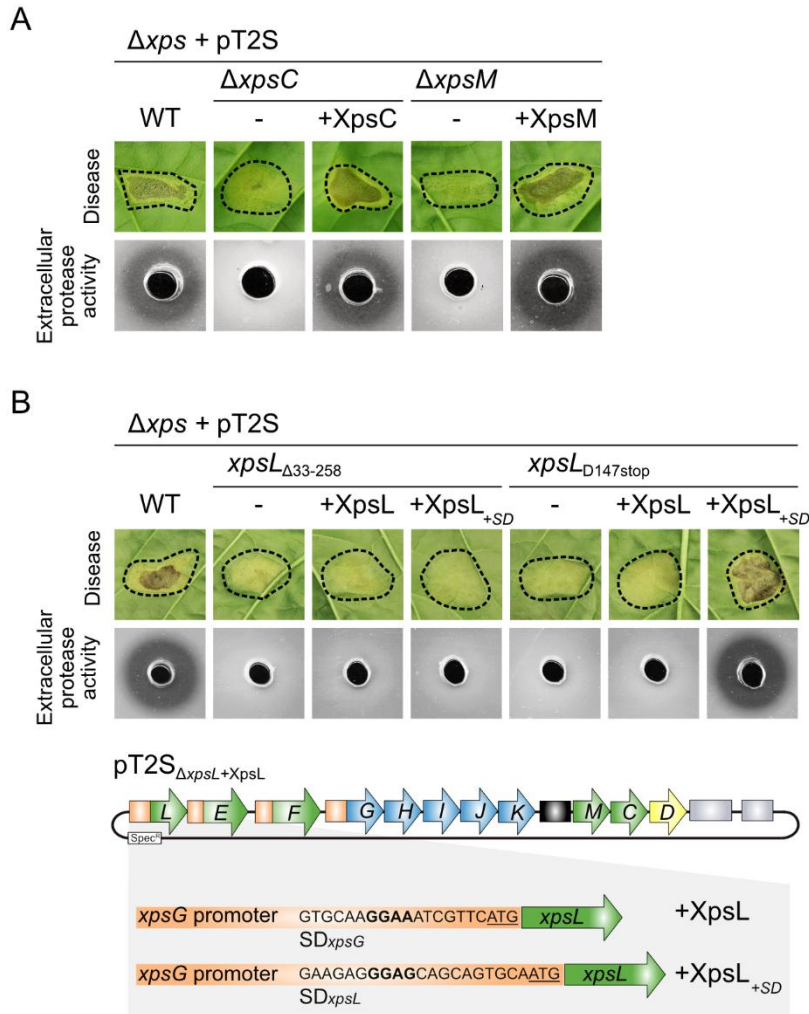


Figure 9: Assembly platform components XpsC, XpsL and XpsM are essential for T2S in *X. euvesicatoria*

A: Complementation studies with *xpsC* and *xpsM* mutants. Infection and protease activity assays were performed with derivatives of *X. euvesicatoria* strain 85-10 Δxps containing modular expression constructs with the wild-type (WT) T2S gene cluster (pT2S) or derivatives thereof lacking *xpsC* ($\Delta xpsC$) or *xpsM* ($\Delta xpsM$). For complementation studies, expression cassettes encoding XpsC (+XpsC) or XpsM (+XpsM) under control of the *xpsG* promoter were inserted at position 1 of T2S gene cluster constructs lacking *xpsC* and *xpsM*, respectively. For infection studies, bacteria were infiltrated at a density of 2×10^7 CFU ml⁻¹ into leaves of susceptible pepper plants and disease symptoms were photographed 8 dpi. Dashed lines indicate the infiltrated areas. For the analysis of extracellular protease activity, bacteria were grown on 1% milk plates for 2 days and halo formation was documented. B: *xpsL* is essential for T2S and depends on its native Shine Dalgarno sequence for efficient expression. The contribution of *xpsL* to virulence and extracellular protease activity was analyzed in derivatives of strain 85-10 Δxps containing the wild-type T2S gene cluster or derivatives thereof lacking *xpsL* ($\Delta xpsL$) with or without expression cassettes encoding XpsL under control of the native *xpsG* promoter (+XpsL). In a second construct, the predicted Shine Dalgarno (SD) sequence of *xpsG* was exchanged by the corresponding sequence upstream of *xpsL* (XpsL_{+SD}) as illustrated. The translation initiation codon (ATG) is underlined. For complementation studies, bacteria were infiltrated into leaves of susceptible pepper leaves or grown on milk-containing agar plates as described in (A).

4.1.5 *In-silico* modeling suggests a structurally conserved trimeric XpsCLM complex in diverse bacterial species

XpsC, XpsL and XpsM are predicted IM proteins with periplasmic domains which presumably surround the central XpsF component of the assembly platform. To predict the architecture of the XpsCLM complex in the context of the T2S system, the corresponding protein structures

were modelled *in silico* using the AlphaFold2 structure prediction algorithm and the molecular visualization program UCSF ChimeraX (Jumper *et al*, 2021; Goddard *et al*, 2018).

When included in one structural model, XpsC, XpsL and XpsM form a trimeric complex with a pTM (predicted template modelling) value of 0.56 and an ipTM (inter-chain predicted template modelling) value of 0.62 (see Figure 10 and appendix, Figure 37). The pTM score assesses the confidence in the relative arrangement of domains within a single protein chain whereas the ipTM score evaluates the reliability of predicted conformations and interactions between protein chains in a multimer structure. pTM and ipTM values range from 0 to 1 and values closer to 1 indicate higher confidence. The cytoplasmic domain of XpsL is predicted to associate with the putative ATPase XpsE at the N1E domain, albeit with lower pTM and ipTM values of 0.48 and 0.51, respectively (see appendix, Figure 37).

According to the AlphaFold2 model, XpsC, XpsL and XpsM insert into the IM with an N-terminal transmembrane helix followed by large C-terminal periplasmic regions. The periplasmic regions of XpsL and XpsM adopt predicted ferredoxin-like folds containing two α helices and an anti-parallel β sheet. These ferredoxin-like fold structures of XpsL and XpsM as well as in the cytosolic domain of XpsL which is predicted to interact with XpsE was significantly more conserved than the rest of the proteins (compare Figure 13). Interaction of XpsL and XpsM are predicted via their transmembrane and periplasmic regions including the ferredoxin-like fold as was previously described for GspL and GspM from *Klebsiella oxytoca* (Dazzoni *et al*, 2023) and *Dickeya dadantii* (Lallemant *et al*, 2013). Furthermore, both XpsL and XpsM were predicted to interact with a relatively unstructured periplasmic region of XpsC between the transmembrane helix and the HR domain of XpsC.

The periplasmic region of XpsC contains an HR domain which is formed by β sheets and is typical of GspC proteins including XcpP from *P. aeruginosa*, OutC from *D. dadantii* and EpsC from *V. cholerae* (Figure 10). This HR domain of XpsC was also predicted by AlphaFold2 to interact with the N0 domain of XpsD and was also more conserved than other regions of XpsC (see Figure 10, Figure 13 and appendix, Figure 37). A second periplasmic region of XpsC, referred to as 2P region, contains a single predicted α helix like in XcpP from *Pseudomonas aeruginosa* (Bleves *et al*, 1999). In contrast, the GspC proteins OutC and EpsC from *D. dadantii* and *V. cholerae* contain a PDZ fold formed by α helices and β sheets in their 2P region (Korotkov *et al*, 2006; Login *et al*, 2010) (Figure 10 and appendix Figure 34). PDZ domains also occur in proteins unrelated to those of the T2S system and are often involved in protein-protein interactions (Sheng & Sala, 2001).

Interestingly, AlphaFold2 modeling revealed a similar structure of trimeric GspCLM complexes from the bacterial pathogens *P. aeruginosa* (XcpPYZ), *D. dadantii* (OutCLM) and *V. cholerae* (EpsCLM), despite limited amino acid sequence similarities of the corresponding

proteins. The pTM values of 0.42 for all three complexes and the ipTM values of 0.41 (for XcpPYZ), 0.42 (for OutCLM) and 0.48 (for EpsCLM) were slightly lower than the corresponding values for XpsCLM from *X. euvesicatoria* (see Figure 10 and appendix, Figure 37). Notably, however, significant portions of the GspC homologs in all models were highly disordered, which might result in lower pTM and ipTM values (see Fig. S6). This suggests that the trimeric XpsCLM complex is not *Xanthomonas*-specific but structurally conserved despite sequence divergence between T2S systems. Interaction sites are similar between the GspL-GspM dimer and GspC homologues, spanning a region between the first N-terminal transmembrane helix and the HR domain (Figure 10 and appendix, Figure 37).

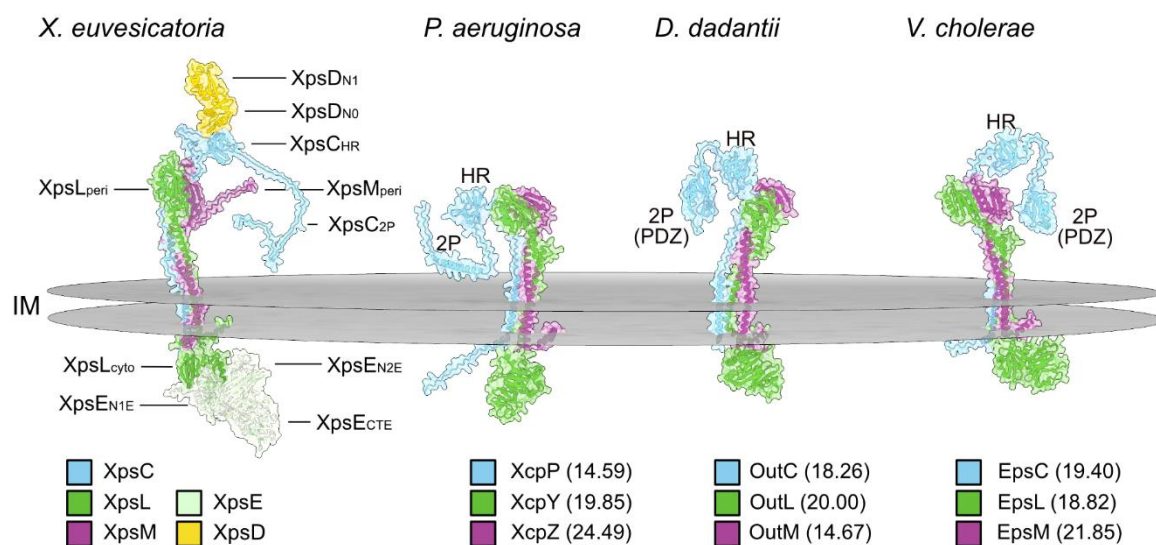


Figure 10: XpsCLM form a predicted trimeric complex which is structurally conserved

The structure of a complex consisting of the periplasmic region of XpsD (referred to as D_{N1} and D_{N0}), XpsC, XpsL, XpsM and XpsE was predicted using the AlphaFold2 algorithm and the molecular visualization program UCSF ChimeraX. Proteins are represented in different colours as indicated. The HR and 2P regions of XpsC, the periplasmic (peri) and cytoplasmic (cyto) domains of XpsL and XpsM and the position of the inner membrane (IM) are indicated. XpsE consists of two N-terminal (N1E and N2E) and one C-terminal (CTE) domain. The per-residue model confidence score (pLDDT) of single protein complexes is shown in Figure 37. AlphaFold2 predictions are also shown for GspCLM proteins from other bacterial species, including XcpPYZ proteins from *P. aeruginosa* strain PAO1, OutCLM proteins from *D. dadantii* strain 3937 and EpsCLM proteins from *V. cholerae* strain N16961. HR and 2P regions of GspC proteins are indicated. The 2P regions of OutC and EpsC contain a PDZ fold. Numbers represent the amino acid identities of the proteins with the corresponding XpsCLM proteins from *X. euvesicatoria*. The following proteins were used for the topology models: XcpP (accession number CAA48581), XcpY (accession number AAG06484) and XcpZ (accession number AAG06483) from *P. aeruginosa* strain PAO1, OutC (accession number CAA46369), OutL (accession number ADM99368) and OutM (accession number ADM99367) from *D. dadantii* strain 3937 and EpsC (accession number P45777), EpsL (accession number P45782) and EpsM (accession number P41851) from *V. cholerae* strain N16961. The predicted alignment errors and pLDDT values are shown in Figure 37 (appendix). Schematic topology models of GspC homologues are shown in Figure 34.

4.1.6 *In vitro* characterization of XpsC, XpsL, XpsM and XpsE interactions

To test predicted interactions between XpsC, XpsL, XpsM and XpsE experimentally, protein-protein interaction studies were performed using the bacterial adenylate cyclase two-hybrid (BACTH) system. This method is based on the reconstitution of the catalytic domain of the

adenylate cyclase (Cya) from two subdomains (T18 and T25) in the bacterial cytoplasm and is suitable for the analysis of soluble and transmembrane proteins (Battesti & Bouveret, 2012; Karimova et al, 1998, Otten 2021). The T18 and T25 subdomains of Cya were analyzed as N-terminal fusion partners of predicted assembly platform components to allow their localization in the cytoplasm (Figure 11). For the cytosolic putative ATPase XpsE, T18 and T25 subdomains were analyzed as both N- or C-terminal fusion partners. Immunoblot analysis of bacterial cell extracts showed that all proteins were stably synthesized (appendix, Figure 35). For BACTH assays, T18 and T25 fusions were co-expressed in the *E. coli* reporter strain DHM1, which lacks the native *cya* gene. Protein-protein interactions led to cAMP production and thus to *lacZ* gene expression which was monitored when bacteria were grown on reporter plates containing X-Gal. Self-interactions of XpsE and XpsC, interactions between XpsE and XpsL as well as of XpsC with XpsM and XpsL were detected (Figure 11). The analyzed fusion proteins did not bind to the T18 or T25 subdomains alone, suggesting that the observed interactions were specific (Figure 11). Interactions between XpsM and XpsL were not detected, potentially due to steric hindrance by the large N-terminal T18 and T25 domains interfering with heterodimer formation of XpsM and XpsL.

To confirm the interaction between the predicted ATPase XpsE and XpsL, an *in vitro* GST (glutathione S-transferase) pull-down assay was employed. For this, GST and GST-XpsE were immobilized on glutathione sepharose and incubated with bacterial lysates containing an N-terminally c-Myc epitope-tagged derivative of XpsL. Immunoblot analyses showed that c-Myc-XpsL coeluted with GST-XpsE but not with GST alone, suggesting a direct interaction between XpsE and XpsL (Figure 11). These results concur with the previous finding that XpsE interacts with XpsL in *X. campestris* pv. *campestris* (Shiue et al, 2006).

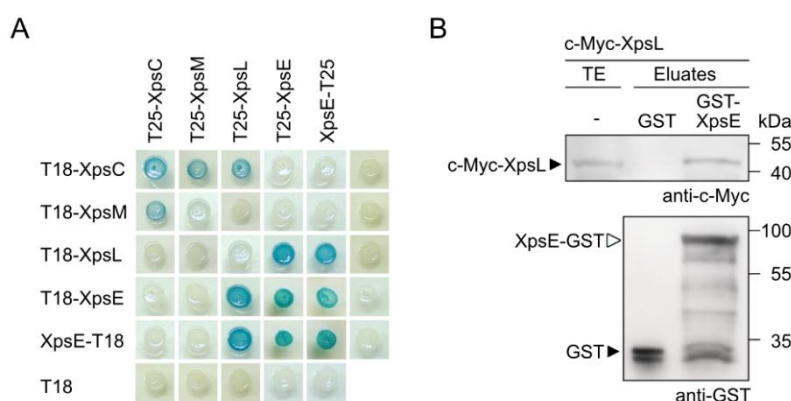


Figure 11: *In vitro* protein-protein interaction studies with assembly platform components from *X. euvesicatoria*

A: BACTH assays with XpsC, XpsL, XpsM and XpsE. T25 and T18 fusions of XpsC, XpsL, XpsM and XpsE as indicated were analyzed in the *E. coli* reporter strain DHM1. Transformants were incubated on indicator plates containing X-Gal and IPTG and representative colonies were photographed after five days. All fusions proteins were stably synthesized as was shown by immunoblot analysis (appendix, Figure 35). B: *In vitro* interaction of XpsL and XpsE. GST and GST-XpsE were immobilized on a glutathione sepharose matrix and incubated with a bacterial lysate containing c-Myc-XpsL. The total cell extract (TE) and eluted proteins (eluate) were analyzed by immunoblotting using c-Myc- or GST-specific antibodies. GST and GST-XpsE are indicated. All experiments were performed at least three times with similar results. One representative result is shown.

4.1.7 Stability of XpsC and XpsL depend on each other and XpsM

To analyze the predicted components of the assembly platform *in vivo* in the context of the native T2S system by immunoblot analysis, epitope-tagged versions of XpsL and XpsC were generated. For the analysis of XpsL, an expression cassette encoding N-terminally c-Myc epitope-tagged XpsL under the control of the *xpsG* promoter and the Shine Dalgarno sequence of *xpsL* was inserted into the flanking region of *xps* gene cluster constructs with a non-sense mutation in *xpsL* or in additional assembly platform genes (see materials and methods cloning). The resulting constructs were transferred into strain 85-10Δ*xps*. Protease activity assays showed that c-Myc-XpsL was functional and restored extracellular protease activity in bacteria containing a nonsense mutation in *xpsL* (Figure 12). When analyzed by immunoblotting, c-Myc-XpsL was detected at the expected molecular size of 48 kDa (Figure 12). An additional protein at a size of approximately 37 kDa, hereafter referred to XpsL', presumably represents a degradation or cleavage product of c-Myc-XpsL lacking the C-terminal protein region. Severely reduced amounts of c-Myc-XpsL were detected in strains lacking the complete *xps*-T2S gene cluster or *xpsM*, suggesting that XpsM contributes to XpsL stability. In contrast to the full-length c-Myc-XpsL protein, the levels of c-Myc-XpsL' appeared to be unaffected, suggesting that the N-terminal region of XpsL is stable in the absence of XpsM (Figure 12).

For the analysis of XpsC, a gene module encoding XpsC-c-Myc under control of the native *xpsG* promoter was inserted into level M constructs containing modular *xps*-T2S gene clusters with deletions in single (*xpsC*) or multiple *xps* genes as described above (see materials and methods cloning). XpsC-c-Myc restored protease activity in a strain lacking the native *xpsC* gene in the modular T2S gene cluster, suggesting that the C-terminal c-Myc epitope did not significantly interfere with XpsC function (Figure 12). When analyzed by immunoblotting in *X. euvesicatoria* protein extracts, XpsC-c-Myc appears to have an aberrant migration pattern because it was detected at a size of approximately 40 kDa instead of the expected size of 34 kDa (28 kDa for XpsC and 6 kDa for the c-Myc epitope) (Figure 12). Furthermore, an additional XpsC-c-Myc-specific signal appeared at a size of 55 kDa (XpsC"). Inspection of the *xpsG* promoter, which is the native promoter of the predicted *xpsG-D* operon and was used to express *xpsC*, revealed the presence of additional potential start codons upstream of the translation initiation site of *xpsC* which may lead to the synthesis of an additional protein corresponding to XpsC-c-Myc with an N-terminal extension. In contrast, c-Myc-XpsL was expressed with the native Shine Dalgarno sequence downstream of the *xpsG* promoter, rendering these alternate start codons out-of-frame, and no similar larger signal was detected for c-Myc-XpsL. An alternative explanation for the 55 kDa signal in the

XpsC-c-Myc derivatives might be the formation of a stable XpsC-c-Myc-containing complex, which was not dissolved during SDS-PAGE.

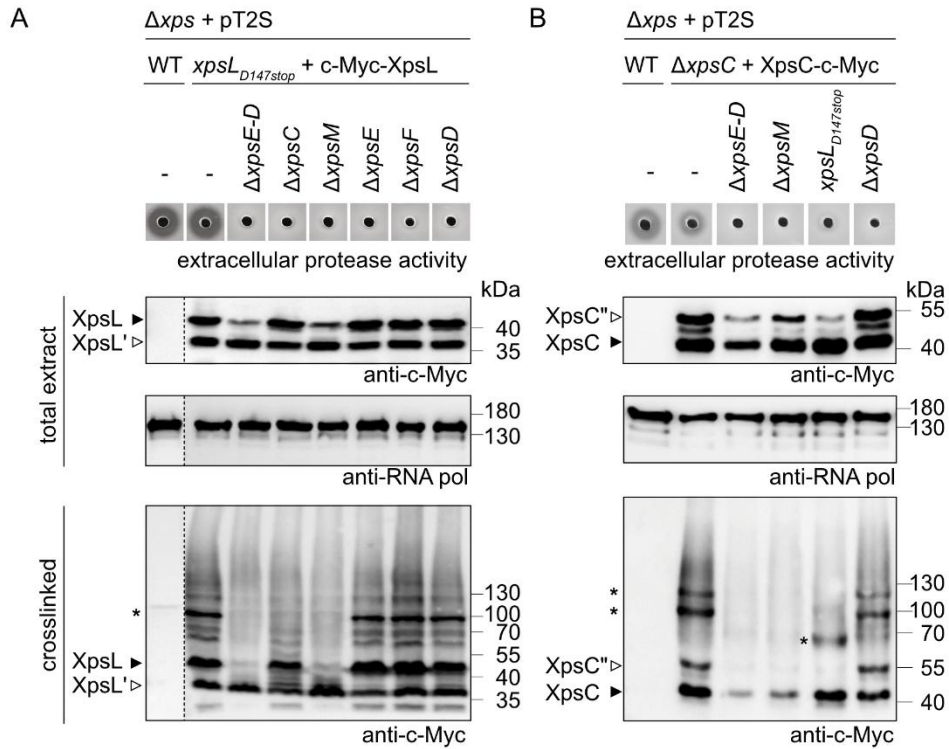


Figure 12: *In vivo* crosslinking experiments verify a trimeric XpsCLM complex

A: Detection of XpsL-containing complexes after *in vivo* crosslinking depends on XpsC and XpsM. Derivatives of strain 85-10 Δxps (Δxps) containing the wild-type (WT) modular T2S gene cluster (+pT2S) or derivatives with a non-sense mutation in *xpsL* and encoding c-Myc-XpsL and with additional deletions in *xpsE-D*, *xpsC*, *xpsM*, *xpsE*, *xpsF* or *xpsD* as indicated were grown in NYG medium. Equal amounts of cell cultures were centrifuged and cells were either resuspended in Laemmli buffer at 99°C (total extract) or incubated with formaldehyde and resuspended in Laemmli buffer at 37°C (crosslinked). Proteins were analyzed by immunoblotting using antibodies specific to the c-Myc epitope or the RNA polymerase β to ensure equal loading. Signals corresponding to the expected sizes of c-Myc-XpsL (48 kDa; black arrow), a probable degradation product of c-Myc-XpsL (37 kDa; white arrow, XpsL') and a c-Myc-XpsL-specific protein complex corresponding in size to XpsC-L-M (100 kDa; asterisk) are indicated. For the analysis of T2S system activity, bacteria were grown on milk protein-containing agar plates to demonstrate extracellular protease activity. Halo formation was documented two days after incubation. B: The formation of XpsC-containing complexes depends on XpsM and XpsL. Derivatives of strain 85-10 Δxps (Δxps) containing the wild-type modular T2S gene cluster or derivatives thereof deleted in *xpsC*, *xpsE-D*, *xpsM*, *xpsL* or *xpsD* and encoding XpsC-c-Myc as indicated were grown in NYG medium and analyzed as described in (A). The signals corresponding to XpsC-c-Myc (black arrow), a potential N-terminal extension or XpsC-c-Myc (white arrow, XpsC'') and an XpsC-c-Myc-specific complexes at 100 kDa, 120 kDa and 60 kDa (only in the *xpsL*_{D147stop} background) are indicated by asterisks. All experiments were performed three times with similar results. One representative example is shown.

4.1.8 Identification of the XpsCLM complex by *in vivo* crosslinking experiments

As AlphaFold2 predicted a trimeric XpsCLM complex and BACTH assays indicated interaction of XpsC, L and M, *in vivo* complex formation of XpsC and XpsL was examined by crosslinking experiments with formaldehyde (FA) which penetrates cells and often interacts with the amino group of lysines (Hoffman *et al*, 2015). FA introduces inter- or intramolecular covalent crosslinks between amino acid residues of proteins which are in close proximity

(2.3–2.7 Å) to each other (Sutherland *et al*, 2008). Immunoblot analysis of cell extracts containing c-Myc-XpsL revealed a specific signal at approximately 100 kDa and additional signals at 60 and 70 kDa after FA treatment, suggesting that c-Myc-XpsL integrates into oligomeric protein complexes (Figure 12). Formation of the 100 kDa complex was abolished in the absence of the entire *xps*-T2S gene cluster as well as in *xpsC* or *xpsM* mutants. In contrast, deletion of *xpsD*, *xpsE* or *xpsF* did not affect complex formation. The signal at 100 kDa corresponds to the size of a predicted trimeric complex of XpsC (28 kDa), XpsM (24 kDa) and XpsL (42 kDa) (see appendix, Table 14).

In addition to c-Myc-XpsL, complex formation by XpsC-c-Myc after FA crosslinking was analyzed. Immunoblot analyses revealed the presence of XpsC-c-Myc-specific protein complexes at molecular sizes of approximately 100 and 120 kDa after FA treatment, also observed in a secretin mutant but was not detectable in the absence of *xpsE-D*, *xpsM* or in an *xpsL_{D147stop}* background (Figure 12). However, when XpsC-c-Myc was expressed in the *xpsL_{D147stop}* background, an XpsC-c-Myc-containing complex at a size of approximately 60 kDa. Again, the signal at 100 kDa corresponds to the size of a trimeric XpsCLM complex, and the 60 kDa complex corresponds to the molecular weight of an XpsC-c-Myc - XpsM dimer. An additional signal for XpsC-c-Myc was detected at 55 kDa (XpsC^{''}), which may arise from an N-terminal extension of XpsC-c-Myc due to an upstream start codon in the *xpsG* promoter sequence used (see above). Incorporation of such an XpsC^{''}-c-Myc into a trimeric complex with XpsL and XpsM could possibly explain the 120 kDa complex observed, which only formed in the presence of both XpsL and XpsM. To test this, an *xpsG* promoter derivative with an upstream stop codon was used to express a c-Myc-XpsC fusion. With this modified promoter, neither XpsC^{''} nor the 120 kDa complex were detected (see below, Figure 14).

Taken together, the results from structural modelling, BACTH assays and formaldehyde crosslinking suggest that XpsCLM forms a trimeric subcomplex in the IM, and that this subcomplex assembles independently of the XpsF, XpsE and XpsD.

4.1.9 Conserved positive charges in the 2P region of XpsC regulate T2S efficiency

As recognition of T2S substrates takes place in the periplasm prior to secretion, periplasmic domains of Xps components probably entail substrate binding sites to facilitate secretion. Two opposite selection pressures on such a substrate binding site are conceivable. If the substrate-binding properties of such a site are required for functional T2S, one would expect to find enhanced conservation of such a region, as mutations in this region would reduce the T2S efficiency and thereby lead to a fitness loss. Alternatively, significant divergence between species in such a substrate binding region could account for the observed species-specificity of T2S substrate recognition (Lindeberg *et al*, 1998). In this line of thought, one would expect that the structural core of the T2S would be conserved while a substrate binding region is adapted to the specific substrates of each species and therefore more variable. Either way, it would be expected that a substrate binding site of the T2S system significantly differs in its conservation from the rest of the system.

Therefore, the conservation of individual amino acids of the assembly platform XpsCLM complex was determined and visualized using the ConSurf web server (Yariv *et al*, 2023; Ashkenazy *et al*, 2016) (Figure 13). Strikingly, a very high degree of conservation was found in multiple positively charged amino acids of the relatively unstructured 2P-region of XpsC. This region seemed like a promising candidate for a substrate binding site, as it is predicted to be freely accessible from the periplasm, highly charged and its conservation is not explained by the restraints of structural properties, such as the ferredoxin-folds of XpsM and XpsL involved in heterodimerization (Dazzoni *et al*, 2023) and the HR-domain of XpsC involved in interaction with the secretin XpsD (Chernyatina & Low, 2019). An elevated degree of variability was only found in individual amino acids, mostly in the proline-rich linker region of XpsC between the HR-domain and the 2P-region as well as in a C-terminal protrusion of XpsM, but these did not appear to form a clustered region. When the conserved 2P-region was modelled with known Xps-substrates using AlphaFold2 (see below, Figure 21 and Figure 22), it was consistently predicted to interact with negative charged regions on substrates via the conserved positively charged interface, formed by multiple arginine residues (R241, R243, R247, R248 and R255) (Figure 13).

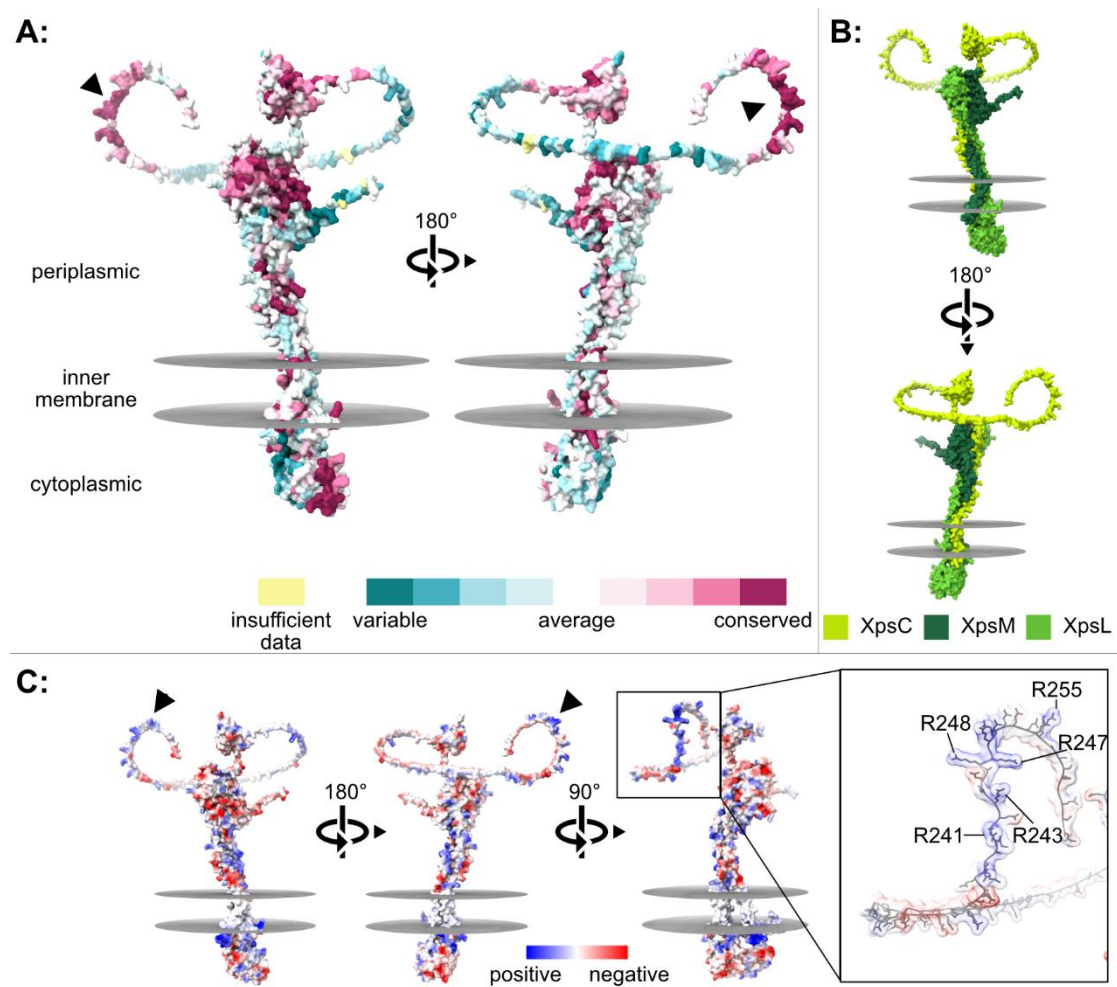


Figure 13: Positively charged residues of 2P-region of XpsC are highly conserved

A: The conservation of individual amino acids of the predicted XpsCLM complex from *X. euvesicatoria* was determined using ConSurf analysis (Yariv *et al*, 2023). The area occupied by the bacterial inner membrane is indicated by grey discs. Significant conservation is shown in purple, significant variation is shown in blue. B: The XpsCLM complex color-coded by protein chains. C: Electrostatic charge distribution of the XpsCLM complex, positive charges are shown in blue and negative ones in red. Highly conserved, positively charged arginine residues in the 2P-region of XpsC are indicated by black triangles and labeled in C.

To investigate a role of this region in substrate recruitment and secretion, N-terminally c-Myc epitope-tagged variants of XpsC were generated in which these positively charged arginine residues were mutated to neutral alanine (XpsC_{5xR→A}: R241A, R243A, R247A, R248A and R255A) or negative glutamic acid (XpsC_{5xR→E}: R241E, R243E, R247E, R248E and R255E) and assembled in the modular T2S gene cluster containing an in-frame deletion of the native *xpsC*. Alanine and glutamic acid were chosen as substitutions as these residues have helix forming properties comparable to arginine. An N-terminal c-Myc tag was used as a C-terminal epitope tag would be directly adjacent to the putative substrate binding site and might interfere with its function, and the XpsC-c-Myc fusion used in previous crosslinking experiment was functional but did not fully restore an *xpsC* deletion in extracellular protease activity (Figure 12). Additionally, the *xpsG* promoter previously used to express XpsC-c-Myc fusions contained an additional upstream start codon that may account for the observed

additional larger protein product at 55 kDa and a crosslinked complex at 120 kDa. Therefore, c-Myc-XpsC fusions were expressed under the control of an altered *xpsG* promoter with a single-nucleotide substitution that created a stop codon just upstream of the *c-Myc-xpsC* translation start site (Figure 14).

The extracellular protease activity of *Xe 85-10Δxps* strains expressing these XpsC variants was determined using milk plates (Figure 14). While the unmutated c-Myc-XpsC fusion fully restored T2S, both variants (XpsC_{5xR→A} and XpsC_{5xR→E}) led to significantly reduced T2S, as demonstrated by reduced extracellular protease activity. Formaldehyde crosslinking revealed complexes corresponding in size to a trimeric XpsCLM complex for all XpsC variants, suggesting that neither mutation effected complex formation of XpsC (Figure 14). Neither the previously detected additional protein signal at 55 kDa nor the crosslinked 120 kDa complex were detected, suggesting that this upstream start site in the *xpsG* promoter accounts for these larger products. For c-Myc-XpsC_{5xR→E}, a reduction in protein stability was observed, which may account for the diminished T2S in the presence of this derivative. Nevertheless, the c-Myc-XpsC_{5xR→A} derivative showed reduced T2S efficiency with no reduction in protein stability, suggesting that the charges of the 2P-region affect T2S efficiency. However, direct interactions of the 2P-region with T2S proteins remain to be experimentally validated.

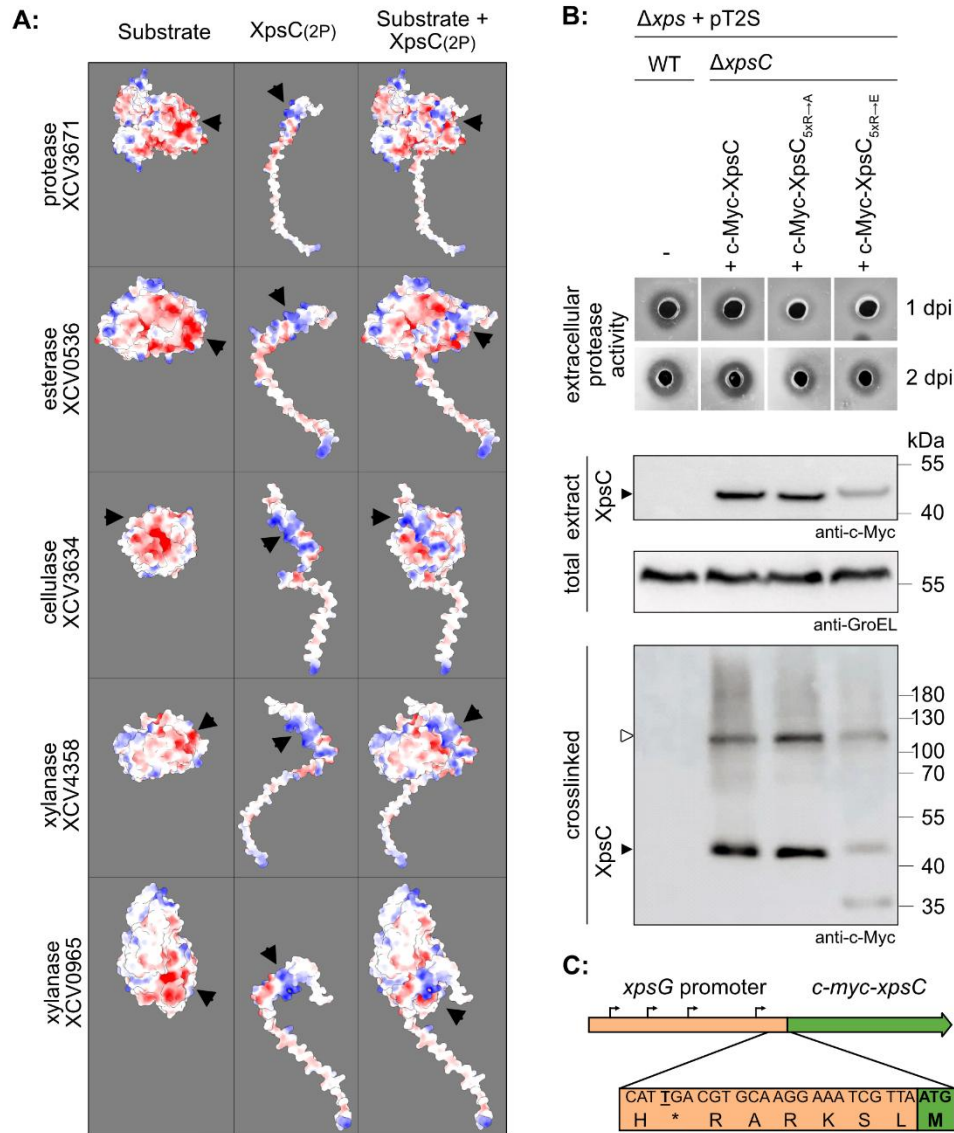


Figure 14: the 2P region of XpsC may interact with substrates electrostatically and regulates T2S efficiency

A: The 2P region of XpsC (XpsC₁₉₅₋₂₆₅) containing conserved, positively charged arginine residues was modelled together with T2S substrates from *X. euvesicatoria* using the AlphaFold2 algorithm. Five interactions representing the functional diversity of T2S substrates are shown: two xylanases, a cellulase, an esterase and a protease. Interactions were consistently predicted to occur via an electrostatic interaction between the positively charged arginine residues of XpsC-2P and negatively charged regions on substrates (black triangles). The predicted alignment errors and pLDDT values are shown in Figure 38 (appendix). **B:** Modular T2S gene clusters with an *xpsC* deletion were complemented with variants of c-Myc-XpsC: the native XpsC protein and two variants with altered electrostatic charges in the conserved positively charged 2P region: neutral alanine substitutions (XpsC_{5xR→A}: R241A, R243A, R247A, R248A and R255A) or negative glutamic acid substitutions (XpsC_{5xR→E}: R241E, R243E, R247E, R248E and R255E). All constructs were expressed in the strain 85-10 Δxps grown in NYG medium. For the analysis of T2S system activity, bacteria were grown on milk protein-containing agar plates to demonstrate extracellular protease activity. Halo formation was documented two days after incubation. Both variants, XpsC_{5xR→A} and XpsC_{5xR→E}, showed reduced extracellular protease activity compared to native XpsC. For the analysis of protein-complex formation, equal amounts of cell cultures were centrifuged, and cells were either resuspended in Laemmli buffer at 99°C (total extract) or incubated with formaldehyde and resuspended in Laemmli buffer at 37°C (crosslinked). Proteins were analyzed by immunoblotting using antibodies specific to the c-Myc epitope or the bacterial chaperonin GroEL to ensure equal loading. Signals corresponding to the expected sizes of c-Myc-XpsC (40 kDa; black triangle) and a protein complex corresponding in size to XpsCLM (100 kDa; white triangle) are indicated. No altered complex formation of the variants XpsC_{5xR→A} and XpsC_{5xR→E} was observed. Experiments were performed three times with similar results. **C:** The *xpsG* promoter derivative used to express c-Myc-XpsC derivatives in these experiments had a single-nucleotide substitution (C→T) generating a stop codon just upstream of the c-Myc-XpsC translation start site to prevent the translation of N-terminally extended proteins from additional start codons further upstream in the promoter.

4.1.10 XpsF and all pseudopilins aside from XpsH are essential to T2S in *X. euvesicatoria*

The pseudopilins XpsGHIJK and XpsF are thought to play a role in the extension of the pseudopilus to push substrates through the secretin in the T2S system. Homologues of XpsHIJK form a tip complex (Korotkov & Hol, 2008; Naskar *et al*, 2021). This tip complex is thought to be pushed up out of the inner membrane as XpsG homologues oligomerize to extend the pseudopilus towards the secretin (López-Castilla *et al*, 2017; Zhang *et al*, 2018). It is unclear how the formation of the pseudopilus and oligomerization of XpsG is regulated, but the enigmatic assembly platform protein XpsF may play a role in this process, as it is thought to be at the center of the assembly platform (Gu *et al*, 2017). Recently, the XpsF homologue of *Klebsiella pneumoniae* was demonstrated to form a trimeric complex with cytoplasmic domains that may be nested at the center of the hexameric ATPase (Guilvout *et al*, 2024).

The role of the membrane protein XpsF and the pseudopilins XpsG, XpsH, XpsI, XpsJ and XpsK was analyzed by generating respective single gene deletions in the modular T2S gene cluster from *X. euvesicatoria*. For complementation studies, respective genes were reinserted under their native promoters upstream of the *xps* genes, as described above. When these constructs were analyzed in strain 85-10 Δ *xps*, deletions of *xpsF*, *xpsG*, *xpsI*, *xpsJ* and *xpsK* led to reduced virulence and extracellular proteases activity, indicating a loss in T2S (Figure 15). Expression of respective genes upstream of the modified *xps* gene clusters restored extracellular protease activity and full virulence, suggesting that the loss of T2S was specific to these respective gene deletions, not due to a polar effect on other genes. Surprisingly, a deletion of *xpsH* did not affect virulence and only slightly reduced extracellular protease activity, suggesting that in contrast to all other Xps proteins, the minor pseudopilin XpsH is not essential for a functional T2S system. This is in agreement with similar findings for the homologue XcpU in *Pseudomonas aeruginosa* (Zhang *et al*, 2018).

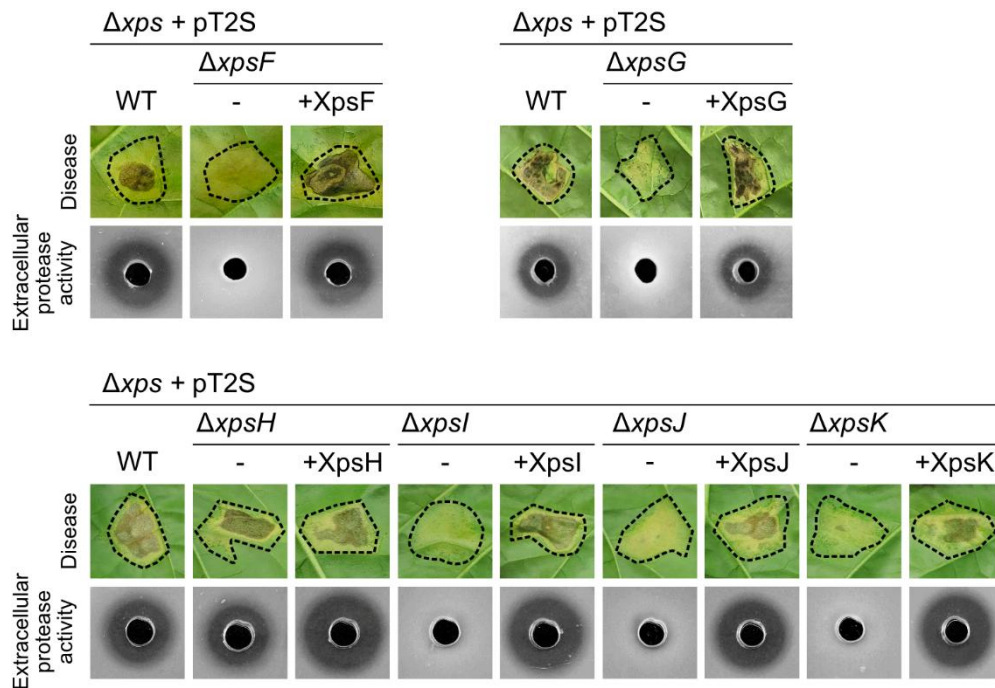


Figure 15: XpsF and the pseudopilins XpsG, XpsI, XpsJ and XpsK are essential to T2S

Infection and protease activity assays were performed with derivatives of *X. euvesicatoria* strain 85-10 Δ *xps* containing modular expression constructs with the wild-type (WT) T2S gene cluster (pT2S) or derivatives thereof lacking *xpsF* (Δ *xpsF*), *xpsG* (Δ *xpsG*), *xpsH* (Δ *xpsH*), *xpsI* (Δ *xpsI*), *xpsJ* (Δ *xpsJ*) or *xpsK* (Δ *xpsK*). For complementation studies, expression cassettes encoding the respective genes under native promoters were inserted upstream of T2S gene cluster constructs lacking respective genes, as indicated. For infection studies, bacteria were infiltrated at a density of 2×10^7 CFU ml⁻¹ into leaves of susceptible pepper plants and disease symptoms were photographed 8 dpi. Dashed lines indicate the infiltrated areas. For the analysis of extracellular protease activity, bacteria were grown on 1% milk plates for 2 days and halo formation was documented.

4.1.11 XpsF oligomerization requires XpsI, XpsJ and XpsK

Recently, the XpsF homologue of *Klebsiella pneumoniae* was demonstrated to oligomerize (Guilvout *et al*, 2024), but whether oligomerization depends on other components of the T2S system was not examined. To inspect whether XpsF also oligomerizes in *Xe* and whether this depends on specific components of the T2S system, *in vivo* formaldehyde crosslinking was performed with a c-Myc-XpsF fusion, as shown in Figure 16.

The c-Myc-XpsF fusion was expressed under the control of the native *xpsF* promoter and inserted into the flanking region of *xps* gene cluster constructs lacking *xpsF* or additional genes (as indicated in Figure 16) and resulting constructs were transferred into strain 85-10 Δ *xps*. Protease activity assays showed that c-Myc-XpsF was functional as it restored extracellular protein activity in a strain lacking the native *xpsF*. However, c-Myc-XpsF was detected slightly lower than the predicted 50 kDa, around 45 kDa (Figure 16). After crosslinking, protein complexes were detected at around 70 kDa, 100 kDa, 110 kDa and 120 kDa. The complex at 70 kDa formed independently of other Xps proteins and seemed more pronounced in the Δ *xpsE-D*, Δ *xpsI*, Δ *xpsJ* or Δ *xpsK* background. The remaining three complexes above 100 kDa formed independently of the secretin XpsD, the assembly

platform components XpsC and XpsM as well as the ATPase XpsE and the pseudopilins XpsG and XpsH, but were not detected or extremely reduced in absence of the pseudopilin tip proteins XpsI, XpsJ and XpsK. This suggests that these three pseudopilins promote XpsF oligomerization, although the composition of the 100 kDa, 110 kDa and 120 kDa c-Myc-XpsF complexes could not be determined.

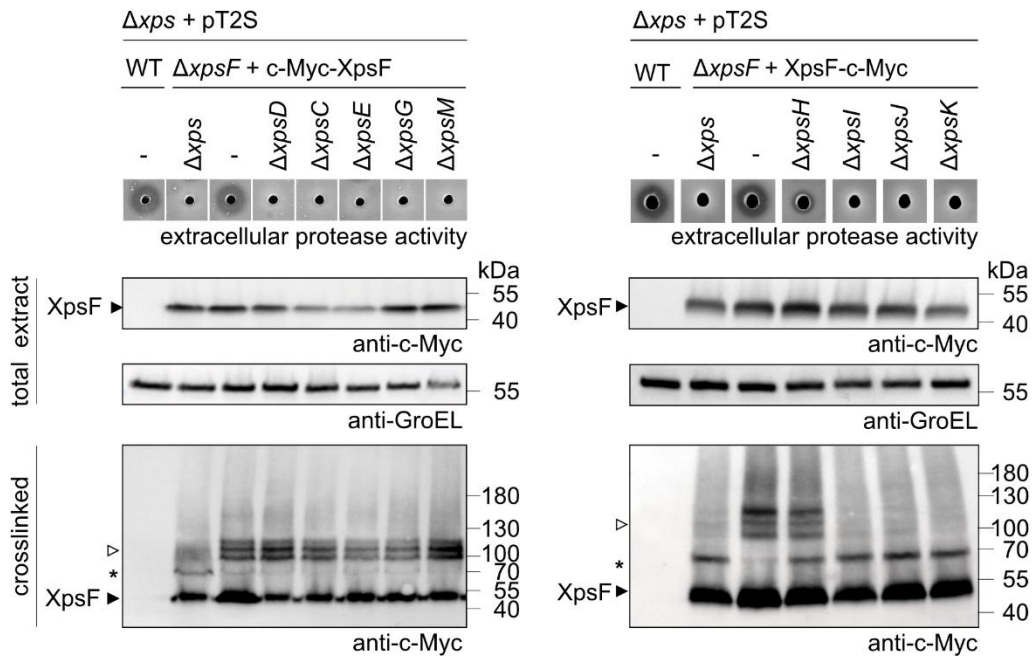


Figure 16: Oligomerization of XpsF requires XpsI, XpsJ and XpsK

Derivatives of strain 85-10 Δ xps (Δ xps) containing the wild-type (WT) modular T2S gene cluster (+pT2S) or a derivative thereof deleted in *xpsE-D*, *xpsD*, *xpsC*, *xpsE*, *xpsG*, *xpsM*, *xpsH*, *xpsI*, *xpsJ* or *xpsK* and encoding c-Myc-XpsF as indicated were grown in NYG medium. Equal amounts of cell cultures were centrifuged, cells were either resuspended in Laemmli buffer at 99°C (total extract) or incubated with formaldehyde and resuspended in Laemmli buffer at 37°C (crosslinked). Proteins were analyzed by immunoblotting using antibodies specific to the c-Myc epitope or the bacterial chaperonin GroEL to ensure equal loading. XpsF was detected at ca. 45 kDa (black triangle) and multiple protein-complexes were detected for c-Myc-XpsF, an Xps-independent complex at 70 kDa (asterisk) and three complexes at around 100 kDa, 110 kDa and 120 kDa (white triangle).

4.1.12 Structural modelling suggests docking of the pseudopilus tip in a trimeric XpsF channel

Recent findings suggest that XpsF homologues form a trimeric membrane channel (Guilvout *et al*, 2024). As formaldehyde crosslinking indicated that the pseudopilins XpsI, XpsJ and XpsK influence oligomerization of XpsF, structural predictions were performed with three monomers of XpsF together with XpsI, XpsJ and XpsK, using AlphaFold2 (Figure 17). This yielded a credible structural model with an ipTM value of 0.6 composed of a trimeric XpsF inner membrane channel with an XpsIJK pseudopilus tip nested inside the channel via the hydrophobic N-terminal regions of the pseudopilin. Strikingly, a very high degree of conservation at the predicted contact sites of the XpsIJK pseudopilus tip complex and the trimeric XpsF channel was revealed by ConSurf analysis (Figure 17). Additionally, a high

degree of conservation was found in the cytoplasmic domains of XpsF, which were predicted to interact with XpsE (see appendix, Figure 36).

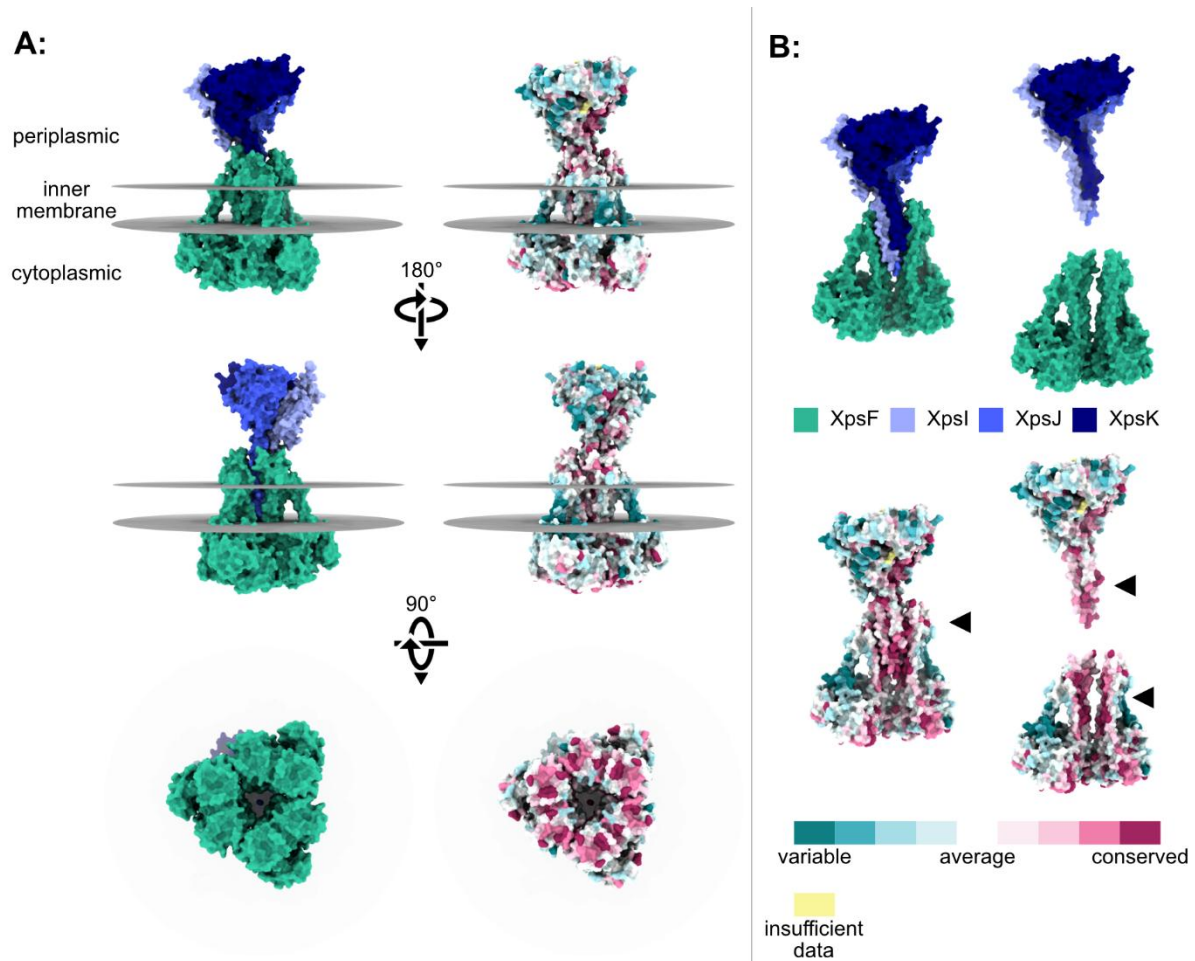


Figure 17: Predicted structure of a XpsI-J-K pseudopilus tip complex nested in a trimeric XpsF channel

A: The predicted structure and amino acid conservation of a complex of three monomers of XpsF (teal) and XpsI (light blue), XpsJ (blue) and XpsK (dark blue) from *X. euvesicatoria* were determined using AlphaFold2 and ConSurf analysis (Yariv *et al*, 2023). The area occupied by the bacterial inner membrane is shown with grey discs. B: The residues at the predicted interaction sites of XpsF and XpsI-J-K are highly conserved. The XpsIJK complex is shown nested in two of three XpsF monomers, and conserved residues are highlighted by black triangles. Significant conservation is shown in purple, significant variation is shown in blue. The predicted alignment errors and pLDDT values are shown in Figure 38 (appendix).

4.1.13 The pseudopilus tip assembles independently of XpsF and XpsE

To experimentally determine whether a trimeric XpsI-J-K pseudopilus tip complex forms *in vivo*, as predicted together with XpsF by AlphaFold2, a targeted cysteine crosslinking approach was employed. To this end, individual amino acids on respective proteins predicted to be in proximity to each other were specifically substituted with cysteines in the modular T2S gene cluster. Strains expressing these modified constructs were then treated with copper chloride as an oxidizing agent which forms covalent disulfide bonds between cysteines of interacting proteins.

To identify a trimeric XpsIJK complex *in vivo* by covalently linking all three proteins to each other simultaneously, cysteines were inserted with the aim of forming two separate disulfide bonds, one between XpsK and XpsJ and a second independent bond between XpsK and XpsI. Amino acid pairs predicted to be in close proximity to each other in the hydrophobic tail of respective pseudopilins were substituted to cysteine: alanine 46 in XpsJ and the aspartic acid 51 in XpsK, as well as alanine 33 in XpsI and alanine 45 in XpsK, respectively (Figure 18). An XpsK-c-Myc fusion was used for these experiments to detect protein complexes by immunoblotting. None of these cysteine substitutions impaired T2S functionality, as shown by milk plates (Figure 18). After treatment with copper chloride, no unspecific XpsK_{A45C+E51C}-c-Myc complexes were detected in absence of cysteine substitutions in XpsI or XpsJ. However, when additional cysteine substitutions were included in XpsI and XpsJ, specific XpsK_{A45C+E51C}-c-Myc-XpsI_{A33C}, XpsK_{A45C+E51C}-c-Myc-XpsJ_{A46C} or XpsK_{A45C+E51C}-c-Myc-XpsI_{A33C}-XpsJ_{A46C} complexes were detected at 45 kDa, 55 kDa and 65 kDa, respectively. While the expected molecular mass of these complexes was slightly higher (50 kDa for XpsI-K, 60 kDa for XpsJ-K and 75 kDa for XpsI-J-K), the aberrant migration pattern may be accounted for by incomplete denaturation of crosslinked samples in Laemmli-buffer lacking β -Mercaptoethanol required for this assay. Furthermore, these XpsI-XpsK, XpsJ-XpsK and XpsI-J-K complexes were also detected in absence of XpsE and XpsF, indicating that the assembly of the XpsI-J-K trimer is independent of XpsE and XpsF.

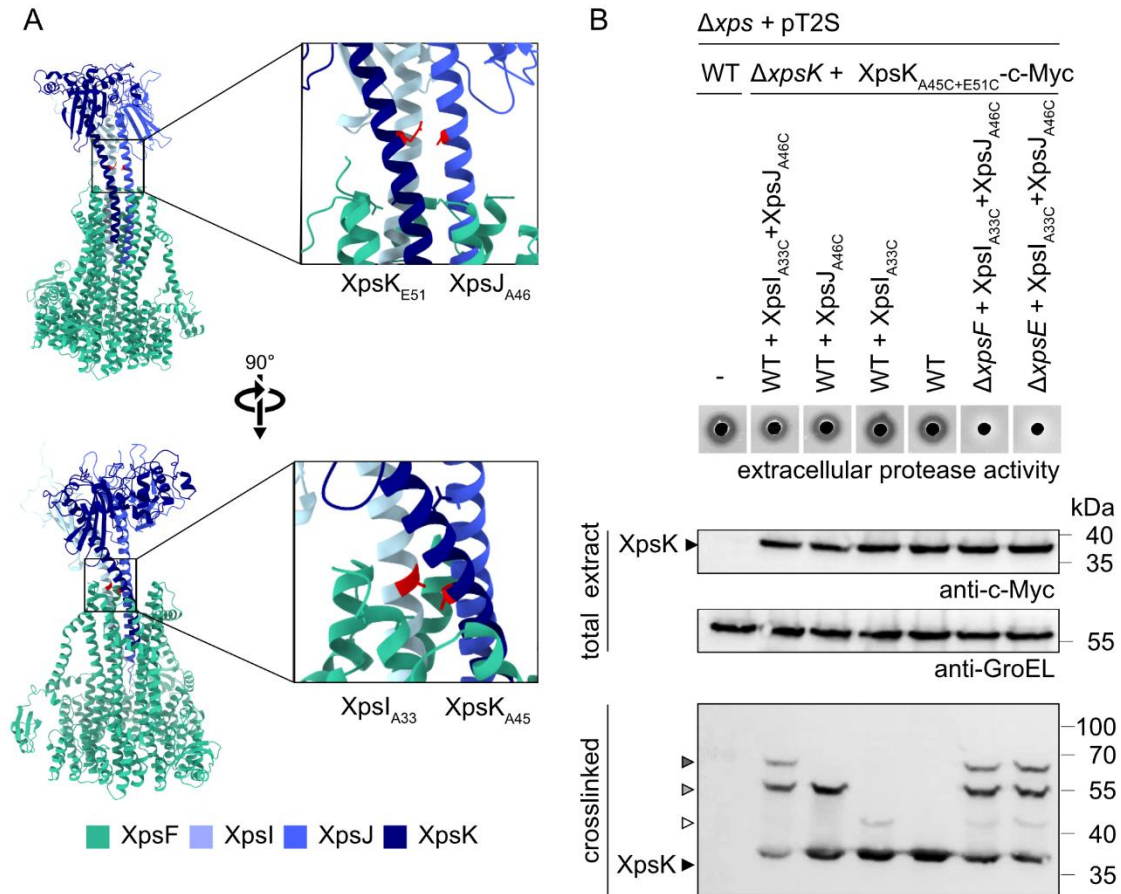


Figure 18: A trimeric XpsIJK complex assembles independently of XpsF and XpsE *in vivo*

A: Amino acids in XpsI, XpsJ and XpsK modelled to be in close proximity with each other are marked in red and were substituted for cysteines to enable crosslinking studies. B: Cysteine crosslinking experiments were performed with derivatives of strain 85-10 Δxps (Δxps) containing the wild-type (WT) modular T2S gene cluster (+pT2S) or derivatives encoding XpsK-c-Myc with alanine 45 and aspartic acid 51 substituted with cysteines and additional substitutions of alanine 33 in XpsI and/or alanine 46 in XpsJ or additional deletion of *xpsF* or *xpsE*, as indicated. Equal amounts of cell cultures grown in NYG medium were centrifuged, cells were either resuspended and boiled in Laemmli buffer (total extract) or incubated with copper chloride to facilitate disulfide bond formation and resuspended and boiled in Laemmli buffer lacking β -Mercaptoethanol (crosslinked). Proteins were analyzed by immunoblotting using antibodies specific to the c-Myc epitope or the bacterial chaperonin GroEL to ensure equal loading. Respective cysteine substitutions in XpsK, XpsI and XpsJ resulted in the formation of an XpsJ-K complex (45 kDa, white triangle), an XpsI-K around (55 kDa, light grey triangle) and a trimeric XpsI-J-K complex (65 kDa, dark grey triangle). Experiments were performed three times, and one representative dataset is shown.

4.1.14 XpsK interacts with XpsF as predicted

To further determine whether the XpsIJK trimer interacts with XpsF as predicted by Alphafold2, an amino acid pair at the interface of XpsF and XpsK were substituted for cysteine: threonine 401 in XpsF and alanine 45 in XpsK, respectively (Figure 19). For analysis of an XpsK-XpsF interaction, the previously constructed XpsK_{A45C+E51C}-c-Myc fusion and an XpsF_{T401C} derivative were used which enable the detection of complexes by immunoblotting. T2S functionality of these derivatives was verified using extracellular protease activity on milk plates (Figure 19).

After treatment with copper chloride, no unspecific XpsK_{A45C+E51C}-c-Myc complexes formed in absence a cysteine substitution in XpsF. However, a single cysteine substitution on XpsF_{T401C} resulted in the formation of two specific protein complexes, with one signal at 75 kDa and another, slightly weaker signal at 180 kDa. The 75 kDa complex corresponds in size to an XpsK_{A45C+E51C}-c-Myc-XpsF_{T401C} complex predicted at 82 kDa. Again, the aberrant migration pattern corresponds to the migration pattern of c-Myc-XpsF slightly below the expected molecular mass in Figure 16 and may be explained by the lack of β -Mercaptoethanol in the Laemmli buffer used for protein denaturation in this assay. The larger XpsK_{A45C+E51C}-c-Myc-XpsF_{T401C} specific complex cannot be directly identified but may arise from XpsF oligomerizing with a further interaction partner. Nevertheless, the cysteine crosslinking results with XpsK_{A45C+E51C}-c-Myc and XpsF_{T401C} very strongly suggest that an interaction between the hydrophobic region of XpsK and the channel interface of XpsF occurs *in vivo*, in agreement with *in silico* predictions.

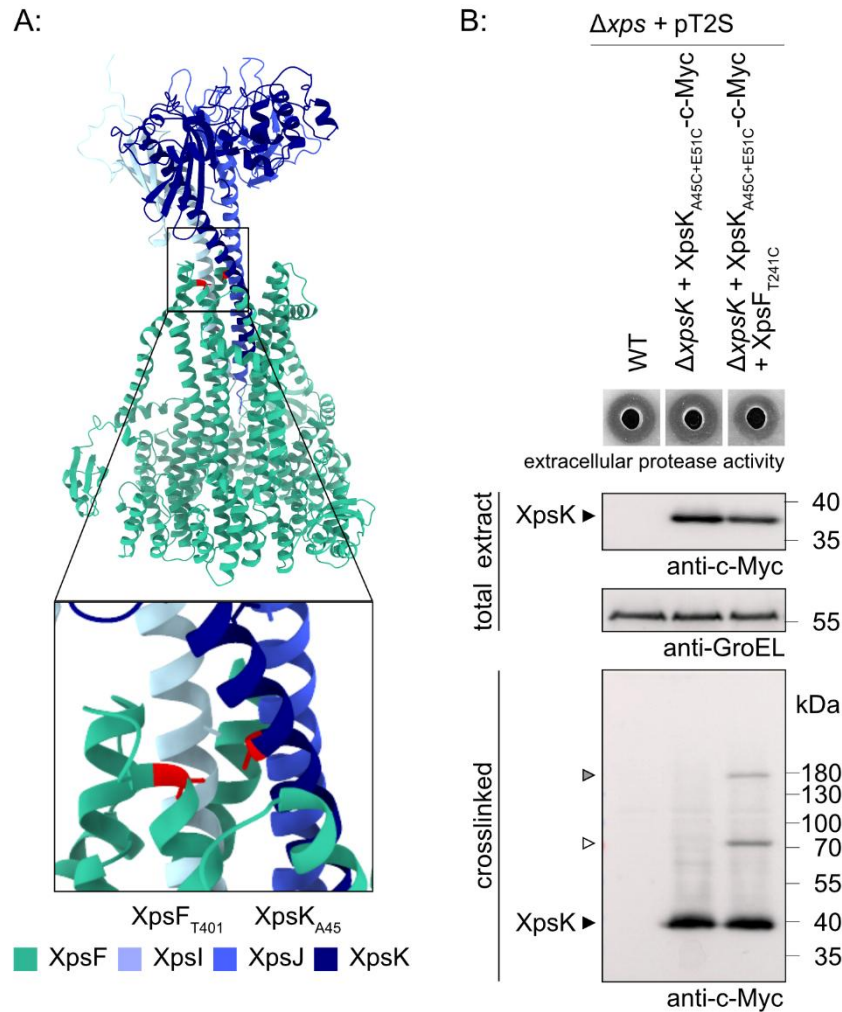


Figure 19: XpsK interacts with XpsF via the hydrophobic tail region

A: Amino acids in XpsK (A45) and XpsF (T401) modelled to be in close proximity with each other are marked in red and were substituted for cysteines to enable crosslinking studies. B: Cysteine crosslinking experiments were performed with derivatives of strain 85-10 Δxps (Δxps) containing the wild-type (WT) modular T2S gene cluster (+pT2S) or derivatives encoding XpsK-c-Myc with alanine 45 and aspartic acid 51 substituted with cysteines with and without an additional cysteine substitution of threonine 401 in XpsF, as indicated. Equal amounts of cell cultures grown in NYG medium were centrifuged, cells were either resuspended and boiled in Laemmli buffer (total extract) or incubated with copper chloride to facilitate disulfide bond formation and resuspended and boiled in Laemmli buffer lacking β -Mercaptoethanol (crosslinked). Proteins were analyzed by immunoblotting using antibodies specific to the c-Myc epitope or the bacterial chaperonin GroEL to ensure equal loading. Respective cysteine substitutions in XpsK and XpsF resulted in the formation of two specific complexes at around 75 kDa (white arrow) and additionally at 180 kDa (dark grey arrow). Experiments were performed thrice, and a representative dataset is shown.

4.1.15 Alphafold3 predictions suggest that XpsHIJK may form the tip of the extending pseudopilus and interact with T2S substrates

It has been suggested that the complex formed by homologues of XpsHIJK is pushed up from the inner membrane by many monomers of XpsG homologues oligomerizing underneath to form an extending pseudopilus structure (López-Castilla *et al*, 2017; Zhang *et al*, 2018). It is thought that the tip complex thus pushes substrates through the secretin channel as the pseudopilus extends (Zhang *et al*, 2018). To model what an extending pseudopilus could look like and to inspect possible substrate binding to the XpsHIJK pseudopilus tip, AlphaFold3 structural predictions of XpsH, XpsI, XpsJ, XpsK and 8 copies of XpsG as well as models of XpsH, XpsI, XpsJ, and XpsK with four different identified T2S substrates, XCV0965, XCV2571, XCV3406 and XCV3634, were generated (Figure 20, for identification of substrates see below, Figure 21 and Figure 22). While XpsH was not essential for T2S function (see Figure 15), it still was included in these models for completeness. A pseudopilus structure with 8 monomers of XpsG positioned under the XpsHIJK complex was predicted with an ipTM value of 0.67 and may be used as a reference for targeted cysteine crosslinking approaches in future studies. Furthermore, models with T2S substrates and the XpsHIJK complex consistently predicted interactions between substrates and XpsK (ipTM values between 0.56 and 0.68, see Figure 39), which may lay the foundation to characterize potential substrate binding sites in future studies. However, due to time restrictions, no experimental validation of these structural predictions was performed.

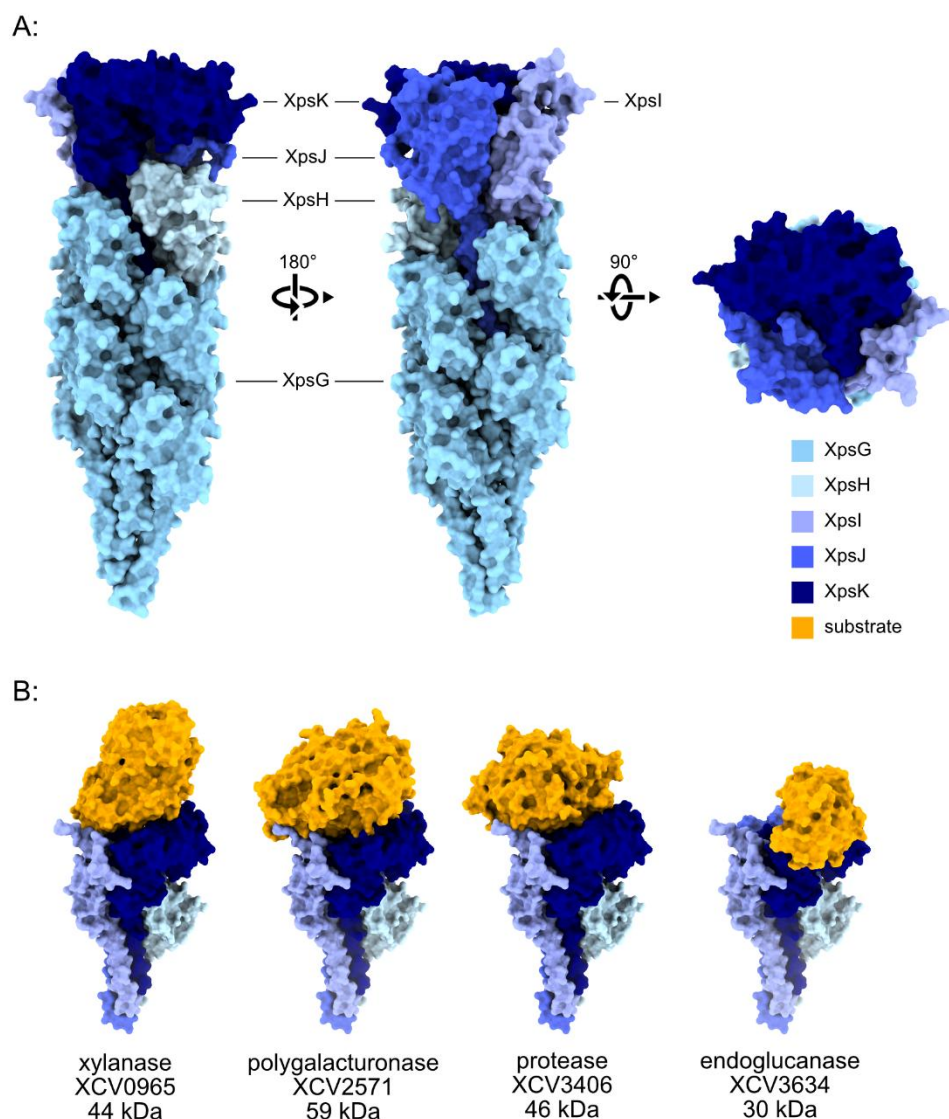


Figure 20: AlphaFold3 predictions of the XpsHIJK tip complex with XpsG and with T2S substrates

The structure of a pseudopilus complex consisting of XpsH, XpsI, XpsJ, XpsK and eight monomers of XpsG (A) or four different T2S substrates (XCV0965, XCV2571, XCV3406 and XCV3634; B) were predicted using the AlphaFold3 algorithm and visualized using UCSF ChimeraX. Proteins are represented in different colours as indicated. The expected prediction errors and pLDDT values are shown in Figure 39 (appendix).

4.2 Function of T2S substrates

4.2.1 *In planta* identification of novel T2S substrates

Thus far, only two xylanases, one esterase and a protease have been characterized as substrates of the Xps-T2S system in *Xe* (Solé *et al*, 2015; Szczesny *et al*, 2010). Previous screens involved overexpression of candidate substrates with a *lac* promoter and secretion assays cells growing in artificial NYG medium rather than *in planta*, and most proteins tested in this manner were secreted in a T2S-independent manner (Szczesny *et al*, 2010; Solé *et al*, 2015). This may be an artefact due to experimental conditions caused by leakage of overexpressed proteins through the outer membrane of rapidly growing cells or due to extracellular vesicles containing overexpressed proteins.

Therefore, a more native assay was employed to characterize T2S substrates expressed and secreted in the native *in planta* setting. Tomato plants were dip infected with *Xe* wild-type and *xps* deletion strains and apoplastic fluid was harvested three days after infection by vacuum infiltration and centrifugation. Soluble proteins were then precipitated in acetone and characterized by mass spectrometry, in collaboration with Jessica Erickson and Susanne Matschi (Leibniz Institute for Plant Biochemistry, Halle). Proteins that are secreted via the Xps-T2S system should be lacking or less abundant samples infected with an *xps* deletion strain compared to the wild-type. Of all *Xanthomonas* proteins detected in infected plants, a total of 23 proteins were less abundant in the apoplast of plants infected with the *xps* deletion strain than in plants infected with the wild-type strain, as shown in Figure 21. These included seven putative proteases and nine carbohydrate-degrading enzymes, including predicted CWDEs such as xylanases, cellulases, polygalacturonases, as well as the lytic transglycosidase HpaJ, potentially involved in remodeling of the bacterial cell wall in T3S system assembly (Hausner *et al*, 2017). Aside from one adhesin, all the identified proteins contained a predicted Sec- or Tat-signal for translocation into the periplasm and were therefore likely T2S substrates. Three proteins were previously identified as T2S substrates: XCV4358, XCV3671 and XCV3013 (Solé *et al*, 2015; Szczesny *et al*, 2010; Siebert, 2019).

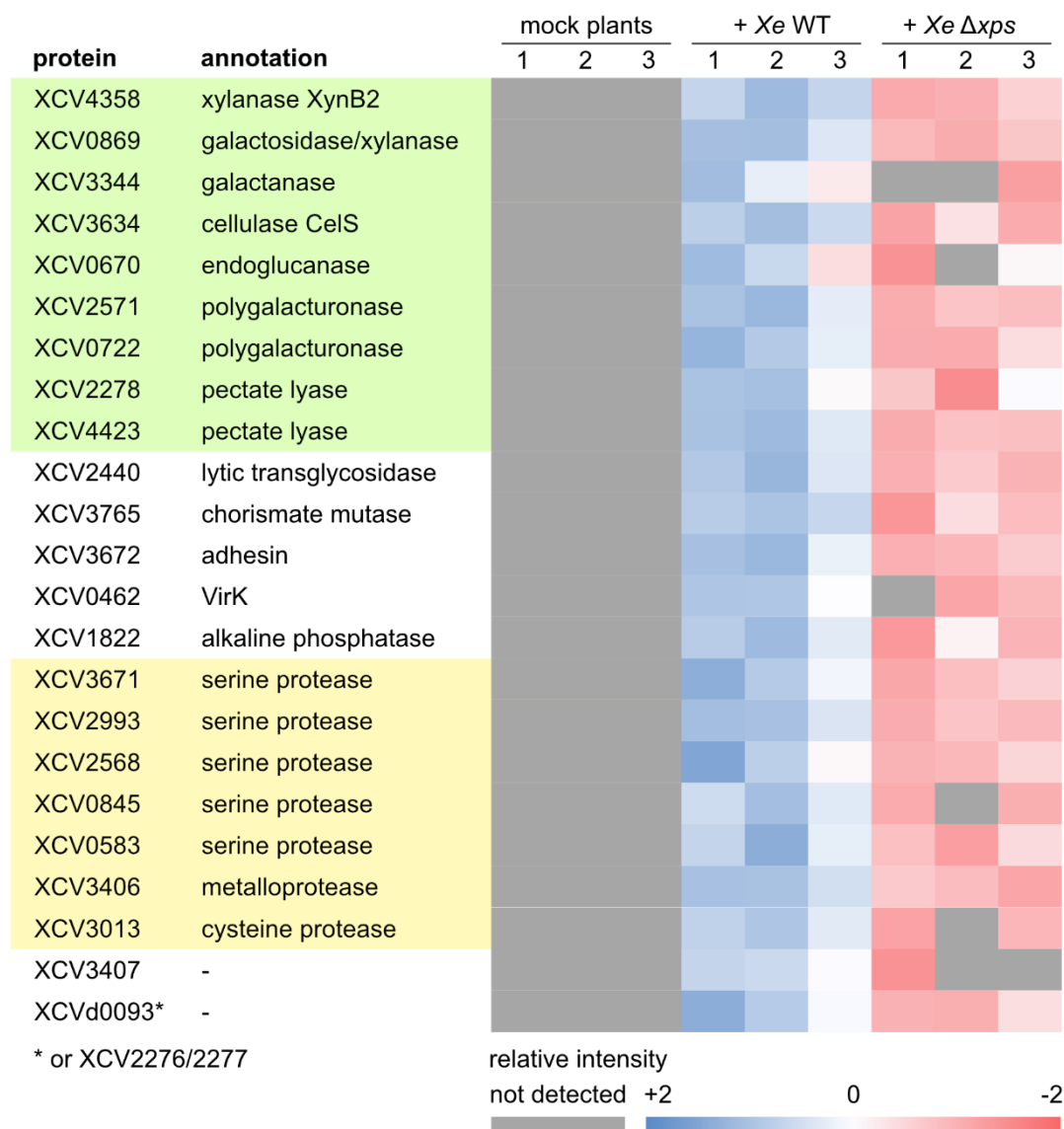


Figure 21: Apoplastic *X. euvesicatoria* proteins reduced in an *xps* mutant

Apoplastic wash fluid from Moneymaker tomato plants infected with wild-type *X. euvesicatoria* strain 85-10 (WT) and a T2S mutant (Δxps) as well as from mock treated plants were quantified using LC-MS/MS. *Xanthomonas* proteins more abundant in WT samples than in Δxps samples as well as GO-annotations and relative intensities of detected unique peptides are shown (blue: high intensity, red: low intensity), predicted proteases are highlighted in yellow and carbohydrate degrading enzymes in green.

Analysis of *in planta* bacterial growth suggested that the *xps* deletion strain grew significantly less than the wild-type (Jessica Erickson, data not shown). Therefore, lower protein abundance in the apoplast may be caused by reduced growth of the *xps* deletion strain, not necessarily due to reduced secretion, and additional verification of candidate substrates was required. To this end, an *in vitro* secretion assay with C-terminal c-Myc-fusions of candidate substrates was modified from Szczesny (Szczesny *et al*, 2010) to more closely resemble native *in planta* conditions. Instead of rich NYG medium, bacteria were cultured in XVM2 medium mimicking plant apoplast conditions and c-Myc-tagged candidate substrates were expressed under their native *Xe* promoters, rather than overexpressed from a *lac* promoter. A

similar approach previously identified the predicted protease XCV3013 as a T2S substrate (Siebert, 2019).

Of the candidate proteins from Figure 21, one xylanase (XCV4358) and six novel T2S substrate candidates were tested in this way: two predicted celluloses (XCV0670 and XCV3634), two putative polygalacturonases (XCV0722 and XCV2571), a predicted metalloprotease (XCV3406) and a protein of unknown function (XCV3407). Secretion assays with the polygalacturonases and xylanase were performed by Akash Shivhare (Shivhare, 2023), and secretion assays of the proteases and the cellulose XCV3634 were performed by Iliyana Kraveva (Kraveva, 2024). All seven T2S substrate candidates were stably expressed and detected in the culture total extracts and supernatants (Figure 22). Furthermore, all seven T2S substrate candidates were significantly less abundant in culture supernatants of the Δxps mutant compared to the wild-type. No GroEL signal was detected in the supernatants, indicating that the detected proteins were not caused by leakage due to cell lysis. Furthermore, these proteins were not reduced in abundance in the total extracts from the Δxps mutant compared to the wild-type, and for XCV3406, XCV3634, XCV0670 and XCV4358, protein abundance was increased in the total extract of the Δxps mutant. Taken together, this suggests that all seven tested proteins are indeed secreted via the Xps-T2S system, as their abundance in culture supernatants is strongly reduced Δxps mutant, while their respective expression in the total extract is not.

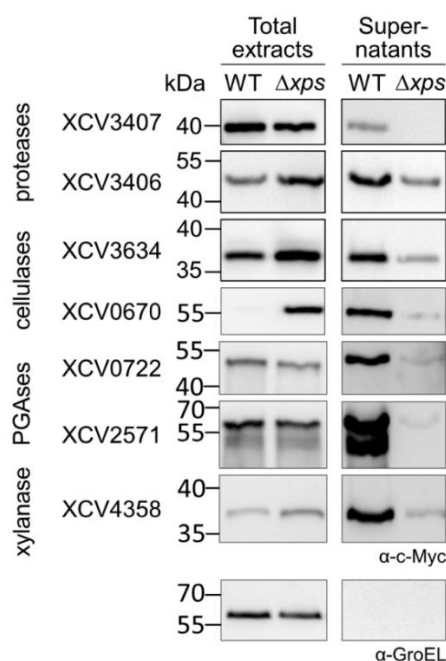


Figure 22: *In vitro* verification of novel *X. euvesicatoria* Xps-T2S substrates

Seven C-terminal c-Myc-fusions of potential T2S substrates were expressed under respective native promoters in Xe 85-10 wild-type (WT) and a T2S mutant (Δxps). Secretion assays were performed in XVM2 media and protein abundance from total cell extracts (total extract) and filtered supernatant (supernatant) were compared by SDS-PAGE and immunoblotting with a c-Myc antibody. As lysis control, the cytoplasmic chaperonin GroEL was detected.

4.2.2 Multiple T2S secreted proteins have proteolytic activity

Structural predictions of the T2S substrate XCV3407 revealed conformational similarities with glutamic proteases such as fungal aspergilloglutamic peptidases, plant-derived neprosins and bacterial scytalidoglutamic peptidases (del Amo-Maestro *et al*, 2022; Kondo *et al*, 2010). To evaluate proteolytic activity of this protein as well as other predicted proteases, a simple assay exploiting the previously reported leakage of periplasmic proteins through the outer membrane of *E. coli* BL21 cells was employed (Zou *et al*, 2012). BL21 cells overexpressing candidate proteins under a *lac* promoter with native Sec- or Tat-signals for translocation into the periplasm were cultured on milk plates. As periplasmic proteins leak through the outer membrane in this *E. coli* strain, these proteins should be released into the extracellular environment where proteolytic degradation of milk proteins would lead to halo formation. This assay was performed with the potential glutamic protease XCV3407, the predicted metalloprotease XCV3406, cysteine protease XCV3013, or the serine proteases XCV3671 and XCV0845 and the predicted polygalacturonase XCV0722 as a negative control (Figure 21). BL21 cells expressing each of the five tested potential proteases led to varying degrees of halo formation, most prominent for the putative serine protease 3671 (Figure 23). No halo formation was detected for a negative control expressing the polygalacturonase XCV0722, indicating that halo formation by BL21 cells was not caused by endogenous proteases. Results were reproduced by Iliyana Krалева (Krалева, 2024).

Structural predictions of XCV3671 suggest that identified a putative active site formed by a typical serine protease catalytic triad composed of serine 448, histidine 258 and aspartate 195 (Figure 24). To experimentally determine whether this serine residue is involved in proteolytic activity, an XCV3671-construct with an alanine substitution of serine 448 generated by Jessica Erickson was tested in BL21 cells together with the other proteases. Cells expressing this variant formed severely reduced halos compared to those with wild-type XCV3671, indicating that serine 448 is functionally important for this serine protease.

It must be noted that this assay only tests for relatively unspecific degradation of milk proteins, composed mostly of casein, and in LB medium at a neutral pH. This does not adequately represent the activity of these proteases when degrading on specific target proteins in the plant apoplast which is slightly acidic in nature (Geilfus, 2017). Additionally, even though all proteins were expressed from the same *lac* promoter in BL21 cells, there may still be differences in their stability that may lead to differing halo sizes. Therefore, deducing the relative proteolytic activity without comparing the stability of different putative proteases by immunoblotting is not possible. Nevertheless, the halo formation in this assay is indicative of proteolytic activity of these five extracellular putative proteases from *Xe*.

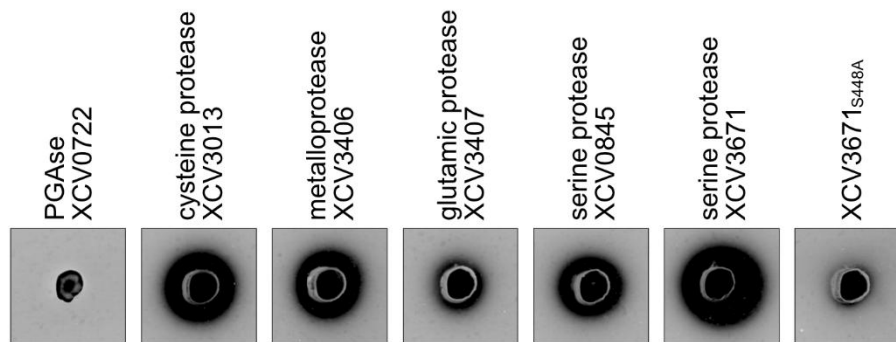


Figure 23: five extracellular proteases from *X. euvesicatoria* show proteolytic activity

Five extracellular putative proteases from *X. euvesicatoria* with their respective Sec-signal were overexpressed under a *lac* promoter in *E. coli* BL21 Star™ (DE3) cells with reported leakage of periplasmic proteins through the outer membrane. Strains were cultured on LB plates containing 2% skim milk powder overnight. Extracellular proteolytic activity resulted in formation of a transparent halo and was specific to XCV3013, XCV3406, XCV3407, XCV0845 and XCV3671. Furthermore, degradation of milk protein was severely impaired for an S448A variant of XCV3671.

4.2.3 The T2S-dependent serine protease XCV3671 requires autocatalytic cleavage for secretion and oligomerization

The serine protease XCV3671 was previously demonstrated to be involved in *in planta* virulence and to form SDS-stable complexes after T2S (Solé *et al*, 2015). This protease is encoded adjacent to the adhesin XadA (XCV3672) directly upstream of the *xps* gene cluster in *X. euvesicatoria*. This appears to be a conserved feature, as homologous proteases, adhesins and *xps* gene clusters are encoded in the same orientation in *Xcc*, *Xag* and even distantly related species such as *Stenotrophomonas maltophilia* strain K279a (Figure 24). Structurally, this serine protease is composed of three relatively distinct domains: an N-terminal domain (1-150) comprised of three α -helices and four β -strands, a central domain (151-527) containing the predicted active site with the catalytic triad composed of an aspartic acid (D195), a histidine (H258) and a serine (S448), and an additional C-terminal domain (528-627) formed by seven β -strands (see Figure 24). To gain insights into the role of each domain of XCV3671 in T2S and oligomerization upon secretion, secretion assays were performed in XVM2 medium as described above (Figure 24) with C-terminally c-Myc epitope-tagged wild-type XCV3671 as well as variants lacking the C-terminal domain (XCV3671 $_{\Delta 528-627}$), lacking the N-terminal domain but retaining the native signal peptide (XCV3671 $_{\Delta 31-150}$) or a carrying a serine to alanine substitution at the catalytic triad of the protease (XCV3671 $_{S448A}$).

In the total extract of cultures, the wild-type XCV3671-c-Myc formed only a faint signal at the expected molecular mass of 69 kDa but a much stronger signal was detected at 55 kDa, and only the 55 kDa signal was detected in the culture supernatant, together with the 100 kDa oligomer formed by XCV3671 upon secretion. Similarly, only a faint signal was detected at

the expected mass of 57 kDa and a much more prominent signal was observed at 45 kDa in total bacterial extracts for XCV3671_{Δ528-627}-c-Myc, lacking the C-terminal domain. Again, only the smaller 45 kDa signal was detected in the culture supernatant, together with a 70 kDa signal corresponding to an oligomer formed upon secretion. For both XCV3671-c-Myc and XCV3671_{Δ528-627}-c-Myc, detection in the supernatant was severely reduced in the *Δxps* mutant strain. Samples with XCV3671_{Δ31-150}, the derivative containing the predicted Sec-signal for translocation into the periplasm but with a deletion of the N-terminal domain, showed a prominent signal at the expected mass of 55 kDa, at the same size as the signal detected in the wild-type XCV3671-c-Myc. However, XCV3671_{Δ31-150} was not detected in the culture supernatant. In contrast to the wild-type XCV3671, a signal for XCV3671_{S448A} was detected with a mass of the unprocessed full-length protein at 69 kDa but was also not detected in the culture supernatant. This may be interpreted to suggest that XCV3671 is autocatalytically processed in the periplasm, cleaving the N-terminal domain prior to secretion (thereby forming the 55 kDa signal). Nevertheless, the N-terminal domain has some important role in the secretion process, as XCV3671_{Δ31-150} lacking this domain was no longer detected in the culture supernatant. The function of the C-terminal domain remains unclear, as it is neither required for secretion nor subsequent oligomerization.

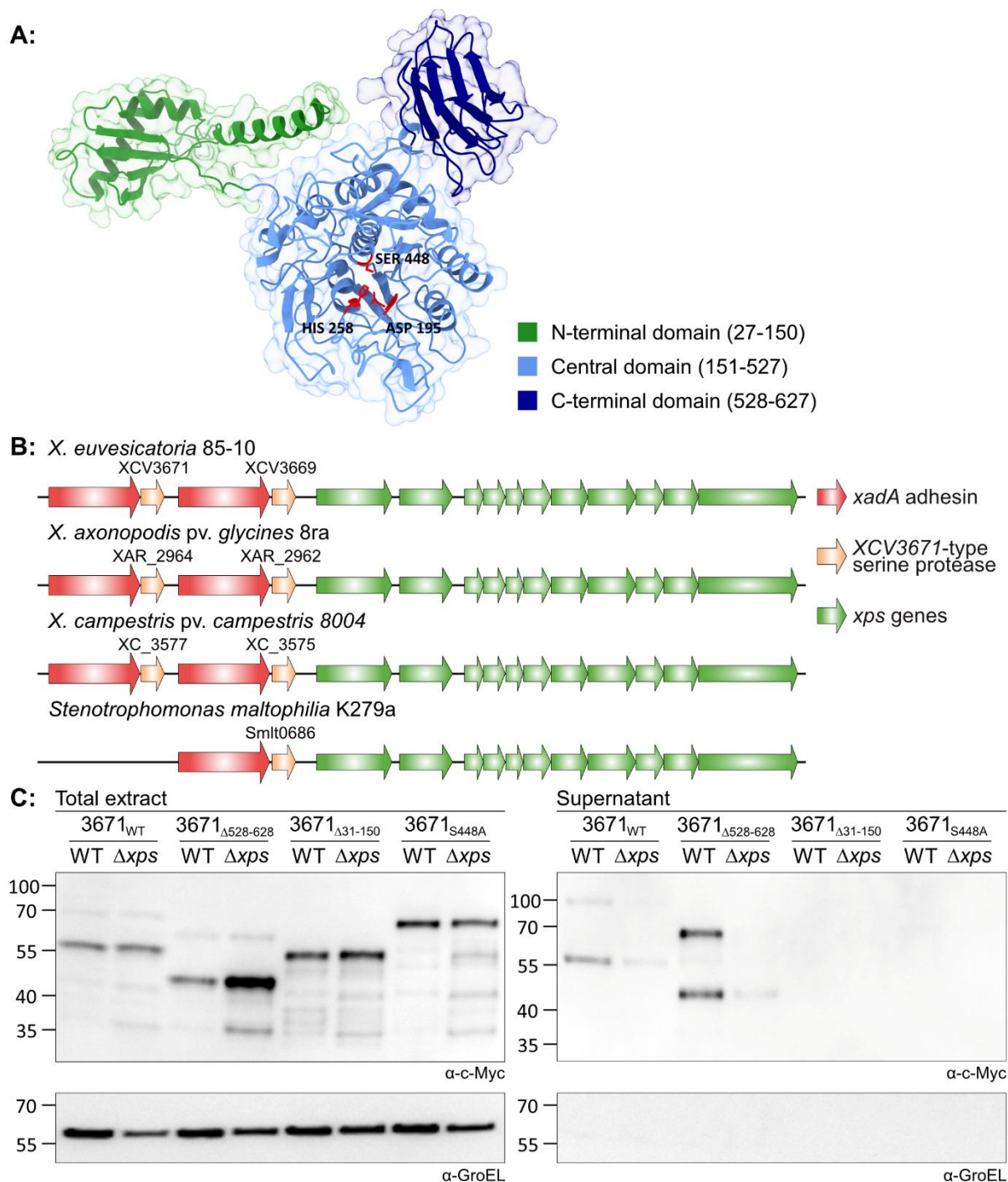


Figure 24: Autocatalytic cleavage of the N-terminal domain of XCV3671 is required for T2S

A: An AlphaFold2 predicted structure of XCV3671 highlighting the N-terminal domain (green), the central domain (light blue) and the C-terminal domain (dark blue), as well as the predicted active site comprised of aspartic acid 195, histidine 258 and serine 448. N-terminal Sec-signal peptides cleaved upon translocation into the periplasm are not shown in this model. B: XCV3671-type proteases are encoded adjacent to adhesins and *xps* gene clusters in *Xe*, *Xag*, *Xcc* and the distantly related *Stenotrophomonas maltophilia* K279a. C: Variants of the T2S serine protease XCV3671 (WT: wild-type, $\Delta 31-150$: deletion of the N-terminal domain, $\Delta 528-627$: deletion of the C-terminal domain, S448A: catalytic mutant) were expressed under the native promoter with a C-terminal c-Myc tag in *X. euvesicatoria* 85-10 wild-type (WT) and a T2S mutant (Δxps). Secretion assays were performed in XVM2 media and protein abundance from total cell extracts (total extract) and filtered supernatant (supernatants) were compared by SDS-PAGE and immunoblotting with a c-Myc antibody. As a lysis control, the cytoplasmic chaperonin GroEL was used. All experiments were performed three times and a representative dataset is shown.

4.2.4 Virulence and protease secretion of the Xps-T2S system are conserved in different *Xanthomonas* species

The Xps-T2S system of members of the *Xanthomonas* genus is involved in the secretion of CWDEs and proteases (Ryan *et al*, 2011). To enable a more thorough investigation of the role of this secretion system in different species of *Xanthomonas* pathogens, the entire *xps* gene cluster was deleted in three different species: the closely related non-vascular pathogens *X. euvesicatoria* (host plants: *Solanum lycopersicum* and *Capsicum annuum*) and *X. axonopodis* pv. *glycines* (host plant: *Glycine max*) as well as the more distantly related vascular pathogen *X. campestris* pv. *campestris* (host plants: Brassicaceae) (Vieira *et al*, 2021; Ryan *et al*, 2011). In agreement with previous findings, an *xps* deletion led to reduced extracellular protease activity in all *Xanthomonas* strains and reduced virulence *in planta* for *Xe* and *Xag*. A plasmid-borne modularized *xps* gene cluster from *Xe* restored extracellular protease activity and *in planta* virulence in all strains (Figure 25). This indicates that the Xps-T2S system from *Xe* can cross-complement in *Xag* and *Xcc*, although in *Xcc*, extracellular protease activity with the *Xe xps* gene cluster was lower with the native system. As *A. thaliana* Col-0 plants are not susceptible to *Xcc* due to an ETI response to the T3S effector AvrAC from *Xcc* (Xu *et al*, 2008), an *Xcc* $\Delta avrAC \Delta xps$ double mutant was generated but *in planta* virulence assays were not yet performed due to time restrictions. Nevertheless, deletions in *xps* genes were shown to reduce *in planta* virulence of *Xcc* in previous studies (Luneau *et al*, 2022; Chen *et al*, 1996; Wang *et al*, 2008).

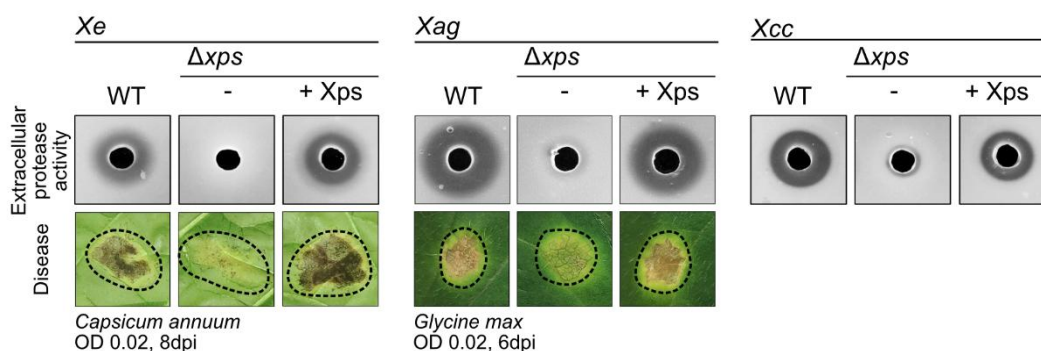


Figure 25: The T2S system contributes to extracellular protease activity and virulence in *Xanthomonas*

Wild-type *X. euvesicatoria* (*Xe*) strain 85-10, *X. axonopodis* pv. *glycines* (*Xag*) strain 8ra and *X. campestris* pv. *campestris* (*Xcc*) strain 8004 and respective T2S deletion mutants (Δxps) with (+Xps) or without (-) the modular *xps*-T2S expression construct from *Xe* were analyzed for bacterial virulence and extracellular protease activity. Bacteria were infiltrated at a density of 2×10^7 CFU ml⁻¹ into leaves of susceptible pepper plants (symptoms documented at 8 dpi) or soya plants (symptoms documented at 6 dpi). Dashed lines indicate the infiltrated areas. For the analysis of extracellular protease activity, bacteria were grown on 2% milk plates for 2 days and halo formation was documented. Bacteria were removed from the holes prior to documentation. Experiments were performed at least three times; one representative dataset is shown.

4.2.5 T2S enables utilization of amino acids from extracellular proteins

Nearly all T2S substrates from *Xanthomonas* species identified thus far are degradative enzymes such as CWDEs and proteases (Solé *et al*, 2015; Szczesny *et al*, 2010; Wang *et al*, 2008). Thus, the question arose whether the secreted proteases may degrade extracellular proteins to fuel bacterial metabolism. To test this, the Xe, Xag and Xcc strains described above were grown on modified XVM2 medium in which free amino acids were replaced with undigested proteins from skim milk powder which must be degraded by the bacteria to support growth (Figure 26). XVM2 medium was used as it mimics the biochemical composition of the apoplastic environment and was previously used for minimal growth experiments (Vieira *et al*, 2021).

Xe, Xag and Xcc could all metabolize amino acids from unprocessed milk as significant growth was detected in XVM2 milk powder medium. However, *xps* deletion mutants in each of these strains displayed a severe reduction in growth, which was restored upon expression of the Xps-T2S system from Xe (see Figure 26). This demonstrates that T2S substrates enable the utilization of amino acids from extracellular proteins.

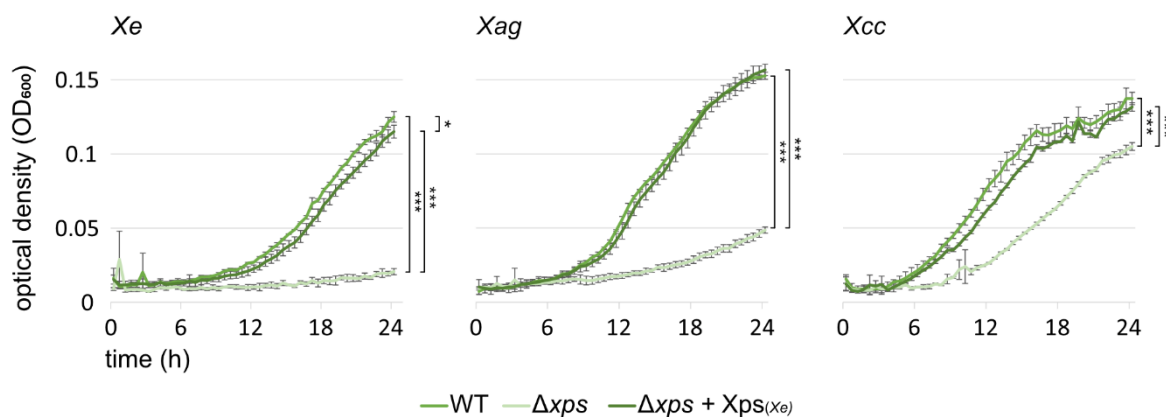


Figure 26: Xps-T2S allows for utilization of amino acids from extracellular proteins

Wild-type *X. euvesicatoria* (Xe) strain 85-10, *X. axonopodis* pv. *glycines* (Xag) strain 8ra and *X. campestris* pv. *campestris* (Xcc) strain 8004 and respective T2S deletion mutants (Δxps) with (+Xps) or without (-) the modular *xps*-T2S expression construct from Xe were grown on XVM2 medium containing 0.03% skim milk powder as the sole amino acid source. Cultures were inoculated with a bacterial density of 2×10^7 CFU ml⁻¹ and monitored for 24h. In all three strains, *xps* deletions showed drastically reduced growth, but growth was restored upon expression of the Xps-T2S system from Xe. Statistically significant differences were determined using one-way ANOVAs with post-hoc Tukey-HSD (P<0.05: "*" P<0.01: "**" P<0.001: "***") Experiments were performed at least three times; one representative dataset is shown.

4.2.6 *Xanthomonas* infection alters plant cell wall composition in a T2S-dependent manner

As T2S substrates include many CWDEs, degradation of the plant cell wall is typically linked to T2S in plant pathogens. However, direct effects of T2S on plant cell wall architecture have not been studied. The cell wall is composed of a very complex polysaccharide network. A

rudimentary characterization of the plant cell wall is the relative quantification of the carbohydrate monomers that make up the complex network cell wall polysaccharides. To this end, alcohol insoluble residue (AIR) containing the cell wall matrix was isolated from plants by extracting and removing soluble short-chain sugars and metabolites soluble in ethanol. Subsequently the polysaccharides are subjected to acid hydrolysis and the resulting monosaccharides are identified and quantified by high-pressure anion-exchange chromatography with pulsed-amperometric detection (HPAEC-PAD). As non-cellulosic glucose originating from hemicelluloses and pectins cannot be differentiated from plant starch, it was therefore not considered in subsequent analyses of plant cell wall carbohydrates. When plant material infected with bacteria is analyzed in this experimental setup, differentiation between monosaccharides derived from plant cell walls and alcohol insoluble bacterial exopolysaccharides is not possible. A characteristic feature of *Xanthomonas* bacteria is the production of an abundant extracellular polysaccharide called xanthan composed of glucose, mannose, and glucuronic acid residues in the molar ratio 2:2:1 (Bhat *et al*, 2022).

Entire pepper leaves were syringe inoculated with either the Xe 85-10 wild-type, the Xe 85-10 Δ xps, Xe 85-10 Δ xps expressing the modular T2S gene cluster or mock-treated with magnesium chloride. Five days after inoculation, at the onset of disease symptoms, *in planta* bacterial growth was quantified and AIR containing the cell wall matrix was extracted. AIR samples subsequently underwent acidic hydrolysis yielding carbohydrate monomers that were quantified using high-pressure liquid anion-exchange chromatography with pulsed amperometric detection in collaboration with Timo Engelsdorf and Kristina Munzert (Philipps-University Marburg). Results are shown in Figure 27, a principal component analysis (PCA) showing the clustering of monosaccharide composition of different treatments is shown in Figure 40 (appendix).

Mannose and glucuronic acid levels are typically relatively rare in plant cell walls, which was also seen in non-inoculated samples (Menna *et al*, 2020; Kleuter *et al*, 2024). Plants infected with Xe showed significantly elevated levels of mannose and glucuronic acid compared to non-inoculated samples, indicating a significant presence of bacterial xanthan, correlating with the bacterial density measured at the time of sampling (Figure 27 B and C).

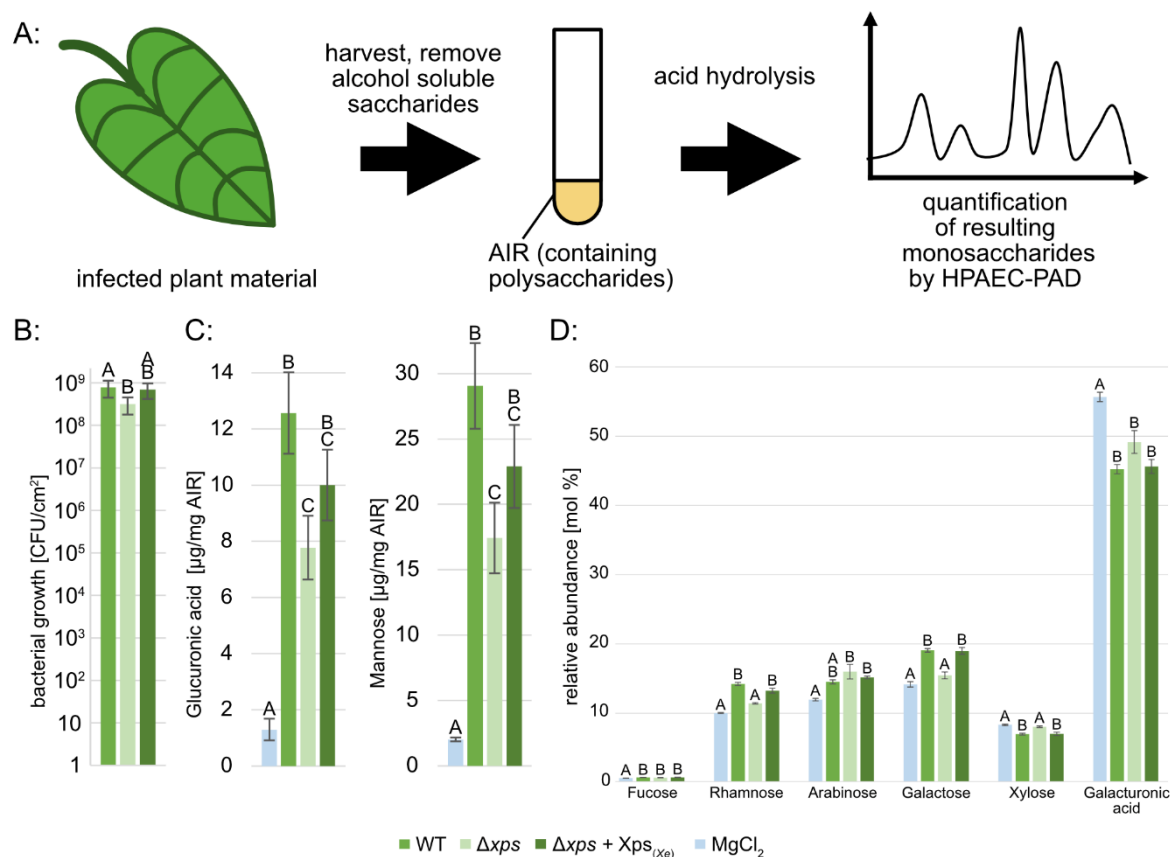


Figure 27: Plant cell wall monosaccharide composition is altered in an Xps-dependent manner during infection

Plants were either infected with wild-type *X. euvesicatoria* strain 85-10 (normal green) and T2S deletion mutants (Δxps) without (light green) or with the modular *xps*-T2S expression construct (+Xps_(Xe), dark green), at a bacterial density of 2×10^7 CFU ml⁻¹ or mock-treated (light blue). A: The experimental workflow to characterize polysaccharides is depicted: alcohol insoluble-residues (AIR) containing complex carbohydrates were isolated and non-cellulosic carbohydrates characterized in monosaccharide composition after acid-hydrolysis by HPAEC-PAD. B: *In planta* bacterial colonization was monitored 5 days after infection, at the time of plant sampling. C: The abundance of mannose and glucuronic acid of non-cellulosic carbohydrates from AIR is significantly increased in plants infected with *X. euvesicatoria*, and correlates with in planta bacterial growth (shown in B). This is indicative of extracellular Xanthan produced by *Xanthomonas* in large quantities which consists of glucose, mannose and glucuronic acid. D: The relative abundance of non-cellulosic plant cell wall carbohydrates is shown in molar percentages (excluding mannose, glucose and glucuronic acid). Non-cellulosic glucose could not be differentiated from starch and is not shown. The relative monosaccharide composition significantly differs between mock treated plants and plants infected with the wild-type strain. The relative monosaccharide composition of plants infected with T2S deletion mutants (Δxps) clustered more like mock-treated plants in rhamnose, galactose and xylose contents, and the complemented strain clustered identical to the wild-type strain (Figure 40). Statistically significant differences were determined using one-way ANOVAs with post-hoc Tukey-HSD (for A and B: $P < 0.05$; for C: $P < 0.01$). Experiments were performed thrice with at least four technical replicates; one representative dataset is shown.

The relative monosaccharide composition of the cell wall significantly differed between mock treated plants and plants infected with the Xe 85-10 wild-type, with an infection with the wild-type strain leading to significantly lower relative xylose and galacturonic acid contents and higher relative rhamnose, galactose, arabinose and fucose contents. The relative monosaccharide composition of plants infected with Xe 85-10 Δxps clustered more like mock-treated plants in rhamnose, galactose and xylose contents and had a slightly increased galacturonic acid content compared to the wild-type treated plants. The T2S deletion strain

with a plasmid-borne modularized *xps* gene cluster (Δxps +Xps) grouped identical to the wild-type strain (compare Figure 40, appendix).

One factor that may contribute to the significantly altered cell wall composition of plants infected with Xe 85-10 Δxps compared to plants infected with wild-type Xe 85-10 may be the slightly reduced *in planta* growth of 85-10 Δxps at the time of sampling. Nevertheless, the difference in growth between 85-10 Δxps and 85-10 Δxps with a plasmid-borne modularized *xps* gene cluster was insignificant, while the differences in plant cell wall composition between these strains were highly significant. This suggests that beyond differences in *in planta* growth of Xe, the presence or absence of the Xps-T2S system itself contributes to changes in plant cell wall architecture. These changes in cell wall monosaccharide composition were quantified in relative contents. Thus, the observed plant cell wall modifications could either be due to a decrease of galacturonic acid and xylose, or alternatively due to an increase in rhamnose, galactose, arabinose and fucose in plants challenged with Xe with a functional Xps-T2S system. Given the finding that the Xps-T2S secretes polygalacturonases and xylanases into the plant apoplast (Figure 21), enzymatic degradation of cell wall pectic polysaccharides containing galacturonic acid and hemicellulosic polysaccharides containing xylose presents one plausible explanation of the observed differences in plant cell wall monosaccharide contents.

4.2.7 Cell wall carbohydrates are utilized by *Xanthomonas* in a T2S dependent manner

To elucidate whether carbohydrates released in the breakdown of the plant cell wall are also utilized as nutrients by *Xanthomonas*, minimal growth experiments in modified XVM2 medium were performed, as in 4.2.5. To this end, the sucrose and fructose carbohydrate sources in XVM2 medium were replaced with either isolated plant cell walls or the complex oligomeric cell wall carbohydrates cellulose, xylan or pectin (Figure 28 and Figure 29).

All three *Xanthomonas* strains, Xe, Xag and Xcc grew on plant cell wall extracts as a sole carbohydrate source (Figure 28). As with protein utilization, cell wall utilization was T2S-dependent, as there was significantly less growth of Δxps mutants for all *Xanthomonas* species growing on cell wall extracts, a phenotype that was restored in all mutants upon expression of the Xps-T2S system from Xe. Growth differences between *Xanthomonas* species were visible, with Xe generally growing less than Xag and Xcc. However, growth for each *Xanthomonas* species was comparable between cell wall extracts from the host plants *S. lycopersicum*, *G. max* and *A. thaliana*. This suggests that the bacterial utilization of cell wall carbohydrates is not highly adapted to host-specific cell wall architecture. Despite some variance between the cell wall extracts of different host plants, the relative monosaccharide

composition was roughly comparable. Cellulosic glucose and galacturonic acid were most abundant (roughly 35-50% and 20%, respectively), followed by arabinose, galactose and xylose (roughly 10% each), and lower levels of rhamnose, mannose, fucose and glucuronic acid.

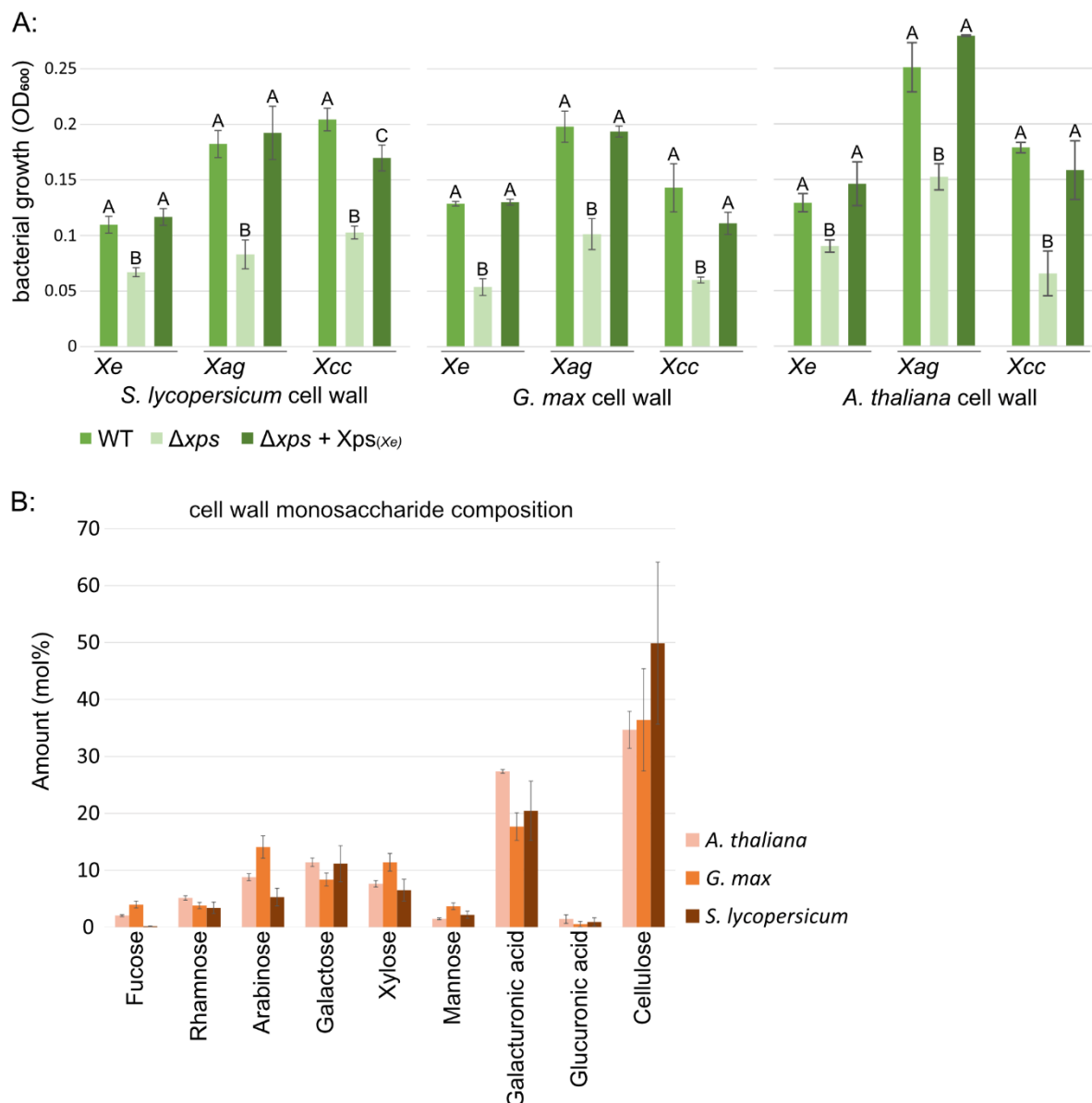


Figure 28: *Xanthomonas* utilization of cell wall carbohydrates depends on the Xps-T2S

A: Wild-type *X. euvesicatoria* (Xe) strain 85-10, *X. axonopodis* pv. *glycines* (Xag) strain 8ra and *X. campestris* pv. *campestris* (Xcc) strain 8004 and respective T2S deletion mutants (Δxps) with (+Xps) or without (-) the modular xps-T2S expression construct from Xe were grown on XVM2 medium containing cell wall extracts from *Solanum lycopersicum*, *Glycine max* or *Arabidopsis thaliana* as the sole carbohydrate source. Cultures were started with a bacterial density of 2×10^7 CFU ml⁻¹ and quantified after 24h of growth. In all three strains, xps deletions showed drastically reduced growth, but growth was restored upon expression of the Xps-T2S system from Xe. Statistically significant differences were determined using one-way ANOVAs with post-hoc Tukey-HSD ($P < 0.05$). Experiments were performed at least three times; one representative dataset is shown. B: The relative monosaccharide composition of the cell wall extracts employed for growth experiments was quantified by HPAEC-PAD and is shown in molar percentages. Non-cellulosic glucose could not be differentiated from starch and is not shown.

Next, the question arose which components of the plant cell wall are preferentially utilized by *Xanthomonas*: cellulose, hemicelluloses or pectin, as T2S substrates are predicted to degrade all three classes of polysaccharides (Figure 21). Furthermore, characterization of pepper cell walls suggested that xylose- and galacturonic acid-containing carbohydrates are removed from the plant cell wall by *Xanthomonas* (see 4.2.6). Therefore, Xe, Xag and Xcc were grown on minimal medium with representative commercial polysaccharides from plant cell walls as a sole carbohydrate source: carboxymethylcellulose as a cellulosic source, xylan from corn cob as a hemicellulose with a large xylose content and citrus peel pectin as a natural source of galacturonic acid. Results are shown in Figure 29.

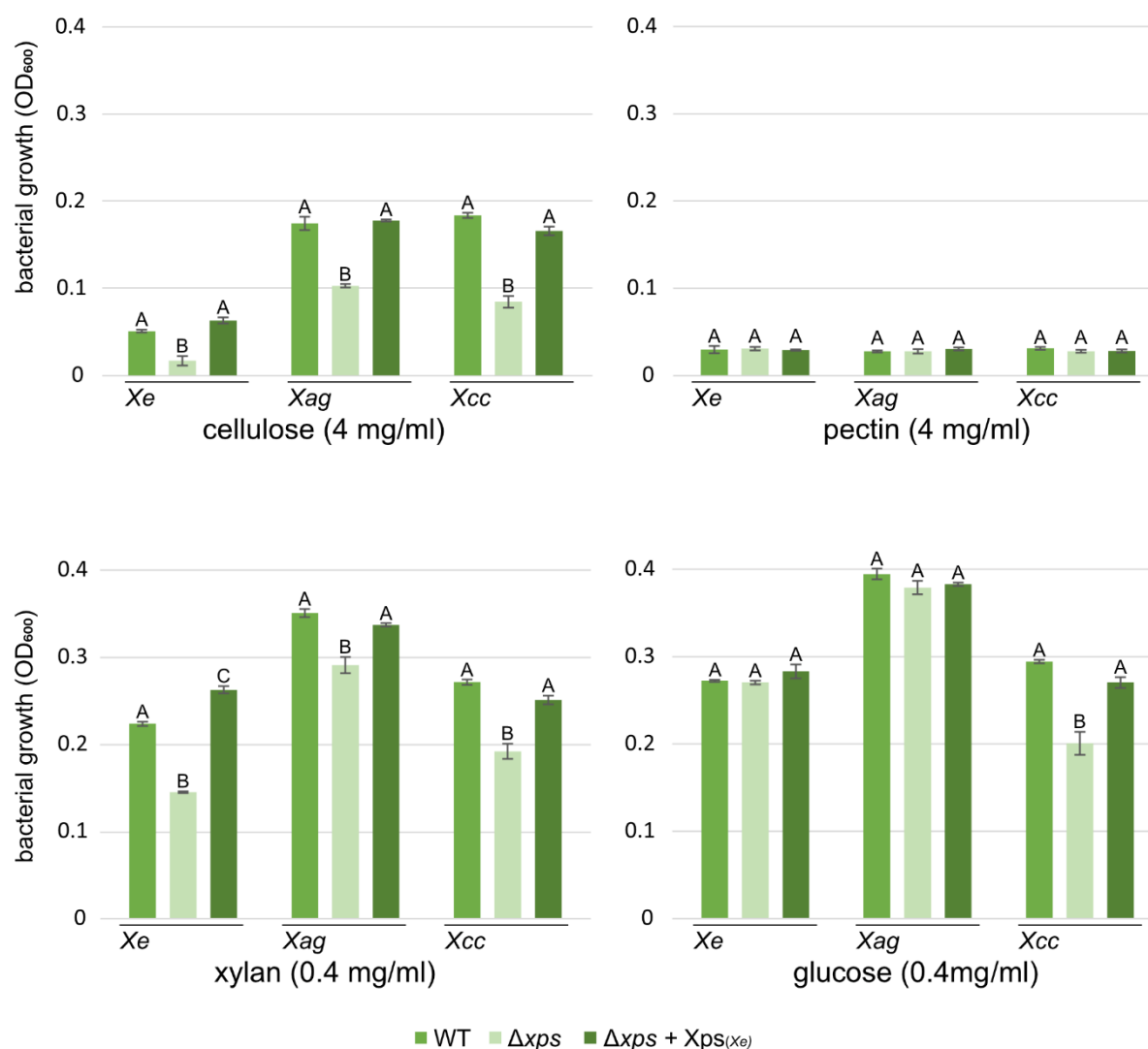


Figure 29: *Xanthomonas* utilization of xylan and cellulose depends on the Xps-T2S system

Wild-type *X. euvesicatoria* strain (Xe) strain 85-10, *X. axonopodis* pv. *glycines* (Xag) strain 8ra and *X. campestris* pv. *campestris* (Xcc) strain 8004 and respective T2S deletion mutants (Δxps) with (+Xps) or without (-) the modular *xps*-T2S expression construct from Xe were grown on XVM2 medium containing either 4mg/ml cellulose or pectin or 0.04mg/ml xylan or glucose as the sole carbohydrate source. Cultures were inoculated with a bacterial density of 2×10^7 CFU ml⁻¹ and quantified after 24h of growth. Statistically significant differences were determined using one-way ANOVAs with post-hoc Tukey-HSD ($P < 0.001$). Significant growth on pectin was not observed for any *Xanthomonas* strain. Experiments were performed at least three times; one representative dataset is shown.

All three *Xanthomonas* species grew on carboxymethylcellulose and xylan as a sole carbon source, but not on pectin. This is surprising as predicted pectin-modifying enzymes such as polygalacturonases and pectate lyases are frequently secreted by *Xanthomonas* and a significant reduction of galacturonic acid in infected plant cell wall material was observed (Figure 21) (Wang *et al*, 2008; Kaewnum *et al*, 2006). Nevertheless, pectin is one of the most complex plant polysaccharides and pectin utilization requires a complex array of catalytic enzymes (Li *et al*, 2024). Utilization of both xylan and cellulose appears T2S-dependent in all three *Xanthomonas* species, with significant reduction in growth for *xps* deletion mutants. While cellulose supported limited slow growth of cultures, much higher growth was observed in a 10-fold lower xylan concentration (0.4 mg/ml compared to 4 mg/ml). In fact, cultures grew to similar bacterial densities when growing on xylan and glucose, indicating that *Xanthomonas* is highly adapted to xylan utilization. Again, as the plasmid-borne modularized *xps* gene cluster from *Xe* restored growth on xylan and carboxymethylcellulose for both *Xag* and *Xcc* Δxps strains, this indicates that the Xps-T2S system from *Xe* can cross-complement in *Xag* and *Xcc*.

No significant growth reductions were observed for *Xe* or *Xag* Δxps mutants compared to respective wild-types growing on glucose, indicating that growth reduction in minimal media is due to reduced utilization of specific carbohydrates for these strains and is not caused by a general growth penalty in XVM2-based media. Nevertheless, reduction in growth of the *Xcc* *xps* mutant growing on glucose was also observed, indicating that for this strain, a deletion of the *xps* gene cluster leads to a general loss in fitness when growing in XVM2 medium.

5 Discussion

Sections of this chapter dealing with XpsD and XpsCLM (5.1-5.2) were originally written as part of an accepted PLOS pathogens manuscript entitled “Modularization of the type II secretion gene cluster from *Xanthomonas euvesicatoria* facilitates the identification of a structurally conserved XpsCLM assembly platform complex” by Samuel Goll, Patrick Martin, Sylvestre Marillonnet and Daniela Büttner.

5.1 Insights into the architecture and the assembly of the Xps-T2S system

The present study sheds light on the architecture of the Xps-T2S system from *X. euvesicatoria*. It was previously reported that the Xps-T2S system is an important virulence factor which depends on the ATPase XpsE and the secretin XpsD for function (Szczesny *et al*, 2010). To expedite functional studies of different components of the system in *X. euvesicatoria*, a modular T2S gene cluster was generated by stepwise and hierarchical assembly of individual promoter- and gene modules using the Golden Gate-based modular cloning strategy in preliminary work by Patrick Martin (Weber *et al*, 2011). Complementation studies confirmed that the modular T2S gene cluster is functional in *X. euvesicatoria* and restores both virulence and extracellular protease activity in a T2S mutant strain. The modular design allows the rapid generation of single or multiple gene deletions and facilitates the reintegration of genes or reporter fusions at different positions in the gene cluster. The generation of deletion mutants and complementation studies using this modular T2S gene cluster in the present study demonstrated that not only the ATPase XpsE and the secretin XpsD are essential for T2S, but all Xps proteins aside from XpsH are required for T2S in *X. euvesicatoria*.

Assembly of a multiprotein nanomachine such as the T2S system is a complex logistical task for a cell. The results presented here suggest that at least three independent subcomplexes of the Xps-T2S system are formed in *X. euvesicatoria*: the outer membrane secretin channel formed by 15 XpsD monomers, an inner membrane assembly platform complex formed by XpsCLM as well as a pseudopilus tip-XpsF complex. Based on the findings from interaction studies and AlphaFold structural predictions, a model of the complete Xps-T2S system from *X. euvesicatoria* was developed, composed of six XpsCLM complexes forming a column-like structure around an XpsF₃IJK complex and connecting the hexameric XpsE ATPase to the XpsD secretin channel, shown in Figure 30. A modular assembly of the T2S is proposed, with an XpsD secretin channel acting as a docking site to which the preformed XpsCLM- and XpsF₃IJK-subcomplexes can assemble, thereby providing a scaffold for the hexameric

ATPase XpsE. This model is based on structural predictions of six XpsCLM complexes, an XpsF₃IJK complex, an XpsF₃E₆ complex, and 15 monomers of an XpsD complex aligned into a crystal structure of the XcpQ secretin complex of *Pseudomonas aeruginosa*, aligned to each other based on predicted interacting regions.

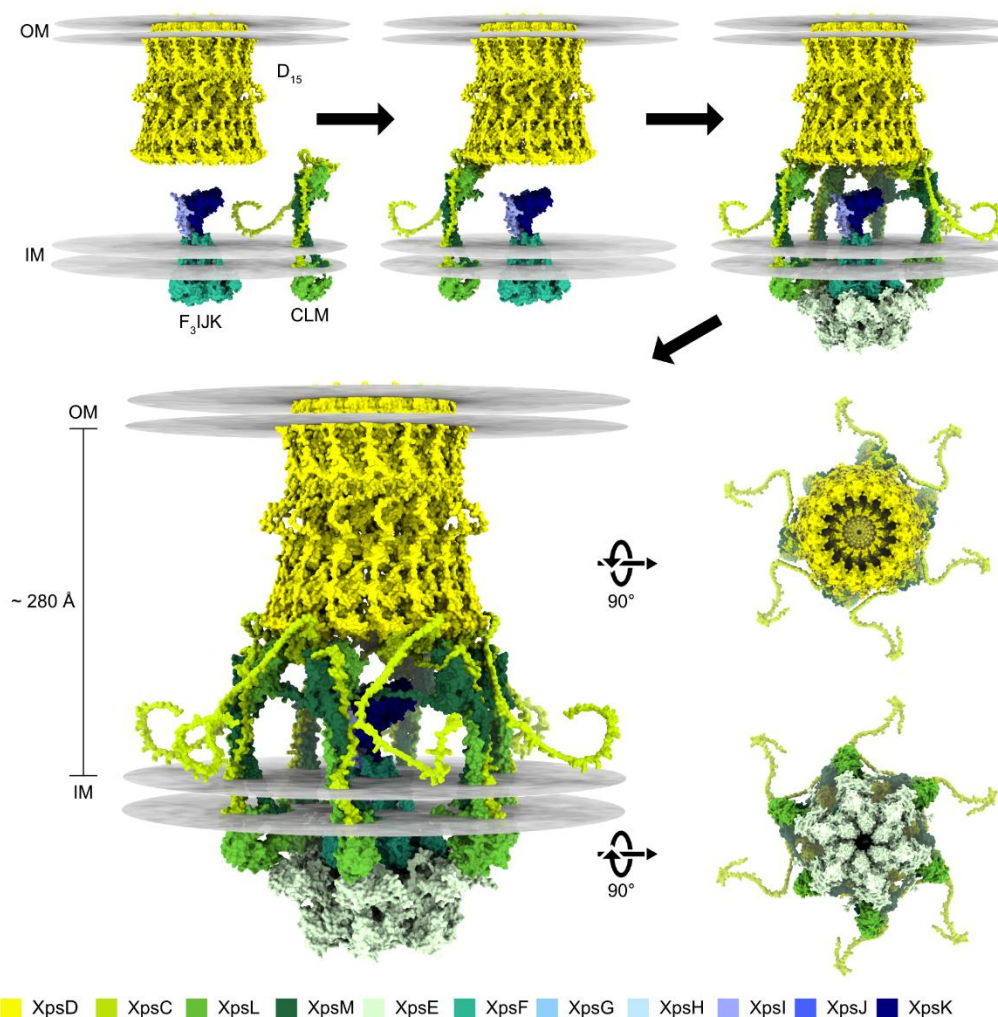


Figure 30: A proposed integrated model of the assembly and function of the T2S system:

The predicted structure of the Xps-T2S system from *X. euvesicatoria*. Top and bottom views of the complex are shown on the bottom right. Modular assembly of the T2S system from preformed XpsCLM, XpsF₃IJK and XpsD subcomplexes is proposed, with six XpsCLM trimers assembling to the pentadecameric XpsD secretin channel around the XpsF₃IJK subcomplex in a cage-like structure, thereby providing a scaffold for the ATPase XpsE to oligomerize and initiate pseudopilus extension. This integrated model was made from AlphaFold structural predictions of the XpsCLM complex, the F₃IJK, the F₃E₆ complex, the XpsD secretin complex as well as predicted interactions between XpsD-N0-XpsC-HR domains and between XpsL-XpsE (appendix, Figure 37, Figure 38 and Figure 39), all visualized and positioned appropriately with UCSF ChimeraX. For the pentadecameric secretin structure, predicted XpsD monomers were aligned to a crystal structure of the pentadecameric *Pseudomonas aeruginosa* PAO1 XcpQ secretin channel (PDB: 5WLN). To include the interaction between the N0 domain of XpsD and the HR domain of XpsC in the model of the XpsCLM complex, slight reposition of the flexible linker of XpsC was required. This short region is predicted with low confidence and high flexibility, located between the second alpha helix and the HR domain (appendix, Figure 34 and Figure 37). Hydrophobic residues in structures were used to predict the position of the outer and inner membranes in the structure (shown by grey discs). Proteins are color-coded as indicated below.

5.1.1 The XpsD secretin channel assembles independently of the remaining T2S system components

Fluorescence microscopy studies with an XpsD-mCherry reporter fusion revealed that the formation of secretin complexes occurred independently of other Xps components. Such secretin complexes formed in the OM are found both in T2S and T3S systems, as well as type IV pili (Majewski *et al*, 2021; Tassinari *et al*, 2023). Often, localization of these secretin complexes to the OM relies on a small protein called a pilotin, however, such a pilotin is absent in *X. euvesicatoria* for both the T3S system and the Xps-T2S system (Büttner, 2012). The secretin has a hinged gate that remains shut unless substrates are actively pushed through it, thus formation of a secretin channel does not lead to leakage of periplasmic proteins without the assembly of the remaining T2S system (Yan *et al*, 2017). As the XpsD secretin complex assembles independently of the remaining T2S components, it is proposed to act as the initiating point of assembly for the remaining T2S system in the model (Figure 30). Interaction of the N0-domain of the secretin and the HR-domain of XpsC was predicted by AlphaFold and demonstrated in other homologous T2S systems (Naskar *et al*, 2021; Yan *et al*, 2017; Chernyatina & Low, 2019), thereby providing a docking site for the IM assembly platform to the OM secretin channel. This concurs with previous findings that polar foci formation of fluorescent fusion proteins of homologues of XpsC, XpsL and XpsM from *V. cholerae* and *K. oxytoca* was decreased in absence of the respective secretin (Buddelmeijer *et al*, 2009; Lybarger *et al*, 2009). Future experiments with GFP-fusions of XpsC, XpsL and XpsM in tandem with the XpsD-mCherry fusion may be performed to verify the co-localization of these assembly platform proteins with the secretin channel. The modularized *xps* gene cluster allows for straightforward generation of the constructs required for these co-localization studies. Additionally, mutating or deleting the HR-domain in XpsC and the N0-domain in XpsD in such fluorescent fusion proteins could assess whether the predicted interactions of these domains facilitate docking of the assembly platform to the secretin. Additionally, direct interaction of these two domains could be assessed by *in vitro* GST-pulldown assays.

5.1.2 The trimeric assembly platform XpsCLM complex links the secretin to the cytoplasmic ATPase

A second independently forming subcomplex is the trimeric assembly platform complex formed by XpsC, XpsL and XpsM. According to structure predictions using the AlphaFold2 algorithm, XpsC, XpsL and XpsM each insert into the IM via a single N-terminal TM helix followed by a C-terminal periplasmic domain. When *X. euvesicatoria* strains with modularized T2S gene clusters expressing c-Myc-fusions of XpsL or XpsC were treated with

formaldehyde, XpsC, XpsL and XpsM formed a trimeric complex as was predicted by AlphaFold2. This concurs with previous reports of XpsL - XpsM complexes in *X. campestris* pv. *campestris* and OutL – OutM complexes in *Dickeya dadantii* (formerly *Erwinia chrysanthemi*) (Tsai *et al*, 2002; Lallemand *et al*, 2013). Protein studies revealed that XpsM stabilizes XpsL as was also shown for homologous proteins from *P. aeruginosa* (Michel *et al*, 1998). The amounts of an XpsL degradation product, however, remained unchanged in the absence of XpsM, indicating that XpsM predominantly stabilizes the full-length XpsL protein. Given that the function of *xpsL* depends on its native Shine Dalgarno sequence, it is assumed that the levels of XpsL are tightly controlled both on the translational level and post-translationally by XpsM. Furthermore, the XpsCLM complex is an independently forming structure in *X. euvesicatoria*, as crosslinking experiments with *xps* deletion mutants showed that the putative ATPase XpsE, the secretin XpsD and XpsF are dispensable for the formation of this complex.

AlphaFold2 predictions suggest that the trimeric XpsCLM complex shares striking structural similarities with GspCLM complexes from *P. aeruginosa*, *D. dadantii* and *V. cholerae*, despite overall low amino acid identities of the corresponding proteins. This suggests that GspCLM complexes represent a conserved structural feature of T2S systems from different bacterial species. The periplasmic domains of GspL and GspM proteins contain predicted ferredoxin-like folds which likely interact with each other as was shown for GspL and GspM proteins from *Klebsiella* spp. and *D. dadantii* (Chernyatina & Low, 2019; Dazzoni *et al*, 2023; Li *et al*, 2023). GspC proteins contain a conserved periplasmic HR domain which interacts with the N0 domain of the secretin as was reported for GspC and GspD proteins from *E. coli* and *D. dadantii* (Korotkov *et al*, 2011; Lee *et al*, 2000; Zhang *et al*, 2022; Wang *et al*, 2012; Gu *et al*, 2012). Thereby, this HR domain likely allows the GspCLM complex to associate with an independently forming GspD secretin complex described above.

In the integrated T2S system model for *X. euvesicatoria* presented here, six XpsCLM complexes dock to the secretin channel via the HR domains of XpsC, arranged within the T2S system like columns. The stoichiometrical mismatch between these six XpsCLM complexes and the predicted XpsD pentadecamer may be resolved by the inherent flexibility of a disordered region in XpsC, located between the HR domain and the binding site for XpsL and XpsM, with the HR domains of six XpsC molecules interacting with six out of 15 N0 domains of XpsD, thus providing positional flexibility and leaving space for T2S substrates to enter the inner vestibule of the secretin channel (Figure 30). In the Pul-T2S of *K. pneumoniae*, however, twelve PulC molecules were predicted to integrate into the assembly platform based on the results of stoichiometry measurements (Chernyatina & Low, 2019). This arrangement could overcome the symmetry mismatch between PulC and PulD by

leaving three N0 domains of PulD being unattached (Chernyatina & Low, 2019). The integration of GspC dimers into the assembly platform of the T2S system has, however, not yet been experimentally confirmed. It is possible that the increased levels of GspC in purified protein fractions are caused by its attachment to the secretin. Alternatively, six additional monomers of GspC could bind to the remaining free N0 domains of the secretin channel, alongside the six copies of the GspCLM complex. This may explain why twelve copies of GspC were identified in *K. pneumoniae* (Chernyatina & Low, 2019).

Furthermore, structural modeling suggests that the XpsCLM complex can bind to the cytoplasmic ATPase XpsE via the cytoplasmic domain of XpsL in *X. euvesicatoria*. This interaction between XpsL and XpsE was verified by BACTH assays and GST pull-down experiments. An interaction with the ATPase was previously also shown for GspL proteins from *K. oxytoca* and *Vibrio* species (Chernyatina & Low, 2019; Dazzoni *et al*, 2023; Lu *et al*, 2014; Abendroth *et al*, 2009). Furthermore, cryo-electron microscopy studies of T2S systems from *K. pneumoniae* revealed that the association of the cytoplasmic domain of GspL with GspE leads to the formation of a GspL-GspM-GspE complex which assembles as a flexible hexameric structure (Chernyatina & Low, 2019). To date, a hexameric GspE structure could not be crystallized without an assistant hexameric protein (Lu *et al*, 2013), suggesting that the formation of the ATPase complex depends on interactions with additional proteins. It remains to be investigated whether the ATPase first binds to GspL as a monomer and only hexamerizes upon docking of the GspCLM complexes to the secretin channel. Taken together, the XpsCLM complex appears to form independently and may subsequently dock to the OM secretin channel and thereby form a scaffold for the binding and oligomerization of the cytoplasmic ATPase.

However, co-localization of the ATPase with the remaining T2S system remains to be demonstrated *in vivo* in *X. euvesicatoria*. One approach to do this would be by generating a GFP-XpsE fusion in the modular *xps* gene cluster, and testing whether this fusion forms fluorescent foci that co-localize with those foci observed for XpsD-mCherry, and whether this co-localization depends on XpsC, XpsL and XpsM, similar to co-localization studies described in 5.1.1. An alternative would be to establish a photo-crosslinking methodology in *X. euvesicatoria*. In photo-crosslinking, a UV-reactive non-canonical amino acid such as p-benzoyl-phenylalanine (pBpa) is inserted at predicted interaction interfaces of the proteins, by mutating the respective codon to an amber stop codon which is suppressed by a pBpa-charged suppressor tRNA generated by an artificial tRNA-synthetase (Singh & Wagner, 2019). In response to UV irradiation, this pBpa forms a covalent crosslink with an interacting protein which can then be visualized by immunoblotting. To characterize interactions of XpsE *in vivo*, amino acids predicted to interact with XpsL could be substituted for pBpa and tested.

However, photo-crosslinking has not yet been established in *X. euvesicatoria*, and suppression of amber stop codons is lethal in many bacteria and only viable in some species such as *E. coli* (Singh & Wagner, 2019).

5.1.3 Pseudopilus initiation at an XpsF channel?

Finally, the findings of this study suggest that a third T2S substructure assembles, composed of XpsF and the pseudopilus tip proteins XpsI, XpsJ and XpsK. The exact stoichiometry of XpsF complexes were difficult to characterize *in vivo* in *X. euvesicatoria*, but in *K. oxytoca*, the homologue PulF was recently demonstrated to form a trimeric ion-channel which fits into the center of the hexameric ATPase PulE (Guilvout *et al*, 2024). GspF is essential for the formation of the pseudopilus and was shown to interact with both GspL and GspE (Chernyatina & Low, 2019; Lu *et al*, 2014; Abendroth *et al*, 2009; López-Castilla *et al*, 2017; Py *et al*, 2001).

XpsF complexes formed by formaldehyde crosslinking were independent of the secretin XpsD, the ATPase XpsE, the assembly platform components XpsC and XpsM and the pseudopilins XpsG and XpsH. As XpsL is unstable in the absence of XpsM, it is assumed that the XpsL does not affect XpsF oligomerization, although this was not validated experimentally due to time constraints. This suggests that XpsF forms a third independent subcomplex of the T2S system in addition to the secretin channel and XpsCLM trimers. Strikingly, XpsF complexes did not form in the absence of the pseudopilus tip proteins XpsI, XpsJ and XpsK. This aligns with structural modelling that proposes a trimeric XpsIJK pseudopilus tip complex nested in a trimeric XpsF inner membrane channel.

The exact protein biochemistry behind formaldehyde crosslinking is not fully understood, and rather than simply crosslinking all proximal amino acids, it has been suggested that formaldehyde mostly effects structured proteins and dominantly leads to the covalent binding of nearby lysine residues (Tayri-Wilk *et al*, 2020). Thereby, in absence of nearby imine containing amino acids, interacting protein regions may not be identified by formaldehyde crosslinking, possibly explaining why no XpsF trimers were directly detected in these experiments, even though trimeric complexes of XpsF homologues were recently found in *K. pneumoniae* (Guilvout *et al*, 2024). Furthermore, formaldehyde crosslinking is unspecific, making it very difficult to identify the exact nature of the detected crosslinked protein complexes.

To work around the limitations of formaldehyde crosslinking, targeted cysteine crosslinking of proposed interaction regions of the pseudopilins XpsI, XpsJ, XpsK and XpsF was employed and demonstrated that the hydrophobic region of XpsK indeed interacts with the XpsF channel as predicted by AlphaFold2 (see Figure 19). In addition to a crosslinked product

corresponding to XpsK-XpsF, additional larger crosslinked product was detected in these experiments which may be due to another free cysteine in XpsF (C183) or a second cysteine substitution (E51C) in the XpsK-c-Myc fusion employed, either forming disulfide bonds between two XpsK-XpsF complexes or with other proteins. However, this remains to be determined in future crosslinking studies without these additional cysteine residues in the interaction partners.

Further, it was determined that the trimeric XpsIJK pseudopilus tip complex assembles independently of both the ATPase XpsE and of XpsF *in vivo*. Taken together with the finding that XpsF oligomers do not form in absence of XpsI, XpsJ and XpsK, this suggests that the XpsIJK complex first assembles independently and subsequently allows for the formation of an XpsF channel, in agreement with findings from *K. pneumoniae* that the trimeric PulF channel only formed in the presence of the other Pul proteins (Guilvout *et al*, 2024). Further insights into the XpsF-XpsIJK complex could be gained by performing cysteine crosslinking studies with c-Myc fusions of XpsI or XpsJ with respective cysteine substitutions and XpsF with corresponding cysteine substitutions in predicted interaction interfaces. Furthermore, additional deletions of the ATPase XpsE or the pseudopilin XpsG or the secretin XpsD would verify that XpsF-XpsIJK complexes form independently, as suggested by formaldehyde crosslinking (see 4.1.11).

Finally, the hexameric ATPase XpsE was predicted to bind to the cytoplasmic interface of a trimeric XpsF channel via the N2E domain of XpsE (appendix, Figure 36). This does not interfere with the predicted Interaction of XpsE with the cytoplasmic domain of XpsL via the N1E domain (Figure 10) and would localize the trimeric XpsF channel in the center of the assembly platform. This concurs with findings from *E. chrysanthemi* that indicate that OutE, OutL and OutF form a complex (Py *et al*, 2001) and similar findings from homologous proteins of the type IVa pilus machine (Bischof *et al*, 2016; Chang *et al*, 2016). In *E. chrysanthemi*, OutL is required for the interaction of OutF and OutE (Py *et al*, 2001). One explanation for this may be that interaction of GspF with GspE may require hexamerization of the ATPase GspE, which in turn requires a scaffold provided by GspL. Such a scaffold would be provided by GspCLM complexes docking to the secretin channel.

Hydrolysis of ATP by GspE is suggested to provide the energy for T2S, but this would require energy transduction from the cytoplasmic ATPase to the extending periplasmic pseudopilus. As GspF appears to connect these two components of the T2S system and may facilitate this process. Furthermore, the predicted interaction sites of GspF and GspE are highly conserved (Guilvout *et al*, 2024). Therefore, understanding the interaction between these two proteins in their native setting may provide insights into energy transduction in the T2S system. The modularized *xps* gene cluster employed here provides a powerful tool to facilitate such

studies in the future. As the interface of XpsF and XpsE is cytosolic rather than periplasmic, it is not accessible for cysteine crosslinking as the interface of XpsF, XpsI, XpsJ and XpsK are. Therefore, future studies need to employ other methods such as proximity labelling with biotin by fusing a biotin ligase to one interacting protein (Sears *et al*, 2019) or photocrosslinking, inserting UV-reactive non-canonical amino acids at predicted interaction interfaces of XpsF and XpsE (see 5.1.2).

It has been proposed that ATP hydrolysis leads to a clockwise sequence of conformational changes in the XpsE homologues, causing XpsF homologues to protrude further into the periplasm and push up the growing pseudopilus to allow for stepwise incorporation of additional XpsG homologues (Naskar *et al*, 2021). Alternatively, the trimeric XpsF channel has been proposed to act as an ion channel for either protons or sodium and T2S was not functional when the potential pore was blocked (Guilvout *et al*, 2024). Furthermore, the XpsIJK complex nested in the trimeric XpsF channel may block passive leakage of ions through the pore until bound by XpsE and aligned to the center of the T2S system to facilitate pseudopilus elongation and substrate secretion. The exact nature of energy transduction needs to be analyzed in future studies for example by specifically mutating amino acids in XpsF to inhibit ion transport, or by establishing a system to measure changes in electromotive force across a plasma-membrane dependent on XpsF oligomerization. This would require more thorough *in silico* modelling to pinpoint target residues potentially involved in ion transport and establishing a system to measure changes in membrane potential poses very significant technical challenges. It would be more feasible and of great interest to perform cysteine crosslinking experiments targeting the interaction sites of the XpsIJK complex and XpsG pseudopilus predicted by AlphaFold3 (compare Figure 20) by inserting specific cysteine substitutions in modelled proximal amino acids of these proteins. If predicted XpsIJK-XpsG interactions would thus be verified *in vivo*, assessing whether other components such as XpsF or XpsE are required for the pseudopilus tip complex to interact with the pseudopilin XpsG would be very straightforward and only require removing the respective gene from the modular *xps* gene cluster.

5.1.4 A proposed functional mechanism of the Xps-T2S system

A model of substrate secretion is also proposed (Figure 31). Substrates may interact with the flexible 2P-region of XpsC (compare Figure 14) and subsequently be brought into the inner vestibule of the T2S system. In the inner vestibule, they may bind to the pseudopilus tip, as predicted by AlphaFold3 and subsequently be secreted into the extracellular milieu through the secretin by pseudopilus extension due to the oligomerization of XpsG (compare Figure 20). Subsequently, the XpsG oligomer disassembles, leading to retraction of the pseudopilus,

so that the next round of substrates can be bound to the pseudopilus tip in the T2S inner vestibule.

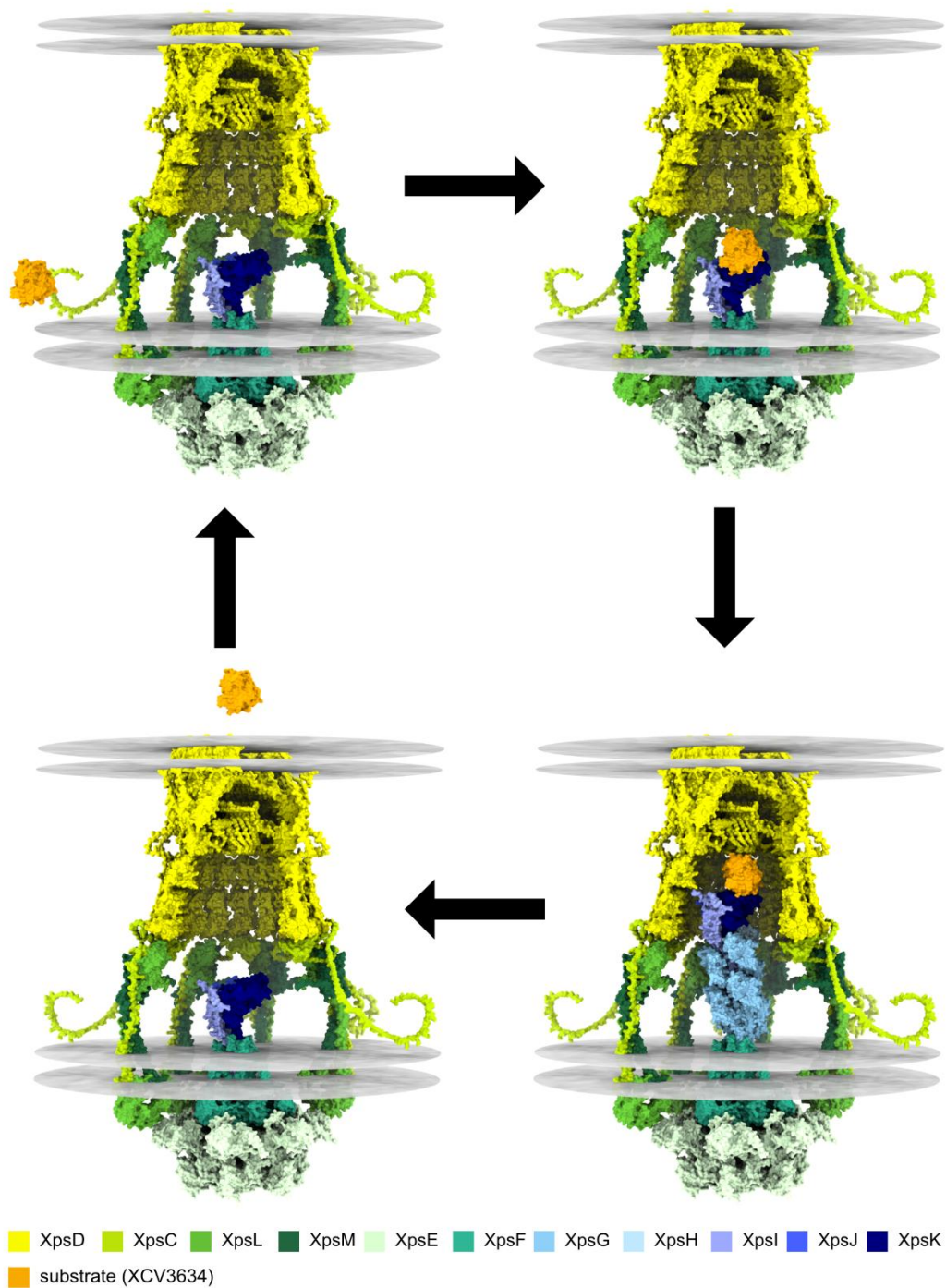


Figure 31: proposed model of substrate secretion via the T2S system

Substrates potentially interact with the 2P-region of XpsC (top left) and are subsequently transported into the inner vestibule of the T2S system, where they are bound by the pseudopilus tip complex (top right) which then extends (bottom right) to push substrates out through the secretin channel. Subsequently the pseudopilus disassembles (bottom left) to push substrates out through the secretin channel. Subsequently the pseudopilus disassembles (bottom left) and the process can begin again. Hydrophobic residues in structures were used to predict the position of the outer and inner membranes in the structure (shown by grey discs). Proteins are color-coded as indicated below.

The 2P-region of XpsC is freely accessible from the periplasm and has conserved positive charges that were modelled to interact with negatively charged regions on substrates. Furthermore, altering these charges of the 2P-region led to reduced protease secretion. 2P-regions in other bacteria have also been suggested to play a role in substrate recognition, even though this region is highly variable between different T2S systems ranging from a simple alpha helix in *P. aeruginosa*, to highly structured PDZ-domains found in *V. cholerae* and *D. dadantii* (Bouley *et al*, 2001; Pineau *et al*, 2014; Bleves *et al*, 1999). Interactions of substrates and the 2P region were shown for *D. dadantii* (Pineau *et al*, 2014, 2021). The 2P region is proposed to act as a binding site for T2S substrates after their Sec- or Tat-dependent transport into the periplasm (Naskar *et al*, 2021; Gu *et al*, 2017). The long relatively unstructured and flexible region connecting the 2P-region of XpsC with the remaining protein may act to enable transport of an interacting substrate from the periplasm into the inner vestibule of the T2S system, where substrates can then bind to the pseudopilus tip complex.

Dynamic association of XpsCLM complexes with the secretin might not only lead to T2S system assembly but might also contribute to the regulation of T2S. It is assumed that T2S substrates bind to the 2P-region of XpsC or to the entire XpsCLM complex and subsequently associate with the tip proteins of the pseudopilus and the secretin. As an alternative T2S substrates interacting with 2P-regions of XpsC in XpsCLM complexes already docked to the T2S system (as shown in Figure 31), substrates may bind to unbound XpsCLM modules which could then dynamically replace “empty” XpsCLM modules docked to the T2S system and thereby deliver their cargo proteins. Such a dynamic assembly of the T2S system could explain why cryo-electron microscopy approaches have so far fallen short in revealing insights into the architecture of T2S systems beyond the structure of the highly stable OM secretin (Gu *et al*, 2017; Chernyatina & Low, 2019).

Once a substrate is brought into the inner vestibule of the T2S system, it is probably bound by the pseudopilus tip complex as modelled by AlphaFold3 (see Figure 20). Interactions between T2S substrates and XpsI, XpsJ or XpsK may be analyzed in future studies by performing GST-pulldown or BACTH assays with respective proteins. Additionally, specific amino acids in T2S substrates and the pseudopilus tip proteins may be substituted for cysteines to analyze such interactions *in vivo* using cysteine crosslinking. Alternatively, photo-crosslinking could be employed to this end, if it can be established in *X. euvesicatoria*. While the exact nature of these interactions remains to be characterized further, interactions of T2S substrates with the pseudopilus tip complex were previously reported for the Xcp system in *P. aeruginosa* (Douzi *et al*, 2011). Located in the pseudopilus tip is XpsK, which was modelled to interact with T2S substrates and appears to be a promiscuous, highly

interactive protein (see Figure 20). A highly interactive pseudopilus tip would make sense considering its central role in secretion of all different T2S substrates. It is conceivable that the pseudopilus tip freely interacts with many different proteins and needs to be shielded by the XpsCLM-complexes arranged around the pseudopilus to keep non-substrate proteins out of the T2S system to prevent their secretion. This would suggest that substrate specificity is determined by biochemical properties of substrate proteins such as size and electrostatic charge distribution that enables passage of substrates into the inner vestibule rather than specific conserved amino acid sequences. These specific biochemical properties that enable a protein to enter the vestibule may be different in different T2S systems, possibly correlating to the highly varying domains found in the 2P-region of XpsC homologues (see 4.1.9).

As an alternative highly dynamic secretion mechanism, it is possible that substrates directly bind to the pseudopilus tip-XpsF subcomplex, followed by assembly of the T2S system from this substrate-bound complex as well as the secretin channel and the XpsCLM subcomplex. Upon substrate secretion, the entire T2S system could again disassemble into its core subcomplexes. For such a T2S mechanism, a conformational change in the pseudopilus tip-XpsF complex due to substrate binding would lead to assembly of the remaining system. This could potentially be by a substrate bound pseudopilus tip-XpsF complex leading to the hexamerization of the ATPase XpsE which in turn could align the XpsCLM modules into a hexameric cage structure via interaction of XpsE with the cytoplasmic domain of XpsL. This hexameric assembly platform cage could subsequently dock to the XpsD secretin channel via interactions of XpsC and XpsD in the periplasm. A weakness of this model is preventing extension of the pseudopilus until the entire T2S system is in place. Extension of the pseudopilus driven by the hexameric ATPase XpsE prior to docking of the assembly platform to the OM secretin channel would waste energy in the form of ATP without secreting substrate proteins through the secretin channel. However, if prior hexamerization of XpsE were required to align XpsCLM complexes into an assembly platform that can dock to the secretin channel, it is difficult to conceive what could prevent such premature pseudopilus extension. The major difference between this mechanism with the one proposed above is the cause of the hexamerization of the ATPase XpsE. The former model relies more on the arrangement of XpsCLM complexes docked to the secretin channel to catalyze XpsE hexamerization, whereas this alternative model predicts a conformational change in XpsF to trigger ATPase assembly. Thus experimentally determining what hexamerization of XpsE depends on *in vivo* (compare 5.1.2) may help discriminating between these two mechanisms.

Interestingly, the highly conserved T2S substrate XCV3671 has an N-terminal domain that is absent in the mature secreted substrate but nevertheless required for secretion (see 4.2.3). This N-terminal domain is composed of roughly 150 amino acids and resembles pseudopilins

of similar size such as XpsG, XpsH and XpsI, with an N-terminal alpha helix and a C-terminal globular structure. This N-terminal region of the substrate XCV3671 may mimic a pseudopilin and facilitate the binding of the substrate to the pseudopilus tip complex prior to being itself autocatalytically cleaved from the mature substrate which is subsequently secreted. This theory is highly speculative and requires further testing to determine whether this N-terminal domain can indeed interact with the pseudopilus and act as a courier for the mature substrate. Interestingly, membrane-bound T2S substrate chaperones have been reported in *Acinetobacter* (Harding *et al*, 2016), which have also been proposed to act as a substrate courier to the T2S system. Perhaps the N-terminal domain of XCV3671 has a similar role to these T2S substrate chaperones, only that it is a part of the unprocessed substrate and probably autocatalytically cleaved from the mature XCV3671 substrate (see 4.2.3). As an interaction between N-terminal domain of XCV3671 and the pseudopilus tip would take place in the periplasm, one could model interactions of these and subsequently substitute amino acid pairs in predicted interaction sites of proteins for cysteine crosslinking.

5.1.5 How does the pseudopilus retract?

Oligomerization of the major pseudopilin XpsG presumably extends the pseudopilus so that substrates can be pushed through the secretin channel. Upon release of substrates into the extracellular space, the pseudopilus needs be retracted so that new substrates can be secreted. In *K. pneumoniae*, oligomerization of the pseudopilus was demonstrated to depend on calcium, with calcium-binding sites in the XpsG homologue PulG, and it has been suggested that lower calcium concentrations in the extracellular milieu compared to the periplasm lead to a release of the bound calcium ions and disassembly of the pseudopilus (López-Castilla *et al*, 2017). However, inside the plant, *X. euvesicatoria* is surrounded by an extracellular apoplastic space which is high in calcium (Stael *et al*, 2011), not a calcium poor environment proposed to facilitate pseudopilus retraction. Nevertheless, it has been described that both plant cell wall polysaccharides and bacterial exopolysaccharides such as xanthan chelate calcium (Lopez-Hernandez *et al*, 2020; Aslam *et al*, 2008). Calcium chelation by bacterial exopolysaccharides can sufficiently lower the apoplastic calcium concentration to inhibit influx of calcium into the plant cell for signaling involved in the plants PTI response (Aslam *et al*, 2008). Additionally, calcium chelation by xanthan may lower the local calcium concentration directly around the bacteria enough to accommodate for a calcium dependent pseudopilus retraction mechanism. Nevertheless, calcium binding of XpsG needs to be verified experimentally. As an alternative mechanism, proteolytic degradation of the extended periplasmic pseudopilus has been suggested, based on findings from homologous T4a pilus formation, but this seems rather energetically inefficient (Nivaskumar & Francetic, 2014; Kapitein *et al*, 2013). On the other hand, the pseudopilus

extension may simply be highly dynamic in nature with simultaneous assembly and disassembly of a metastable pseudopilus, constantly extending and retracting in a stochastic manner. Thereby substrates would remain bound to the pseudopilus tip until a pseudopilus extension is coincidentally long enough to release the substrate into the extracellular milieu.

5.2 The role of T2S in plant infection

Beyond characterization of architecture and assembly of the Xps-T2S system, the results of this study provide insights into the role of T2S in virulence. Prior to this study, four T2S substrates in *X. euvesicatoria* were known, two putative xylanases, an esterase and a serine protease (Solé *et al*, 2015; Szczesny *et al*, 2010). Mass-spectrometry based characterization of the *X. euvesicatoria* “secretome” in the tomato apoplast during infection expanded this list to include 19 candidate T2S substrates, of which seven representing a diversity of enzyme classes were validated *in vitro*. These include predicted CWDEs such as cellulases and polygalacturonases, as well as cysteine- metallo- and glutamic proteases. While homologues of these candidates such as the putative cysteine protease XCV3013 and the predicted polygalacturonases XCV0722 and XCV2571 as well as the putative cellulase XCV0670 have been shown to be T2S substrates in other *Xanthomonas* strains, this present study represents the most extensive characterization of T2S substrates from a single *Xanthomonas* strain (Pfeilmeier *et al*, 2024; Wang *et al*, 2008; Szczesny *et al*, 2010; Solé *et al*, 2015; Jha *et al*, 2007). Concurring with this, it was shown that the plant cell wall is altered during bacterial colonization in a T2S-dependent manner, with a reduction of relative abundance of xylose and galacturonic acid (see 4.2.6).

Potential roles of T2S in bacterial virulence include: (I) Facilitating bacterial nutrient acquisition through enzymatic degradation of extracellular polysaccharides and proteins; (II) Degrading apoplastic plant defense components; (III) generating plant-derived metabolites such as xylose that may be perceived by the bacteria, subsequently activating virulence genes such as the T3S system *in planta*; (IV) Supporting T3S effector delivery by degrading the plant cell wall for penetration of the T3S pilus. As previously mentioned, differentiating between these different potential roles is difficult (see 2.3.2 and Figure 4).

5.2.1 T2S and nutrient acquisition

Growth experiments in minimal media with plant cell wall polysaccharides as the sole carbohydrate source enabled an investigation into the role of the T2S in nutrient acquisition independently of plant immunity and effects T3S *in planta* (see 4.2.7). It was demonstrated that *Xanthomonas* can utilize plant cell carbohydrates, specifically cellulose and hemicelluloses, and that the Xps-T2S is implicated in this process, as growth in Δxps mutants in all three *Xanthomonas* spp. tested was reduced compared to the respective wild-

types. For one species, *X. campestris* pv. *campestris*, a general growth reduction of T2S mutants in minimal media was observed even with glucose as the carbon source. Thus for *X. campestris* pv. *campestris* one must be careful with attributing reduced growth in other carbohydrate sources to reduced utilization of extracellular carbohydrates via secreted CWDEs. This general growth reduction might be due to detrimental effects of T2S substrate proteins retained in the periplasm of this species.

Xylan- and cellulose utilization concurs with the T2S-secreted cellulases and xylanases of *X. euvesicatoria*. Xylan from corn cob contains a xylose backbone with arabinose and glucuronic acid side chains (Oliveira *et al*, 2010). It lacks the β -1,4 glucose backbone found in the predominant hemicellulose xyloglucan and therefore cannot be degraded by cellulases. While xylan is less prevalent in the primary cell wall of most non-*Poaceae* plants, such as *Brassicaceae* and soybean host of *X. campestris* pv. *campestris* and *X. axonopodis* pv. *glycines*, xylan is highly abundant in the primary cell walls of tomato as the host of *X. euvesicatoria* (Broxterman & Schols, 2018). Interestingly, all *Xanthomonas* strains grew most efficiently on xylan compared to other polysaccharides, suggesting that highly efficient utilization of xylose-containing polysaccharides is a conserved feature. This concurs with findings that secreted xylanases are important for plant infection in non-related vascular and non-vascular *Xanthomonas* species (Jha *et al*, 2007; Déjean *et al*, 2013; Vieira *et al*, 2021; Solé *et al*, 2015), and that xylan and xyloglucan utilization genes are conserved in the genus (Déjean *et al*, 2013; Vieira *et al*, 2021). This seems particularly important for vascular pathogens, surrounded by non-living xylem cells which cannot be reprogrammed by T3S for nutrient export into the apoplast, further exemplified by the related vascular pathogen *Xylella fastidiosa* lacking a T3S system requires the Xps-T2S system for virulence on grapevine (Ingel *et al*, 2023).

Surprisingly, pectin did not support growth, even though multiple predicted polygalacturonases and other pectin-degrading enzymes are secreted by the Xps system (see Figure 22) and polygalacturonic acid content is reduced in the cell walls of plants during *Xanthomonas* infection (see Figure 27). Similarly, no major contribution to virulence was observed for pectin-degrading enzymes in *X. oryzae* pv. *oryzae* (Tayi *et al*, 2016), although a role in virulence was reported for two polygalacturonases from *X. campestris* pv. *campestris* (Wang *et al*, 2008). Pectins are the most complex carbohydrates found in plant cell walls and bacterial pectin-utilizing bacteria require a complex set of enzymes, far more than simple polygalacturonases and pectinases (Li *et al*, 2024). However, rather than direct utilization, partial degradation of the various cell wall pectins by these enzymes may be required for *Xanthomonas* to access cellulose and hemicellulose carbohydrates which are metabolized. This would explain why the relative galacturonic acid contents of infected plants are reduced,

possibly resulting from degradation of pectins such as homogalacturonan. Growth of *X. campestris* pv. *campestris* on cell wall extracts specifically released galactose and rhamnose from these (Vorhölter *et al*, 2012), which could be attributed to degradation of complex pectins such as Rhamnogalacturonan I (compare Figure 5). In contrast to this, the relative levels of rhamnose and galactose were not reduced but significantly elevated in cell walls of plants challenged with *X. euvesicatoria* (see Figure 27), suggesting that the details of pectin degradation vary between *Xanthomonas* species.

In future experiments, sequentially deleting individual T2S substrates implicated in carbohydrate metabolism in *X. euvesicatoria* could provide insights into their respective roles. To this end, *X. euvesicatoria* strains lacking the predicted T2S-dependent cellulases (XCV0670 and XCV3634) or pectin-degrading enzymes (XCV0722, XCV2571, XCV2278 and XCV4423) as well as the predicted xylanases would need to be generated. Subsequently, quantifying the growth of these strains in minimal medium with cell wall extracts, cellulose or xylan as a sole carbon source may provide insights into the respective roles of these enzymes in carbohydrate metabolism. Additionally, quantification of the monosaccharide composition of plant cell walls in pepper plants challenged with these deletion mutants could provide insights into what role individual enzymes play in altering the cell wall architecture. However, functional redundancy poses a major challenge to such endeavors, as multiple homologues of each predicted enzyme class (cellulases, xylanases, pectin-degrading enzymes) are found in *X. euvesicatoria*, which probably can cross-complement individual gene deletions. Therefore, multiple subsequent gene deletions would have to be performed to generate strains devoid of all homologues of different enzyme classes in a time-consuming process.

In addition to carbohydrates, the apoplast also contains glycoproteins which pose a potential amino acid source for *Xanthomonas*, and *X. euvesicatoria* secretes multiple different classes of proteases via the T2S system. Interestingly, degradation of arabinose side-chains of glycoproteins was previously reported for *X. euvesicatoria* (Nakamura *et al*, 2018). Secreted proteases hydrolyze extracellular proteins into metabolizable amino acids or polysaccharides, as *Xanthomonas* strains grew on unprocessed extracellular milk protein as a sole amino acid source in a T2S-dependent manner *in vitro*. It remains to be determined whether apoplastic proteins are also degraded and metabolized in this way *in planta*. An interesting experiment to gain insight into this would be isolating plant cell walls in their native state, together with bound glycoproteins and performing minimal growth experiments with these native cell wall extracts as the sole carbohydrate and amino acid source or with only extracted glycoproteins as an amino acid source (Feiz *et al*, 2006). Again, one could attempt to delete individual T2S-dependent proteases to determine their respective contribution, but

functional redundancy of the many different T2S-dependent proteases in *X. euvesicatoria* poses a major challenge to such an endeavor (compare Figure 21 and Figure 23).

Taken together, these findings strongly implicate the *Xanthomonas* Xps-T2S with nutrient acquisition, without excluding additional roles of the system *in planta*.

5.2.2 Degradation of apoplastic defense components by the T2S system

In addition to contributing to nutrient acquisition, T2S may prevent PTI responses *in planta* (Figure 32). PTI responses are triggered by PAMPs such as flagellin and DAMPs such as short oligosaccharides released in cell wall degradation, which are detected by plant receptors (Xiao *et al*, 2024). To prevent PTI responses, bacterial pathogens may use the T2S system to secrete additional CWDEs that quickly degrade intermediate cell wall oligosaccharides to undetectable monomers, exemplified by exo-xylanases secreted together with endo-xylanases in *Xanthomonas axonopodis* pv. *citri* (Santos *et al*, 2014). Secreted proteases may also inhibit PTI, and proteomics of apoplastic proteins identified many different T2S-dependent proteases, including serine- metallo- cysteine- and glutamic proteases (see Figure 21 and Figure 23). Proteolytic degradation of plant receptors may prevent detection of PAMPs and subsequent signaling cascades triggering PTI. A frequent PTI response of the plant is the production and release of short extracellular danger-associated plant elicitor peptides (PEPs) that are sensed by and activate immune responses in surrounding cells (Yu *et al*, 2024). Apoplastic bacterial proteases may degrade these PEPs, thus inhibiting plant signaling. Additionally, plants secrete CWDE-inhibiting proteins such as xylanase- and polygalacturonase-inhibiting-proteins (XIPs and PGIPs) into the apoplast in response to pathogens (Xiao *et al*, 2024; Tundo *et al*, 2022). Degradation of these plant XIPs and PGIPs by bacterial proteases may be the pathogens way of defending the function of its' own CWDEs.

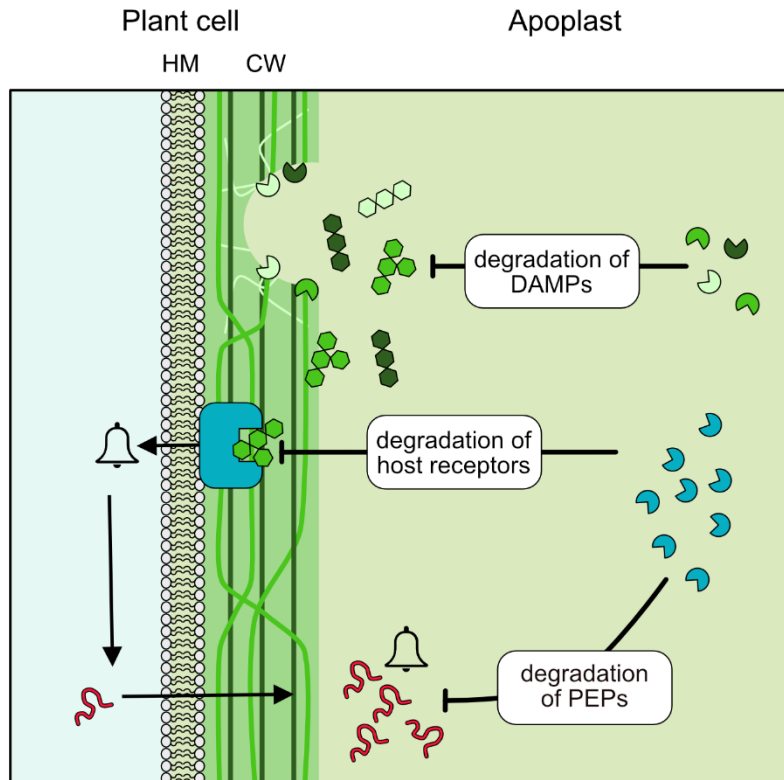


Figure 32: Potential inhibition of PTI responses by T2S substrates

The interface of a plant cell and the apoplast containing T2S substrates is shown. In the course of infection, DAMPs such as plant cell wall oligosaccharides may be detected by plant receptors (blue rectangle), triggering PTI responses such as the production and release of plant elicitor peptides (PEPs, red). These DAMPs may be degraded by specialized T2S-dependent CWDEs (green, above). Additionally, T2S-dependent proteases (blue, below) may degrade plant receptor proteins or PEPs. HM: host membrane, CW: cell wall

The potential role of T2S substrates in inhibiting PTI was not addressed in this study, and future experiments should therefore focus on this aspect of T2S in *Xanthomonas*. Perception of PAMPs and DAMPs triggers the transcriptional activation of plant genes involved in PTI, such as genes involved in salicylic acid production or PEP precursor genes (Li *et al*, 2016).

To determine whether T2S substrates interfere with induction of PTI, future studies could assess the transcriptional induction of such PTI-induced genes in tomato plants by qRT-PCR, comparing plants infected with wild-type *X. euvesicatoria* to plants challenged with Δxps mutants. It would be expected that induction of PTI-responsive genes is stronger in latter plants if T2S substrates inhibit induction of PTI. Additionally, as a first screen to see if T2S substrates affect DAMP recognition or PEP-signaling, synthetic oligosaccharides that act as DAMPs or synthetic PEPs could be syringe-inoculated into host plants alone or with respective wild-type and T2S mutant *Xanthomonas* strains. As a readout, the activation of DAMP- or PEP-induced genes would be determined by qRT-PCR and compared between different treatments, to see if co-inoculation with bacteria secreting proteases decreases DAMP-recognition or PEP signaling *in planta*. A more elegant approach would be constructing and analyzing a *Xanthomonas* strain with deletions of all secreted proteases but

still with a functional T2S system. However, as many different proteases are secreted, this would be very cumbersome.

5.2.3 Functional interplay between T2S and T3S in virulence?

Two alternative ways of the T2S system supporting the T3S system in *Xanthomonas* are conceivable: either degradative functions of T2S substrates release plant-derived signals such as cell wall saccharides that are perceived by bacteria to upregulate T3S genes (Vieira *et al*, 2021), or degradation of the plant cell wall assists the T3S pilus assembly and subsequent effector delivery (Szczesny *et al*, 2010). However, these two potential T2S functions are beyond the scope of the present study.

The T3S system of *X. euvesicatoria* is encoded by *hrp* (hypersensitive response and pathogenicity) genes. These are transcriptionally controlled by two regulators, an AraC-type transcriptional activator called HrpX and HrpG, related to OmpR family two-component regulators (Büttner & Bonas, 2002), and can be activated *in planta* or in minimal media mimicking *in planta* conditions (Lindgren, 1997). Upon expression of *hrp* genes, an additional signal is required for assembly of the system and functional T3S. *In vitro*, this can be achieved by lowering the pH (Rossier *et al*, 1999). There seem to be species-specific differences in carbohydrate dependent regulation of the T3S system (Wengelnik *et al*, 1996). While fructose and sucrose are sufficient to induce the expression of *hrp* genes in *X. euvesicatoria*, xylose and galactose are required to activate these genes in *X. oryzae* pv. *oryzae* and *X. citri* pv. *citri* (Ikawa *et al*, 2018; Tsuge & Ikawa, 2023; Vieira *et al*, 2021). Both xylose and galactose are probably released *in planta* in T2S-mediated degradation of the plant cell wall. It would therefore be interesting to systematically analyze the role of the T2S system in releasing monosaccharides from the plant cell wall that activate *hrp* genes in different *Xanthomonas* species. To this end, the induction of T3S system *hrp* genes would be quantified by qRT-PCR in wild-type and T2S mutants of different *Xanthomonas* species cultivated in minimal media with selected carbohydrate sources such as plant cell wall extracts, xylan, xyloglucan or cellulose, as well as monosaccharides such as glucose, xylose, galactose.

Whether the breakdown of the cell wall assists T3S pilus assembly is difficult to determine experimentally. However, *X. euvesicatoria* T2S mutants still induce an HR response in resistant pepper plants due to the delivery of T3S effectors. Thus cell wall degradation by T2S substrates does not appear essential for T3S pilus assembly (Szczesny *et al*, 2010).

5.3 Employing the Xps-T2S to expand the metabolic capabilities of *E. coli*

A potential application of the T2S substrates characterized in this study could be the generation of *E. coli* strains able to utilize other nutrient sources to reduce costs in protein production. Typically, *E. coli* strains are cultured with complex but processed amino acid- and carbohydrate-sources such as tryptone, yeast extract, glycerol or glucose (Shahzadi et al, 2021; Ferreira et al, 2018). While these are not dramatically expensive, costs could be reduced if non-processed industrial waste products were used to culture *E. coli*, like carbohydrate-rich agricultural waste products such as corn cob. *E. coli* should be able to metabolize various monosaccharides once they are released from complex plant carbohydrates, as in its native habitat in the human gut, *E. coli* utilizes the mono- and disaccharides released from complex plant-derived polysaccharides degraded by other gut bacteria (Conway & Cohen, 2015). Costs could be further reduced if processed amino acid-sources such as tryptone were replaced with protein-rich dairy waste products such as cheese whey which can be used to culture *Xanthomonas* strains (Silva et al, 2009). As extensive expression toolkits have already been developed and optimized for *E. coli* (Rosano et al, 2019), expanding its nutrient utilization capacities may be simpler for industrial protein production than establishing and optimizing expression systems in other metabolically diverse bacteria such as *Cellvibrio japonicus* (Attia et al, 2018).

Employing the Xps-T2S system from *X. euvesicatoria* in *E. coli* requires some genetic reorganization of the gene cluster. The *Xanthomonas*-specific promoters of the *xps* genes need to be replaced with promoters functional in *E. coli*. Furthermore, the different *xps* genes need to be expressed in the correct stoichiometric ratio in *E. coli* to form a functional T2S system in the cell. To achieve this, the ribosome-binding sites that control the translation of the *xps* genes may need to be exchanged to suit the translation machinery of *E. coli*. A simple way of optimizing the transcriptional and translational nuances of protein expression is to employ promoter- and RBS-libraries. Thereby, the *xps* genes would be cloned under the control of many different promoter- and RBS-variants simultaneously, and all varying constructs subsequently screened to find combinations of promoters and RBSs that yield a functional T2S system in *E. coli*. Appropriate Golden Gate-compatible promoter- and RBS-libraries have already been generated (S. Marillonnet, unpublished). To accommodate for a simple screen of T2S, a T2S-dependent protease such as XCV3671 would be included in the genetic constructs, and cells carrying the *xps* gene clusters for *E. coli* could be cultured on solid medium containing skim milk powder. Functional T2S would lead to the secretion of the protease, resulting in halo formation around the colony. Subsequently, such an optimized *xps* gene cluster for *E. coli* could be expressed together with appropriate T2S substrates,

including proteases and/or CWDEs, to facilitate growth on protein rich industrial waste or complex carbohydrate sources from agricultural waste. Furthermore, as photo-crosslinking was optimized for *E. coli* but may not be possible in *Xanthomonas* (see 5.1.2), a heterologous functional Xps-T2S system could also facilitate targeted photo-crosslinking approaches to characterize specific protein-protein interactions of the system.

A previous attempt to generate such an *E. coli*-compatible Xps-T2S replaced the promoters of the system and some RBSs but retained the native *xpsG-D* operon structure from *X. euvesicatoria* (Kraleva, 2024). No functional *xps* gene clusters could be generated with this approach (Kraleva, 2024), and future experiments should therefore reorganize this *xpsG-D* operon as well, so that each individual gene is expressed under an RBS-library. However, it is possible that differences in the organization of the cell envelope of *E. coli* and *X. euvesicatoria* like peptidoglycan organization may impede Xps-T2S function in *E. coli*.

As an alternative to expressing an entire heterologous Xps-T2S system to deliver T2S substrates, one could simply express respective T2S substrates in the *E. coli* BL21 strain, in which leakage of periplasmic proteins occurs (see 4.2.2). One could test if the BL21 cells secreting the proteases XCV3671, XCV3406, XCV3407, XCV3013 can be cultured in minimal medium with unprocessed milk protein, as shown for *Xanthomonas* (see 4.2.5). This may be cheaper than culturing in media that require processed amino acid sources such as tryptone. However, protease-secreting cells may not be conducive to heterologous protein production, as the desired recombinant proteins may also be degraded.

Culturing *E. coli* BL21 cells expressing *Xanthomonas* CWDEs on complex carbohydrates may be more conducive to reducing industrial protein production costs. Initially, growth of *E. coli* strains secreting specific CWDEs such as xylanases or cellulases would be examined in minimal medium with the respective polysaccharide as sole carbohydrate source, such as xylan or cellulose. Similar approaches have previously led to cellulose and xylan utilization in *E. coli* (Gao *et al*, 2015, 2020; Zhang *et al*, 2024a; Salamanca-Cardona *et al*, 2014). Subsequently, growth on minimal medium with plant cell wall extracts as a sole carbon source would be assessed for strains producing multiple different secreted CWDEs simultaneously, including xylanases, cellulases and polygalacturonases. Testing different combinations of CWDEs would provide a platform to determine what CWDEs are required to access cell wall monosaccharides and how these mutually benefit from one another. By excluding polygalacturonases, it could be determined whether pectin degradation is required to access cellulose and hemicelluloses, as postulated above (see 5.2.1). On the long run, this may lay the foundation to generate *E. coli* strains capable of recycling agricultural waste products such as corn cob to produce high-value enzymes, potentially reducing protein production costs.

6 References

- Abby SS, Cury J, Guglielmini J, Néron B, Touchon M & Rocha EPC (2016) Identification of protein secretion systems in bacterial genomes. *Scientific Reports* 2016 6:1 6: 1–14
- Abendroth J, Mitchell DD, Korotkov K V., Johnson TL, Kreger A, Sandkvist M & Hol WGJ (2009) The three-dimensional structure of the cytoplasmic domains of EpsF from the type 2 secretion system of *Vibrio cholerae*. *J Struct Biol* 166: 303–315
- Albers SV, Szabó Z & Driessen AJM (2006) Protein secretion in the Archaea: multiple paths towards a unique cell surface. *Nature Reviews Microbiology* 2006 4:7 4: 537–547
- Alvarez-Martinez CE, Sgro GG, Araujo GG, Paiva MRN, Matsuyama BY, Guzzo CR, Andrade MO & Farah CS (2020) Secrete or perish: The role of secretion systems in *Xanthomonas* biology. *Comput Struct Biotechnol J* 19: 279–302
- del Amo-Maestro L, Mendes SR, Rodríguez-Banqueri A, Garzon-Flores L, Girbal M, Rodríguez-Lagunas MJ, Guevara T, Franch À, Pérez-Cano FJ, Eckhard U, *et al* (2022) Molecular and *in vivo* studies of a glutamate-class prolyl-endopeptidase for coeliac disease therapy. *Nature Communications* 2022 13:1 13: 1–16
- An SQ, Potnis N, Dow M, Vorhölter FJ, He YQ, Becker A, Teper D, Li Y, Wang N, Bleris L, *et al* (2020) Mechanistic insights into host adaptation, virulence and epidemiology of the phytopathogen *Xanthomonas*. *FEMS Microbiol Rev* 44: 1–32
- Apama G, Chatterjee A, Sonti R V. & Sankaranarayanan R (2009) A Cell Wall–Degrading Esterase of *Xanthomonas oryzae* Requires a Unique Substrate Recognition Module for Pathogenesis on Rice. *Plant Cell* 21: 1860
- Ashkenazy H, Abadi S, Martz E, Chay O, Mayrose I, Pupko T & Ben-Tal N (2016) ConSurf 2016: an improved methodology to estimate and visualize evolutionary conservation in macromolecules. *Nucleic Acids Res* 44: W344–W350
- Aslam SN, Newman MA, Erbs G, Morrissey KL, Chinchilla D, Boller T, Jensen TT, De Castro C, Ierano T, Molinaro A, *et al* (2008) Bacterial polysaccharides suppress induced innate immunity by calcium chelation. *Curr Biol* 18: 1078–1083
- Attia MA, Nelson CE, Offen WA, Jain N, Davies GJ, Gardner JG & Brumer H (2018) *In vitro* and *in vivo* characterization of three *Cellvibrio japonicus* glycoside hydrolase family 5 members reveals potent xyloglucan backbone-cleaving functions. *Biotechnol Biofuels* 11: 45
- Baptista JC, Machado MA, Homem RA, Torres PS, Vojnov AA & Do Amaral AM (2010) Mutation in the xpsD gene of *Xanthomonas axonopodis* pv. *citri* affects cellulose degradation and virulence. *Genet Mol Biol* 33: 146–153
- Barbat B, Douzi B, Ball G, Tribout M, Karkouri K El, Kellenberger C & Voulhoux R (2023) Insights into dynamics and gating properties of T2SS secretins. *Sci Adv* 9
- Beckwith J (2013) The Sec-dependent pathway. *Res Microbiol* 164: 497
- Benz I & Schmidt MA (2011) Structures and functions of autotransporter proteins in microbial pathogens. *International Journal of Medical Microbiology* 301: 461–468
- Bernstein HD (2019) Type V Secretion in Gram-Negative Bacteria. *EcoSal Plus* 8: 10.1128/ecosalplus.ESP-0031–2018
- Bertani G (1951) Studies on lysogenesis. I. The mode of phage liberation by lysogenic *Escherichia coli*. *J Bacteriol* 62: 293–300
- Bhardwaj N, Kumar B & Verma P (2019) A detailed overview of xylanases: an emerging biomolecule for current and future prospective. *Bioresources and Bioprocessing* 2019 6:1 6: 1–36
- Bhat IM, Wani SM, Mir SA & Masoodi FA (2022) Advances in xanthan gum production, modifications and its applications. *Biocatal Agric Biotechnol* 42: 102328
- Bischof LF, Friedrich C, Harms A, Søgaard-Andersen L & Van Der Does C (2016) The Type IV pilus assembly ATPase PilB of *Myxococcus xanthus* interacts with the inner membrane platform protein PilC and the nucleotide-binding protein PilM. *Journal of Biological Chemistry* 291: 6946–6957
- Bleves S, Gérard-Vincent M, Lazdunski A & Filloux A (1999) Structure-function analysis of XcpP, a component involved in general secretory pathway-dependent protein secretion in *Pseudomonas aeruginosa*. *J Bacteriol* 181: 4012–4019

- Block A & Alfano JR (2011) Plant targets for *Pseudomonas syringae* type III effectors: virulence targets or guarded decoys? *Curr Opin Microbiol* 14: 39–46
- Boch J, Scholze H, Schornack S, Landgraf A, Hahn S, Kay S, Lahaye T, Nickstadt A & Bonas U (2009) Breaking the code of DNA binding specificity of TAL-type III effectors. *Science* (1979) 326: 1509–1512
- Bouley J, Condemine G & Shevchik VE (2001) The PDZ domain of OutC and the N-terminal region of OutD determine the secretion specificity of the type II out pathway of *Erwinia chrysanthemi*. *J Mol Biol* 308: 205–219
- Braet J, Catteeuw D & Van Damme P (2022) Recent Advancements in Tracking Bacterial Effector Protein Translocation. *Microorganisms* 10
- Brown PJB, Chang JH & Fuqua C (2023) *Agrobacterium tumefaciens*: a Transformative Agent for Fundamental Insights into Host-Microbe Interactions, Genome Biology, Chemical Signaling, and Cell Biology. *J Bacteriol* 205: e00005–23
- Broxterman SE & Schols HA (2018) Characterisation of pectin-xylan complexes in tomato primary plant cell walls. *Carbohydr Polym* 197
- Buddelmeijer N, Krehenbrink M, Pecorari F & Pugsley AP (2009) Type II secretion system secretin PulD localizes in clusters in the *Escherichia coli* outer membrane. *J Bacteriol* 91: 161–168
- Büttner D (2012) Protein Export According to Schedule: Architecture, Assembly, and Regulation of Type III Secretion Systems from Plant- and Animal-Pathogenic Bacteria. *Microbiol Mol Biol Rev* 76: 262
- Büttner D (2016) Behind the lines-actions of bacterial type III effector proteins in plant cells. *FEMS Microbiol Rev* 40: 894–937
- Büttner D & Bonas U (2002) Getting across - Bacterial type III effector proteins on their way to the plant cell. *EMBO Journal* 21: 5313–5322 doi:10.1093/emboj/cdf536
- Büttner D & Bonas U (2010) Regulation and secretion of *Xanthomonas* virulence factors. *FEMS Microbiol Rev* 34: 107–133 doi:10.1111/j.1574-6976.2009.00192.x
- Cascales E & Christie PJ (2004) Definition of a Bacterial Type IV Secretion Pathway for a DNA Substrate. *Science* 304: 10.1126/science.1095211
- Chang YW, Rettberg LA, Treuner-Lange A, Iwasa J, Søgaard-Andersen L & Jensen GJ (2016) Architecture of the type IVa pilus machine. *Science* (1979) 351
- Chen LQ, Hou BH, Lalonde S, Takanaga H, Hartung ML, Qu XQ, Guo WJ, Kim JG, Underwood W, Chaudhuri B, *et al* (2010) Sugar transporters for intercellular exchange and nutrition of pathogens. *Nature* 468: 527–532
- Chen LY, Chen DY, Miaw J & Hu NT (1996) XpsD, an outer membrane protein required for protein secretion by *Xanthomonas campestris* pv. *campestris*, forms a multimer. *Journal of Biological Chemistry* 271: 2703–2708
- Chernyatina AA & Low HH (2019) Core architecture of a bacterial type II secretion system. *Nat Commun* 10
- Cherrak Y, Flaugnatti N, Durand E, Journet L & Cascales E (2019) Structure and Activity of the Type VI Secretion System. *Microbiol Spectr* 7: 10.1128/microbiolspec.psib-0031–2019
- Chylińska M, Szymańska-Chargot M & Zdunek A (2014) Imaging of polysaccharides in the tomato cell wall with Raman microspectroscopy. *Plant Methods* 10: 1–9
- Cianciotto NP & White RC (2017) Expanding role of type II secretion in bacterial pathogenesis and beyond. *Infect Immun* 85
- Conway T & Cohen PS (2015) Commensal and Pathogenic *Escherichia coli* Metabolism in the Gut . *Microbiol Spectr* 3
- Cosgrove DJ (2023) Structure and growth of plant cell walls. *Nature Reviews Molecular Cell Biology* 2023 25:5 25: 340–358
- Costa TRD, Harb L, Khara P, Zeng L, Hu B & Christie PJ (2021) Type IV secretion systems: Advances in structure, function, and activation. *Mol Microbiol* 115: 436–452
- Coulthurst S (2019) The Type VI secretion system: A versatile bacterial weapon. *Microbiology (United Kingdom)* 165: 503–515
- Daniels MJ, Barber CE & Turner PC (1984a) Isolation of mutants of *Xanthomonas campestris* pv. *campestris* showing altered pathogenicity. *J Gen Microbiol* 130: 2447–2455

- Daniels MJ, Barber CE, Turner PC, Sawczyc MK, Byrde RJW & Fielding AH (1984b) Cloning of genes involved in pathogenicity of *Xanthomonas campestris* pv. *campestris* using the broad host range cosmid pLAFR1. *EMBO J* 3: 3323–3328
- Dazzoni R, Li Y, López-Castilla A, Brier S, Mechaly A, Cordier F, Haouz A, Nilges M, Francetic O, Bardiaux B, *et al* (2023) Structure and dynamic association of an assembly platform subcomplex of the bacterial type II secretion system. *Structure* 31: 152-165.e7
- Déjean G, Blanvillain-Baufumé S, Boulanger A, Darrasse A, De Bernonville TD, Girard AL, Carrère S, Jamet S, Zischek C, Lautier M, *et al* (2013) The xylan utilization system of the plant pathogen *Xanthomonas campestris* pv. *campestris* controls epiphytic life and reveals common features with oligotrophic bacteria and animal gut symbionts. *New Phytologist* 198: 899–915
- Deng W, Marshall NC, Rowland JL, McCoy JM, Worrall LJ, Santos AS, Strynadka NCJ & Finlay BB (2017) Assembly, structure, function and regulation of type III secretion systems. *Nat Rev Microbiol* 15: 323–337 doi:10.1038/nrmicro.2017.20
- Desvaux M, Parham NJ, Scott-Tucker A & Henderson IR (2004) The general secretory pathway: A general misnomer? *Trends Microbiol* 12: 306–309
- Douzi B, Ball G, Cambillau C, Tegoni M & Voulhoux R (2011) Deciphering the Xcp *Pseudomonas aeruginosa* Type II Secretion Machinery through Multiple Interactions with Substrates. *J Biol Chem* 286: 40792
- Drehkopf S, Otten C, Hausner J, Seifert T & Büttner D (2020) HrpB7 from *Xanthomonas campestris* pv. *vesicatoria* is an essential component of the type III secretion system and shares features of HrpO/FliJ/YscO family members. *Cell Microbiol* 22: e13160
- Engler C, Kandzia R & Marillonnet S (2008) A one pot, one step, precision cloning method with high throughput capability. *PLoS One* 3
- Fatima U & Senthil-Kumar M (2015) Plant and pathogen nutrient acquisition strategies. *Front Plant Sci* 6: 162246
- Feiz L, Irshad M, Pont-Lezica RF, Canut H & Jamet E (2006) Evaluation of cell wall preparations for proteomics: A new procedure for purifying cell walls from *Arabidopsis* hypocotyls. *Plant Methods* 2: 1–13
- Figurski DH & Helinski DR (1979) Replication of an origin-containing derivative of plasmid RK2 dependent on a plasmid function provided in trans. *Proceedings of the National Academy of Sciences* 76: 1648–1652
- Filloux A (2004) The underlying mechanisms of type II protein secretion. *Biochimica et Biophysica Acta (BBA) - Molecular Cell Research* 1694: 163–179
- Filloux A (2022) Bacterial protein secretion systems: Game of types. *Microbiology (United Kingdom)* 168: 001193
- Francetic O, Belin D, Badaut C & Pugsley AP (2000) Expression of the endogenous type II secretion pathway in *Escherichia coli* leads to chitinase secretion. *EMBO J* 19: 6697–6703
- Fry SC (2004) Primary cell wall metabolism: tracking the careers of wall polymers in living plant cells. *New Phytologist* 161: 641–675
- Gao C, Guo L, Ding Q, Hu G, Ye C, Liu J, Chen X & Liu L (2020) Dynamic consolidated bioprocessing for direct production of xylonate and shikimate from xylan by *Escherichia coli*. *Metab Eng* 60: 128–137
- Gao D, Luan Y, Wang Q, Liang Q & Qi Q (2015) Construction of cellulose-utilizing *Escherichia coli* based on a secretable cellulase. *Microb Cell Fact* 14: 159
- Gao L, Guan Z, Gao P, Zhang W, Qi Q & Lu X (2020b) *Cytophaga hutchinsonii* gldN, Encoding a Core Component of the Type IX Secretion System, Is Essential for Ion Assimilation, Cellulose Degradation, and Cell Motility. *Appl Environ Microbiol* 86: e00242-20
- Gardner JG & Keating DH (2010) Requirement of the type II secretion system for utilization of cellulosic substrates by *Cellvibrio japonicus*. *Appl Environ Microbiol* 76: 5079–5087
- Geilfus CM (2017) The pH of the Apoplast: Dynamic Factor with Functional Impact Under Stress. *Mol Plant* 10: 1371–1386
- Ghosal D, Kim KW, Zheng H, Kaplan M, Truchan HK, Lopez AE, McIntire IE, Vogel JP, Cianciotto NP & Jensen GJ (2019) *In vivo* structure of the *Legionella* type II secretion system by electron cryotomography. *Nature Microbiology* 2019 4:12 4: 2101–2108

- Gluck-Thaler E, Cerutti A, Perez-Quintero AL, Butchacas J, Roman-Reyna V, Madhavan VN, Shantharaj D, Merfa M V., Pesce C, Jauneau A, *et al* (2020) Repeated gain and loss of a single gene modulates the evolution of vascular plant pathogen lifestyles. *Sci Adv* 6
- Goddard TD, Huang CC, Meng EC, Pettersen EF, Couch GS, Morris JH & Ferrin TE (2018) UCSF ChimeraX: Meeting modern challenges in visualization and analysis. *Protein Science* 27: 14–25
- Gorasia DG, Veith PD & Reynolds EC (2020) The Type IX Secretion System: Advances in Structure, Function and Organisation. *Microorganisms* 8: 1173
- Gralka M, Pollak S & Cordero OX (2023) Genome content predicts the carbon catabolic preferences of heterotrophic bacteria. *Nature Microbiology* 2023 8:10 8: 1799–1808
- Greenberg JT & Yao N (2004) The role and regulation of programmed cell death in plant–pathogen interactions. *Cell Microbiol* 6: 201–211
- Grossman AS, Mauer TJ, Forest KT & Goodrich-Blair H (2021) A widespread bacterial secretion system with diverse substrates. *mBio* 12
- Gu S, Kelly G, Wang X, Frenkiel T, Shevchik VE & Pickersgill RW (2012) Solution Structure of Homology Region (HR) Domain of Type II Secretion System. *Journal of Biological Chemistry* 287: 9072–9080
- Gu S, Shevchik VE, Shaw R, Pickersgill RW & Garnett JA (2017) The role of intrinsic disorder and dynamics in the assembly and function of the type II secretion system. *Biochimica et Biophysica Acta (BBA) - Proteins and Proteomics* 1865: 1255–1266
- Guilvout I, Samsudin F, Huber RG, Bond PJ, Bardiaux B & Francetic O (2024) Membrane platform protein PulF of the *Klebsiella* type II secretion system forms a trimeric ion channel essential for endopilus assembly and protein secretion. *mBio* 15
- Guo S, Stevens CA, Vance TDR, Olijve LLC, Graham LA, Campbell RL, Yazdi SR, Escobedo C, Bar-Dolev M, Yashunsky V, *et al* (2017) Structure of a 1.5-MDa adhesin that binds its Antarctic bacterium to diatoms and ice. *Sci Adv* 3
- Halte M & Erhardt M (2021) Protein Export via the Type III Secretion System of the Bacterial Flagellum. *Biomolecules* 11: 1–19
- Harding CM, Kinsella RL, Palmer LD, Skaar EP & Feldman MF (2016) Medically Relevant *Acinetobacter* Species Require a Type II Secretion System and Specific Membrane-Associated Chaperones for the Export of Multiple Substrates and Full Virulence. *PLoS Pathog* 12: e1005391
- Hausner J, Hartmann N, Jordan M & Büttner D (2017) The predicted lytic transglycosylase HpaH from *Xanthomonas campestris* pv. *vesicatoria* associates with the type III secretion system and promotes effector protein translocation. *Infect Immun* 85: 788–804
- Hausner J, Jordan M, Otten C, Marillonnet S & Büttner D (2019) Modular Cloning of the Type III Secretion Gene Cluster from the Plant-Pathogenic Bacterium *Xanthomonas euvesicatoria*. *ACS Synth Biol* 8: 532–547
- Henderson IR & Nataro JP (2005) Autotransporter Proteins. *EcoSal Plus* 1
- Hoffman EA, Frey BL, Smith LM & Auble DT (2015) Formaldehyde crosslinking: a tool for the study of chromatin complexes. *J Biol Chem* 290: 26404–26411
- Hou S, Liu Z, Shen H & Wu D (2019) Damage-associated molecular pattern-triggered immunity in plants. *Front Plant Sci* 10: 453679
- Hu NT, Lee PF & Chen C (1995) The type IV pre-pilin leader peptidase of *Xanthomonas campestris* pv. *campestris* is functional without conserved cysteine residues. *Mol Microbiol* 18: 769–777
- Huguet E, Hahn K, Wengelnik K & Bonas U (1998) hpaA mutants of *Xanthomonas campestris* pv. *vesicatoria* are affected in pathogenicity but retain the ability to induce host-specific hypersensitive reaction. *Mol Microbiol* 29: 1379–1390
- Hwang I (1992) Use of Detached Soybean Cotyledons for Testing Pathogenicity of *Xanthomonas campestris* pv. *glycines*. *Plant Dis* 76: 182
- Ikawa Y, Ohnishi S, Shoji A, Furutani A & Tsuge S (2018) Concomitant regulation by a LacI-Type transcriptional repressor XylR on genes involved in xylan and xylose metabolism and the type III secretion system in rice pathogen *Xanthomonas oryzae* pv. *oryzae*. *Molecular Plant-Microbe Interactions* 31: 605–613

- Ingel B, Castro C, Burbank L, Her N, De Anda NI, Way H, Wang P & Roper MC (2023) *Xylella fastidiosa* Requires the Type II Secretion System for Pathogenicity and Survival in Grapevine. *Molecular Plant-Microbe Interactions* 36: 636–646
- Izadi-Pruneyre N, Karami Y & Nilges M (2024) Structure and Dynamics of Type 4a Pili and Type 2 Secretion System Endopili. *Subcell Biochem* 104: 549–563
- Jacobs JM, Pesce C, Lefeuvre P & Koebnik R (2015) Comparative genomics of a cannabis pathogen reveals insight into the evolution of pathogenicity in *Xanthomonas*. *Front Plant Sci* 6: 148004
- Jacq A, Burlat V & Jamet E (2017) Plant Cell Wall Proteomics as a Strategy to Reveal Candidate Proteins Involved in Extracellular Lipid Metabolism. *Curr Protein Pept Sci* 19: 190–199
- Jha G, Rajeshwari R & Sonti R V. (2005) Bacterial type two secretion system secreted proteins: Double-edged swords for plant pathogens. *Molecular Plant-Microbe Interactions* 18: 891–898 doi:10.1094/MPMI-18-0891
- Jha G, Rajeshwari R & Sonti R V. (2007) Functional Interplay Between Two *Xanthomonas oryzae* pv. *oryzae* Secretion Systems in Modulating Virulence on Rice. <https://doi.org/10.1094/MPMI-20-0031> 20: 31–40
- Jones JDG & Dangl JL (2006) The plant immune system. *Nature* 2006 444:7117 444: 323–329
- Jones JDG, Staskawicz BJ & Dangl JL (2024) The plant immune system: From discovery to deployment. *Cell* 187: 2095–2116
- Jumper J, Evans R, Pritzel A, Green T, Figurnov M, Ronneberger O, Tunyasuvunakool K, Bates R, Židek A, Potapenko A, *et al* (2021) Highly accurate protein structure prediction with AlphaFold. *Nature* 2021 596:7873 596: 583–589
- Kaewnum S, Prathuangwong S & Burr TJ (2006) A Pectate Lyase Homolog, xagP, in *Xanthomonas axonopodis* pv. *glycines* Is Associated with Hypersensitive Response Induction on Tobacco. *Phytopathology* 96: 1230–1236
- Kapitein N, Bönenmann G, Pietrosiuk A, Seyffer F, Hausser I, Locker JK & Mogk A (2013) ClpV recycles VipA/VipB tubules and prevents non-productive tubule formation to ensure efficient type VI protein secretion. *Mol Microbiol* 87: 1013–1028
- Karimova G, Dautin N & Ladant D (2005) Interaction network among *Escherichia coli* membrane proteins involved in cell division as revealed by bacterial two-hybrid analysis. *J Bacteriol* 187: 2233–2243
- Kleuter M, Yu Y, Pancaldi F, Nagtzaam M, van der Goot AJ & Trindade LM (2024) Cell wall as a barrier for protein extraction from tomato leaves: A biochemical study. *Plant Physiology and Biochemistry* 208: 108495
- Kondo MY, Okamoto DN, Santos JAN, Juliano MA, Oda K, Pillai B, James MNG, Juliano L & Gouvea IE (2010) Studies on the catalytic mechanism of a glutamic peptidase. *J Biol Chem* 285: 21437–21445
- Korotkov K V., Gonen T & Hol WGJ (2011) Secretins: dynamic channels for protein transport across membranes. *Trends Biochem Sci* 36: 433–443
- Korotkov K V. & Hol WGJ (2008) Structure of the GspK-GspI-GspJ complex from the enterotoxigenic *Escherichia coli* type 2 secretion system. *Nat Struct Mol Biol* 15: 462–468
- Korotkov K V., Krumm B, Bagdasarian M & Hol WGJ (2006) Structural and functional studies of EpsC, a crucial component of the type 2 secretion system from *Vibrio cholerae*. *J Mol Biol* 363: 311–321
- Korotkov K V. & Sandkvist M (2019) Architecture, function, and substrates of the type II secretion system. *EcoSal Plus* 8
- Kousik CS & Ritchie DF (1998) Response of bell pepper cultivars to bacterial spot pathogen races that individually overcome major resistance genes. *Plant Dis* 82: 181–186
- Krалева I (2024) Understanding substrate recognition and translocation in bacterial type II secretion systems.
- Lallemant M, Login FH, Guschinskaya N, Pineau C, Effantin G, Robert X & Shevchik VE (2013) Dynamic interplay between the periplasmic and transmembrane domains of GspL and GspM in the type II secretion system. *PLoS One* 8
- Lee Erickson J & Schuster M (2024) Extracellular proteases from microbial plant pathogens as virulence factors. *Curr Opin Plant Biol* 82: 102621
- Lee HM, Chen JR, Lee HL, Leu WM, Chen LY & Hu NT (2004) Functional dissection of the XpsN (GspC) protein of the *Xanthomonas campestris* pv. *campestris* type II secretion machinery. *J Bacteriol* 186: 2946–2955

- Lee HM, Wang KC, Liu YL, Yew HY, Chen LY, Leu WM, Chen DC & Hu NT (2000) Association of the cytoplasmic membrane protein XpsN with the outer membrane protein XpsD in the type II protein secretion apparatus of *Xanthomonas campestris* pv. *campestris*. *J Bacteriol* 182: 1549–1557
- Leo JC, Grin I & Linke D (2012) Type V secretion: mechanism(s) of autotransport through the bacterial outer membrane. *Philosophical Transactions of the Royal Society B: Biological Sciences* 367: 1088
- Li B, Meng X, Shan L & He P (2016) Transcriptional regulation of pattern-triggered immunity in plants. *Cell Host Microbe* 19: 641
- Li J, Peng C, Mao A, Zhong M & Hu Z (2024) An overview of microbial enzymatic approaches for pectin degradation. *Int J Biol Macromol* 254: 127804
- Li Y, Santos-Moreno J & Francetic O (2023) The periplasmic coiled coil formed by the assembly platform proteins Pull and PulM is critical for function of the *Klebsiella* type II secretion system. *Res Microbiol* 174: 104075
- Lindeberg M, Boyd CM, Keen NT & Collmer A (1998) External loops at the C terminus of *Erwinia chrysanthemi* pectate lyase C are required for species-specific secretion through the out type II pathway. *J Bacteriol* 180: 1431–1437
- Lindgren PB (1997) The role of hrp genes during plant-bacterial interactions. *Annu Rev Phytopathol* 35: 129–152
- Llosa M & Alkorta I (2017) Coupling Proteins in Type IV Secretion. *Curr Top Microbiol Immunol* 413: 143–168
- Login FH, Fries M, Wang X, Pickersgill RW & Shevchik VE (2010) A 20-residue peptide of the inner membrane protein OutC mediates interaction with two distinct sites of the outer membrane secretin OutD and is essential for the functional type II secretion system in *Erwinia chrysanthemi*. *Mol Microbiol* 76: 944–955
- López-Castilla A, Thomassin JL, Bardiaux B, Zheng W, Nivaskumar M, Yu X, Nilges M, Egelman EH, Izadi-Pruneyre N & Francetic O (2017) Structure of the calcium-dependent type 2 secretion pseudopilus. *Nature Microbiology* 2: 1686–1695
- Lopez-Hernandez F, Tryfona T, Rizza A, Yu XL, Harris MOB, Webb AAR, Kotake T & Dupree P (2020) Calcium Binding by Arabinogalactan Polysaccharides Is Important for Normal Plant Development. *Plant Cell* 32: 3346–3369
- Lorrai R & Ferrari S (2021) Host Cell Wall Damage during Pathogen Infection: Mechanisms of Perception and Role in Plant-Pathogen Interactions. *Plants* 2021, Vol 10, Page 399 10: 399
- Lu C, Korotkov K V. & Hol WGJ (2014) Crystal structure of the full-length ATPase GspE from the *Vibrio vulnificus* type II secretion system in complex with the cytoplasmic domain of GspL. *J Struct Biol* 187: 223–235
- Lu C, Turley S, Marionni ST, Park YJ, Lee KK, Patrick M, Shah R, Sandkvist M, Bush MF & Hol WGJ (2013) Hexamers of the Type II Secretion ATPase GspE from *Vibrio cholerae* with Increased ATPase Activity. *Structure* 21: 1707–1717
- Luneau JS, Baudin M, Quiroz Monnens T, Carrère S, Bouchez O, Jardinaud MF, Gris C, François J, Ray J, Torralba B, et al (2022) Genome-wide identification of fitness determinants in the *Xanthomonas campestris* bacterial pathogen during early stages of plant infection. *New Phytologist* 236: 235–248
- Lybarger SR, Johnson TL, Gray MD, Sikora AE & Sandkvist M (2009) Docking and assembly of the type II secretion complex of *Vibrio cholerae*. *J Bacteriol* 191: 3149–3161
- Majewski DD, Okon M, Heinkel F, Robb CS, Vuckovic M, McIntosh LP & Strynadka NCJ (2021) Characterization of the Pilotin-Secretin Complex from the *Salmonella enterica* Type III Secretion System Using Hybrid Structural Methods. *Structure* 29: 125-138.e5
- Marsh JW & Taylor RK (1998) Identification of the *Vibrio cholerae* type 4 prepilin peptidase required for cholera toxin secretion and pilus formation. *Mol Microbiol* 29: 1481–1492
- Meiresonne NY, van der Ploeg R, Hink MA & den Blaauwen T (2017) Activity-related conformational changes in D,D-carboxypeptidases revealed by *in vivo* periplasmic Förster resonance energy transfer assay in *Escherichia coli*. *mBio* 8
- Menna A, Fischer-Stettler M, Pfister B, Andrés GS, Holbrook-Smith D & Sánchez-Rodríguez C (2020) Single-run HPLC Quantification of Plant Cell Wall Monosaccharides. *Bio Protoc* 10
- Meuskens I, Saragliadis A, Leo JC & Linke D (2019) Type V Secretion Systems: An Overview of Passenger Domain Functions. *Front Microbiol* 10: 1163
- Michel G, Bleves S, Ball G, Lazdunski A & Filloux A (1998) Mutual stabilization of the XcpZ and XcpY components of the secretory apparatus in *Pseudomonas aeruginosa*. *Microbiology (N Y)* 144: 3379–3386

- Michel-Souzy S, Douzi B, Cadoret F, Raynaud C, Quinton L, Ball G & Voulhoux R (2018) Direct interactions between the secreted effector and the T2SS components GspL and GspM reveal a new effector-sensing step during type 2 secretion. *Journal of Biological Chemistry* 293: 19441–19450
- Minsavage G V. (1990) Gene-For-Gene Relationships Specifying Disease Resistance in *Xanthomonas campestris* pv. *vesicatoria* - Pepper Interactions . *Molecular Plant-Microbe Interactions* 3: 41
- Mirdita M, Schütze K, Moriwaki Y, Heo L, Ovchinnikov S & Steinegger M (2022) ColabFold: making protein folding accessible to all. *Nature Methods* 2022 19:6 19: 679–682
- Mithani A, Hein J & Preston GM (2011) Comparative Analysis of Metabolic Networks Provides Insight into the Evolution of Plant Pathogenic and Nonpathogenic Lifestyles in *Pseudomonas*. *Mol Biol Evol* 28: 483–499
- Morbitzer R, Elsaesser J, Hausner J & Lahaye T (2011) Assembly of custom TALE-type DNA binding domains by modular cloning. *Nucleic Acids Res* 39: 5790–5799
- Nakamura M, Yasukawa Y, Furusawa A, Fuchiwaki T, Honda T, Okamura Y, Fujita K & Iwai H (2018) Functional characterization of unique enzymes in *Xanthomonas euvesicatoria* related to degradation of arabinofuranoligosaccharides on hydroxyproline-rich glycoproteins. *PLoS One* 13: e0201982
- Naskar S, Hohl M, Tassinari M & Low HH (2021) The structure and mechanism of the bacterial type II secretion system. *Mol Microbiol* 115: 412–424 doi:10.1111/mmi.14664
- Nivaskumar M & Francetic O (2014) Type II secretion system: A magic beanstalk or a protein escalator. *Biochimica et Biophysica Acta (BBA) - Molecular Cell Research* 1843: 1568–1577
- Notti RQ & Stebbins CE (2016) The Structure and Function of Type III Secretion Systems. *Microbiol Spectr* 4: 10.1128/microbiolspec.VMBF-0004–2015
- Nunn DN & Lory S (1991) Product of the *Pseudomonas aeruginosa* gene *pilD* is a prepilin leader peptidase. *Proc Natl Acad Sci U S A* 88: 3281–3285
- O'Leary BM, Neale HC, Geilfus CM, Jackson RW, Arnold DL & Preston GM (2016) Early changes in apoplast composition associated with defence and disease in interactions between *Phaseolus vulgaris* and the halo blight pathogen *Pseudomonas syringae* pv. *phaseolicola*. *Plant Cell Environ* 39: 2172
- O'Leary BM, Rico A, McCraw S, Fones HN & Preston GM (2014) The infiltration-centrifugation technique for extraction of apoplastic fluid from plant leaves using *Phaseolus vulgaris* as an example. *J Vis Exp*
- Oliveira EE, Silva AE, Júnior TN, Gomes MCS, Aguiar LM, Marcelino HR, Araújo IB, Bayer MP, Ricardo NMPS, Oliveira AG, *et al* (2010) Xylan from corn cobs, a promising polymer for drug delivery: Production and characterization. *Bioresour Technol* 101: 5402–5406
- Otten C & Büttner D (2021) HrpB4 from *Xanthomonas campestris* pv. *vesicatoria* acts similarly to SctK proteins and promotes the docking of the predicted sorting platform to the type III secretion system. *Cell Microbiol* 23
- Paauw M, Giesbers M, Pfeilmeier S & Burg HA van den (2024) Four cell wall-degrading enzymes of *Xanthomonas campestris* pv. *campestris* determine bacterial escape from hydathodes to the leaf vasculature. *bioRxiv*: 2024.10.09.617435
- Palmer T & Berks BC (2012) The twin-arginine translocation (Tat) protein export pathway. *Nature Reviews Microbiology* 2012 10:7 10: 483–496
- Patrick M, Gray MD, Sandkvist M & Johnson TL (2010) Type II Secretion in *Escherichia coli* . *EcoSal Plus* 4
- Patrick M, Korotkov K V., Hol WGJ & Sandkvist M (2011) Oligomerization of EpsE Coordinates Residues from Multiple Subunits to Facilitate ATPase Activity. *Journal of Biological Chemistry* 286: 10378–10386
- Pfeilmeier S, Werz A, Ote M, Bortfeld-Miller M, Kirner P, Keppler A, Hemmerle L, Gäbelein CG, Petti GC, Wolf S, *et al* (2024) Leaf microbiome dysbiosis triggered by T2SS-dependent enzyme secretion from opportunistic *Xanthomonas* pathogens. *Nature Microbiology* 2024 9:1 9: 136–149
- Pineau C, Guschinskaya N, Gonçalves IR, Ruau del F, Robert X, Gouet P, Ballut L & Shevchik VE (2021) Structure-function analysis of pectate lyase Pel3 reveals essential facets of protein recognition by the bacterial type 2 secretion system. *Journal of Biological Chemistry* 296
- Pineau C, Guschinskaya N, Robert X, Gouet P, Ballut L & Shevchik VE (2014) Substrate recognition by the bacterial type II secretion system: More than a simple interaction. *Mol Microbiol* 94: 126–140

- Platt R, Drescher C, Park SK & Phillips GJ (2000) Genetic system for reversible integration of DNA constructs and lacZ gene fusions into the *Escherichia coli* chromosome. *Plasmid* 43: 12–23
- Potnis N, Timilsina S, Strayer A, Shantharaj D, Barak JD, Paret ML, Vallad GE & Jones JB (2015) Bacterial spot of tomato and pepper: diverse *Xanthomonas* species with a wide variety of virulence factors posing a worldwide challenge. *Mol Plant Pathol* 16: 907–920
- Pourhassan N. Z, Cui H, Khosa S, Davari MD, Jaeger KE, Smits SHJ, Schwaneberg U & Schmitt L (2022) Optimized Hemolysin Type 1 Secretion System in *Escherichia coli* by Directed Evolution of the Hly Enhancer Fragment and Including a Terminator Region. *ChemBiochem* 23
- Py B, Loiseau L & Barras F (2001) An inner membrane platform in the type II secretion machinery of Gram-negative bacteria. *EMBO Rep* 2: 244–248
- Rêgo AT, Chandran V & Waksman G (2010) Two-step and one-step secretion mechanisms in Gram-negative bacteria: contrasting the type IV secretion system and the chaperone-usheer pathway of pilus biogenesis. *Biochem J* 425: 475–488
- Rico A & Preston GM (2008) *Pseudomonas syringae* pv. *tomato* DC3000 Uses Constitutive and Apoplast-Induced Nutrient Assimilation Pathways to Catabolize Nutrients That Are Abundant in the Tomato Apoplast. <https://doi.org/10.1094/MPMI-21-2-0269> 21: 269–282
- Rosano GL, Morales ES & Ceccarelli EA (2019) New tools for recombinant protein production in *Escherichia coli*: A 5-year update. *Protein Sci* 28: 1412
- Rossier O, Wengelnik K, Hahn K & Bonas U (1999) The *Xanthomonas* Hrp type III system secretes proteins from plant and mammalian bacterial pathogens. *Proc Natl Acad Sci U S A* 96: 9368–9373
- Ryan RP, Vorhölter FJ, Potnis N, Jones JB, Van Sluys MA, Bogdanove AJ & Dow JM (2011) Pathogenomics of *Xanthomonas*: understanding bacterium–plant interactions. *Nature Reviews Microbiology* 2011 9:5 9: 344–355
- Salamanca-Cardona L, Ashe CS, Stipanovic AJ & Nomura CT (2014) Enhanced production of polyhydroxyalkanoates (PHAs) from beechwood xylan by recombinant *Escherichia coli*. *Appl Microbiol Biotechnol* 98: 831–842
- Santos CR, Hoffmam ZB, De Matos Martins VP, Zanphorlin LM, De Paula Assis LH, Honorato RV, De Oliveira PSL, Ruller R & Murakami MT (2014) Molecular mechanisms associated with xylan degradation by *Xanthomonas* plant pathogens. *Journal of Biological Chemistry* 289: 32186–32200
- Savary S, Willocquet L, Pethybridge SJ, Esker P, McRoberts N & Nelson A (2019) The global burden of pathogens and pests on major food crops. *Nat Ecol Evol* 3: 430–439
- Schulze S, Kay S, Büttner D, Egler M, Eschen-Lippold L, Hause G, Krüger A, Lee J, Müller O, Scheel D, *et al* (2012) Analysis of new type III effectors from *Xanthomonas* uncovers XopB and XopS as suppressors of plant immunity. *New Phytologist* 195: 894–911
- Sears RM, May DG & Roux KJ (2019) BioID as a Tool for Protein-Proximity Labeling in Living Cells. *Methods Mol Biol* 2012: 299
- Shahzadi I, Al-Ghamdi MA, Nadeem MS, Sajjad M, Ali A, Khan JA & Kazmi I (2021) Scale-up fermentation of *Escherichia coli* for the production of recombinant endoglucanase from *Clostridium thermocellum*. *Scientific Reports* 2021 11:1 11: 1–10
- Sheng M & Sala C (2001) PDZ domains and the organization of supramolecular complexes. *Annu Rev Neurosci* 24: 1–29
- Shi Y, Queller DC, Tian Y, Zhang S, Yan Q, He Z, He Z, Wu C, Wang C & Shu L (2021) The ecology and evolution of amoeba-bacterium interactions. *Appl Environ Microbiol* 87
- Shiue SJ, Kao KM, Leu WM, Chen LY, Chan NL & Hu NT (2006) XpsE oligomerization triggered by ATP binding, not hydrolysis, leads to its association with XpsL. *EMBO J* 25: 1426–1435
- Shivhare AK (2023) Identifying Novel Type II Secretion Substrates and Understanding the Substrate Recognition by the Type II Secretion System from the Plant- Pathogenic Bacterium *Xanthomonas euvesicatoria*.
- Siebert J (2019) Funktionelle Charakterisierung von drei kleinen Proteinen aus *Xanthomonas*.
- Silva MF, Fornari RCG, Mazutti MA, de Oliveira D, Padilha FF, Cichoski AJ, Cansian RL, Di Luccio M & Treichel H (2009) Production and characterization of xanthan gum by *Xanthomonas campestris* using cheese whey as sole carbon source. *J Food Eng* 90: 119–123

- Singh N & Wagner S (2019) Investigating the assembly of the bacterial type III secretion system injectisome by *in vivo* photocrosslinking. *International Journal of Medical Microbiology* 309 doi:10.1016/j.ijmm.2019.151331
- Singh PK & Donnenberg MS (2023) High throughput and targeted screens for prepilin peptidase inhibitors do not identify common inhibitors of eukaryotic gamma-secretase. *Expert Opin Drug Discov* 18: 563–573
- Skare JT, Ahmer BMM, Seachord CL, Darveau RP & Postle K (1993) Energy transduction between membranes. TonB, a cytoplasmic membrane protein, can be chemically cross-linked *in vivo* to the outer membrane receptor FepA. *Journal of Biological Chemistry* 268: 16302–16308
- Solé M, Scheibner F, Hoffmeister AK, Hartmann N, Hause G, Rother A, Jordan M, Lautier M, Arlat M & Büttner D (2015) *Xanthomonas campestris* pv. *vesicatoria* secretes proteases and xylanases via the Xps type II secretion system and outer membrane vesicles. *J Bacteriol* 197: 2879–2893
- Soni J, Sinha S & Pandey R (2024) Understanding bacterial pathogenicity: a closer look at the journey of harmful microbes. *Front Microbiol* 15: 1370818
- Souza DP, Oka GU, Alvarez-Martinez CE, Bisson-Filho AW, Dunger G, Hobeika L, Cavalcante NS, Alegria MC, Barbosa LRS, Salinas RK, *et al* (2015) Bacterial killing via a type IV secretion system. *Nature Communications* 2015 6:1 6: 1–9
- Stael S, Wurzing B, Mair A, Mehler N, Vothknecht UC & Teige M (2011) Plant organellar calcium signalling: an emerging field. *J Exp Bot* 63: 1525
- Sutherland BW, Toews J & Kast J (2008) Utility of formaldehyde cross-linking and mass spectrometry in the study of protein-protein interactions. *J Mass Spectrom* 43: 699–715
- Szczesny R, Jordan M, Schramm C, Schulz S, Cogez V, Bonas U & Büttner D (2010) Functional characterization of the Xcs and Xps type II secretion systems from the plant pathogenic bacterium *Xanthomonas campestris* pv. *vesicatoria*. *New Phytologist* 187: 983–1002
- Tartoff K & Hobbs C (1987) Improved media for growing plasmid and cosmid clones. *Bethesda Res Lab Focus* 12: 12–
- Tassinari M, Rudzite M, Filloux A & Low HH (2023) Assembly mechanism of a Tad secretion system secretin-pilolin complex. *Nat Commun* 14
- Tayi L, Maku R V., Patel HK & Sonti R V. (2016) Identification of pectin degrading enzymes secreted by *Xanthomonas oryzae* pv. *oryzae* and determination of their role in virulence on rice. *PLoS One* 11
- Tayri-Wilk T, Slavin M, Zamel J, Blass A, Cohen S, Motzik A, Sun X, Shalev DE, Ram O & Kalisman N (2020) Mass spectrometry reveals the chemistry of formaldehyde cross-linking in structured proteins. *Nature Communications* 2020 11:1 11: 1–9
- Teulet A, Camuel A, Perret X & Giraud E (2022) The Versatile Roles of Type III Secretion Systems in Rhizobium-Legume Symbioses. *Annu Rev Microbiol* 76: 45–65
- Thieme F, Koebnik R, Bekel T, Berger C, Boch J, Büttner D, Caldana C, Gaigalat L, Goesmann A, Kay S, *et al* (2005) Insights into genome plasticity and pathogenicity of the plant pathogenic bacterium *Xanthomonas campestris* pv. *vesicatoria* revealed by the complete genome sequence. *J Bacteriol* 187: 7254–7266
- Thomassin JL, Santos Moreno J, Guilvout I, Tran Van Nhieu G & Francetic O (2017) The trans-envelope architecture and function of the type 2 secretion system: new insights raising new questions. *Mol Microbiol* 105: 211–226
- Timilsina S, Potnis N, Newberry EA, Liyanapathirana P, Iruegas-Bocardo F, White FF, Goss EM & Jones JB (2020) *Xanthomonas* diversity, virulence and plant-pathogen interactions. *Nat Rev Microbiol* 18: 415–427
- Tsai RT, Leu WM, Chen LY & Hu NT (2002) A reversibly dissociable ternary complex formed by XpsL, XpsM and XpsN of the *Xanthomonas campestris* pv. *campestris* type II secretion apparatus. *Biochemical Journal* 367: 865
- Tsuge S & Ikawa Y (2023) Close relationships between *hrp* gene expression and sugars/sugar metabolism in *Xanthomonas oryzae* pv. *oryzae*. *Physiol Mol Plant Pathol* 125: 102003
- Tundo S, Mandalà G, Sella L, Favaron F, Bedre R & Kalunke RM (2022) Xylanase Inhibitors: Defense Players in Plant Immunity with Implications in Agro-Industrial Processing. *Int J Mol Sci* 23: 14994
- Vieira PS, Bonfim IM, Araujo EA, Melo RR, Lima AR, Fessel MR, Paixão DAA, Persinoti GF, Rocco SA, Lima TB, *et al* (2021) Xyloglucan processing machinery in *Xanthomonas* pathogens and its role in the transcriptional activation of virulence factors. *Nature Communications* 2021 12:1 12: 1–15

- Voegelé A, O'Brien DP, Subrini O, Sapay N, Cannella SE, Enguéné VYN, Hessel A, Karst J, Hourdel V, Perez ACS, *et al* (2018) Translocation and calmodulin-activation of the adenylate cyclase toxin (CyaA) of *Bordetella pertussis*. *Pathog Dis* 76
- Vorhölter FJ, Wiggerich HG, Scheidle H, Sidhu VK, Mrozek K, Küster H, Pühler A & Niehaus K (2012) Involvement of bacterial TonB-dependent signaling in the generation of an oligogalacturonide damage-associated molecular pattern from plant cell walls exposed to *Xanthomonas campestris* pv. *campestris* pectate lyases. *BMC Microbiol* 12: 239
- Waack U, Johnson TL, Chedid K, Xi C, Simmons LA, Mobley HLT & Sandkvist M (2017) Targeting the Type II Secretion System: Development, Optimization, and Validation of a High-Throughput Screen for the Identification of Small Molecule Inhibitors. *Front Cell Infect Microbiol* 7: 380
- Wagner C, Polke M, Gerlach RG, Linke D, Stierhof YD, Schwarz H & Hensel M (2011) Functional dissection of SiiE, a giant non-fimbrial adhesin of *Salmonella enterica*. *Cell Microbiol* 13: 1286–1301
- Wang L, Rong W & He C (2008) Two *Xanthomonas* extracellular polygalacturonases, *pghAxc* and *pghBxc*, are regulated by type III secretion regulators HrpX and HrpG and are required for virulence. *Molecular Plant-Microbe Interactions* 21: 555–563
- Wang X, Pineau C, Gu S, Guschinskaya N, Pickersgill RW & Shevchik VE (2012) Cysteine scanning mutagenesis and disulfide mapping analysis of arrangement of GspC and GspD protomers within the type 2 secretion system. *J Biol Chem* 287: 19082–19093
- Wang Y, Pruitt RN, Nürnberger T & Wang Y (2022) Evasion of plant immunity by microbial pathogens. *Nature Reviews Microbiology* 20:8 20: 449–464
- Weber E, Engler C, Gruetzner R, Werner S & Marillonnet S (2011) A modular cloning system for standardized assembly of multigene constructs. *PLoS One* 6
- Wengelnik K, Marie C, Russel M & Bonas U (1996) Expression and localization of HrpA1, a protein of *Xanthomonas campestris* pv. *vesicatoria* essential for pathogenicity and induction of the hypersensitive reaction. *J Bacteriol* 178: 1061–1069
- Xiao Y, Sun G, Yu Q, Gao T, Zhu Q, Wang R, Huang S, Han Z, Cervone F, Yin H, *et al* (2024) A plant mechanism of hijacking pathogen virulence factors to trigger innate immunity. *Science* (1979) 383: 732–739
- Xu RQ, Blanvillain S, Feng JX, Jiang B, Le, Li XZ, Wei HY, Kroj T, Lauber E, Roby D, Chen B, *et al* (2008) AvrAC(Xcc8004), a type III effector with a leucine-rich repeat domain from *Xanthomonas campestris* pathovar *campestris* confers avirulence in vascular tissues of *Arabidopsis thaliana* ecotype Col-0. *J Bacteriol* 190: 343–355
- Yadeta KA & Thomma BPHJ (2013) The xylem as battleground for plant hosts and vascular wilt pathogens. *Front Plant Sci* 4: 43568
- Yan Z, Yin M, Xu D, Zhu Y & Li X (2017) Structural insights into the secretin translocation channel in the type II secretion system. *Nature Structural & Molecular Biology* 2017 24:2 24: 177–183
- Yanisch-Perron C, Vieira J & Messing J (1985) Improved M13 phage cloning vectors and host strains: nucleotide sequences of the M13mp18 and pUC19 vectors. *Gene* 33: 103–119
- Yariv B, Yariv E, Kessel A, Masrati G, Chorin A Ben, Martz E, Mayrose I, Pupko T & Ben-Tal N (2023) Using evolutionary data to make sense of macromolecules with a 'face-lifted' ConSurf. *Protein Sci* 32
- Yu X, Huang Z, Cheng Y, Hu K, Zhou Y, Yao H, Shen J, Huang Y, Zhuang X & Cai Y (2024) Comparative Genomics Screens Identify a Novel Small Secretory Peptide, SiSolP12, which Activates Both Local and Systemic Immune Response in Tomatoes and Exhibits Broad-Spectrum Activity. *J Agric Food Chem* 72: 18507–18519
- Zhang B, Gao Y, Zhang L & Zhou Y (2021) The plant cell wall: Biosynthesis, construction, and functions. *J Integr Plant Biol* 63: 251–272
- Zhang S, Gu S, Rycroft P, Ruau del F, Delolme F, Robert X, Ballut L, Pickersgill RW & Shevchik VE (2022) Scaffolding Protein GspB/OutB Facilitates Assembly of the *Dickeya dadantii* Type 2 Secretion System by Anchoring the Outer Membrane Secretin Pore to the Inner Membrane and to the Peptidoglycan Cell Wall. *mBio* 13
- Zhang S, Wang J, Chen Y, Zheng Z & Xu Z (2024a) Efficient secretion of an enzyme cocktail in *Escherichia coli* for hemicellulose degradation. *Int J Biol Macromol* 259: 129205
- Zhang Y, Faucher F, Zhang W, Wang S, Neville N, Poole K, Zheng J & Jia Z (2018) Structure-guided disruption of the pseudopilus tip complex inhibits the Type II secretion in *Pseudomonas aeruginosa*. *PLoS Pathog* 14: e1007343

- Zhang Y, Li Y, de Zeeuw T, Duijts K, Kawa D, Lamers J, Munzert KS, Li H, Zou Y, Jessica Meyer A, *et al* (2024) Root branching under high salinity requires auxin-independent modulation of LATERAL ORGAN BOUNDARY DOMAIN 16 function. *Plant Cell* 36: 899–918
- Zou HS, Song X, Zou LF, Yuan L, Li YR, Guo W, Che YZ, Zhao WX, Duan YP & Chen GY (2012) EcpA, an extracellular protease, is a specific virulence factor required by *Xanthomonas oryzae* pv. *oryzicola* but not by *X. oryzae* pv. *oryzae* in rice. *Microbiology (Reading)* 158: 2372–2383

7 Appendix

7.1 Supplemental tables

Table 11: Modular Cloning vectors used in this study

| Plasmid | description | Reference |
|-----------|---|------------------------------|
| pAGM9121 | Derivative of pUC19, contains <i>lacZα</i> fragment flanked by <i>Bpil</i> sites, CTCA/CGAG overhangs; Sm ^R | (Weber <i>et al.</i> , 2011) |
| pAGM1311 | pUC19-derived level -1 vector, <i>lacZα</i> fragment flanked by <i>Bsal</i> sites, ACAT/TTGT overhangs; Km ^R | (Weber <i>et al.</i> , 2011) |
| pICH41331 | pUC19-derived level 0 vector, <i>lacZα</i> fragment flanked by <i>Bpil</i> sites, GGAG/CGCT overhangs; Sm ^R | (Weber <i>et al.</i> , 2011) |
| pICH41308 | pUC19-derived level 0 vector, <i>lacZα</i> fragment flanked by <i>Bpil</i> sites, AATG/GCTT overhangs; Sm ^R | (Weber <i>et al.</i> , 2011) |
| pICH41295 | pUC19-derived level 0 vector, <i>lacZα</i> fragment flanked by <i>Bpil</i> sites, GGAG/AATG overhangs; Sm ^R | (Weber <i>et al.</i> , 2011) |
| pICH47732 | Level 1 destination vector derived from pBIN19 and pUC19, <i>lacZα</i> fragment flanked by <i>Bsal</i> - (GGAG/CGCT overhangs) and <i>Bpil</i> sites (AATG/GCTT overhangs), for level M position 1; Ap ^R | (Weber <i>et al.</i> , 2011) |
| pICH47742 | Level 1 destination vector derived from pBIN19 and pUC19, <i>lacZα</i> fragment flanked by <i>Bsal</i> - (GGAG/CGCT overhangs) and <i>Bpil</i> sites (GCAA/ACTA overhangs),for level M position 2; Ap ^R | (Weber <i>et al.</i> , 2011) |
| pICH47751 | Level 1 destination vector derived from pBIN19 and pUC19, <i>lacZα</i> fragment flanked by <i>Bsal</i> - (GGAG/CGCT overhangs) and <i>Bpil</i> sites (ACTA/TTAC overhangs), for level M position 3; Ap ^R | (Weber <i>et al.</i> , 2011) |
| pICH47761 | Level 1 destination vector derived from pBIN19 and pUC19, <i>lacZα</i> fragment flanked by <i>Bsal</i> - (GGAG/CGCT overhangs) and <i>Bpil</i> sites (TTAC/CAGA overhangs), for level M position 4; Ap ^R | (Weber <i>et al.</i> , 2011) |
| pICH47772 | Level 1 destination vector derived from pBIN19 and pUC19, <i>lacZα</i> fragment flanked by <i>Bsal</i> - (GGAG/CGCT overhangs) and <i>Bpil</i> sites (CAGA/TGTG overhangs),for level M position 5; Ap ^R | (Weber <i>et al.</i> , 2011) |
| pAGM8031 | Level M vector derived from pBIN19 and pUC19, <i>lacZα</i> fragment flanked by <i>Bpil</i> sites,TGCC/GGGA overhangs, Sm ^R | (Weber <i>et al.</i> , 2011) |
| pICH54011 | Dummy module derived from pBIN19 and pUC19, 15-bp insert for level M position 1 with TGCC/GCAA <i>Bpil</i> fusion sites, Ap ^R | (Weber <i>et al.</i> , 2011) |
| pICH54022 | Dummy module derived from pBIN19 and pUC19, 15-bp insert for level M position 2 with GCAA/ACTA <i>Bpil</i> fusion sites; Ap ^R | (Weber <i>et al.</i> , 2011) |
| pICH54033 | Dummy module derived from pBIN19 and pUC19, 15-bp insert for level M position 3 with ACTA/TTAC <i>Bpil</i> fusion sites; Ap ^R | (Weber <i>et al.</i> , 2011) |
| pICH54044 | Dummy module derived from pBIN19 and pUC19, 15-bp insert for level M position 4 with TTAC/CAGA <i>Bpil</i> fusion sites; Ap ^R | (Weber <i>et al.</i> , 2011) |
| pICH54055 | Dummy module derived from pBIN19 and pUC19, 15-bp insert for level M position 5 with CAGA/TGTG <i>Bpil</i> fusion -sites; Ap ^R | (Weber <i>et al.</i> , 2011) |
| pICH50872 | Level M end-linker for position 6; derived from pUC19, GCAA/- <i>Bsal</i> and GCAA/GGGA <i>Bpil</i> fusion sites; Ap ^R | (Weber <i>et al.</i> , 2011) |
| pICH50914 | Level M end-linker for position 6; derived from pUC19, TGTG/- <i>Bsal</i> and TGTG/GGGA <i>Bpil</i> fusion sites; Ap ^R | (Weber <i>et al.</i> , 2011) |

Table 12: Modular Cloning constructs designed in this study

| Plasmid | description | Assembly | Reference |
|---|--|---|-------------------|
| Constructs for the generation of the modular <i>xps</i> gene cluster | | | |
| Level -2 constructs (unless otherwise noted, assembled with <i>Bpi</i> I and T4 ligase) | | | |
| pT2S011 | Level -2 module containing <i>xpsG</i> promoter (213 bp upstream of <i>xpsG</i>); Sm ^R | pAGM9121 and PCR with: Promoter 3 nt -209 fw / Promoter 3 nt +4 rv | P. Martin, unpub. |
| pT2S012 | Level -2 module containing <i>xpsG</i> ; Sm ^R | pAGM9121 and PCR with: <i>xpsG</i> nt1 fw / <i>xpsG</i> nt492 rv | P. Martin, unpub. |
| pT2S013 | Level -2 module containing <i>xpsH</i> ; Sm ^R | pAGM9121 and PCR with: <i>xpsH</i> nt -13 fw / <i>xpsH</i> nt 510 rv | P. Martin, unpub. |
| pT2S014 | Level -2 module containing <i>xpsI</i> ; Sm ^R | pAGM9121 and PCR with: <i>xpsI</i> nt 1 fw / <i>xpsI</i> nt 417 rv | P. Martin, unpub. |
| pT2S016 | Level -2 module containing bp 1-429 of <i>xpsJ</i> ; Sm ^R | pAGM9121 and PCR with: <i>xpsJ</i> nt 1 fw / <i>xpsJ</i> nt 429 rv | P. Martin, unpub. |
| pT2S017 | Level -2 module containing bp 426-636 of <i>xpsJ</i> ; Sm ^R | pAGM9121 and PCR with: <i>xpsJ</i> nt 426 fw / <i>xpsJ</i> nt 636 rv | P. Martin, unpub. |
| pT2S018 | Level -2 module containing <i>xpsK</i> ; Sm ^R | pAGM9121 and PCR with: <i>xpsK</i> nt 1 fw / <i>xpsK</i> nt 852 rv | P. Martin, unpub. |
| pT2S019 | Level -2 module containing bp 1-449 of <i>xpsL</i> ; Sm ^R | pAGM9121 and PCR with: <i>xpsL</i> nt 1 fw / <i>xpsL</i> nt 449 rv | P. Martin, unpub. |
| pT2S020 | Level -2 module containing bp 446-1122 of <i>xpsL</i> ; Sm ^R | pAGM9121 and PCR with: <i>xpsL</i> nt 446 fw / <i>xpsL</i> nt 1122 rv | P. Martin, unpub. |
| pT2S022 | Level -2 module containing bp 14-654 of <i>xpsM</i> ; Sm ^R | pAGM9121 and PCR with: <i>xpsM</i> nt 14 fw / <i>xpsM</i> nt 654 rv | P. Martin, unpub. |
| pT2S023 | Level -2 module containing bp 8-227 of <i>xpsC</i> ; Sm ^R | pAGM9121 and PCR with: <i>xpsC</i> nt 8 fw / <i>xpsC</i> nt 227 rv | P. Martin, unpub. |
| pT2S024 | Level -2 module containing bp 223-795 of <i>xpsC</i> ; Sm ^R | pAGM9121 and PCR with: <i>xpsC</i> nt 223 fw / <i>xpsC</i> nt 795 rv | P. Martin, unpub. |
| pT2S025 | Level -2 module containing bp 1-1572 of <i>xpsD</i> ; Sm ^R | pAGM9121 and PCR with: <i>xpsD</i> nt 1 fw / <i>xpsD</i> nt 1572 rv | P. Martin, unpub. |
| pT2S026 | Level -2 module containing bp 1568-2292 of <i>xpsD</i> ; Sm ^R | pAGM9121 and PCR with: <i>xpsD</i> nt 1568 fw / <i>xpsD</i> nt 2292 rv | P. Martin, unpub. |
| Level -1 (unless otherwise noted, assembled with <i>Bsa</i> I and T4 ligase) | | | |
| pT2S001 | Level -1 module containing the <i>xpsE</i> promoter (365 bp upstream of <i>xpsE</i>) and <i>xpsE</i> ; Km ^R | pAGM1311 with 4 PCRs: Promoter 1 nt -365 fw / Promoter 1 nt +4 rv <i>XpsE</i> nt 1 fw / <i>XpsE</i> nt 936 rv <i>XpsE</i> nt 932 fw / <i>XpsE</i> nt 1069 rv <i>XpsE</i> nt 1065 fw / <i>XpsE</i> nt 1728 rv | P. Martin, unpub. |
| pT2S005 | Level -1 module containing the <i>xpsF</i> promoter (175 bp upstream of <i>xpsF</i>) and <i>xpsF</i> ; Km ^R | pAGM1311 with 3 PCRs: Promoter 2 nt -175 fw / Promoter 2 nt +4 rv <i>XpsF</i> nt 1 fw / <i>XpsF</i> nt 270 rv <i>XpsF</i> nt 266 fw / <i>XpsF</i> nt 1218 rv | P. Martin, unpub. |
| pT2S015 | Level -1 module containing <i>xpsG</i> , <i>xpsH</i> , <i>xpsI</i> downstream of the <i>xpsG</i> promoter; Km ^R | pAGM1311 with pT2S011+012+013+014 | P. Martin, unpub. |
| pT2S021 | Level -1 module containing <i>xpsJ</i> , <i>xpsK</i> and <i>xpsL</i> ; Km ^R | pAGM1311 with pT2S016+017+018+019+020 | P. Martin, unpub. |
| pT2S028 | Level -1 module containing <i>xpsM</i> , <i>xpsC</i> and <i>xpsD</i> ; Km ^R | pAGM1311 with pT2S022+023+024+025+026 | P. Martin, unpub. |
| Level 0 (unless otherwise noted, assembled with <i>Bpi</i> I and T4 ligase) | | | |
| pT2S002 | Level 0 module containing <i>xpsE</i> downstream of the <i>xpsE</i> promoter; Sm ^R | pICH41331 with pT2S001 | P. Martin, unpub. |
| pT2S006 | Level 0 module containing <i>xpsF</i> downstream of the <i>xpsF</i> promoter; Sm ^R | pICH41331 with pT2S005 | P. Martin, unpub. |
| pT2S030 | Level 0 module containing the <i>xpsG</i> - <i>xpsD</i> operon downstream of the <i>xpsG</i> promoter; Sm ^R | pICH41331 with pT2S015+021+028 | P. Martin, unpub. |

| Plasmid | description | Assembly | Reference |
|---|---|---|-------------------|
| Level 1 (unless otherwise noted, assembled with <i>Bsal</i> and T4 ligase) | | | |
| pT2S032 | Level 1 module containing <i>xpsE</i> downstream of the <i>xpsE</i> promoter; Ap ^R | pICH47742 with pT2S002 | P. Martin, unpub. |
| pT2S034 | Level 1 module containing <i>xpsF</i> downstream of the <i>xpsF</i> promoter; Ap ^R | pICH47751 with pT2S006 | P. Martin, unpub. |
| pT2S036 | Level 1 module containing the <i>xpsG</i> - <i>xpsD</i> operon downstream of the <i>xpsG</i> promoter; Ap ^R | pICH47761 with pT2S030 | P. Martin, unpub. |
| Level M (unless otherwise noted, assembled with <i>Bpil</i> and T4 ligase) | | | |
| pT2S038 | Level M module containing <i>xpsE</i> - <i>xpsD</i> with native promoters; Sm ^R | pAGM8031 with pICH54011+pT2S032+034+036 +pICH54055+pICH50914 | P. Martin, unpub. |
| Constructs for deletion of <i>xps</i> genes | | | |
| Level -2 (unless otherwise noted, assembled with <i>Bpil</i> and T4 ligase) | | | |
| pT2S091 | Level -2 module encoding amino acids 259 - 373 of XpsL and XpsM; Sm ^R | pAGM9121 and PCR with: dxpsL fw / xpsM nt 654 rv | this study |
| pT2S096 | Level -2 module encoding XpsK and amino acids 1-32 of XpsL; Sm ^R | pAGM9121 and PCR with: xpsK nt 1 fw / dxpsL rv | this study |
| pT2S174 | Level -2 module encoding amino acids 1 - 146 of XpsL with a nonsense mutation (GAT → TGA) at codon 147 (XpsL _{D147stop}); Sm ^R | pAGM9121 and PCR with: xpsL part 1 fw / dxpsL 147stop rv | this study |
| pT2S097 | Level -2 module encoding amino acids 149 - 373 of XpsL and amino acids 1 - 33 of XpsM; Sm ^R | pAGM9121 and PCR with: xpsK nt 1 fw / dxpsL rv | this study |
| pT2S092 | Level -2 module encoding amino acids 179 - 217 of XpsM and XpsC; Sm ^R | pAGM9121 and PCR with: dxpsM fw / xpsC nt 795 rv | this study |
| pT2S051 | Level -2 module encoding amino acids 162 - 265 of XpsC; Sm ^R | pAGM9121 and PCR with: dxpsC fw / xpsC nt 795 rv | P. Martin, unpub. |
| pT2S056 | Level -2 module encoding amino acids 1 - 102 of XpsD; Sm ^R | pAGM9121 and PCR with: xpsD nt 1 fw / dxpsD rv | P. Martin, unpub. |
| pT2S175 | Level -2 module encoding amino acids 179 - 217 of XpsM and XpsC _{Δ73-162} ; Sm ^R | pAGM9121 and PCR with: dxpsM fw / dxpsC rv | this study |
| pT2S106 | Level -2 module encoding XpsG _{Δ30-121} and XpsH; Sm ^R | pAGM9121 and 2 PCRs: xpsG nt 1 fw / dxpsG rv dxpsG fw + xpsH nt 510 rv | this study |
| pT2S087 | Level -2 module encoding XpsG, XpsH _{Δ14-107} and XpsI; Sm ^R | pAGM9121 and 2 PCRs: xpsG nt 1 fw / dxpsH1 rv dxpsH2 fw / xpsI nt 417 rv | this study |
| pT2S089 | Level -2 module encoding XpsH and amino acids 1-20 of XpsI; Sm ^R | pAGM9121 and PCR with: xpsH nt 1 fw / dxpsI1 rv | this study |
| pT2S095 | Level -2 module encoding amino acids 126-138 of XpsI and amino acids 1-143 of XpsJ; Sm ^R | pAGM9121 and PCR with: dxpsI2 fw / xpsJ nt 449 rv | this study |
| pT2S105 | Level -2 module encoding XpsI and amino acids 1-13 of XpsJ; Sm ^R | pAGM9121 and PCR with: xpsI nt 1 fw / dxpsJ rv | this study |
| pT2S090 | Level -2 module encoding amino acids 184-211 of XpsJ and XpsK; Sm ^R | pAGM9121 and PCR with: dxpsJ fw / xpsK nt 852 rv | this study |
| pT2S088 | Level -2 module encoding for amino acids 152-211 of XpsJ and XpsK _{Δ29-205} ; Sm ^R | pAGM9121 and 2 PCRs: xpsJ nt 426 fw / dxpsK rv dxpsK fw / xpsL nt 449 rv | this study |
| pT2S431 | Level -2 module encoding for amino acids 184-211 of XpsJ and XpsK _{Δ29-205} ; Sm ^R | pAGM9121 and PCR with: dxpsJ fw + xpsK nt 852 rv (template: pT2S088) | this study |
| pT2S435 | Level -2 module encoding XpsI _{Δ21-125} and amino acids 1-13 of XpsJ; Sm ^R | pAGM9121 and PCR with: xpsI nt 1 fw / dxpsJ rv (template: pT2S131) | this study |
| Level -1 (unless otherwise noted, assembled with <i>Bsal</i> and T4 ligase) | | | |
| pT2S103 | Level -1 module encoding XpsJ, XpsK and amino acids 1 - 32 of XpsL; Km ^R | pAGM1311 with pT2S016+017+096 | this study |
| pT2S099 | Level -1 module encoding amino acids 259 - 373 of XpsL, XpsM, XpsC and XpsD; Km ^R | pAGM1311 with pT2S091+023+024+025+026 | this study |
| pT2S178 | Level -1 module encoding XpsJ, XpsK and XpsL _{D147stop} ; Km ^R | pAGM1311 with pT2S016+017+018+174+020 | this study |

| Plasmid | description | Assembly | Reference |
|---|---|---------------------------------------|-------------------|
| pT2S104 | Level -1 module encoding XpsJ, XpsK, XpsL and amino acids 1 - 33 of XpsM; Km ^R | pAGM1311 with pT2S016+017+018+019+097 | this study |
| pT2S100 | Level -1 module encoding amino acids 179 - 217 of XpsM, XpsC and XpsD; Km ^R | pAGM1311 with pT2S092+025+026 | this study |
| pT2S052 | Level -1 module encoding XpsM, XpsC _{Δ73-162} and XpsD; Km ^R | pAGM1311 with pT2S022+023+051+025+026 | P. Martin, unpub. |
| pT2S57 | Level -1 module encoding XpsM, XpsC and XpsD _{Δ103-523} ; Km ^R | pAGM1311 with pT2S022+023+024+056+026 | P. Martin, unpub. |
| pT2S179 | Level -1 module encoding amino acids 179 - 217 of XpsM, XpsC _{Δ73-162} and XpsD; Km ^R | pAGM1311 with pT2S175+025+026 | this study |
| pT2S188 | Level -1 module encoding XpsJ, XpsK, XpsL _{D147stop} and amino acids 1 - 33 of XpsM; Km ^R | pAGM1311 with pT2S016+017+018+174+097 | this study |
| pT2S137 | Level -1 module encoding XpsM, XpsC _{Δ73-162} and XpsD _{Δ103-523} ; Km ^R | pAGM1311 with pT2S022+023+051+056+026 | This study |
| pT2S117 | Level -1 module encoding XpsG _{Δ30-121} , XpsH, XpsI under the <i>xpsG</i> promoter; Km ^R | pAGM1311 with pT2S011+106+014 | this study |
| pT2S093 | Level -1 module encoding XpsG, XpsH _{Δ14-107} , XpsI under the <i>xpsG</i> promoter; Km ^R | pAGM1311 with pT2S011+087 | this study |
| pT2S101 | Level -1 module encoding for XpsG, XpsH, amino acids 1-20 of XpsI under the <i>xpsG</i> promoter; Km ^R | pAGM1311 with pT2S011+012+089 | this study |
| pT2S102 | Level -1 module encoding for amino acids 126-138 of XpsI, XpsJ, XpsK and XpsL; Km ^R | pAGM1311 with pT2S095+017+018+019+020 | this study |
| pT2S116 | Level -1 module encoding for XpsG, XpsH, XpsI, amino acids 1-13 of XpsJ under the <i>xpsG</i> promoter; Km ^R | pAGM1311 with pT2S011+012+013+105 | this study |
| pT2S098 | Level -1 module encoding for amino acids codons 184-211 of XpsJ, XpsK and XpsL; Km ^R | pAGM1311 with pT2S090+019+020 | this study |
| pT2S094 | Level -1 module encoding for XpsJ, XpsK _{Δ29-205} and XpsL; Km ^R | pAGM1311 with pT2S016+088+020 | this study |
| pT2S432 | Level -1 module encoding for amino acids codons 126-138 of XpsI, XpsJ, XpsK _{Δ29-205} and XpsL; Km ^R | pAGM1311 with pT2S095+088+020 | this study |
| pT2S441 | Level -1 module encoding for amino acids codons 184-211 of XpsJ, XpsK _{Δ29-205} and XpsL; Km ^R | pAGM1311 with pT2S431+019+020 | this study |
| pT2S442 | Level -1 module encoding for XpsG, XpsH, XpsI _{Δ21-125} , amino acids 1-13 of XpsJ under the <i>xpsG</i> promoter; Km ^R | pAGM1311 with pT2S011+012+013+435 | this study |
| Level 0 (unless otherwise noted, assembled with <i>Bpi</i> I and T4 ligase) | | | |
| pT2S107 | Level 0 module encoding XpsG, H, I, J, K, L _{Δ33-258} , M, C and D under control of the <i>xpsG</i> promoter; Sm ^R | pICH41331 with pT2S015+103+099 | this study |
| pT2S187 | Level 0 module encoding XpsG, H, I, J, K, XpsL _{D147stop} , M, C and D under control of the <i>xpsG</i> promoter; Sm ^R | pICH41331 with pT2S015+178+028 | this study |
| pT2S108 | Level 0 module encoding XpsG, H, I, J, K, L, M _{Δ34-178} , C and D under control of the <i>xpsG</i> promoter; Sm ^R | pICH41331 with pT2S015+104+100 | this study |
| pT2S053 | Level 0 module encoding XpsG, H, I, J, K, L, M, C _{Δ73-162} and D under control of the <i>xpsG</i> promoter; Sm ^R | pICH41331 with pT2S015+021+052 | P. Martin, unpub. |
| pT2S058 | Level 0 module encoding XpsG, H, I, J, K, L, M, C and XpsD _{Δ103-523} under control of the <i>xpsG</i> promoter; Sm ^R | pICH41331 with pT2S015+021+057 | P. Martin, unpub. |
| pT2S170 | Level 0 module encoding XpsG, H, I, J, K, XpsL, M, C _{Δ73-162} and XpsD _{Δ103-523} under control of the <i>xpsG</i> promoter; Sm ^R | pICH41331 with pT2S015+021+137 | This study |
| pT2S180 | Level 0 module encoding XpsG, H, I, J, K, L, M _{Δ34-178} , C _{Δ73-162} , D under control of the <i>xpsG</i> promoter; Sm ^R | pICH41331 with pT2S015+104+179 | this study |
| pT2S181 | Level 0 module encoding XpsG, H, I, J, K, XpsL _{D147stop} , M, C _{Δ73-162} , D under control of the <i>xpsG</i> promoter; Sm ^R | pICH41331 with pT2S015+178+052 | this study |

| Plasmid | description | Assembly | Reference |
|---|---|--------------------------------|-------------------|
| pT2S182 | Level 0 module encoding XpsG, H, I, J, K, XpsL _{D147stop} , M, C and XpsD _{Δ103-523} under control of the <i>xpsG</i> promoter; Sm ^R | pICH41331 with pT2S015+178+057 | this study |
| pT2S193 | Level 0 module encoding XpsG, H, I, J, K, XpsL _{D147stop} , M _{Δ34-178} , C and D under control of the <i>xpsG</i> promoter; Sm ^R | pICH41331 with pT2S015+188+100 | this study |
| pT2S129 | Level 0 module encoding XpsG _{Δ30-121} , H, I, J, K, L, M, C, D under the <i>xpsG</i> promoter; Sm ^R | pICH41331 with pT2S117+021+028 | this study |
| pT2S130 | Level 0 module encoding XpsG, H _{Δ14-107} , I, J, K, L, M, C, D under the <i>xpsG</i> promoter; Sm ^R | pICH41331 with pT2S093+021+028 | this study |
| pT2S131 | Level 0 module encoding XpsG, H, I _{Δ21-125} , J, K, L, M, C, D under the <i>xpsG</i> promoter; Sm ^R | pICH41331 with pT2S101+021+028 | this study |
| pT2S132 | Level 0 module encoding XpsG, H, I, J _{Δ14-183} , K, L, M, C, D under the <i>xpsG</i> promoter; Sm ^R | pICH41331 with pT2S116+098+028 | this study |
| pT2S133 | Level 0 module encoding XpsG, H, I, J, K _{Δ29-205} , L, M, C, D under the <i>xpsG</i> promoter; Sm ^R | pICH41331 with pT2S015+094+028 | this study |
| pT2S436 | Level 0 module encoding XpsG, H, I _{Δ21-125} , J, K _{Δ29-205} , L, M, C, D under the <i>xpsG</i> promoter; Sm ^R | pICH41331 with pT2S101+432+028 | this study |
| pT2S449 | Level 0 module encoding XpsG, H, I, J _{Δ14-183} , K _{Δ29-205} , L, M, C, D under the <i>xpsG</i> promoter; Sm ^R | pICH41331 with pT2S116+441+028 | this study |
| pT2S464 | Level 0 module encoding XpsG, H, I _{Δ21-125} , J _{Δ14-183} , K, L, M, C, D under the <i>xpsG</i> promoter; Sm ^R | pICH41331 with pT2S442+098+028 | this study |
| pT2S527 | Level 0 module encoding XpsG, H, I, J _{Δ14-183} , K, L, M, C _{Δ73-162} , D under the <i>xpsG</i> promoter; Sm ^R | pICH41331 with pT2S116+098+052 | this study |
| Level 1 (unless otherwise noted, assembled with <i>Bsa</i> I and T4 ligase) | | | |
| pT2S126 | Level 1 module with <i>xpsG</i> operon encoding XpsL _{Δ33-258} ; Ap ^R | pICH47761 with pT2S107 | this study |
| pT2S192 | Level 1 module with <i>xpsG</i> operon encoding XpsL _{D147stop} ; Ap ^R | pICH47761 with pT2S187 | this study |
| pT2S127 | Level 1 module with <i>xpsG</i> operon encoding XpsM _{Δ34-178} ; Ap ^R | pICH47761 with pT2S108 | this study |
| pT2S054 | Level 1 module with <i>xpsG</i> operon encoding XpsC _{Δ73-162} ; Ap ^R | pICH47761 with pT2S053 | P. Martin, unpub. |
| pT2S059 | Level 1 module with <i>xpsG</i> operon encoding XpsD _{Δ103-523} ; Ap ^R | pICH47761 with pT2S058 | P. Martin, unpub. |
| pT2S172 | Level 1 module with <i>xpsG</i> operon encoding XpsC _{Δ73-162} and XpsD _{Δ103-523} ; Ap ^R | pICH47761 with pT2S170 | this study |
| pT2S189 | Level 1 module with <i>xpsG</i> operon encoding XpsM _{Δ34-178} and XpsC _{Δ73-162} ; Ap ^R | pICH47761 with pT2S180 | this study |
| pT2S194 | Level 1 module with <i>xpsG</i> operon encoding XpsL _{D147stop} and XpsC _{Δ73-162} ; Ap ^R | pICH47761 with pT2S181 | this study |
| pT2S190 | Level 1 module with <i>xpsG</i> operon encoding XpsL _{D147stop} and XpsD _{Δ103-523} ; Ap ^R | pICH47761 with pT2S182 | this study |
| pT2S198 | Level 1 module with <i>xpsG</i> operon encoding XpsL _{D147stop} , and XpsM _{Δ34-178} ; Ap ^R | pICH47761 with pT2S193 | this study |
| pT2S140 | Level 1 module with <i>xpsG</i> operon encoding XpsG _{Δ30-121} ; Ap ^R | pICH47761 with pT2S129 | this study |
| pT2S141 | Level 1 module with <i>xpsG</i> operon encoding XpsH _{Δ14-107} ; Ap ^R | pICH47761 with pT2S130 | this study |
| pT2S142 | Level 1 module with <i>xpsG</i> operon encoding XpsI _{Δ21-125} ; Ap ^R | pICH47761 with pT2S131 | this study |
| pT2S143 | Level 1 module with <i>xpsG</i> operon encoding XpsJ _{Δ14-183} ; Ap ^R | pICH47761 with pT2S132 | this study |
| pT2S144 | Level 1 module with <i>xpsG</i> operon encoding XpsK _{Δ29-205} ; Ap ^R | pICH47761 with pT2S133 | this study |
| pT2S466 | Level 1 module with <i>xpsG</i> operon encoding XpsI _{Δ21-125} and XpsK _{Δ29-205} ; Ap ^R | pICH47761 with pT2S436 | this study |

| Plasmid | description | Assembly | Reference |
|---|---|--|-------------------|
| pT2S465 | Level 1 module with <i>xpsG</i> operon encoding XpsJ _{Δ14-183} and XpsK _{Δ29-205} ; Ap ^R | pICH47761 with pT2S449 | this study |
| pT2S480 | Level 1 module with <i>xpsG</i> operon encoding XpsI _{Δ21-125} and XpsJ _{Δ14-183} ; Ap ^R | pICH47761 with pT2S464 | this study |
| pT2S538 | Level 1 module with <i>xpsG</i> operon encoding XpsJ _{Δ14-183} and XpsC _{Δ73-162} ; Ap ^R | pICH47761 with pT2S527 | this study |
| Level M (unless otherwise noted, assembled with <i>Bpil</i> and T4 ligase) | | | |
| pT2S069 | Level M module with an <i>xps</i> gene cluster lacking <i>xpsE</i> , Sm ^R | pAGM8031 with pICH54011+ pICH54022+034+036+pICH54055+pICH50914 | P. Martin, unpub. |
| pT2S085 | Level M module with an <i>xps</i> gene cluster lacking <i>xpsF</i> , Sm ^R | pAGM8031 with pICH54011+ pT2S032+pICH54033+pT2S036+pICH54055+pICH50914 | this study |
| pT2S156 | Level M module with an <i>xps</i> gene cluster encoding XpsL _{Δ33-258} ; Sm ^R | pAGM8031 with pICH54011+ pT2S032+034+126+pICH54055+pICH50914 | this study |
| pT2S200 | Level M module with an <i>xps</i> gene cluster encoding XpsL _{D147stop} ; Sm ^R | pAGM8031 with pICH54011+ pT2S032+034+192+pICH54055+pICH50914 | this study |
| pT2S138 | Level M module with an <i>xps</i> gene cluster encoding XpsM _{Δ34-178} ; Sm ^R | pAGM8031 with pICH54011+ pT2S032+034+127+pICH54055+pICH50914 | this study |
| pT2S055 | Level M module with an <i>xps</i> gene cluster encoding XpsC _{Δ73-162} ; Sm ^R | pAGM8031 with pICH54011+ pT2S032+034+054+pICH54055+pICH50914 | P. Martin, unpub. |
| pT2S060 | Level M module with an <i>xps</i> gene cluster encoding XpsD _{Δ103-523} ; Sm ^R | pAGM8031 with pICH54011+ pT2S032+034+059+pICH54055+pICH50914 | P. Martin, unpub. |
| pT2S145 | Level M module with an <i>xps</i> gene cluster encoding XpsG _{Δ30-121} ; Sm ^R | pAGM8031 with pICH54011+ pT2S032+034+140+pICH54055+pICH50914 | this study |
| pT2S148 | Level M module with an <i>xps</i> gene cluster encoding XpsH _{Δ14-107} ; Sm ^R | pAGM8031 with pICH54011+ pT2S032+034+141+pICH54055+pICH50914 | this study |
| pT2S150 | Level M module with an <i>xps</i> gene cluster encoding XpsI _{Δ21-125} ; Sm ^R | pAGM8031 with pICH54011+ pT2S032+034+142+pICH54055+pICH50914 | this study |
| pT2S152 | Level M module with an <i>xps</i> gene cluster encoding XpsJ _{Δ14-183} ; Sm ^R | pAGM8031 with pICH54011+ pT2S032+034+143+pICH54055+pICH50914 | this study |
| pT2S154 | Level M module with an <i>xps</i> gene cluster encoding XpsK _{Δ29-205} ; Sm ^R | pAGM8031 with pICH54011+ pT2S032+034+144+pICH54055+pICH50914 | this study |
| Constructs for complementation studies | | | |
| Level -1 (unless otherwise noted, assembled with <i>Bsal</i> and T4 ligase) | | | |
| pT2S003 | Level -1 module encoding XpsE-FLAG under control of the <i>xpsE</i> promoter; Km ^R | pAGM1311 with 4 PCRs: Promoter 1 nt -365 fw / Promoter 1 nt +4 rv XpsE nt 1 fw / XpsE nt 936 rv XpsE nt 932 fw / XpsE nt 1069 rv XpsE nt 1065 fw / xpsE-FLAG rev | P. Martin, unpub. |
| pT2S044 | Level -1 module containing 209 bp of the <i>xpsG</i> promoter; Km ^R | pAGM1311 with PCR P3 compC fw / rv | P. Martin, unpub. |
| pT2S045 | Level -1 module encoding XpsC; Km ^R | pAGM1311 with PCR xpsC comp fw / rv | P. Martin, unpub. |
| pT2S448 | Level -1 module encoding XpsG; Km ^R | pAGM1311 with PCR xpsG comp fw / rv | this study |
| pT2S242 | Level -1 module c-terminal 1×FLAG epitope tag; Km ^R | pUC57 with annealed oligos: 1×FLAG-C fw / rv, (assembled with EcoRV and T4 ligase) | this study |

| Plasmid | description | Assembly | Reference |
|--|---|---|-------------------|
| Level 0 (unless otherwise noted, assembled with <i>Bpil</i> and T4 ligase) | | | |
| pT2S004 | Level 0 module encoding XpsE-FLAG under control of the <i>xpsE</i> promoter; Sm ^R | pICH41331 with pT2S003 | P. Martin, unpub. |
| pT2S075 | Level 0 module containing 209 bp of the <i>xpsG</i> promoter; Sm ^R | pICH41331 with PCR P3 comp fw / rv | P. Martin, unpub. |
| pT2S119 | Level 0 module encoding XpsL; Sm ^R | pAGM9121 with PCR xpsL comp fw / rv | this study |
| pT2S203 | Level 0 module containing <i>xpsL</i> and 21 upstream bp encompassing the native <i>xpsL</i> Shine Dalgarno sequence; Sm ^R | pAGM9121 with PCR xpsL comp fw / xpsL+SD comp rv | this study |
| pT2S114 | Level 0 module encoding XpsM; Sm ^R | pAGM9121 with PCR xpsM comp fw / rv | this study |
| pT2S046 | Level 0 module encoding XpsC under control of the <i>xpsG</i> promoter; Sm ^R | pICH41331 with pT2S044+045 | P. Martin, unpub. |
| pT2S209 | Level 0 module encoding XpsD; Sm ^R | pAGM9121 with PCR xpsD comp fw / rv | this study |
| pT2S451 | Level 0 module encoding XpsG-FLAG; Sm ^R | pICH41308 with pT2S448+242 | this study |
| pT2S110 | Level 0 module encoding XpsH; Sm ^R | pAGM9121 with PCR xpsH comp fw / rv | this study |
| pT2S111 | Level 0 module encoding XpsI; Sm ^R | pAGM9121 with PCR xpsI comp fw / rv | this study |
| pT2S112 | Level 0 module encoding XpsJ; Sm ^R | pAGM9121 with PCR xpsJ comp fw / rv | this study |
| pT2S113 | Level 0 module encoding XpsK; Sm ^R | pAGM9121 with PCR xpsK comp fw / rv | this study |
| Level 1 (unless otherwise noted, assembled with <i>Bsal</i> and T4 ligase) | | | |
| pT2S072 | derivative of pICH47732 encoding XpsE-FLAG under control of the <i>xpsE</i> promoter; Ap ^R | pICH47732 with pT2S004 | P. Martin, unpub. |
| pT2S084 | derivative of pICH47732 encoding XpsF under control of the <i>xpsF</i> promoter; Ap ^R | pICH47732 with pT2S006 | this study |
| pT2S135 | derivative of pICH47732 encoding XpsL under control of the <i>xpsG</i> promoter; Ap ^R | pICH47732 with pT2S075+119 | this study |
| pT2S206 | derivative of pICH47732 containing <i>xpsL</i> and 21 upstream bp encompassing the native <i>xpsL</i> Shine Dalgarno sequence under control of the <i>xpsG</i> promoter; Ap ^R | pICH47732 with pT2S075+203 | this study |
| pT2S125 | derivative of pICH47732 encoding XpsM under control of the <i>xpsG</i> promoter; Ap ^R | pICH47732 with pT2S075+114 | this study |
| pT2S049 | derivative of pICH47732 encoding XpsC under control of the <i>xpsG</i> promoter; Ap ^R | pICH47732 with pT2S046 | P. Martin, unpub. |
| pT2S225 | derivative of pICH47732 encoding XpsD under control of the <i>xpsG</i> promoter; Ap ^R | pICH47732 with pT2S075+209 | this study |
| pT2S463 | derivative of pICH47732 encoding XpsG-FLAG under the <i>xpsG</i> promoter; Ap ^R | pICH47732 with pT2S075+451+pAGB232 | this study |
| pT2S121 | derivative of pICH47732 encoding XpsH under the <i>xpsG</i> promoter; Ap ^R | pICH47732 with pT2S075+110 | this study |
| pT2S122 | derivative of pICH47732 encoding XpsI under the <i>xpsG</i> promoter; Ap ^R | pICH47732 with pT2S075+111 | this study |
| pT2S123 | derivative of pICH47732 encoding XpsJ under the <i>xpsG</i> promoter; Ap ^R | pICH47732 with pT2S075+112 | this study |
| pT2S124 | derivative of pICH47732 encoding XpsK under the <i>xpsG</i> promoter; Ap ^R | pICH47732 with pT2S075+113 | this study |
| Level M (unless otherwise noted, assembled with <i>Bpil</i> and T4 ligase) | | | |
| pT2S077 | Level M module with an <i>xps</i> gene cluster lacking <i>xpsE</i> , encoding XpsE-FLAG under control of the native promoter inserted outside the <i>xps</i> -gene cluster; Sm ^R | pAGM8031 with pT2S072+ pICH54022+034+036+pICH54055+pICH50914 | P. Martin, unpub. |
| pT2S086 | Level M module with an <i>xps</i> gene cluster lacking <i>xpsF</i> , encoding XpsF under control of the native promoter inserted outside the <i>xps</i> -gene cluster; Sm ^R | pAGM8031 with pT2S084+ pT2S032+pICH54033+pT2S036 +pICH54055+pICH50914 | this study |

| Plasmid | description | Assembly | Reference |
|--|--|---|-----------------------|
| pT2S157 | Level M module with an <i>xps</i> gene cluster encoding XpsL Δ_{33-258} , encoding XpsL under control of the native promoter inserted outside the <i>xps</i> -gene cluster; Sm ^R | pAGM8031 with pT2S135+ pT2S032+034+126+pICH54055 +pICH50914 | this study |
| pT2S208 | Level M module with an <i>xps</i> gene cluster encoding XpsL Δ_{33-258} , encoding XpsL under control of the native promoter containing the <i>xpsL</i> Shine Dalgarno sequence outside the <i>xps</i> gene cluster; Sm ^R | pAGM8031 with pT2S206+ pT2S032+034+126+pICH54055 +pICH50914 | this study |
| pT2S201 | Level M module with an <i>xps</i> gene cluster encoding XpsL $\Delta_{147stop}$, encoding XpsL under control of the native promoter inserted outside the <i>xps</i> -gene cluster; Sm ^R | pAGM8031 with pT2S135+ pT2S032+034+192+pICH54055 +pICH50914 | this study |
| pT2S207 | Level M module with an <i>xps</i> gene cluster encoding XpsL $\Delta_{147stop}$, encoding XpsL under control of the native promoter containing the <i>xpsL</i> Shine Dalgarno sequence outside the <i>xps</i> gene cluster; Sm ^R | pAGM8031 with pT2S206+ pT2S032+034+192+pICH54055 +pICH50914 | this study |
| pT2S158 | Level M module with an <i>xps</i> gene cluster encoding XpsM Δ_{34-178} , and encoding XpsM under control of the native promoter outside the <i>xps</i> gene cluster; Sm ^R | pAGM8031 with pT2S125+ pT2S032+034+127+pICH54055 +pICH50914 | this study |
| pT2S073 | Level M module with an <i>xps</i> gene cluster encoding XpsC Δ_{73-162} , and encoding XpsC under control of the native promoter outside the <i>xps</i> gene cluster; Sm ^R | pAGM8031 with pT2S049+ pT2S032+034+054+pICH54055 +pICH50914 | P. Martin, unpub. |
| pT2S230 | Level M module with an <i>xps</i> gene cluster encoding XpsD $\Delta_{103-523}$, and encoding XpsD under control of the native promoter outside the <i>xps</i> gene cluster; Sm ^R | pAGM8031 with pT2S225+ pT2S032+034+059+pICH54055 +pICH50914 | this study |
| pT2S467 | Level M module with an <i>xps</i> gene cluster encoding XpsG Δ_{30-121} , , and encoding XpsG under control of the native promoter outside the <i>xps</i> gene cluster; Sm ^R | pAGM8031 with pT2S463+ pT2S032+034+140+pICH54055 +pICH50914 | this study |
| pT2S149 | Level M module with an <i>xps</i> gene cluster encoding XpsH Δ_{14-107} , and encoding XpsH under control of the native promoter outside the <i>xps</i> gene cluster; Sm ^R | pAGM8031 with pT2S121+ pT2S032+034+141+pICH54055 +pICH50914 | this study |
| pT2S151 | Level M module with an <i>xps</i> gene cluster encoding XpsI Δ_{21-125} , and encoding XpsI under control of the native promoter outside the <i>xps</i> gene cluster; Sm ^R | pAGM8031 with pT2S122+ pT2S032+034+142+pICH54055 +pICH50914 | this study |
| pT2S153 | Level M module with an <i>xps</i> gene cluster encoding XpsJ Δ_{14-183} , , and encoding XpsJ under control of the native promoter outside the <i>xps</i> gene cluster; Sm ^R | pAGM8031 with pT2S123+ pT2S032+034+143+pICH54055 +pICH50914 | this study |
| pT2S155 | Level M module with an <i>xps</i> gene cluster encoding XpsK Δ_{29-205} , , and encoding XpsK under control of the native promoter outside the <i>xps</i> gene cluster; Sm ^R | pAGM8031 with pT2S124+ pT2S032+034+144+pICH54055 +pICH50914 | this study |
| tagged genes | | | |
| Level -1 (unless otherwise noted, assembled with <i>Bsa</i> I and T4 ligase) | | | |
| pAGB1000 | derivative of pICH41021 containing a linker (2× AKLEGPAGL)-encoding sequence; Ap ^R | | Drehkopf et al., 2022 |
| pAGB1048 | derivative of pICH41021 containing <i>mCherry</i> for generation of C-terminal translational fusions; Ap ^R | | Drehkopf et al., 2022 |
| pT2S210 | Level -1 module encoding XpsD lacking a stop codon for the generation of C-terminal translational fusions; Km ^R | pAGM1311 with PCR <i>xpsD</i> tagC fw / rv | this study |
| pICSL50010 | derivative of pAGM1301 encoding a C terminal 4×c-Myc epitope, Sm ^R | | (Engler et al., 2014) |
| pAGB872 | Level -1 module with a 4×c-Myc epitope for generation of N-terminal fusions; Ap ^R | pICH41021 with PCR 4×Myc-N fw / rv (template: pICSL50010) | C. Otten |

| Plasmid | description | Assembly | Reference |
|--|--|--|-----------------------|
| pAGB873 | Level -1 module with a 4×c-Myc epitope for generation of C-terminal fusions; Ap ^R | pICH41021 with PCR 4×Myc-C fw / rv (template: pICSL50010) | C. Otten |
| pT2S065 | Level -1 module encoding XpsC for the generation of N-terminal fusions; Km ^R | pAGM1311 with PCR xpsC tagN fw / rv | P. Martin, unpub. |
| pT2S066 | Level -1 module encoding XpsC lacking a stop codon for the generation of C-terminal fusions; Km ^R | pAGM1311 with PCR xpsC tagC fw / rv | P. Martin, unpub. |
| pT2S205 | Level -1 module encoding XpsL for the generation of N-terminal fusions; Km ^R | pAGM1311 with PCR xpsL tagN fw / rv | this study |
| pT2S336 | Level -1 module encoding XpsF for the generation of N-terminal fusions; Km ^R | pAGM1311 with PCR xpsF tagN fw / rv | this study |
| pT2S342 | Level -1 module encoding XpsK lacking a stop codon for the generation of C-terminal fusions; Km ^R | pAGM1311 with PCR xpsK tagC fw / rv | this study |
| Level 0 (unless otherwise noted, assembled with <i>Bpil</i> and T4 ligase) | | | |
| pT2S219 | Level 0 module encoding XpsD-2×AKLEG PAGL-mCherry; Sm ^R | pICH41308 with pT2S210+pAGB1000+pAGB1048 | this study |
| pAGB232 | derivative of pICH41276 containing a transcriptional terminator from <i>X. euvesicatoria</i> ; Sm ^R | | Drehkopf et al., 2022 |
| pT2S285 | Level 0 module containing 209 bp of the <i>xpsG</i> promoter followed by 21 bp upstream region of <i>xpsL</i> encompassing the native <i>xpsL</i> Shine Dalgarno sequence; Ap ^R | pUC57 with PCR P3 comp fw / P3xpsLSD rv (template: pT2S206) (assembled with EcoRV and T4 ligase) | this study |
| pT2S289 | Level 0 module encoding 4×c-Myc-XpsL; Sm ^R | pICH41308 with pT2S205+pAGB872 | this study |
| pT2S293 | Level 0 module encoding XpsC-4×c-Myc; Sm ^R | pICH41308 with pT2S066+pAGB873 | this study |
| pT2S294 | Level 0 module encoding 4×c-Myc-XpsC; Sm ^R | pICH41308 with pT2S065+pAGB872 | this study |
| pT2S487 | Level 0 module encoding 4×c-Myc-XpsC _{5xR→A} ; Sm ^R | Quickchange PCR on pT2S294 with xpsC _{R5A} fw / rv | this study |
| pT2S488 | Level 0 module encoding 4×c-Myc-XpsC _{5xR→E} ; Sm ^R | Quickchange PCR on pT2S294 with xpsC _{R5E} fw / rv | this study |
| pT2S337 | Level 0 module encoding 4×c-Myc-XpsF; Sm ^R | pICH41308 with pT2S336+pAGB872 | this study |
| pT2S349 | Level 0 module encoding XpsK-4×c-Myc; Sm ^R | pICH41308 with pT2S342+pAGB873 | this study |
| pT2S351 | Level 0 module containing 175 bp of the <i>xpsF</i> promoter, Sm ^R | pICH41295 with PCR P2 new fw / rv | this study |
| pT2S352 | Level 0 module containing 209 bp of the <i>xpsG</i> promoter without additional start codons, Sm ^R | pICH41295 with PCR P3 new fw / rv | this study |
| Level 1 (unless otherwise noted, assembled with <i>Bsal</i> and T4 ligase) | | | |
| pT2S236 | Level 1 module encoding XpsD-2×AKLEG PAGL-mCherry under control of the <i>xpsG</i> promoter; Ap ^R | pICH47732 with pT2S075+219+pAGB232 | this study |
| pT2S290 | Level 1 module encoding 4×c-Myc-XpsL under control of the <i>xpsG</i> promoter with the native <i>xpsL</i> Shine Dalgarno sequence; Ap ^R | pICH47732 with pT2S285+289+pAGB232 | this study |
| pT2S301 | Level 1 module encoding XpsC-4×c-Myc under control of the <i>xpsG</i> promoter; Ap ^R | pICH47732 with pT2S075+293+pAGB232 | this study |
| pT2S495 | Level 1 module encoding 4×c-Myc-XpsC under control of the <i>xpsG</i> promoter; Ap ^R | pICH47732 with pT2S352+294+pAGB232 | this study |
| pT2S496 | Level 1 module encoding 4×c-Myc-XpsC _{5xR→A} under control of the <i>xpsG</i> promoter; Ap ^R | pICH47732 with pT2S352+487+pAGB232 | this study |
| pT2S497 | Level 1 module encoding 4×c-Myc-XpsC _{5xR→E} under control of the <i>xpsG</i> promoter; Ap ^R | pICH47732 with pT2S352+488+pAGB232 | this study |
| pT2S353 | Level 1 module encoding 4×c-Myc-XpsF under control of the <i>xpsF</i> promoter; Ap ^R | pICH47732 with pT2S351+294+pAGB232 | this study |

| Plasmid | description | Assembly | Reference |
|--|--|---|------------|
| Level M (unless otherwise noted, assembled with <i>Bpil</i> and T4 ligase) | | | |
| pT2S238 | Level M module with an <i>xps</i> gene cluster encoding XpsD _{Δ103-523} , and encoding XpsD-mCherry under control of the native promoter outside the <i>xps</i> gene cluster; Sm ^R | pAGM8031 with pT2S236+032+034+059+plCH54055+plCH50914 | this study |
| pT2S253 | Level M module encoding XpsD-mCherry under control of the native promoter; Sm ^R | pAGM8031 with pT2S236+plCH50872 | this study |
| pT2S296 | Level M module with an <i>xps</i> gene cluster encoding XpsL _{D147stop} , encoding 4×c-Myc-XpsL under control of the native promoter containing the <i>xpsL</i> Shine Dalgarno sequence outside the <i>xps</i> gene cluster; Sm ^R | pAGM8031 with pT2S290+032+034+192+plCH54055+plCH50914 | this study |
| pT2S318 | Level M module encoding 4×c-Myc-XpsL under control of the native promoter and containing the <i>xpsL</i> Shine Dalgarno sequence; Sm ^R | pAGM8031 with pT2S290+plCH50872 | this study |
| pT2S297 | Level M module with an <i>xps</i> gene cluster encoding XpsL _{D147stop} and XpsM _{Δ34-178} encoding 4×c-Myc-XpsL under control of the native promoter containing the <i>xpsL</i> Shine Dalgarno sequence outside the <i>xps</i> gene cluster; Sm ^R | pAGM8031 with pT2S290+032+034+198+plCH54055+plCH50914 | this study |
| pT2S298 | Level M module with an <i>xps</i> gene cluster encoding XpsL _{D147stop} and XpsC _{Δ73-162} encoding 4×c-Myc-XpsL under control of the native promoter containing the <i>xpsL</i> Shine Dalgarno sequence outside the <i>xps</i> gene cluster; Sm ^R | pAGM8031 with pT2S290+032+034+194+plCH54055+plCH50914 | this study |
| pT2S299 | Level M module with an <i>xps</i> gene cluster encoding XpsL _{D147stop} and lacking <i>xpsE</i> encoding 4×c-Myc-XpsL under control of the native promoter containing the <i>xpsL</i> Shine Dalgarno sequence outside the <i>xps</i> gene cluster; Sm ^R | pAGM8031 with pT2S290+plCH54022+pT2S034+192+plCH54055+plCH50914 | this study |
| pT2S300 | Level M module with an <i>xps</i> gene cluster encoding XpsL _{D147stop} and XpsD _{Δ103-523} encoding 4×c-Myc-XpsL under control of the native promoter containing the <i>xpsL</i> Shine Dalgarno sequence outside the <i>xps</i> gene cluster; Sm ^R | pAGM8031 with pT2S290+032+034+190+plCH54055+plCH50914 | this study |
| pT2S322 | Level M module with an <i>xps</i> gene cluster encoding XpsL _{D147stop} and lacking <i>xpsF</i> encoding 4×c-Myc-XpsL under control of the native promoter containing the <i>xpsL</i> Shine Dalgarno sequence outside the <i>xps</i> gene cluster; Sm ^R | pAGM8031 with pT2S290+032+plCH54033+pT2S192+plCH54055+plCH50914 | this study |
| pT2S306 | Level M module with an <i>xps</i> gene cluster encoding XpsC _{Δ73-162} encoding XpsC-4×c-Myc under control of the native promoter outside the <i>xps</i> gene cluster; Sm ^R | pAGM8031 with pT2S301+032+034+054+plCH54055+plCH50914 | this study |
| pT2S319 | Level M module encoding XpsC-4×c-Myc under control of the native promoter; Sm ^R | pAGM8031 with pT2S301+plCH50872 | this study |
| pT2S307 | Level M module with an <i>xps</i> gene cluster encoding XpsL _{D147stop} and XpsC _{Δ73-162} encoding XpsC-4×c-Myc under control of the native promoter outside the <i>xps</i> gene cluster; Sm ^R | pAGM8031 with pT2S301+032+034+194+plCH54055+plCH50914 | this study |
| pT2S317 | Level M module with an <i>xps</i> gene cluster encoding XpsM _{Δ34-178} and XpsC _{Δ73-162} encoding XpsC-4×c-Myc under control of the native promoter outside the <i>xps</i> gene cluster; Sm ^R | pAGM8031 with pT2S301+032+034+189+plCH54055+plCH50914 | this study |

| Plasmid | description | Assembly | Reference |
|---------|--|---|------------|
| pT2S333 | Level M module with an <i>xps</i> gene cluster encoding XpsC _{Δ73-162} and XpsD _{Δ103-523} encoding XpsC-4×c-Myc under control of the native promoter outside the <i>xps</i> gene cluster; Sm ^R | pAGM8031 with pT2S301+032+034+172+plCH54055+plCH50914 | this study |
| pT2S503 | Level M module with an <i>xps</i> gene cluster encoding XpsC _{Δ73-162} encoding 4×c-Myc-XpsC under control of the native promoter outside the <i>xps</i> gene cluster; Sm ^R | pAGM8031 with pT2S495+032+034+054+plCH54055+plCH50914 | this study |
| pT2S504 | Level M module with an <i>xps</i> gene cluster encoding XpsC _{Δ73-162} encoding 4×c-Myc-XpsC _{5xR→A} under control of the native promoter outside the <i>xps</i> gene cluster; Sm ^R | pAGM8031 with pT2S496+032+034+054+plCH54055+plCH50914 | this study |
| pT2S505 | Level M module with an <i>xps</i> gene cluster encoding XpsC _{Δ73-162} encoding 4×c-Myc-XpsC _{5xR→E} under control of the native promoter outside the <i>xps</i> gene cluster; Sm ^R | pAGM8031 with pT2S497+032+034+054+plCH54055+plCH50914 | this study |
| pT2S365 | Level M module with an <i>xps</i> gene cluster lacking <i>xpsF</i> encoding 4×c-Myc-XpsF under control of the native promoter outside the <i>xps</i> gene cluster; Sm ^R | pAGM8031 with pT2S353+032+plCH54033+pT2S036+plCH54055+plCH50914 | this study |
| pT2S394 | Level M module encoding 4×c-Myc-XpsF under control of the native promoter outside the <i>xps</i> gene cluster; Sm ^R | pAGM8031 with pT2S353+plCH50872 | this study |
| pT2S390 | Level M module with an <i>xps</i> gene cluster encoding XpsD _{Δ103-523} and lacking <i>xpsF</i> encoding 4×c-Myc-XpsF under control of the native promoter outside the <i>xps</i> gene cluster; Sm ^R | pAGM8031 with pT2S353+032+plCH54033+pT2S059+plCH54055+plCH50914 | this study |
| pT2S392 | Level M module with an <i>xps</i> gene cluster encoding XpsC _{Δ73-162} and lacking <i>xpsF</i> encoding 4×c-Myc-XpsF under control of the native promoter outside the <i>xps</i> gene cluster; Sm ^R | pAGM8031 with pT2S353+032+plCH54033+pT2S054+plCH54055+plCH50914 | this study |
| pT2S399 | Level M module with an <i>xps</i> gene cluster encoding lacking <i>xpsE</i> and <i>xpsF</i> encoding 4×c-Myc-XpsF under control of the native promoter outside the <i>xps</i> gene cluster; Sm ^R | pAGM8031 with pT2S353+plCH54022+54033+pT2S036+plCH54055+plCH50914 | this study |
| pT2S393 | Level M module with an <i>xps</i> gene cluster encoding XpsG _{Δ30-121} and lacking <i>xpsF</i> encoding 4×c-Myc-XpsF under control of the native promoter outside the <i>xps</i> gene cluster; Sm ^R | pAGM8031 with pT2S353+032+plCH54033+pT2S140+plCH54055+plCH50914 | this study |
| pT2S414 | Level M module with an <i>xps</i> gene cluster encoding XpsM _{Δ34-178} and lacking <i>xpsF</i> encoding 4×c-Myc-XpsF under control of the native promoter outside the <i>xps</i> gene cluster; Sm ^R | pAGM8031 with pT2S353+032+plCH54033+pT2S127+plCH54055+plCH50914 | this study |
| pT2S415 | Level M module with an <i>xps</i> gene cluster encoding XpsH _{Δ14-107} and lacking <i>xpsF</i> encoding 4×c-Myc-XpsF under control of the native promoter outside the <i>xps</i> gene cluster; Sm ^R | pAGM8031 with pT2S353+032+plCH54033+pT2S141+plCH54055+plCH50914 | this study |
| pT2S416 | Level M module with an <i>xps</i> gene cluster encoding XpsI _{Δ21-125} and lacking <i>xpsF</i> encoding 4×c-Myc-XpsF under control of the native promoter outside the <i>xps</i> gene cluster; Sm ^R | pAGM8031 with pT2S353+032+plCH54033+pT2S142+plCH54055+plCH50914 | this study |
| pT2S417 | Level M module with an <i>xps</i> gene cluster encoding XpsJ _{Δ14-183} and lacking <i>xpsF</i> encoding 4×c-Myc-XpsF under control of the native promoter outside the <i>xps</i> gene cluster; Sm ^R | pAGM8031 with pT2S353+032+plCH54033+pT2S143+plCH54055+plCH50914 | this study |

| Plasmid | description | Assembly | Reference |
|---|---|---|------------|
| pT2S418 | Level M module with an <i>xps</i> gene cluster encoding XpsK _{Δ29-205} and lacking <i>xpsF</i> encoding 4×c-Myc-XpsF under control of the native promoter outside the <i>xps</i> gene cluster; Sm ^R | pAGM8031 with pT2S353+032+plCH54033+pT2S144+plCH54055+plCH50914 | this study |
| Cysteine crosslinking | | | |
| Level -2 (unless otherwise noted, assembled with <i>Bpil</i> and T4 ligase) | | | |
| pT2S476 | Level -2 module encoding XpsI _{A33C} ; Sm ^R | Quickchange PCR on pT2S014 with xpsI _{A33C} fw / rv | this study |
| pT2S477 | Level -2 module containing bp 1-429 of <i>xpsJ</i> with a missense mutation leading to a A to C substitution (A46C); Sm ^R | Quickchange PCR on pT2S016 with xpsJ _{A46C} fw / rv | this study |
| Level -1 (unless otherwise noted, assembled with <i>Bsal</i> and T4 ligase) | | | |
| pT2S483 | Level -1 module encoding XpsG, XpsH, XpsI _{A33C} downstream of the <i>xpsG</i> promoter; Km ^R | pAGM1311 with pT2S011+012+013+476 | this study |
| pT2S484 | Level -1 module encoding XpsJ _{A46C} , XpsK _{Δ29-205} and XpsL; Km ^R | pAGM1311 with pT2S477+088+020 | this study |
| Level 0 (unless otherwise noted, assembled with <i>Bpil</i> and T4 ligase) | | | |
| pT2S478 | Level 0 module encoding XpsK _{A45C+E51C} -4×c-Myc; Sm ^R | Quickchange PCR on pT2S349 with xpsK _{A45C+E51C} fw / rv | this study |
| pT2S490 | Level 0 module with <i>xpsG</i> operon encoding XpsJ _{A46C} and XpsK _{Δ29-205} ; Sm ^R | plCH41331 with pT2S015+484+028 | this study |
| pT2S491 | Level 0 module with <i>xpsG</i> operon encoding XpsI _{A33C} , XpsJ _{A46C} and XpsK _{Δ29-205} ; Sm ^R | plCH41331 with pT2S483+484+028 | this study |
| pT2S494 | Level 0 module with <i>xpsG</i> operon encoding XpsI _{A33C} and XpsK _{Δ29-205} ; Sm ^R | plCH41331 with pT2S483+094+028 | this study |
| Level 1 (unless otherwise noted, assembled with <i>Bsal</i> and T4 ligase) | | | |
| pT2S498 | Level 1 module encoding XpsK _{A45C+E51C} -4×c-Myc under control of the native promoter; Ap ^R | plCH47732 with pT2S351+478+pAGB232 | this study |
| pT2S500 | Level 1 module with <i>xpsG</i> operon encoding XpsJ _{A46C} and XpsK _{Δ29-205} ; Ap ^R | plCH47761 with pT2S490 | this study |
| pT2S499 | Level 1 module with <i>xpsG</i> operon encoding XpsI _{A33C} , XpsJ _{A46C} and XpsK _{Δ29-205} ; Ap ^R | plCH47761 with pT2S491 | this study |
| pT2S508 | Level 1 module with <i>xpsG</i> operon encoding XpsI _{A33C} and XpsK _{Δ29-205} ; Ap ^R | plCH47761 with pT2S494 | this study |
| pT2S551 | Level 1 module encoding XpsF _{T241C} downstream of the <i>xpsF</i> promoter; Ap ^R | Quickchange PCR on pT2S034 with xpsF _{T241C} fw / rv | this study |
| Level M (unless otherwise noted, assembled with <i>Bpil</i> and T4 ligase) | | | |
| pT2S506 | Level M module with an <i>xps</i> gene cluster encoding XpsI _{A33C} , XpsJ _{A46C} and XpsK _{Δ29-205} and encoding XpsK _{A45C+E51C} -4×c-Myc under control of the native promoter outside the <i>xps</i> gene cluster; Sm ^R | pAGM8031 with pT2S498+032+034+499+plCH54055+plCH50914 | this study |
| pT2S507 | Level M module with an <i>xps</i> gene cluster encoding XpsJ _{A46C} and XpsK _{Δ29-205} and encoding XpsK _{A45C+E51C} -4×c-Myc under control of the native promoter outside the <i>xps</i> gene cluster; Sm ^R | pAGM8031 with pT2S498+032+034+500+plCH54055+plCH50914 | this study |
| pT2S511 | Level M module with an <i>xps</i> gene cluster encoding XpsI _{A33C} and XpsK _{Δ29-205} and encoding XpsK _{A45C+E51C} -4×c-Myc under control of the native promoter outside the <i>xps</i> gene cluster; Sm ^R | pAGM8031 with pT2S498+032+034+508+plCH54055+plCH50914 | this study |
| pT2S512 | Level M module with an <i>xps</i> gene cluster encoding XpsK _{Δ29-205} and encoding XpsK _{A45C+E51C} -4×c-Myc under control of the native promoter outside the <i>xps</i> gene cluster; Sm ^R | pAGM8031 with pT2S498+032+034+144+plCH54055+plCH50914 | this study |

| Plasmid | description | Assembly | Reference |
|---------|---|---|------------|
| pT2S525 | Level M module with an <i>xps</i> gene cluster encoding XpsI _{A33C} , XpsJ _{A46C} and XpsK _{Δ29-205} , lacking <i>xpsE</i> and encoding XpsK _{A45C+E51C-4×C} -Myc under control of the native promoter outside the <i>xps</i> gene cluster; Sm ^R | pAGM8031 with pT2S498+plCH54022+pT2S034+499+plCH54055+plCH50914 | this study |
| pT2S526 | Level M module with an <i>xps</i> gene cluster encoding XpsI _{A33C} , XpsJ _{A46C} and XpsK _{Δ29-205} , lacking <i>xpsF</i> and encoding XpsK _{A45C+E51C-4×C} -Myc under control of the native promoter outside the <i>xps</i> gene cluster; Sm ^R | pAGM8031 with pT2S498+032+plCH54033+T2S499+plCH54055+plCH50914 | this study |
| pT2S553 | Level M module with an <i>xps</i> gene cluster encoding XpsF _{T241C} , XpsK _{Δ29-205} and encoding XpsK _{A45C+E51C-4×C} -Myc under control of the native promoter outside the <i>xps</i> gene cluster; Sm ^R | pAGM8031 with pT2S498+032+551+144+plCH54055+plCH50914 | this study |

Table 13: primers used in this study

| Name | Sequence (5'-3'; <i>Bpi</i> I and <i>Bsa</i> I sites are written in bold, overhangs in italics) |
|--|---|
| Deletion of the <i>xps</i> gene cluster | |
| <i>Xe Δxps</i> -5'-fw | TTT GGTCTC T CGAC GCTGAGCATTTCTGCCAGAT |
| <i>Xe Δxps</i> -5'-rv | TTT GGTCTC T ATGC AGCCACTTGAGAAGGGT |
| <i>Xe Δxps</i> -3'-fw | TTT GGTCTC T GCAT CGATGCTCGATTGGATCGAC |
| <i>Xe Δxps</i> -3'-rv | TTT GGTCTC T ATGG CTCCGGTAGCTATACCTATA |
| <i>Xag Δxps</i> -5'-fw | TTT GGTCTC T CGAC GCTGGCGTCCAGGCCACCGG |
| <i>Xag Δxps</i> -5'-rv | TTT GGTCTC T ATTG CAGGGGGGTGAGTCAAC |
| <i>Xag Δxps</i> -3'-fw | TTT GGTCTC T CAAT ACTCGTCTCCACTGGTCCGG |
| <i>Xag Δxps</i> -3'-rv | TTT GGTCTC T ATGG ACCCTGCGATTCCGCCACCC |
| <i>Xcc Δxps</i> -5'-fw | TTT GGTCTC T CGAC GCAGTTGCCGCAGCCAGCCTG |
| <i>Xcc Δxps</i> -5'-rv | TTT GGTCTC T TTCG CTAGATTAAATAGGT |
| <i>Xcc Δxps</i> -3'-fw | TTT GGTCTC T CGAA CATTCCGGTCACACTATTGCAG |
| <i>Xcc Δxps</i> -3'-rv | TTT GGTCTC T ATGG GCCACCCGCATCACCGGCGG |
| Expression constructs for protease and secretion assays | |
| P4361 fw | TTT GGTCTC T ATTC AGGACAACGCGGTTCTGTG |
| P4361 rv | TTT GGTCTC T CATA GCGCGTGGCCTATGCG |
| 4358 fw | TT GGTCTC A TATG TTGAAACTCCGTTATCCGCTCAC |
| 4358 rv | TT GGTCTC G CACC GGGCCTGCTGGCAACGTAG |
| p0722 fw | TT GGTCTC A ATTC GGCCGCGTCGCTGCACTGCA |
| p0722 rv | TT GGTCTC G CATG GAAGAGATCACCCGAAAG |
| 0722fw | TT GGTCTC A TATG AAAGTCTTACCGCTGC |
| 0722rv | TT GGTCTC G CACC CAGTGCCGGGAAGCGGGGTG |
| p2571 1 fw | TT GAAGAC AA CTCA ATTCCTGTGATCCGGCGTGACCG |
| p2571 1 rv | TT GAAGAC AA TCTG TGCGTTGCTGTTTCGACC |
| p2571 2 fw | TT GAAGAC AA CAGA CCACGCATGTGCAGGGC |
| p2571 2 rv | TT GAAGAC AA CTCG CATAGTGCTTTCTCCGGTTAATG |
| 2571 1 fw | TT GGTCTC A TATG CCGTACCATCGCCTTGTTT |
| 2571 1 rv | TT GGTCTC G CCTT TCCACCTTCCAGCACC |
| 2571 2 fw | TT GGTCTC G AAGG TGTCGTTTCGCAAAGCC |
| 2571 2 rv | TT GGTCTC G CACC GATCGGCGAATCCGGCAGCAC |
| p0670 fw | TT GGTCTC A ATTC TGAGGGACACTCCGGGGGAC |

| Name | Sequence (5'-3'; <i>Bpi</i> I and <i>Bsa</i> I sites are written in bold, overhangs in italics) |
|---|---|
| p0670 rv | TT GGTCTC G <i>CGTC</i> TCCCTGGATGACCGAAC |
| 0670 1 fw | TT GGTCTC A <i>GACG</i> ATCATGCCCATTTTCAG |
| 0670 1 rv | TT GGTCTC G <i>CGTC</i> TCGAAGCCGAACACGTTG |
| 0670 2 fw | TT GGTCTC A <i>GACG</i> GGCAACCATGTCATGC |
| 0670 2 rv | TT GGTCTC G <i>CACC</i> ACCTGCAGCGCAGAAGC |
| p3634 fw | TT GGTCTC A <i>ATTC</i> GTCGCCCCCTCCGGCTGTTG |
| p3634 rv | TT GGTCTC G <i>CATA</i> GTGACTCTCCGTATGATTG |
| 3634 fw | TT GGTCTC A <i>TATG</i> CACAACCTGCCATCCAGCT |
| 3634 rv | TT GGTCTC G <i>CACC</i> CTTCGCATCCAAGGTCGCGCTG |
| p3406 fw | TT GGTCTC A <i>ATTC</i> TGCCTCAGGTGTTGAAACTG |
| p3406 rv | TT GGTCTC G <i>CATA</i> AATACCTATTTTATTTTGG |
| 3406 fw | TT GGTCTC A <i>TATG</i> AAAATAAATTTTCTAGCAGCGGCG |
| 3406 rv | TT GGTCTC A <i>CACC</i> TCGCTTGGTCGGCCTAAAGTTG |
| p3407 fw | TT GGTCTC A <i>ATTC</i> GTCACCTGTGAGCACGGATG |
| p3407 rv | TT GGTCTC G <i>CATA</i> GTATTTCTTTGTTAAC |
| 3407 fw | TT GGTCTC A <i>TATG</i> AAACACAGTAAATTTCTGTTAGTAACTG |
| 3407 rv | TT GGTCTC A <i>CACC</i> GAGCTTCCCGGTAAATTCATTGAG |
| p3672 fw | TT GAAGAC AA <i>CTCA</i> ATTCGGCACCTGGTCATTTGAAATAAC |
| p3672 rv | TT GAAGAC AA <i>CTCG</i> CATAAACGCCTAACTCCCCATTTTG |
| 3671 fw | TTT GGTCTC G <i>TATG</i> GTGATCCAGAGTTCTTCTAC |
| 3671 rv | TTT GGTCTC G <i>CACC</i> TTGGCGCGCCAGCAGGCTCA |
| 3671 _{Δ31-150} fw | TT GAAGAC AA <i>GTTG</i> GGGTTGGCGGCCAACG |
| 3671 _{Δ31-150} rv | TT GAAGAC AA <i>CAAC</i> ACCAGCGGCGCATTGCCGAACG |
| 3671 _{Δ527-627} rv | TTT GGTCTC T <i>CACC</i> ATCCACCTGACATCCCACATCG |
| Expression constructs for BACTH and pull-down assays | |
| xpsL BACTH fw | TT GGTCTC A <i>TATG</i> ACCGCATGGCGGGACACC |
| xpsL BACTH rv | TT GGTCTC G <i>CACC</i> ACGCTGCGTGGCATCGGCC |
| xpsM BACTH fw | T GAAGAC AA <i>CTCA</i> TATGCCACGCAGCGTTAAGCGCG |
| xpsM BACTH rv | T GAAGAC AA <i>CTCG</i> CACCAGGCGCATTGCTGGCCTCCG |
| xpsC BACTH fw | TTT GGTCTC T <i>TATG</i> CGCCTTGACATGATC |
| xpsC BACTH rv | TTT GGTCTC T <i>CACC</i> TTGGGTCTGACCGGGGGTAG |
| xpsE BACTH fw | TTT GGTCTC T <i>TATG</i> GTGAACGCGGTTGCCGTC |
| xpsE BACTH rv | TTT GGTCTC T <i>CACC</i> CGCATCCTCCGTGAC |
| xpsF BACTH fw | TT GGTCTC A <i>TATG</i> CCCCTCTACCGTTACAAGG |
| xpsF BACTH rv | TT GGTCTC G <i>CACC</i> GCCGATTGCATTGGTGAGGTC |
| Modularization of the xps gene cluster | |
| Amplification of <i>xpsE</i> including the native promoter | |
| Promoter 1 nt -365 fw | TTT GGTCTC A <i>ACAT</i> GGAGGCTTCGAGGCCAAGGCCGGC |
| Promoter 1 nt +4 rv | TTT GGTCTC A <i>TCAC</i> ACTCGTCTCCACTGGT |
| xpsE nt 1 fw | TTT GGTCTC A <i>GTA</i> ACGCGGTTGCCGTCGA |
| xpsE nt 936 rv | TTT GGTCTC A <i>CTCG</i> GTAAAGCCCAGCTTGTA |
| xpsE nt 932 fw | TTT GGTCTC A <i>CGAG</i> GACTTCTTGCCGCAGTTCCG |
| xpsE nt 1069 rv | TTT GGTCTC A <i>ATCT</i> TCGACGGTGATGATTTT |
| xpsE nt 1065 fw | TTT GGTCTC A <i>AGAT</i> CCGGTGGAATACCAGATCGA |

| Name | Sequence (5'-3'; <i>Bpi</i> I and <i>Bsa</i> I sites are written in bold, overhangs in italics) |
|--|---|
| xpsE nt 1728 rv | TTT GGTCTC A ACAA AGCGTCACGCATCCTCCGTGACGC |
| Amplification of <i>xpsF</i> including the native promoter | |
| Promoter 2 nt -175 fw | TTT GGTCTC A ACAT GGAGTCGGTAAGGCAGCAGAAACA |
| Promoter 2 nt +4 rv | TTT GGTCTC A GCAT CAGGCTGGGAGGCCGG |
| xpsF nt 1 fw | TTT GGTCTC A ATGC CCCTCTACCGTTACAA |
| xpsF nt 270 rv | TTT GGTCTC A CTCG GGCAGATCCATCAGAAT |
| xpsF nt 266 fw | TTT GGTCTC A CGAG GACGAAAAAGCCGGCGGGT |
| xpsF nt 1218 rv | TTT GGTCTC A ACAA AGCGTCAGCCGATTGCATTGGTGA |
| Amplification of <i>xpsG</i> - <i>xpsD</i> including the native promoter | |
| Promoter 3 nt -209 fw | TTT GAAGAC AA CTCA ACATGGAGGAGCGGAGCTCTGCGCAACGGTGCACTCTTCAC |
| Promoter 3 nt +4 rv | TTT GAAGAC AA CTCG GCATTGCAAAGGTTCCCGCA |
| xpsG nt 1 fw | TTT GAAGAC AA CTCA ATGCCCGCCGTGTCATGTGT |
| xpsG nt 492 rv | TTT GAAGAC AA CTCG TTATTGGTACTTGATGTCCG |
| xpsH nt -13 fw | TTT GAAGAC AA CTCA ATAAGCGCTCGCCATGCGCG |
| xpsH nt 510 rv | TTT GAAGAC AA CTCG TCATGGCGCCGGCGTCCGCA |
| xpsI nt 1 fw | TTT GAAGAC AA CTCA ATGAAGCGTCAGCGCGGTTA |
| xpsI nt 417 rv | TTT GAAGAC AA CTCG ACAACTCATGGCGGGCTGCCCTGC |
| xpsJ nt 1 fw | TTT GAAGAC AA CTCA ACATTGAGCCGTTGCGCAGCGCA |
| xpsJ nt 429 rv | TTT GAAGAC AA CTCG TTCCGGCGGCAGCGGGCTGCT |
| xpsJ nt 426 fw | TTT GAAGAC AA CTCA GGAAACCCTTGCCCAAGGCGTGCA |
| xpsJ nt 636 rv | TTT GAAGAC AA CTCG TCATTGCCCTGCCCGGGGT |
| xpsK nt 1 fw | TT GAAGAC AA CTCA ATGAGTCGTTGCGCGGTGC |
| xpsK nt 852 rv | TTT GAAGAC AA CTCG GTCATTGCACTGCTGCTCCC |
| xpsL nt 1 fw | TTT GAAGAC AA CTCA TGACCGCATGGCGGGACACC |
| xpsL nt 449 rv | TTT GAAGAC AA CTCG CTCGCGCACATCGAGCACGCG |
| xpsL nt 446 fw | TTT GAAGAC AA CTCA CGAGGACGGCCAGCTCGATGCCGA |
| xpsL nt 1122 rv | AAA GAAGAC AA CTCG ACAATTAACGCTGCGTGGCATCGG |
| xpsM nt 14 fw | TTT GAAGAC AA CTCA ACATTAAAGCGGATCGCTGGATC |
| xpsM nt 654 rv | TTT GAAGAC AA CTCG TCAAGGCGCATTGCTGGCCT |
| xpsC nt 8 fw | TTT GAAGAC AA CTCA TTGACATGATCGGCCTGCGC |
| xpsC nt 227 rv | TTT GAAGAC AA CTCG CTCGGCAAACGCCGGGTGCGC |
| xpsC nt 223 fw | TTT GAAGAC AA CTCA CGAGGACCGCCTGCCGCATCCGTT |
| xpsC nt 795 rv | TTT GAAGAC AA CTCG TCATTGGGTCTGACCGGGGG |
| xpsD nt 1 fw | TTT GAAGAC AA CTCA ATGAGTGAACGCATGACGCC |
| xpsD nt 1572 rv | TTT GAAGAC AA CTCG GCCAGCACCGCCCGTACCATC |
| xpsD nt 1568 fw | TTT GAAGAC AA CTCA TGGCCTCCCATCAGCTGCTGGTAG |
| xpsD nt 2292 rv | TTT GAAGAC AA CTCG ACAAAGCGCTATCTACCCTTCTCAAGTG |
| Deletion constructs of individual <i>xps</i> genes | |
| dxpsL rv | AAA GAAGAC AA CTCG ACAAGGCCAGCAGCGATTGTTGCC |
| dxpsL fw | TTT GAAGAC AA CTCA ACATGGCCGAACGGCAGCAATTGATG |
| dxpsM rv | AAA GAAGAC AA CTCG ACAAGGGTGAACCATGGGTGCACCAG |
| dxpsM fw | TTT GAAGAC AA CTCA ACATACCCTGGATATCGCCTTCGAGCTG |
| dxpsL 147stop rv | TTT GAAGAC AA CTCG CTCGCGCACATCAGAGCACGCG |
| dxpsC nt 485 fw | TTT GAAGAC AA CTCA CGAGGGGCGGGCAGCCGCCACCG |

| Name | Sequence (5'-3'; <i>Bpi</i> I and <i>Bsa</i> I sites are written in bold, overhangs in italics) |
|--|---|
| dxpsD rv | TTT GAAGAC AA <i>CTCG</i> GCCAGCGAAATTGAAGGTGGCACTG |
| dxpsG rv | TTT GAAGAC AA <i>GATC</i> AGCACAATGACGATGATGATTTCCAG |
| dxpsG fw | TTT GAAGAC AA <i>GATC</i> AGCCTGGGCAAGGACGGC |
| dxpsH rv | TTT GAAGAC AA <i>CACT</i> CCATGCCGATGACGCAACG |
| dxpsH fw | TTT GAAGAC AA <i>AGTG</i> CGCTTCACCGGCGCGC |
| dxpsI rv | TTT GAAGAC AA <i>CTCG</i> ACAAACGCCAGCAACGCGAAGGC |
| dxpsI fw | TTT GAAGAC AA <i>CTCA</i> ACATCGTTGCGGCTGGTGGCGGCC |
| dxpsJ rv | TTT GAAGAC AA <i>CTCG</i> ACAATCGATCAAGGTGAAGCCTGCG |
| dxpsJ fw | TTT GAAGAC AA <i>CTCA</i> ACATTCGACATCCGCAGCGACGATG |
| dxpsK rv | TTT GAAGAC AA <i>CGGT</i> GAGCGCGAACGCACCG |
| dxpsK fw | TTT GAAGAC AA <i>ACCG</i> CGATGGGGCTGGACG |
| Expression constructs for complementation studies | |
| xpsE-FLAG rev | T GGTCTC A ACAA AGCGTC ACTTATCGTCGTCATCTTTGTAATCCGCATCCTCCGTGACGC |
| P3 comp fw | TTT GGTCTC A GGAG GAGCGGAGCTCTGCGCAACG |
| P3 comp rv | TTT GGTCTC A <i>CATT</i> TGCAAAGGTTCCCGCATGGG |
| xpsL comp fw | TTT GAAGAC AA <i>CTCA</i> AATGACCGCATGGCGGGACAC |
| xpsL comp rv | TTT GAAGAC AA <i>CTCG</i> AGCGTTAACGCTGCGTGGCATCGGC |
| xpsL+SD comp fw | TTT GAAGAC AA <i>CTCAA</i> ATGGGAAGAGGGAGCAGCAGTGC |
| xpsM comp fw | TTT GAAGAC AA <i>CTCA</i> AATGCCACGCAGCGTTAAGCGC |
| xpsM comp rv | TTT GAAGAC AA <i>CTCG</i> AGCGTCAAGGCGCATTGCTGGCCTC |
| P3 compC fw | TT GGTCTC A ACAT GGAGGAGCGGAGCTCTGCGCAACG |
| P3 compC rv | TT GGTCTC A ACAA GCATTGCAAAGGTTCCCGCATGGG |
| xpsC comp fw | TT GGTCTC A ACAT ATGCGCCTTGACATGATCGG |
| xpsC comp rv | TT GGTCTC A ACAA AGCGTCATTGGGTCTGACCGGGGG |
| xpsD comp fw | TTT GAAGAC AA <i>CTCA</i> AATGAGTGAACGCATGACGCC |
| xpsD comp rv | TTT GAAGAC AA <i>CTCG</i> AGCG CTATCTACCCTTCTCAAGTGG |
| xpsG comp fw | TT GGTCTC A ACAT AATGCCCGCCGTGTCATGTGTTG |
| xpsG comp rv | TT GGTCTC A ACAA TAGCTTGGTACTTGATGTCCGCGTC |
| xpsH comp fw | TTT GAAGAC AA <i>CTCA</i> AATGCGCGTTGCGTGTACGCC |
| xpsH comp rv | TTT GAAGAC AA <i>CTCG</i> AGCGTCATGGCGCCGGCGTCCG |
| xpsI comp fw | TTT GAAGAC AA <i>CTCA</i> AATGAAGCGTCAGCGCGGTTAC |
| xpsI comp rv | TTT GAAGAC AA <i>CTCG</i> AGCGTCATGGCGGGCTGCCCTGC |
| xpsJ comp fw | TTT GAAGAC AA <i>CTCA</i> AATGAGCCGTTGCGCGAGCG |
| xpsJ comp rv | TTT GAAGAC AA <i>CTCG</i> AGCGTCATTGCCCTGCCCGGGG |
| xpsK comp fw | TTT GAAGAC AA <i>CTCA</i> AATGAGTCGTTGCGCGGTGC |
| xpsK comp rv | TTT GAAGAC AA <i>CTCG</i> AGCGTCATTGCACTGCTGCTCCCTC |
| Generation of fluorescence- and epitope-tagged constructs | |
| 4×Myc-N fw | TTT GAAGAC AA <i>AATG</i> GAACAAAAGTTGATCTCTGAAGAGG |
| 4×Myc-N rv | TTT GAAGAC AA <i>CAGG</i> TTAAGGTCTCTTCAGAAATAAGTTTTG |
| 4×Myc-C fw | TTT GAAGAC AA <i>GCTA</i> AGGAACAAAAGTTGATCTCTGAAGAGGAC |
| 4×Myc-C rv | TTT GAAGAC AA <i>AAGC</i> TCAAAGGTCCTCTTCAGAAATAAG |
| 1×FLAG-C fw | TT GAAGAC AA <i>GCTA</i> CAGACTACAAGGATGACGATGACAAGTGAAGCTTTTGTCTTCAA |
| 1×FLAG-C rv | TT GAAGAC AA <i>AAGC</i> TTCAC TTGTCATCGTCATCCTTG TAGTCTGTAGCTTGTCTTCAA |

| Name | Sequence (5'-3'; <i>Bpi</i> I and <i>Bsa</i> I sites are written in bold, overhangs in italics) |
|------------------------------|---|
| xpsL tagN fw | TT GGTCTC A ACAT CCTGATGACCGCATGGCGGGACAC |
| xpsL tagN rv | TT GGTCTC A ACAA AAGCTTAACGCTGCGTGGCATCGG |
| P3xpsLSD rv | TTT GGTCTC A CATT GCACTGCTGCTCCCTCTCC |
| xpsD tagC fw | TT GGTCTC A ACAT AATGAGTGAACGCATGACGCC |
| xpsD_tagC rv | TT GGTCTC A ACAA TAGCTCTACCCTTCTCAAGTGGCT |
| xpsC tagC fw | TT GGTCTC A ACAT AATGATGCGCCTTGACATGATCGG |
| xpsC tagC rv | TT GGTCTC A ACAA TAGCTTGGGTCTGACCGGGGGTAG |
| xpsC tagN fw | TT GGTCTC A ACAT CCTGATGCGCCTTGACATGATCGG |
| xpsC tagN rv | TT GGTCTC A ACAA AAGCTCATTGGGTCTGACCGGGGG |
| xpsF tagN fw | TT GGTCTC A ACAT CCTG ATGCCCCTCTACCGTTACAAGGC |
| xpsF tagN rv | TT GGTCTC A ACAA AAGCTCAGCCGATTGCATTGGTGAGGTC |
| xpsK tagC fw | TT GGTCTC A ACAT AATG AGTCGTTGCGCGGTGCCGC |
| xpsK tagC rv | TT GGTCTC A ACAA TAGC TTGCACTGCTGCTCCCTCTTC |
| P2 fw | TT GAAGAC TT GGAG CGCTACTAGAATTGAGCTCGGAG |
| P2 rv | TT GAAGAC TT CATT AGGCTGGGAGGCCGGG |
| P3 new fw | TT GAAGAC TT GGAG CGCTTTACGAATTCCTATGGGGAG |
| P3 new rv | TT GAAGAC TT CATT AACGATTTCCTTGACACGTCAATG |
| XpsC variants | |
| xpsC _{R5E} fw | TT GAAGAC AA CTTT GGCTTCGATCTCTTCTCGATGGCACGCATC |
| xpsC _{R5E} rv | TT GAAGAC AA GAAG AGCGCCAGCTGCAACAGCAGGAACAGAGCGGC |
| xpsC _{R5A} fw | TT GAAGAC AA CTGC GGCTTCGATGGCTTCGGCGATGGCACGCATC |
| xpsC _{R5A} rv | TT GAAGAC AA GCAG CCCGCCAGCTGCAACAGCAGGCCAGAGCGGC |
| Cysteine crosslinking | |
| xpsI _{A33C} fw | TT GAAGAC AA TGTG CACGCCAGGTGCGCGCGG |
| xpsI _{A33C} rv | TT GAAGAC AA CACA GCCGGACAACGACCCAGC |
| xpsJ _{A46C} fw | TT GAAGAC AA TGTC AGCGCAGCGAGCGCGTAC |
| xpsJ _{A46C} rv | TT GAAGAC AA GACA GATCGCTTCGCCGCGCTG |
| xpsK _{A45C+E51C} fw | TT GAAGAC AA GCAC GCGTGTGTGCGCTGCAGGGCAGCATGCTG |
| xpsK _{A45C+E51C} rv | TT GAAGAC AA GTGC GGTGAGACAGAACGCACCGATCATCGCGG |
| xpsF _{T241C} fw | TT GGTCTC A TCTG TAATGCAATCGGCTGA |
| xpsF _{T241C} rv | TT GGTCTC A CAGA GGTCATACAGCGGGAC |

Table 14: predicted molecular masses of Xps proteins

| Protein | Size (amino acids) | Expected size (kDa) |
|------------|--------------------|---------------------|
| XpsE | 575 | 65 kDa |
| XpsF | 405 | 44 kDa |
| XpsG | 163 | 17 kDa |
| XpsH | 169 | 18 kDa |
| XpsI | 138 | 15 kDa |
| XpsJ | 211 | 23 kDa |
| XpsK | 301 | 32 kDa |
| XpsL | 373 | 42 kDa |
| XpsM | 217 | 24 kDa |
| XpsC | 265 | 28 kDa |
| XpsD | 759 | 77 kDa |
| XpsO | 287 | 32 kDa |
| c-Myc- tag | | ca. 6kDa |

7.2 Supplemental figures



Figure 33: The modular T2S system restores bacterial spot formation in an *xps*-T2S gene cluster mutant

Leaves of susceptible ECW pepper plant were dip-infected with the wild-type strain 85-10 and the T2S deletion mutant 85-10 Δxps (Δxps) with (+) or without (-) the modular *xps*-T2S expression construct (pT2S). Disease symptom formation was photographed seven weeks after infections. The experiment was performed three times with similar results. Spot formation on one representative leaf per strain is shown.

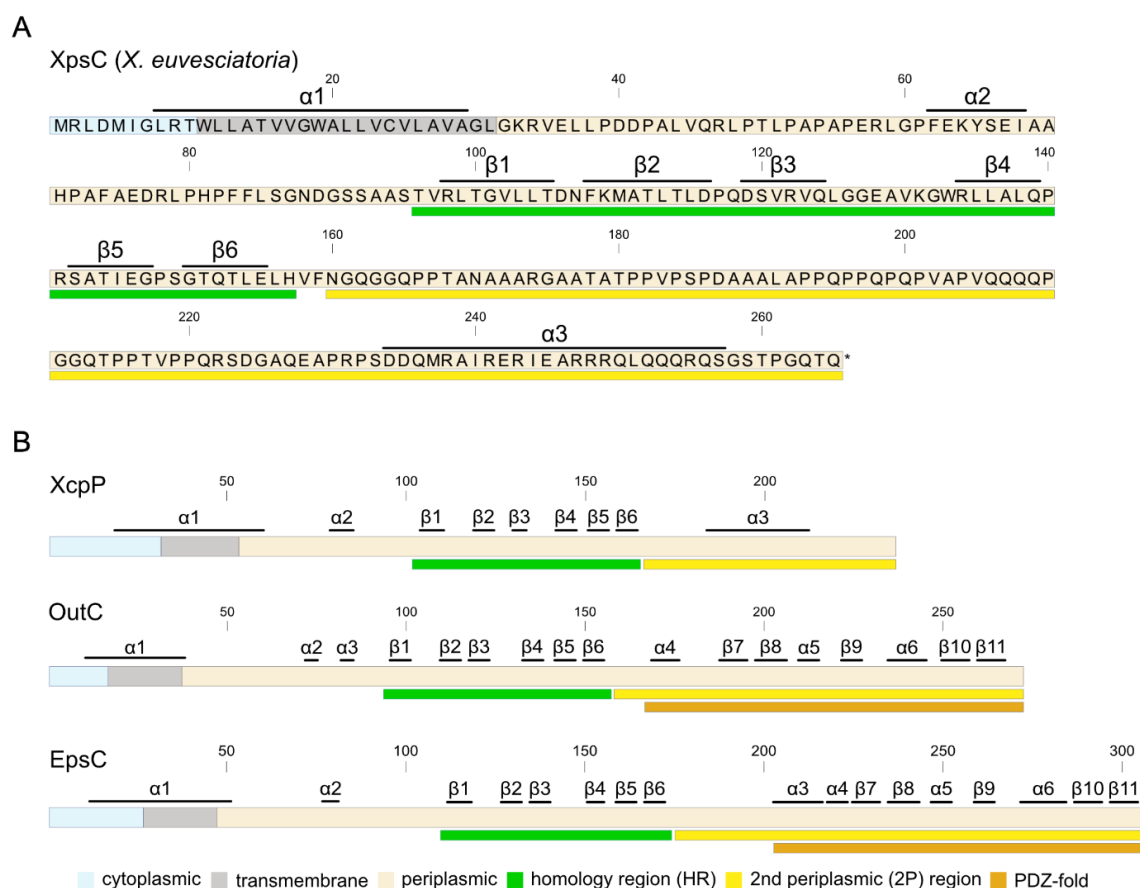


Figure 34: Predicted secondary structures in XpsC and corresponding GspC proteins

A: Predicted α -helices and β -sheets in XpsC from *X. euvesicatoria*. The amino acid sequence of XpsC (accession number CAJ25390) and the positions of predicted α -helices and β -sheets predicted by AlphaFold2 are shown. Coloured rectangles refer to cytoplasmic, transmembrane and periplasmic regions as well as to the HR and 2P regions as indicated. Numbers indicate amino acid positions. B: Predicted secondary structure elements in GspC proteins. α -helices and β -sheets were predicted and indicated as described in (A). The following proteins were analyzed: XcpP from *P. aeruginosa* strain PAO1 (accession number CAA48581), OutC proteins from *D. dadantii* strain 3937 (accession number CAA46369) and EpsC proteins from *V. cholerae* strain N16961 (accession number P45777).

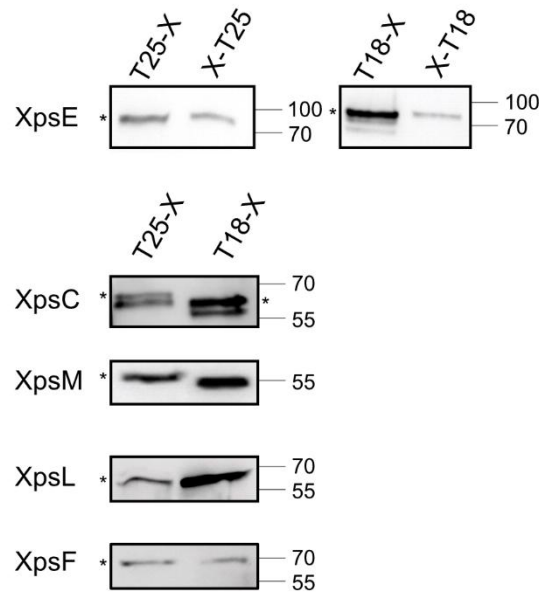


Figure 35: Synthesis and immunological detection of T18 and T25 fusions of assembly platform components

Cell extracts from *E. coli* strain JM109 containing expression constructs encoding T18 and T25 fusions of XpsC, XpsL, XpsM and XpsE as indicated were analyzed by immunoblotting, using a FLAG epitope-specific antibody.

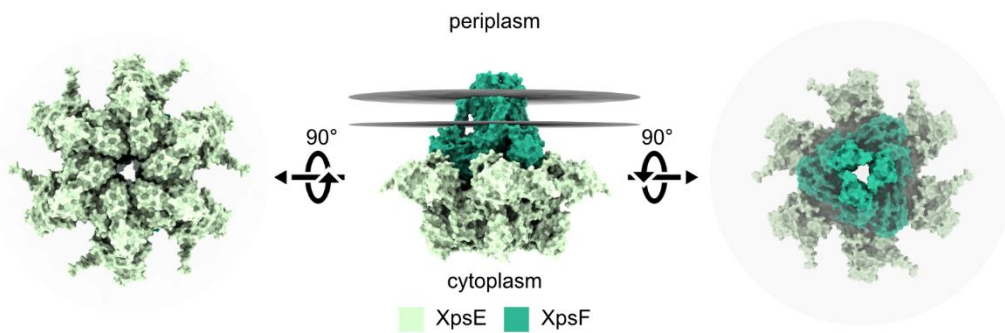


Figure 36: AlphaFold3 structural model of XpsE₆-XpsF₃ complex:

A: The structure of a hexameric-trimeric XpsE₆-XpsF₃ complex of the ATPase XpsE and the inner membrane protein XpsF from *X. euvesicatoria* was predicted using AlphaFold3 and visualized using UCSF ChimeraX. Top and bottom views of the complex are shown on the right and left. Hydrophobic residues in structures were used to predict the position of the outer and inner membranes in the structure (shown by grey discs). Proteins are color-coded as indicated below.

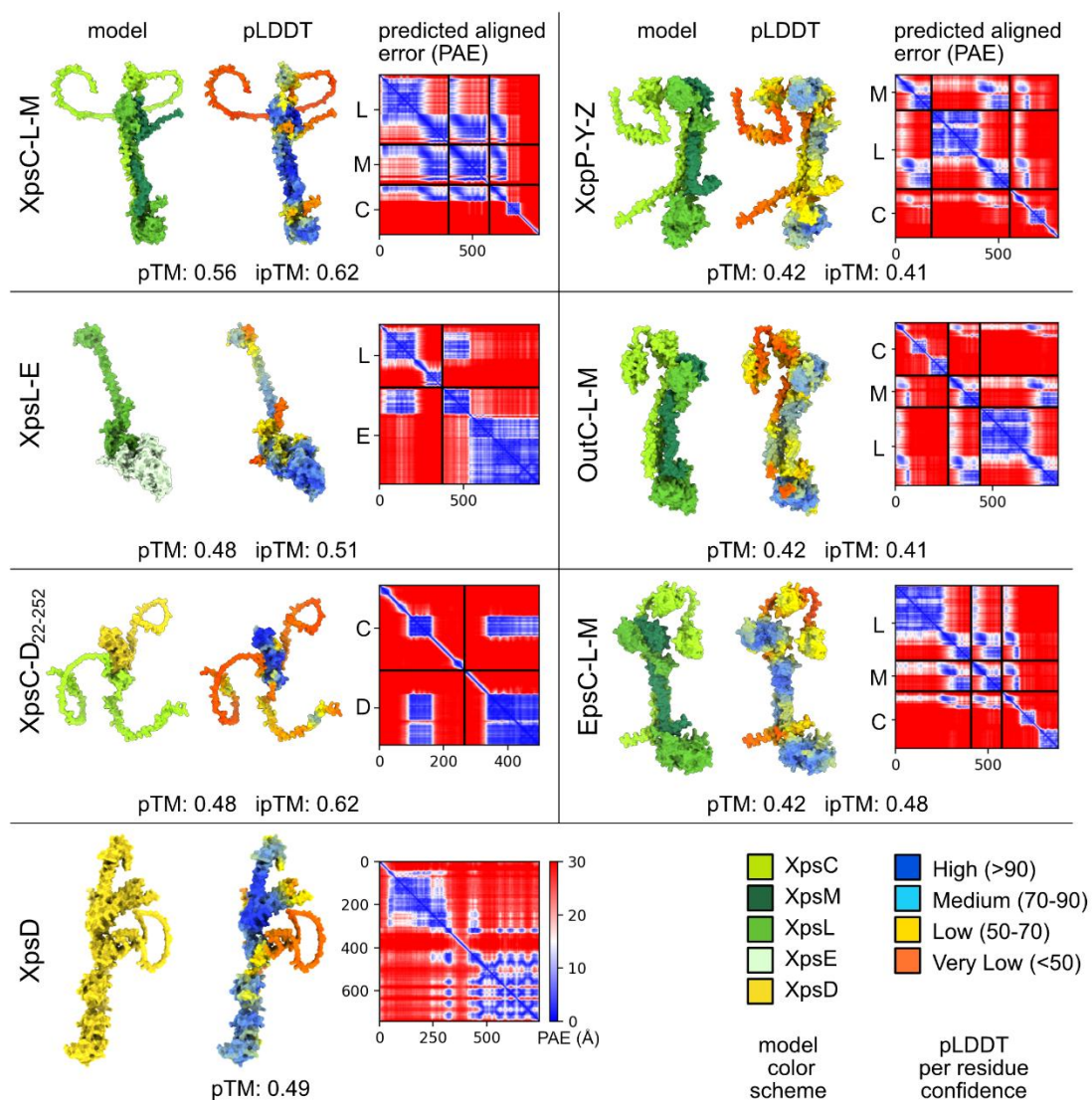


Figure 37: AlphaFold2 Structure predictions of assembly platform components from *X. euvesicatoria*, *P. aeruginosa*, *D. dadantii* and *V. cholerae*.

Complexes containing XpsCLM from *X. euvesicatoria* or corresponding proteins from *P. aeruginosa*, *D. dadantii* and *V. cholerae* were predicted using the AlphaFold2 algorithm and the molecular visualization program UCSF ChimeraX. Similarly, XpsD as well as complexes between XpsL and XpsE, XpsC and the N-terminal region of XpsD (XpsD₂₂₋₂₅₂) were modeled. In the models on the left side, proteins are shown in different colours as indicated. The models on the right side show the per-residue model confidence score (pLDDT, predicted local distance difference test) which is scaled from 0 to 100 with different colours referring to different scores as indicated. In addition, a predicted aligned error (PAE) plot shows regions of high (blue colour, low PAE value) and low (red colour, high PAE value) confidence for the predicted structures. The pTM and ipTM values are shown below the models.

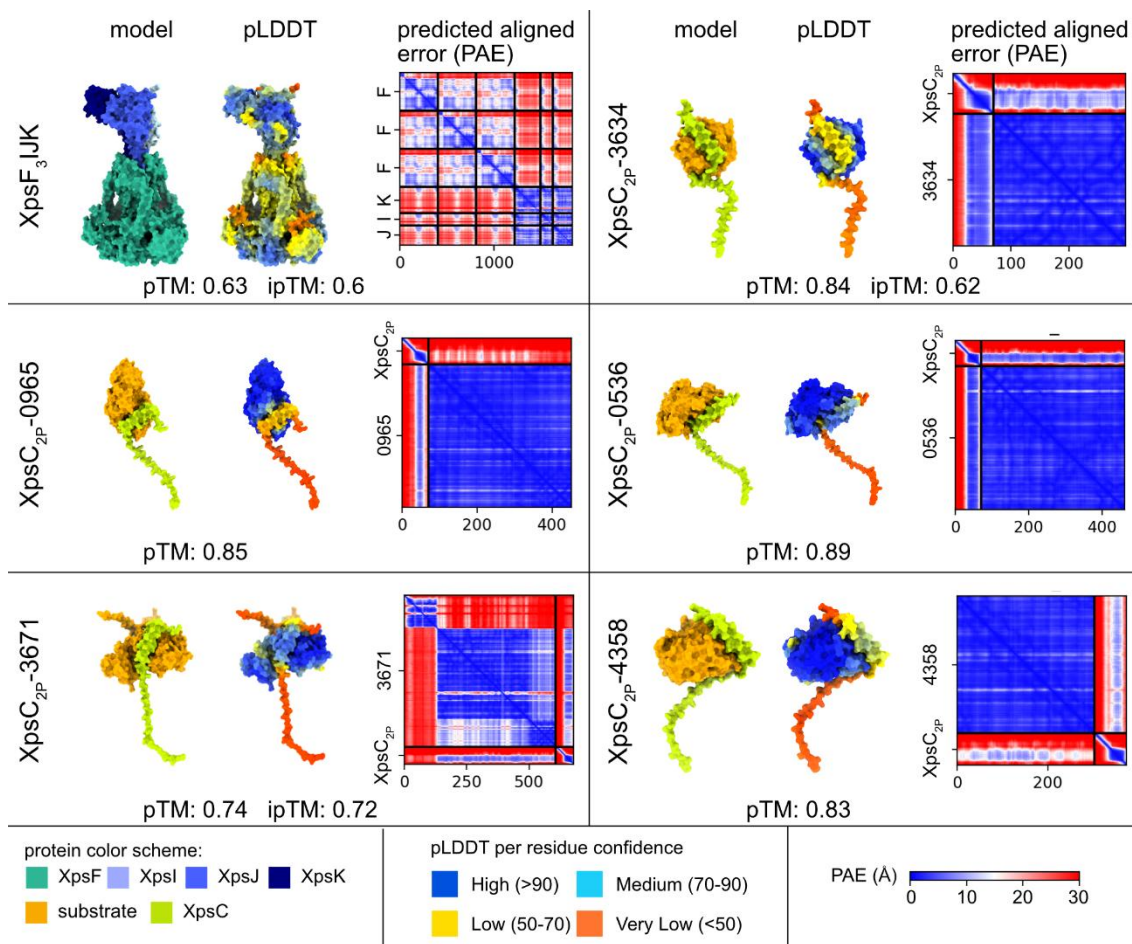


Figure 38: AlphaFold2 structure predictions of additional T2S proteins

Complexes containing XpsF₃IJK as well as interactions between the XpsC-2P region (XpsC₁₉₅₋₂₆₅) and T2S substrates XCV3634, XCV0965, XCV0536, XCV3671 and XCV4358 from *X. euvesicatoria* were predicted using the AlphaFold2 algorithm and visualized with UCSF ChimeraX. In the models on the left side, proteins are shown in different colours as indicated. The models on the right side show the per-residue model confidence score (pLDDT, predicted local distance difference test) which is scaled from 0 to 100 with different colours referring to different scores as indicated. In addition, a predicted aligned error (PAE) plot shows regions of high (blue colour, low PAE value) and low (red colour, high PAE value) confidence for the predicted structures. The pTM and ipTM values are shown below the models.

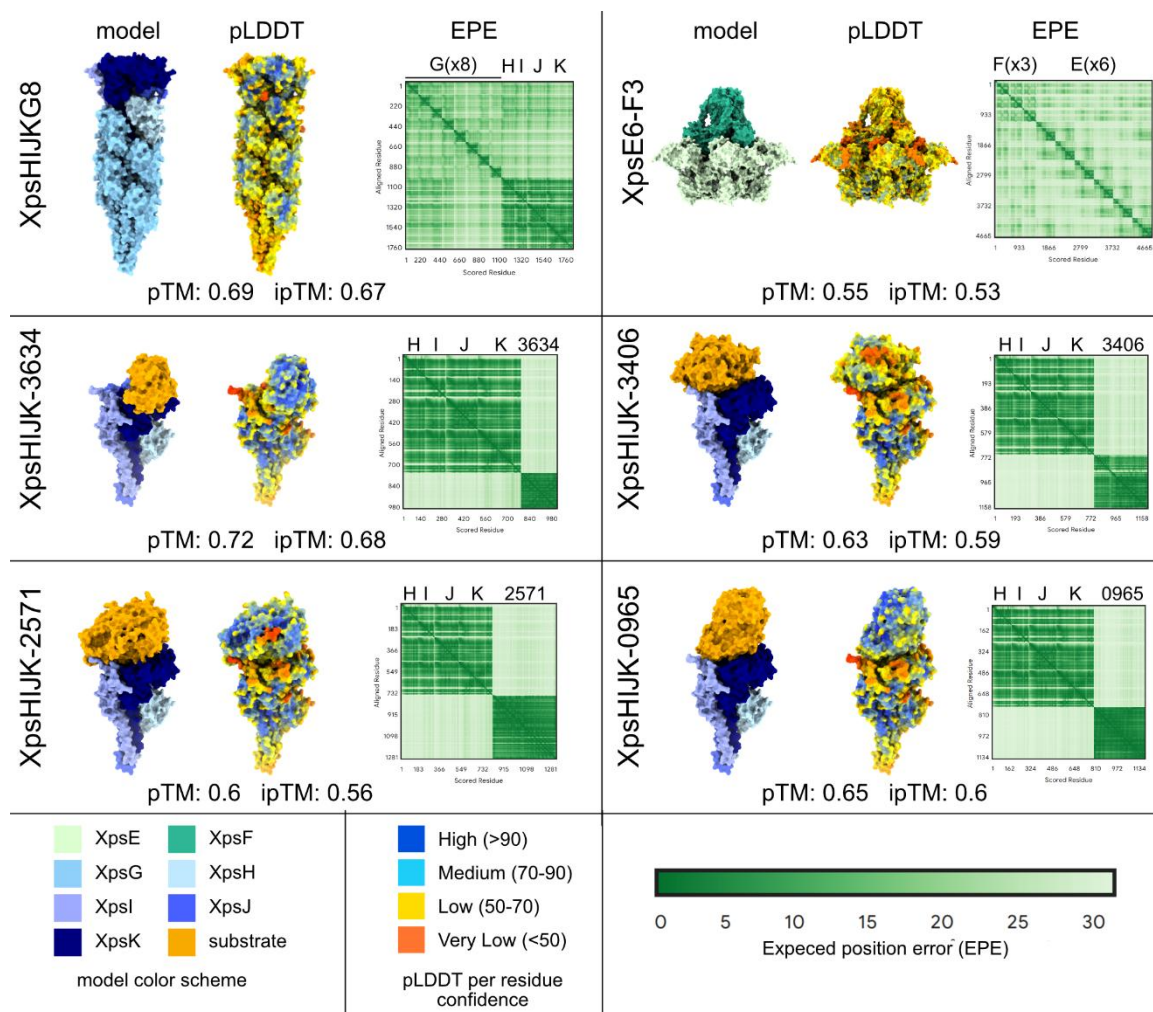


Figure 39: AlphaFold3 structure predictions of proteins used in this study

Complexes containing XpsHIJG₈ as well as interactions between the XpsHIJK pseudopilus tip complex and T2S substrates XCV3634, XCV3406, XCV2571 and XCV0965 from *X. euvesicatoria* were predicted using the AlphaFold3 algorithm and visualized with UCSF ChimeraX. In the models on the left side, proteins are shown in different colours as indicated. The models on the right side show the per-residue model confidence score (pLDDT, predicted local distance difference test) which is scaled from 0 to 100 with different colours referring to different scores as indicated. In addition, an expected position error (EPE) plot shows regions of high (green colour, low EPE value) and low (white colour, high EPE value) confidence for the predicted structures. The pTM and ipTM values are shown below the models.

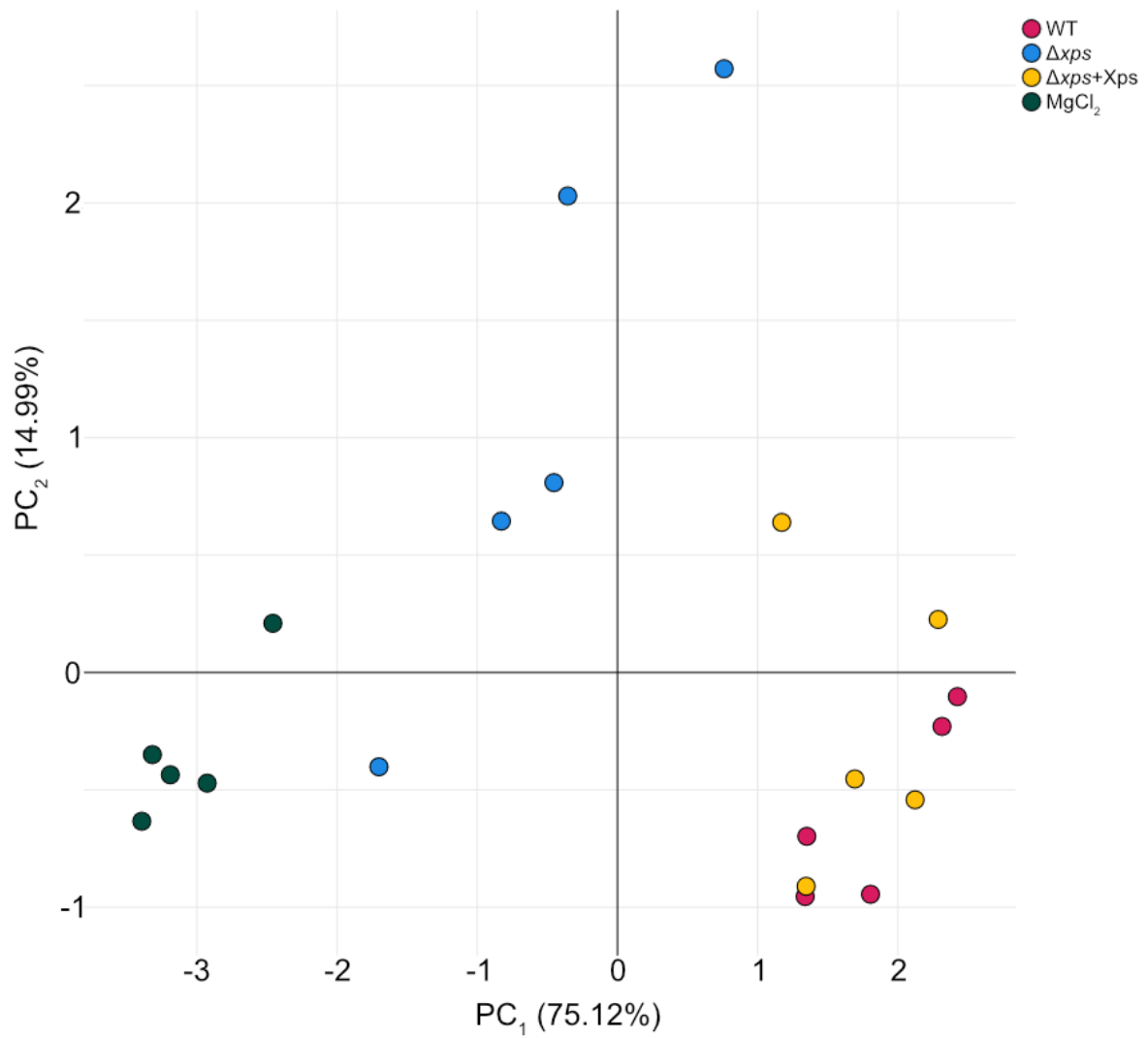


Figure 40: Principal component analysis of the cell wall monosaccharide composition of infected plants

Composition Principal component analysis of the cell wall monosaccharide composition depicted in Figure 27 revealed that 90.11% of the variation was contained in the first two principal components (PC1 and PC2), where PC1 (75.12% of the variation) separates between treatments, with a distinct cluster for $MgCl_2$ -treated samples, a cluster of wild-type and $\Delta xps+Xps$ -treated samples and the Δxps -treated samples appearing between these two.

7.3 Acknowledgements

It is my deep conviction that good science springs from collaboration of people with different backgrounds, convictions and worldviews. The myth of a lone scientific genius is exactly that, a myth with little truth to it.

I am deeply grateful to Daniela Büttner for the supervision of this thesis. Thank you for the hours of talking through data, pointing out mistakes, discussing ways forward and encouraging in challenging times. Both M.Sc. students involved in studying the T2S system in our group, Akash Shivhare and Iliyana Kraleva, have my deep appreciation and helped me ask better questions. Thank you for being the humorous, open and sharp-minded people that you both are. I'm much obliged to Patrick Martin for many preliminary experiments and conceiving and constructing the modular T2S plasmid. Additionally, I am grateful for the other lab mates in the AG Büttner and the AG Laubinger, especially Matze, Luise, Sabine, Christian and Cornelius. I'll remember lunch breaks and endless political discussions with many of you for a long time.

Collaborating with Jessica Erickson (now in Tübingen) really helped both of us understand the function of the T2S substrates *in planta*. I don't want to know what this thesis would look like without you, and I really appreciate discussing and ranting together and building each other up in setbacks. Special thanks to Vivian Linke and Akash Shivhare for helping us have the manpower required for these mass-spec experiments. Beyond that, I really benefitted from collaborating and discussing with Sylvestre Marillonnet and Susanne Matschi (both IPB Halle), Stephanie Krüger (MLU Halle). Finally, I appreciate the assistance of Timo Engelsdorf and Kristina Munzert (PU Marburg) in characterizing the cell wall monosaccharides of infected plants.

Four other people I would like to mention here that contributed to this thesis in valuable ways are Torsten Waldminghaus, David Huber, and my parents, Martin and Mirjam. Working in Torstens lab shaped my scientific critical thinking more than any other lab. David, as a flatmate helped me discuss T2S in normal human terms and built me up as an encouraging friend in the dark seasons of this PhD journey. Finally, my parents, especially my mom, invested more into my education and formation as a person than any other people I know. Thank you for that.

Finally, I am grateful to God for making life so intricate, complex and worth studying, and especially for granting me life a second time after I had Leukemia as a four-year-old.

7.4 Curriculum vitae

Name: Samuel Goll
Nationality: German
Fields of interest: Molecular Microbiology and Genetics, Synthetic Biology, Plant-Pathogen-Interactions,



Formal Education

2022-2025: **Ph.D. in Molecular Genetics in the Group of Daniela Büttner**
Martin-Luther-University Halle-Wittenberg
“Understanding the architecture and biology of the type II protein secretion system in plant-pathogenic *Xanthomonas* bacteria”

2019-2021: **M.Sc. Molecular and Cellular Biology** (grade average: 0.8)
Philipps-University of Marburg
Majors: Plant-Pathogen-Interactions, Genetics, Microbial Ecology
Master’s thesis in the lab of Lars Voll:
“The Role of Carbohydrate Availability and Allocation in the Interaction of *Arabidopsis thaliana* and *Colletotrichum higginsianum*”

2016-2019: **B.Sc. Biology** (grade average: 1.2)
Philipps-University of Marburg
Majors: Genetics, Molecular Microbiology
Bachelor’s thesis in the lab of Torsten Waldminghaus:
“Characterization of the Chromosome 2 Replication Triggering Site (*crtS*) of *Vibrio cholerae* using Synthetic Biology”

2015: **Deutsche Internationale Abiturprüfung (DIAP)** (grade average: 1.0)
German School of Kuala Lumpur, Malaysia
(awarded with a Abiturientenpreis from the Gesellschaft Deutscher Chemiker (GDCh))

Funding

2023-2025: funded by the **Studienstiftung des Deutschen Volkes**

2022: funded by the **Graduiertenförderung des Landes Sachsen-Anhalt**

2016-2020: funded by the **Deutschlandstipendium** (4 years of funding)

7.5 Declaration of authorship

I hereby declare that I am the sole author of this thesis and that no other sources or learning aids, other than those listed, have been used. Furthermore, I declare that all direct or indirect sources used are clearly identified as references.

I also hereby declare that my thesis has not been prepared for another examination or assignment, either in its entirety or excerpts thereof.

Halle (Saale), 24. 03. 2025

Samuel Goll